A Window into Selective Catalytic Reduction: a RAIRS Study of NO and NH_3 on Cu{311}

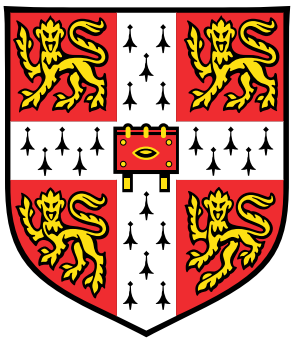

Krit Sitathani

Department of Chemistry

University of Cambridge

This dissertation is submitted for the degree of

Doctor of Philosophy

Downing College

April 2016

I would like to dedicate this thesis to my friends and family who have provided me with unconditional support and care throughout my studies.

Declaration

I hereby declare that except where specific reference is made to the work of others, the contents of this dissertation are original and have not been submitted in whole or in part for consideration for any other degree or qualification in this, or any other University. This dissertation is the result of my own work and includes nothing which is the outcome of work done in collaboration, except where specifically indicated in the text. This dissertation contains less than 60,000 words, including tables, footnotes, bibliography and appendices, but excluding photographs and diagrams as specified by the Degree Committee for Physics and Chemistry.

Krit Sitathani

April 2016

Acknowlegements

First and foremost, I would like to extend my most genuine thanks to my supervisor, Dr Steven Jenkins for providing me with so much support during my time here and guidance whenever I needed it.

I am grateful to all of my colleagues at the Surface Science group as I would not have been able to finish my PhD without their constant help. I want to express my gratitude to Dr Israel Temprano, who taught me about importance of a good work ethic and provided me with motivation during my PhD. I am also extremely grateful to Dr Steven Driver, who has spent a considerable amount of time helping me, especially teaching me the principles behind LEED and providing me with constant moral support. Many thanks also go to Dr David Madden and Dr Tao Liu for helping me in getting to grips with my RAIRS machine, especially to overcome its daily nuisances.

Next, I would like to say thank you to my family - my father, mother, and brother - who have provided me with constant love and unconditional care even though they are far away in another country. Words cannot describe how grateful I am to have such a supportive family.

To all of my friends that I have met during my time in Cambridge, I would not be the person I am today if I had not met every single one of them. My time in Cambridge has been defined by my experiences with everyone one of you, especially those I met during my time at Downing College MCR, rowing with DCBC, and shooting for CURA. I will cherish these memories and friendships for life. I would like to give special mention and thanks to a few people: Nicholas Soane for his friendship and for housing me when I needed it. Dr Daisy Hessenberger for being an amazing friend through both the good and tough times.

Dr Pablo Aran-Terol for the many years of friendship and providing me with far too many delicious meals. Dr Matthias Grein for all the life advice and teaching me the joys of gin. Dr Erika Davies, Bianca Provost, Dr Camilla d'Angelo, Laura Clarke, and Porndee Chua for putting up with me and helping me whenever I needed it. Christopher Rowe, Dr Michiel Kamp, and Kyle Sutherland-Cash for the many hours playing games together over the years. Calum MacDonald and Dr Jake Harris, for the countless pints at various pubs.

I also would not have been able to start my PhD without the help of my friends and colleagues during my time at the University of Liverpool. Special thanks go to Dr Heike Arnolds for being my first ever supervisor and for introducing me to surface science. I would also like to thank Dr John Greenwood, Dr Liban Saleh, Dr Danny Dawson, and George Prempeh for their many years of friendship.

I would also like to extend my gratitude to Dr Carl Doige, who sparked my interest in Chemistry due his passion and kind words during my time at Ruamrudee International School.

Abstract

This thesis studies the interaction between the bare Cu{311} surface with NO and NH_3, individually and co-adsorbed using reflection-absorption infrared spectroscopy (RAIRS). In addition to the bare Cu{311} surface, the interaction of NO and NH_3 with the various oxygen phases of the Cu{311} surface phases was also studied. Several other techniques were used in tandem to support the study, such as low energy electron diffraction (LEED) and temperature programmed desorption (TPD) experiments using mass spectrometry. The study was carried out in pursuit an understanding of the underlying mechanism of the selective catalytic reduction (SCR) of NO using NH_3 in current diesel engines.

The dosing of NO onto the Cu{311} surface at 100 K leads to the initial adsorption of intact NO. After an exposure threshold is reached, individual NO molecules react with another NO molecule to form $(NO)_2$ dimers. These dimer species subsequently form N_2O, leaving $O_{(a)}$ on the surface. Oxygen was found to be an inhibitor for the reaction, either due to the reaction in a self-poisoning process or from oxygen pre-dosing onto the Cu{311} surface. Temperature plays a minor role with regards to NO/Cu{311}, as it only affects the amount of NO on the surface along with adsorbate surface mobility.

Similarly, NH_3 was found to adsorb intact onto the Cu{311} surface and not to react or dissociate at 100 K. Oxygen acts as a site blocker for the adsorption, but can also stabilise NH_3 to remain on the surface at higher temperatures due to electronic effects. At 300 K, it was found that both the bare and oxygen pre-covered Cu{311} surface was able to dissociate NH_3 into NH_2.

The co-adsorption of NO and that of NH_3 onto the Cu{311} surface were found to be largely independent of each other and the interaction is dominated by the displacement of

NO by NH_3. However, as NO adsorption on the Cu{311} surface forms $O_{(a)}$, it indirectly affects the adsorption of NH_3 by creating an oxygen covered Cu{311} surface, which changes how NH_3 adsorbs onto the surface.

Contents

Contents **vii**

1 Introduction - NO and the Environment **1**

1.1 Nitrogen Oxide 1

1.1.1 Environmental Effects of Nitrogen Oxide 2

1.2 Car Exhaust and Catalytic Converters 3

1.2.1 Selective Catalytic Reduction 5

1.3 Background of NH_3 8

1.4 Overview of this Thesis 9

1.5 Surface Science 10

1.5.1 Ultra High Vacuum 10

1.5.2 Single Crystals 11

2 Experimental - Surface Science **14**

2.1 Surface Science 14

2.1.1 Ultra High Vacuum System 14

2.1.2 Vacuum System 16

2.1.3 Pressure Detection 17

2.1.4 Manipulator and Temperature Control System 18

2.2 Single Crystals 20

2.3 Reflection-Absorption Infrared Spectroscopy 20

2.4 Secondary Techniques 26

2.4.1 Ion Sputtering 26
2.4.2 Low Energy Electron Diffraction 27
2.4.3 Auger Spectroscopy 28
2.4.4 Mass Spectroscopy 31

3 Cu{311} and Oxides of Cu{311} 35
3.1 Bare Cu{311} 35
3.2 Oxygen Pre-Covered Cu{311} 35
3.2.1 O(1×2)/Cu{311} 36
3.2.2 O(Runways)/Cu{311} 38
3.2.3 O(Oxide Clusters)/Cu{311} 39
3.3 Residual CO Adsorption 40
3.3.1 Past CO Adsorption Studies 40
3.3.2 Experimental 46
3.3.3 CO/Cu{311} Results 46
3.3.4 TPD Studies of CO/Cu{311} 51
3.3.5 Discussion 54
3.3.6 Conclusion 56

4 NO and Cu{311} 57
4.1 Literature Review 57
4.1.1 Catalytic Studies of NO 57
4.1.2 Surface Science Studies of NO 62
4.2 Experimental 70
4.3 Results 70
4.3.1 NO and Bare Cu{311} 71
4.3.2 NO and Oxygen Pre-Covered Cu{311} 79
4.3.3 Temperature Effects 86
4.4 Discussion 91
4.4.1 RAIRS Analysis 91

4.4.2 Reaction Mechanism 99
4.5 Conclusion 100

5 NH_3 and Cu{311} 101
5.1 Literature Review 101
5.1.1 Surface Science Studies of NH_3 101
5.2 Experimental 112
5.3 Results 112
5.3.1 NH_3 and Bare Cu{311} 112
5.3.2 NH_3 and Oxygen Pre-Covered Cu{311} 116
5.3.3 Temperature Effects 120
5.4 Discussion 124
5.4.1 NH_3 and Bare Cu{311} 124
5.4.2 NH_3 and Oxygen Pre-covered Cu{311} 126
5.4.3 Temperature Effects 129
5.5 Conclusion 131

6 NH_3 and NO Co-Adsorption on Cu{311} 132
6.1 Literature Review 132
6.2 Experimental 135
6.3 Results 136
6.3.1 RAIRS Experiments 136
6.3.2 Temperature Programmed Desorption Experiments 142
6.4 Discussion 143
6.4.1 RAIRS Analysis 143
6.4.2 Temperature Programmed Desorption Analysis 146
6.4.3 Co-Adsorption and Mechanism 150
6.5 Conclusion 151

7 Conclusion **152**

7.1 Conclusion 152

7.2 Further Work 155

References **157**

Chapter 1

Introduction - NO and the Environment

1.1 Nitrogen Oxide

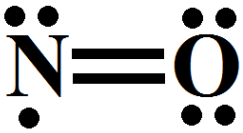

Fig. 1.1 A Lewis structure diagram of the NO molecule, showing the nitrogen and oxygen bond along with the radical.

Nitric Oxide is a molecule with the chemical formula NO and a molecular weight of 30 g mol^{-1}. It is a free radical consisting of nitrogen bonded directly to oxygen (Figure 1.1). NO is formed naturally from lightning strikes and is a major by-product of combustion. Natural sources make up less than 10% of the total amount of NO produced globally, with the remaining 90% originating from human activity. Of this 90%, up to 50% of human-produced NO emissions are from automobiles, 20% from electric power plants, with the remaining 30% from a combination of other smaller sources [1]. From combustion, the production of NO follows Equation 1.1 - 1.3.

$$2N_2 + O \rightarrow 2NO + 2N \tag{1.1}$$

$$2N_2 + O_2 \rightarrow 2NO + 2N \tag{1.2}$$

$$N + OH \rightarrow NO + H \tag{1.3}$$

NO readily reacts in air to form N_2O and NO_2, both of which are greenhouse gases [1]. The worldwide creation of NO related gases increased from 15 tons per year in 1860 to 156 tons per year in 1997 [2]. There has been a global effort to reduce emissions, which is spearheaded by the Intergovernmental Panel on Climate Change (IPCC), a scientific intergovernmental body under the direction of the United Nations [3].

The difficulty in reducing the amount of NO emitted by human sources is its direct effect on a country's economy. The use of NO is deeply intertwined with a country's manufacturing processes and energy use, which are essential for economic prosperity. Thus the solution which will reduce NO emissions must come both from a more effective use of technologies that produce NO as a by-product and from the removal of NO before it is release into the atmosphere.

1.1.1 Environmental Effects of Nitrogen Oxide

NO emissions are of environmental concern due to their effects on the environment, causing damage both directly and indirectly [2, 4, 5]. NO causes soil and water enrichment due to nitrate injection/cascading, which can cause uncontrolled algae and plant growth in water sources. This growth can cause the death of other plant and animal species.

NO readily reacts with volatile organic compounds in the presence of sunlight to produce ozone in the troposphere, causing damage to human life and the environment [6]. Ozone in the troposphere is known to damage the human respiratory system, causing health concerns such as asthma or inflammation of the lung. Conversely, NO reacts with ozone in the stratosphere to form O_2. This depletes the amount of ozone in the stratosphere and creates ozone holes [7]. Ozone holes expose humans and the environment to harmful UV radiation from the sun.

On a smaller scale, NO readily reacts with NH_3 and H_2O to form nitric acid, which can end up as acid rain [1]. Acid rain does not directly harm human life but can damage buildings and soil. The main danger from acid rain is due to how it kills insects, plants, and aquatic life forms.

1.2 Car Exhaust and Catalytic Converters

Automobiles are responsible for up to 50% of global NO emissions [1], so any curtailing thier emissions will significantly impact global NO levels. Considerable effort hast been made to find ways to convert NO into environmentally friendly N_2 and O_2. Thermodynamically, NO is unstable and the decomposition reaction to form N_2 and O_2 has a ΔG_f^0 of -86 kJ mol^{-1} [8]. However, there is an activation energy of 310 kJ mol^{-1} [9]. Therefore catalysts are needed to overcome the high activation energy requirement. Unsurprisingly, one of the approaches to reduce global emissions has been the introduction of catalytic converters into cars in the late 20th century.

In the UK, the Environmental Protection Act of 1990 [10] introduced emission standards for industrial and automobile processes. This led to the widespread use of catalytic converters in cars from 1992; as a result, most cars on today's roads in the UK are now installed with one. The use of catalytic converters allows the same number of cars to function while simultaneously reducing emission, achieving the goal of emission reduction with minimum disruption to the automobile industry.

In most cars, the current standard for catalytic converters are Pt three-way catalysts, an example of which is shown in Figure 1.2. Three-way catalytic converters offer an effective way to reduce emission from car exhaust by converting it to more environmentally friendly gases such N_2 or H_2O [11–13]. Their basic form is a precious metal catalyst (Pt) supported on a substrate (ceramic or zeolites) on a honeycomb-like grid. The term "three-way catalyst" refer to its ability to conduct three simultaneous reactions: the reduction of nitrogen oxides, the oxidation of carbon monoxide, and the oxidation of unburnt hydrocarbons, as shown in Equations 1.4 - 1.6.

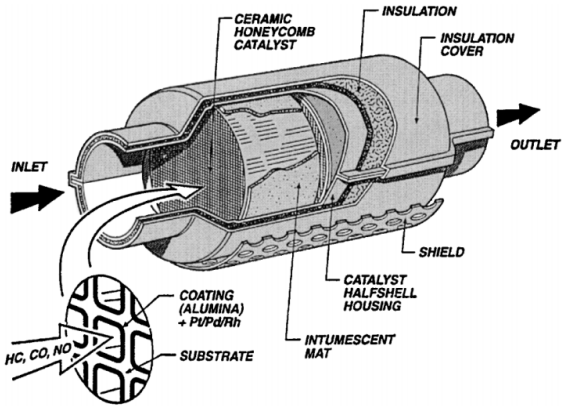

Fig. 1.2 An example of a three-way catalytic converter in the exhaust area of a car. Hydrocarbons, CO, and NOx enter from the left and flow through the honey-comb three-way catalyst grid. (Heck and Farraguto [13])

$$2\mathrm{NO} \rightarrow \mathrm{O}_2 + \mathrm{N}_2 \tag{1.4}$$

$$2\mathrm{CO} + \mathrm{O}_2 \rightarrow 2\mathrm{CO}_2 \tag{1.5}$$

$$\mathrm{C}_x\mathrm{H}_y + (1 + \frac{y}{4})\mathrm{O}_2 \rightarrow x\mathrm{CO}_2 + \frac{y}{2}\mathrm{H}_2\mathrm{O} \tag{1.6}$$

Three-way catalysts are able to effectively reduce emissions from car exhaust to an amount that falls within emission standards. However, three-way catalysts do not work with all automobile exhaust, in particular that which is emitted by automobiles that use "lean burn" engines.

Diesel engines are used by a substantial percentage of automobiles and many of them run under "lean burn" conditions. Lean burn conditions are when the air:fuel ratio during combustion is high, which causes the exhaust to have a high oxygen content, rendering it an oxidising environment. Although this allows for the oxidation of CO into CO_2 and hydrocarbons to be possible, the reduction of NO into N_2 remains difficult, despite a catalyst. Thus, in order to reduce NO emissions in cars fitted with catalysts, a new method of converting NO into N_2 in an oxidising environment must be developed. In addition to lean burn

conditions, the temperature of diesel exhaust is also 200 K lower than that of petroleum gasoline engines. This puts it outside the optimal operating temperature range of Pt three-way catalysts, which is an additional reason why new catalysts should be developed for diesel engines. Several efforts are being made to overcome these problems, and one of the leading techniques is called selective catalytic reduction (SCR).

1.2.1 Selective Catalytic Reduction

As mentioned in the previous section, selective catalytic reduction (SCR) is a technique used to reduce NO emissions of diesel engines. The resulting exhaust gas from diesel engines is "lean" - where the air:fuel ratio is high. This causes the conditions inside the catalytic converter to be an oxidising environment. Therefore, NH_3 is injected into exhaust gas before it reaches the catalytic converter in order to selectively reduce NO into N_2 and H_2O [14]. The use of SCR, in combination with an effective catalyst, is able to reduce NO emission by up to 90% [15, 16]. Typically, NH_3 is used as the reductant (or alternatively, urea - which breaks down to form NH_3 but can also directly reduce NO [17]). A simple visual representation of this process is shown in Figure 1.3.

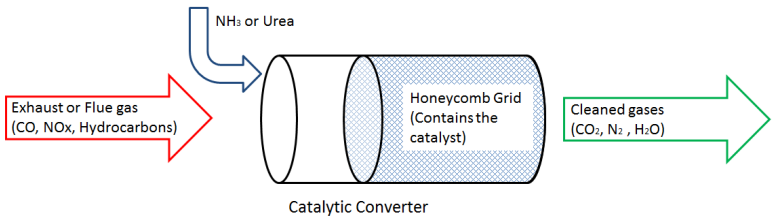

Fig. 1.3 A simple visualisation of the how selective catalytic process occurs when NH_3 is injected into the arriving exhaust before it enters the catalytic converter.

Controlling the stoichiometry of the gas environment inside the catalytic converter is vital in order for the reaction to take place. It must be controlled so the stoichiometry of this process follows the chemical equations below [18].

$$4NO + 4NH_3 + O_2 \rightarrow 4N_2 + 6H_2O \tag{1.7}$$

$$6NO_2 + 8NH_3 \rightarrow 7N_2 + 12H_2O \tag{1.8}$$

Similarly, when urea is used as the reductant, instead of NH_3, the overall reaction follows Equation 1.9.

$$4NO + 2(NH_2)_2CO + O_2 \rightarrow 4N_2 + 4H_2O + 2CO_2 \tag{1.9}$$

In addition to the complex stoichiometric requirement of SCR, the nature of the catalyst is also vital for the success of the reaction. Similar to Pt three-way catalysts, the catalyst used for the SCR reaction is metal supported on a substrate, encased in a ceramic honeycomb grid. When combined with catalysts that are able to oxidise CO and hydrocarbons, the use of SCR allows for the reduction of NO in the oxidising conditions produced by lean burn diesel engines.

New legislation has introduced tighter regulation of emissions from diesel engines. This has caused SCR based catalytic converters to become a standard within the automobile industry. Therefore, due to the widespread use of SCR, there has been motivation to investigate the mechanism behind the process. In addition to its use in the automobile industry, SCR is also used to clean NO from power generation, especially from the flue gas emitted by boilers [18].

Limitations of SCR

In an ideal world, the SCR reaction would occur with 100% efficiency and convert all NO into N_2. However, there are several side reactions that can also occur, which are shown in Equations 1.10 - 1.12.

$$2SO_2 + O_2 \rightarrow 2SO_3 \tag{1.10}$$

$$SO_3 + 2NH_3 + H_2O \rightarrow (NH_4)_2SO_4 \tag{1.11}$$

$$SO_3 + NH_3 + H_2O \rightarrow NH_4HSO_4 \tag{1.12}$$

SO_2 poisons the reactivity of the catalyst and requires removal via heating or replacing the catalyst [19]. In addition, SO_2 can react with O_2 to form SO_3, which can further react with NH_3 to produce ammonium sulfate salts which can clog the catalyst.

Besides the possible formation of chemical by-products, there exist several other limitations of selective catalytic reduction. First, one of the major issues is the degradation of the catalyst, either through chemical poisoning or particulate build up [20, 21]. Oxidation of the catalyst can also occur, especially in lean burn engines due to their high air:fuel ratio, which can render the catalyst ineffective. This is prevented by precisely controlling the stoichiometry inside the catalytic converter.

Secondly, there is the issue of particulate build up inside the catalytic converter, especially soot which is a significant by-product of diesel engines [22]. Soot is a carbon particulate which is the result of incomplete combustion of hydrocarbons. Due to the porous nature of the catalyst, it becomes easily filled with soot, making it ineffective. The most common method to deal with soot is to use pre-filters, which prevent soot from reaching the catalyst. In addition to soot, ammonium salts (a by-product of the reaction between NH_3 and SO_3, as shown in Equation 1.11 - 1.12) can also clog up the catalytic converter.

Another major issue is NH_3 slip, which is when NH_3 is leaked into the atmosphere instead of being completely used up in the catalytic converter [20]. This could occur due to excess NH_3 being injected into the catalyst, or the catalyst being destroyed by poisoning or from soot. NH_3 slip past the catalytic converter can cause corrosion of car components due to its corrosive nature. It also causes environmental problems because NH_3 is a toxic gas if leaked into the atmosphere. Excess NH_3 injection can be prevented through the use of sensors, and by precisely controlling the dosing of NH_3 into the reaction chamber.

Temperature is also an issue for SCR, as a catalyst will have a minimum working temperature and a narrow temperature margin in which it has maximum efficiency [20, 21]. Often, during the initial start-up phase of a diesel engine or gas turbine, the catalyst will not have had time to heat up to its optimum temperature. Conversely, excess temperature will cause

degradation of the catalyst, either through degrading the metal catalyst directly, or through destroying the zeolite. The optimum working temperature for the SCR reaction is typically in the range of 523 - 700 K. Therefore, precise control over the working temperature of the reaction chamber and catalyst must be exercised.

1.3 Background of NH_3

NH_3 is a very important chemical, which is primarily used in agriculture - in the manufacture of fertilizer. It is also used in industrial processes; such as the such as the creation of explosives or as a cleaning agent. A brief chronological review by Galloway *et al* in 2013 [23] and an extensive encyclopedia by Appl published in 2006 [24] outline the and importance of this chemical. A Lewis structure diagram of NH_3 is shown in Figure 1.4.

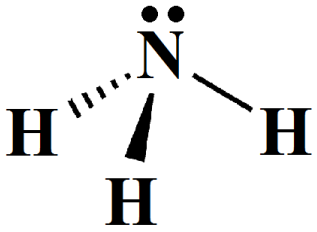

Fig. 1.4 A Lewis structure diagram of the gas phase NH_3 molecule, showing the nitrogen and hydrogen bonds. The bond length between nitrogen and hydrogen is 101.7 pm and the bond angle between the hydrogen atoms is 107.8°

.

The large-scale production of NH_3 became widely available due to the discovery of the Haber–Bosch process in 1909, which led to Fritz Haber winning the Nobel prize in 1920 [25]. Since this discovery, several thousand million tonnes of NH_3 have been produced. As of 2012, more than 140 million tonnes of NH_3 are produced annually (Figure 1.5) [26]. The resulting increase in the availability of NH_3 has allowed it to be used for agricultural and industrial purposes globally.

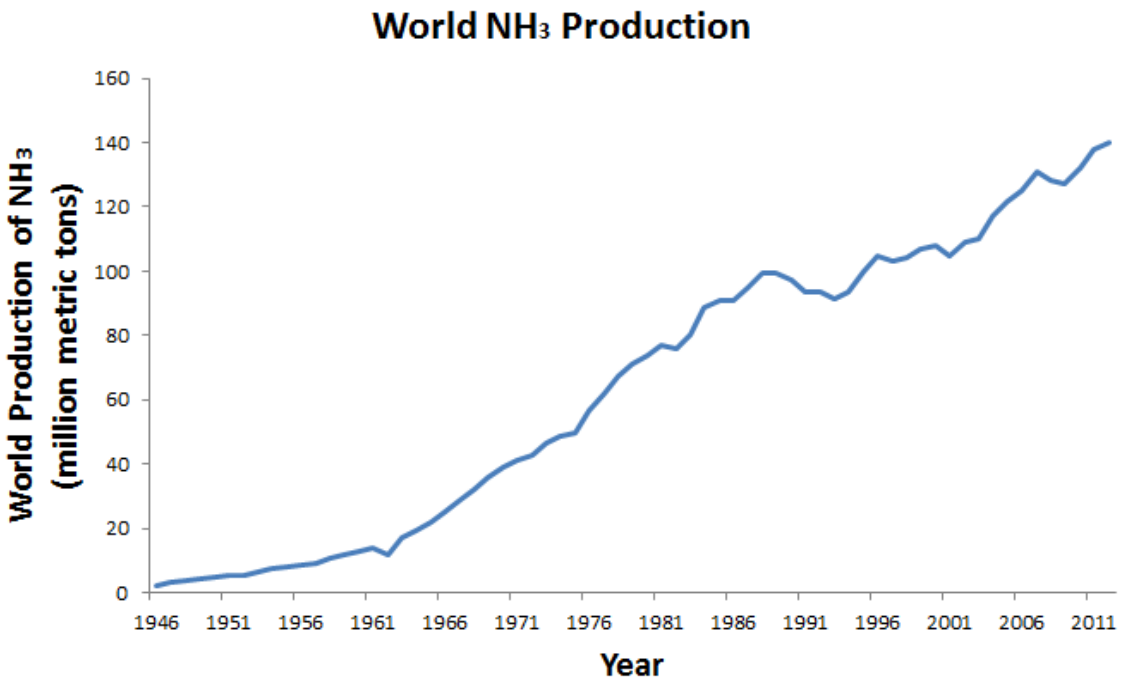

Fig. 1.5 Worldwide annual production of NH_3 [26].

1.4 Overview of this Thesis

Although Pt is one of the most widely used catalysts for catalytic converters, car manufacturers have started to approach base materials to replace it in an effort to cut costs. One of the most promising base materials is Cu, which is both cheap and an active catalyst for both NO reduction and CO oxidation. The aim of this thesis is therefore to study Cu as a catalyst for the SCR reaction.

To gain an understanding of interaction processes involved in Cu based SCR catalysis, the work in this thesis studies the interaction of NO and NH_3 with Cu as well as the effects of oxygen. In order to break down the process, the interactions of NO and NH_3 with a Cu surface were initially studied separately (e.g. through only absorbing NO onto Cu, studying one chemical at a time). Then, expanding this study, the effects of oxygen pre-covered phases of the Cu{311} surface on each interaction were investigated. Once the interaction of NO and NH_3 on Cu is understood separately, the co-adsorption of NO and NH_3 co-adsorption on Cu could then be explored.

The study of these interactions will increase our understanding of the SCR process enabling the development of better catalysts. The approach adopted in this thesis uses surface science methodology, which allows for fundamental processes to be studied.

1.5 Surface Science

Surface science is a discipline that examines the fundamental interactions between molecules and surfaces in order to understand the underlying mechanism for a chemical process. This understanding is achieved by taking a "reductionist" approach to studying a process: breaking it down into its fundamental components. The process is examined under highly controlled conditions by the use of ultra high vacuum conditions, single crystals, and high purity gases.

In practice, surface scientists study chemical processes by introducing gases (referred to as "adsorbates" when they adsorb onto the surface) onto single crystals (referred to as the "substrate"). This process of adsorption is then examined using various techniques such as reflection-absorption infrared spectroscopy (RAIRS) or Low Energy Electron Diffraction (LEED), explored further in Chapter 2. In addition to the process of adsorption, chemical reactions, and desorption may also be studied.

1.5.1 Ultra High Vacuum

One of the core principles of surface science is its extensive use of Ultra High Vacuum (UHV) conditions to study the reaction processes. UHV is used out of necessity to reduce the amount of undesired reactive species or contaminants adsorbing onto a surface. Therefore experiments are performed at 1×10^{-10} - 1×10^{-11} mbar of pressure, to reduce the presence of contaminants thereby diminishing their effects. Equation 1.13 (based on the kinetic theory of gases) highlights this by providing a rate at which gas molecules arrive onto a surface. Where R is the impact rate, m is atomic mass of a gas, P is pressure (in Pascal), T

is temperature, and k_b is the Boltzmann constant.

$$R = \frac{P}{\sqrt{2\pi m k_b T}} \tag{1.13}$$

To illustrate this, consider for example, a 1 cm^2 single crystal exposed to CO. If we use a single crystal with a surface area of 1 cm^2, surface atom density of 10^{15} atoms per cm^2, a pressure of 10^{-5} mbar, and assume that CO has a 100% sticking probability (every molecule that strikes the surface sticks), it would take 35 seconds for the crystal to be covered by a layer of CO. If the pressure is reduced even further to the standard UHV working conditions of 10^{-10} mbar, it would take up to 35,000 seconds or roughly 10 hours. UHV conditions therefore provide enough time to conduct experiments without contaminants affecting results.

In surface science, a unique unit known as "Langmuir" is used to define the exposure of a surface to an amount of adsorbate. One langmuir is 10^{-6} torr per second, which gives exposure. For example, a pressure of 1.0 x 10^{-4} Pa for 30 minutes would give 18,000 L of exposure and 1.0 x 10^{-7} Pa for 30 minutes would give 18 L of exposure. It is worth noting that the definition of Langmuir is independent of the size of the surface.

1.5.2 Single Crystals

Most catalysts used for industrial or automobile application commonly take the form of a composite powder mixture containing a metal catalyst (Cu, Fe, Au, Zn, etc) supported on a substrate such as a zeolite sieve of molecular porosity 5 (ZSM-5) [27]. Instead, surface scientists employ single crystals that are cut with high precision to give them control over the surface structure. A single crystal is a solid with a single continuous lattice structure that has no edges or grain boundaries. It can be cut using diffraction and high precision lasers to reveal well-defined surface structures, for example the surfaces shown in Figure 1.6. When there is no reconstruction or re-arranging of the surface atoms, the surface is referred to as "bulk-terminated".

The interaction of gas molecules with surface atoms is generally quite complex, as the

surface structure plays an important role in chemical processes. Molecules interact differently with the different aspects of the surface such as terraces, vacancies, adatoms, and steps. Due to this intricacy, surface scientists simplify the process by controlling the complexity of the structure of the surface atoms. For example, Figure 1.6 shows a ball model schematic representation for low Miller index face centred cubic single crystals. The Miller indices are a notation used to define the surface plane in terms of the lattice of the single crystal.

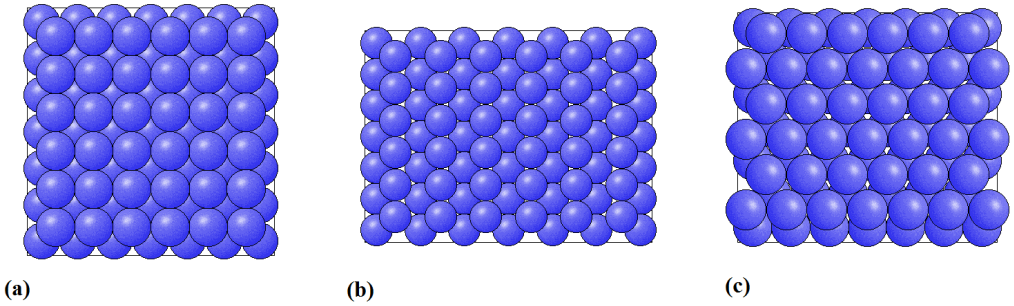

Fig. 1.6 Low Miller Index surface structures of a FCC (a) {100} (b) {110} and (c){111} surface [28].

One of the significant factors that has implications for surface chemistry is the differing coordination numbers (neighboring atoms). In the bulk of a crystal, an atom can have up to 12 neighboring atoms. At the surface of a single crystal, due to the cut - the atoms at the surface usually have a maximum of 9 atomic neighbors (as those above the plane of the surface have been removed). These exposed atoms are less stable than their bulk counterparts, this often leads to effects such as surface relaxation (which causes the distance between the substrate atoms to shrink in order to maximise electron density) or surface reconstruction. The substrate atoms may also bind to gas molecules in order to maximise coordination, which can cause reconstruction and other effects.

In addition, surfaces can also have "defects" on them, such as steps, kinks, vacancies, and adatoms. The atoms near or at these defect sites have a lower coordination number than bulk-terminated surfaces. The reactivity of these defects tends to be much higher than that of highly coordinated surface atoms; consequently, even though they might be a minority structure (having less than 1% prevalence), they may be up to several times more reactive. Thus the presence of defects must be taken into account when studying the reactions at

surfaces.

The surface structure can be altered by the surface itself or can be induced by adsorbates. For example, the Cu{110} surface can have an "added row" reconstruction after the surface has been exposed to oxygen [29]. There are many other factors that can affect the interaction and chemistry of adsorbates with the surface atoms. For example, the exposure of the second (or third row) of substrate atoms to adsorbed molecules can alter the chemistry of the whole surface, as these atoms will have a different coordination number and/or electronic structure than the first row.

Chapter 2

Experimental - Surface Science

2.1 Surface Science

In this chapter, the science behind the experimental techniques used in this thesis, as well as their day-to-day usage will be discussed.

2.1.1 Ultra High Vacuum System

A commonly used apparatus in surface science is an ultra high vacuum (UHV) chamber. This is a stainless steel chamber that maintains a pressure as low as 1×10^{-10} to 1×10^{-11} mbar. The UHV chamber used for this thesis is shown in Figure 2.1 along with a schematic labeling of the important components of the system. The normal operating pressure during experiments (when not dosing gases) was 2×10^{-11} mbar.

The UHV system is divided into three different levels, each containing different components. The top level of the UHV chamber is where the system is connected to a Leybold Turbovac 151 turbomolecular pump, ionization gauge, and gas dosing leak valve. The middle level contains a Physical Electronics sputter ion gun and an Ar leak valve, an Edwards E603 diffusion pump, and a VG Scienta retractable rear view LEED optics. The bottom level is where the Mattson RS1 IR Spectrometer and a Hiden Hal 2 Analytical mass spectrometer is located. Both leak valves are connected to a gas line, which is pumped by an

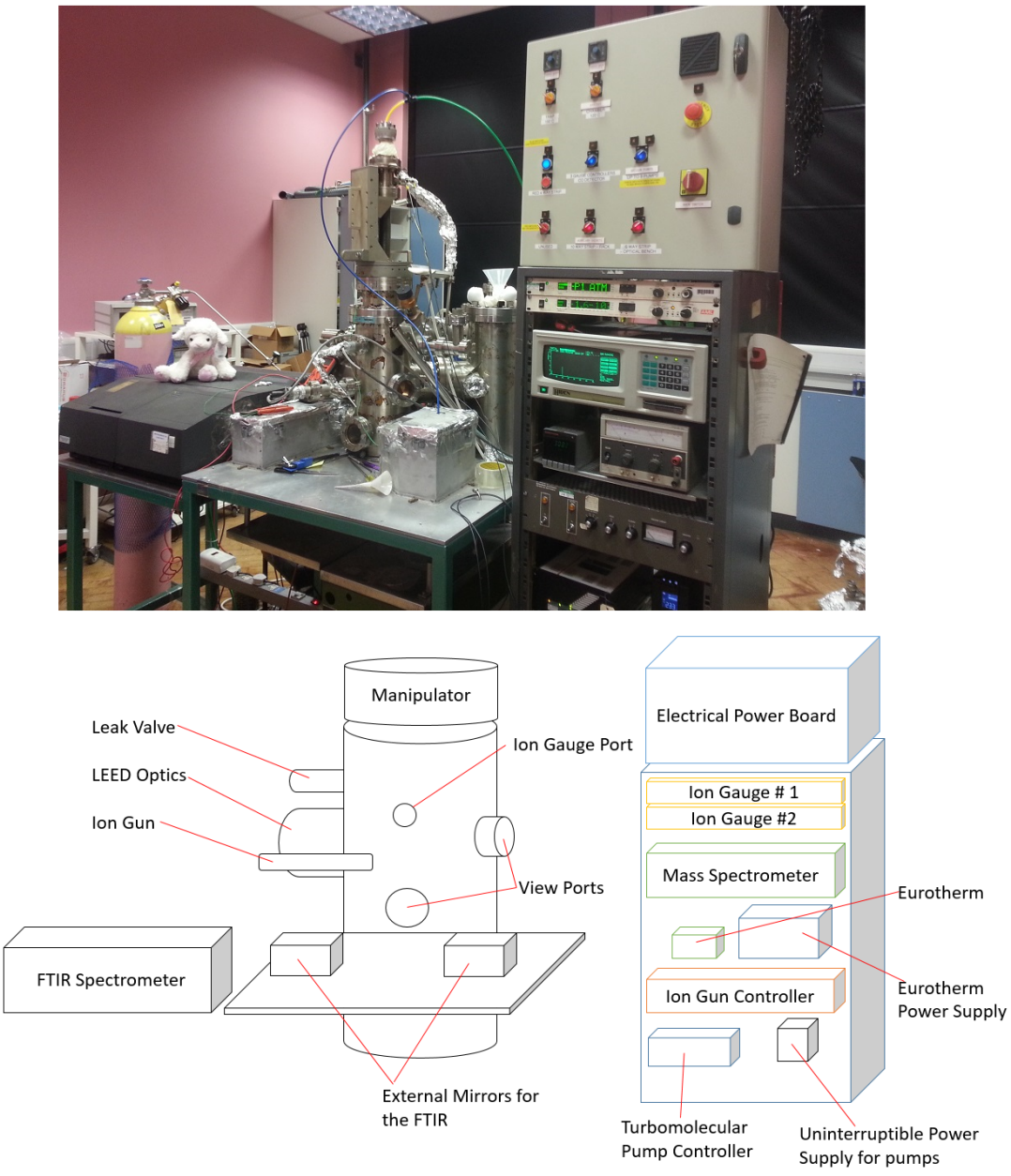

Fig. 2.1 The apparatus used for used for experiments discussed in this thesis. It is comprised of an ultra high vacuum chamber, a Mattson RS1 FTIR Spectrometer, and an electronics rack. A wired schematic is provided detailing the key components of the system from the Eurotherm to LEED optics.

Edwards E02 diffusion pump and backed by an Edwards E2M5 rotary pump. The Cu{311} single crystal is moved between the levels by a manipulator that has movement along the x, y, and z Cartesian axis, along with full 360° rotation around the z axis. Each of the major components will be described in more detail in their respective sections.

The separate UHV components are connected using ConFlat flanges, which are necessary to achieve UHV pressures. At each connection joint there is a ConFlat flange which has multiple outside bolts and an inner knife edge. A joint is made by placing a Cu gasket on the knife edges. The outside bolts are then tightened, which causes the ConFlat's inner knife edge to cut into the Cu gasket, creating a UHV-suitable seal.

2.1.2 Vacuum System

The UHV system is pumped by two separate pumping systems which allows it to achieve pressures in the range of 10^{-11} mbar. The main pump is a Leybold Turbovac 151 turbomolecular pump, which is backed by an Edwards E2M18 rotary pump, that provides a back vacuum of 10^{-2} mbar. The secondary pump is an Edwards E603 diffusion pump, backed by an Edwards E2M12 rotary pump.

When setting up the UHV chamber to conduct experiments, undertaking maintenance of its parts, or changing the crystal used, the entire chamber is often unavoidably exposed to air. The inner chamber wall is therefore exposed to contaminants, the most significant being water from the air.

Once the necessary calibrations, changes, or maintenance is finished, the system is sealed using the ConFlat flange and Cu gaskets, and pumped down using both turbomolecular and diffusion pumps. Pumping for 24 hours is usually sufficient to bring the system's pressure down to the 10^{-8}-10^{-9} mbar range. After pumping down, an additional procedure commonly referred to as "baking out" is conducted to allow the system to reach pressures on the order of 10^{-11} mbar.

One of the major contaminants when exposing the inside of the UHV chamber to air is H_2O. H_2O readily adsorbs to the inner wall of the chamber, and this inhibits the chamber from reaching a pressure that is suitable for surface science experiments. While most con-

taminants can be pumped out either using the turbomolecular and / or the diffusion pump, it is difficult to completely remove H_2O at room temperature. Therefore, a "bake out" procedure must be performed in order to remove H_2O from the inside of the UHV chamber. The procedure involves heating the entire metal chamber to remove gases from the internal walls of the UHV system. The higher temperature provides thermal energy for molecules to desorb from the inner chamber walls; these molecules can then be removed by the pumps.

To cause this process to occur, the UHV system is covered with a fibre glass tent and bake-out heaters are used to heat up the entire stainless steel chamber. Due to temperature limitations imposed by electronic components, bellows, and view ports, the system is heated to 130-135°C. Furthermore, areas near the KBr windows are only heated to 120°C because the KBr windows used in this system have a temperature limit of 130°C. The system is baked out for at least 48 hours to allow for the full removal of contaminants - mainly the H_2O reservoir. During this heating process, the system's pressure rises to 10^{-7} mbar, and then gradually lowers back down into the 10^{-9} - 10^{-10} mbar range. Once the bake out stage is complete, the heaters are turned off and the UHV system is cooled back down to room temperature, where a normal operating pressure in the order of 10^{-11} mbar is achieved.

2.1.3 Pressure Detection

The pressure inside the UHV system is constantly monitored by a hot-filament ionisation gauge, while the gas line and backing pumps are monitored by pirani gauges.

Hot-filament ionization gauges, known simply as "Ion Gauges", are designed to function under low pressures between 10^{-4} and 10^{-11} mbar. Ion gauges are ideal for work under UHV conditions; their pressure sensitivity can be changed to suit different working pressures by simply varying the emission current. Varying the emission current between 0.1 μA, 1 mA, and 10 mA is used to monitor pressures between 10^{-4} and 10^{-6}, 10^{-6} and 10^{-9}, and 10^{-9} and $^{-11}$ mbar, respectively. Ion gauges are not used at pressures above 10^{-4} mbar, as the filaments tend to burn out when exposed to higher pressures.

Ion gauges work by running a current through a tungsten filament - this filament thermionically emits electrons that are attracted to a nearby metal grid which is positively charged

due to a voltage being applied. Once inside the metal grid, the electrons transverse repeatedly in it. If the electron collides with a gas-phase species, ionisation may occur, which positively charges the gas species. Within the metal grid, there is a negatively charged wire. The positively charged ions move towards the negatively charged wire. This wire is earthed through an electrometer, so when an ion impacts it, the change in voltage can be measured. The fluctuation of the voltage is used to estimate the pressure of the system.

Pirani gauges are used to monitor atmospheric and near atmospheric pressures. They have a limited functioning range - their pressure sensitivity drops off when the pressure is 3×10^{-3} mbar - so they are only used for gas line and backing pressure tracking. Pirani gauges work by tracking the resistance change when a heated wire is placed inside a vacuum; the resistance changes depending on the pressure and thermal conductivity of residual gases around it.

2.1.4 Manipulator and Temperature Control System

The single crystal used in the experiments for this thesis was mounted on a custom made manipulator which allows for movement of the crystal in x, y, and z axis and 360° rotation around the z axis. This permits the single crystal to move into positions inside the UHV chamber which enable the undertaking of procedures such as Ar ion sputtering or RAIRS experiments.

The Cu{311} single crystal used in this thesis was mounted to the manipulator using 0.4 mm diameter Ta wires. The Ta wires were placed inside the grooves on the top and bottom edges of the single crystal and secured in place by 0.125 mm diameter Ta wires tied through holes at the corners of the single crystal. This can be seen in Figure 2.2.

The crystal temperature is controlled by an Eurotherm PID controller. The controller monitors the temperature of the single crystal with a "K-Type" thermocouple: the combination of 0.25 mm chromel and alumel wires that are mounted directly onto the crystal. The Eurotherm is able to heat the single crystal by controlling a power supply that passes a current through the two 0.4 mm diameter Ta wires that are attached to the top and bottom of the single crystal; the wires heat up from resistive heating, which then warms the Cu{311}

single crystals to temperatures up to 900 K. In addition, there is a cold finger which can be filled with liquid N_2, which is able to cool the single crystal down to 95 K by conduction. Therefore, by using combination of the resistive heating provided by the manipulating the power supply coupled with the cooling effect of liquid nitrogen, the temperature of the single crystal can be precisely controlled. The Eurotherm is also able to create a linear ramp of the temperature, which allows for temperature programmed desorption (TPD) experiments to be performed.

Fig. 2.2 The single crystal mounted onto the manipulator during the preparatory stage outside the UHV chamber.

2.2 Single Crystals

The single crystal used in these experiments was a MaTecK GmBH Cu{311} single crystal, with a purity of 99.9999%, and dimensions of 15.00 mm $\times$ 10.00 mm $\times$ 1.00 mm. It has grooves running along the long edge (for the attaching of the heating wires) and a 0.5 mm hole (for the attaching of the thermocouple so that temperature can be measured). When the crystal was cut, the crystal orientation was measured to an accuracy of $< 0.1^{\circ}$. The single crystal was polished so that one side of has a roughness of 0.03 micron. The concept of single crystals will be discussed in Section 1.5.2 and the specifics of the Cu{311} are discussed in Chapter 3.

2.3 Reflection-Absorption Infrared Spectroscopy

The main spectroscopic technique used for experiments in this thesis was reflection-absorption infrared spectroscopy (RAIRS). RAIRS is based on the use of infrared (IR) light. When molecules are irradiated with IR light, they will absorb it at the frequencies that match the vibrational mode if that mode is associated with a change in dipole moment [30]. IR based spectroscopy is often used to identify the species of molecules present in samples or solutions; molecules have unique IR vibrational frequencies and lineshapes which allow them to be "fingerprinted".

In surface science, RAIRS is used to study the vibrational modes of adsorbed species on a single crystal [31]. The surface of the crystal is irradiated with a broad spectrum IR light source (600 - 4,000 cm^{-1}), which is reflected off the crystal and into a detector. Vibrational modes that are active absorb the IR light at those frequencies and are attenuated. The resulting spectrum can then be referenced against a spectrum obtained from a clean surface and will indicate the active vibrational modes of molecules present on the surface. The information gathered using this technique can provide information on adsorption sites, configuration, reaction pathways, or active species.

A key component of RAIRS is the angle of incidence at which the IR beam strikes the surface. The angle of incidence is the angle between the incoming IR beam and normal (or z

in Figure 2.3). When light is reflected off a crystal, it can be separated into two portions, the incident (E') and reflected (E") electric field vectors. Each of these vectors can be resolved into two components: which are p-polarised and s-polarised (parallel and perpendicular to the plane of incidence, respectively). This is shown as a schematic in Figure 2.3.

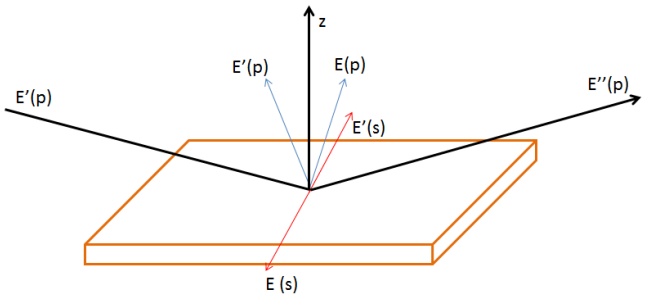

Fig. 2.3 Schematic of the components of the incoming beam, reflected light, and both the p and s polarised light intensities.

The ratio of the reflected intensity to incident intensity follows Equations 2.1 and 2.2 [32, 33]. The ratio is defined as R, where R_s and R_p are the s and p components of the reflection, respectively. While n is the refractive index, k is absorption coefficient, and ϕ is angle of incidence.

$$R_p = (n - sec\phi)^2 + k^2/(n + sec\phi)^2 + k^2 \tag{2.1}$$

$$R_s = (n - cos\phi)^2 + k^2/(n + cos\phi)^2 + k^2 \tag{2.2}$$

On reflection off the surface, both R_s and R_p experience a phase shift (δ). Figure 2.4 shows the change in the reflection coefficient and phase shifts upon reflection at different incidence angles. The schematic illustrates that for the s-polarized component there is a phase shift which causes the cancelation of its electric vector. This is because there is a phase change of nearly 180° upon reflection, independent of the angle of incidence, and since the reflection coefficient of Cu is nearly 1, this makes the s-polarized component effectively zero at the surface. However, as we can see from Figure 2.4, the intensity of the p-polarized component (E_p) is dependent on the angle of incidence.

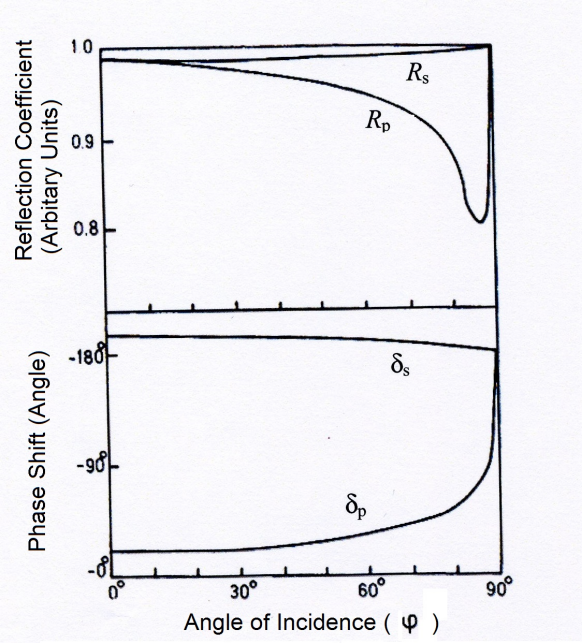

Fig. 2.4 Schematic calculations for the intensity coefficients (R_p and R_s) and phase shift (δ_p and δ_s) for the p and s-polarised light components as a function of angle of incidence(ϕ). (Hayden [34])

In addition, the electric field vector (E_p) of the p-polarised light can be further resolved into a parallel ($E_p^{\parallel}$) and perpendicular ($E_p^{\perp}$) component with respect to the surface. Through symmetry, the ($E_p^{\parallel}$) components are effectively cancelled out. The magnitude of the ($E_p^{\perp}$) component with respect to angle of incidence is summarised in Figure 2.5. The schematic shows that the ($E_p^{\perp}$) is enhanced when the angle approaches 90° (with a maximum at 88°). Therefore, RAIRS is performed at near grazing incidence to increase the intensity of p-polarised light.

Apart from enhancing ($E_p^{\perp}$), another benefit of the use of grazing incident is the increase in the illumination of the surface. Due to the angle, the IR light beam spreads out over a larger area, thereby maximising the amount of surface area that it illuminates. As most experiments conducted in this thesis are in the order of a few monolayers of adsorbates, which have a weak IR signal due to the very low amounts, therefore any additional enhancement of the signal is beneficial.

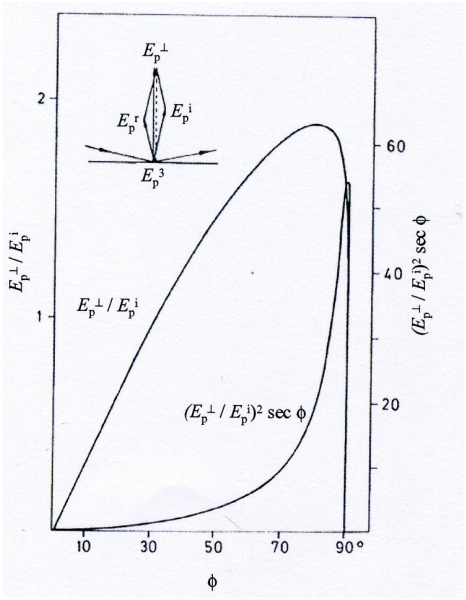

Fig. 2.5 Schematic calculations for magnitude of both the parallel ($E_p^{\parallel}$) and perpendicular ($E_p^{\perp}$) components of (E_p) as a function of the angle of incidence. (Hayden [34])

Selection Rule

It is important to note that only certain vibrational modes are actually RAIRS active; this is commonly referred to as the "selection rule". Vibrational modes of molecules that have a dynamic dipole moment component, that is parallel to the ($E_p^{\perp}$) component are active because they overlap and are constructively enhanced. In contrast, dynamic dipole moments that are perpendicular interfere destructively and cancel out.

In addition to this, the free electrons in the metal will also create an opposite dipole image when an adsorbate with a dipole moment is present on the surface. If the dipole moment is parallel to the surface, the opposite image will cancel out the electric field, whereas a perpendicular image dipole will reinforce the electric field of the adsorbate. Therefore, vibrational modes are only RAIRS active if they contain a non-zero component perpendicular to the surface. By using this rule, via an examination of the presence or absence of vibrational modes (such as symmetric or antisymmetric modes), information regarding the orientation of the adsorbate with respect to the surface can be inferred.

Spectral Interpretation

When a molecule forms a bond with the atoms of a solid surface, its electronic structure is altered. In the simplest form of this alternation of the electronic structure, the vibrational frequency of the bands sshifts due to the extra interactions with the surface of the metal and the reduction in degrees of freedom. Therefore, the vibrational frequencies of a molecule on a surface will be different from its gas phase. Additional information can be gained from analysis of the subtle differences in the spectrum and by using the surface selection rule.

To highlight an example of this, let us consider how the IR frequency can be used to identify the adsorption site of a CO molecule. A simple molecule such as CO binds to the Cu surface directly by the creation of a Cu-CO bond. Electrons from the surface back donate into CO's $2\pi^*$ anti-bonding orbital which causes a shift in the C-O stretching frequency. Theoretically, the larger the electron density, the larger the number of electrons that back donate into CO, which causes a greater shift in frequency. Therefore, the larger the number of Cu atoms that CO is bonded to, the larger the shift of the C-O stretching frequency. This knowledge can be used to infer the adsorption site of CO, whether it be onto an atop site, bridge, 3-fold hollow, or 4-fold hollow site.

Figure 2.6 shows a visual representation of CO adsorption onto a FCC{111} surface, showing it bonded to an atop, bridge, and hollow site. When adsorbing onto an atop site (where bonding only occurs with one substrate atom), there is a minimum shift of the C-O stretching frequency from the gas phase. When CO bonds to an increasing number of Cu atoms, the frequency shift increases. The difference in frequency is compared in Table 2.1 [35]. This difference in frequency allows the molecules' adsorption sites to be determined.

Table 2.1 Compilation of CO stretching frequency onto different adsorption sites [35]

Frequency (cm^{-1})	CO State
2143	Gas
2130-2000	Atop Site
2000-1860	Bridge-Site
1820-1800	Hollow Site

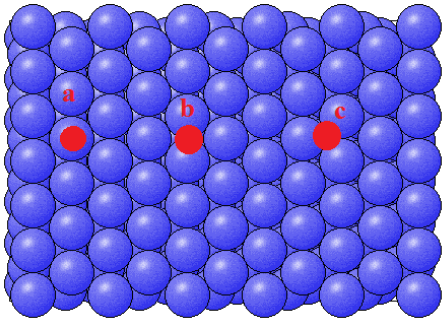

Fig. 2.6 A simple ball model visual representation of the adsorption of CO onto a FCC{111} surface showing the adsorption onto an (a) atop site, (b) bridge-site, and (c) hollow site [28].

In addition to determining adsorption sites, other information can be gathered from analysing a spectrum. For example, the appearance of vibration modes for NH_2 after adsorption of NH_3 onto a Cu surface could indicate the reaction or fragmentation of the NH_3 molecule. For complex molecules such as amino acids, the orientation of the molecule can be determined by analysing the presence or absence of certain vibrational modes to identify which functional groups present.

However, in practice, the intensity of RAIRS peaks is often more complex than can be accounted for by only dipole moments or angle of incidence. Other factors must be taken into account when analysing the spectrum. For example, whilst at low coverage the intensity of the peak is often directly proportional to coverage, at higher coverage, dipole-dipole coupling starts to reduce the dipole moment per molecule. This phenomenon starts to reduce the effects of intensity per molecule as coverage increases, thereby reducing the range of the increase in intensity as coverage increases. Other factors, such as a change in temperature can also affect the broadening of peaks.

In the data analysis, RAIRS peak assignments were made by comparing IR frequencies with similar work in the literature. The frequencies used as a reference are chosen from the combination of IR studies and use of structural surface science techniques (such as LEED or STM).

The spectrometer used for the work in this thesis is a Mattson RS1 FTIR spectrometer. To perform a RAIRS experiment, the single crystal is aligned so that the IR beam is reflected off the surface near grazing incidence. The spectrum is obtained by the averaging of 300

scans at a resolution of 4 cm^{-1}, which allowed a spectrum to be taken once every 2 minutes. The first spectrum is taken as the single crystal is cooled to 400 K subsequently, spectrum are continuously recorded every 2 minutes until the end of the experiment. Depending on the experimental conditions, a spectrum that was recorded before gas exposure is used as a reference for data analysis. Then once, a gas (NO or NH_3) is leaked into the chamber and a RAIR spectrum is taken every 2 minutes. This allows the surface species (and any changes) to be monitored using RAIRS. By varying the pressure, the length of exposure time, type of gas, the effects of coverages, time, and the process of co-adsorption can be studied.

2.4 Secondary Techniques

2.4.1 Ion Sputtering

An Ion gun was used to accelerate Ar ions towards the Cu{311} crystal inside the UHV chamber. When an Ar ion impacts the surface, there is a transfer of energy to the atom or molecule that it collides with. If the the amount of energy transferred is higher than the desorption energy threshold, this impact will cause the atom or molecule to desorb from the surface. Adsorbates or impurities (such as CO, O, or NO) are generally lighter than metal atoms so they readily desorb from the surface after a sputtering cycle. This technique is used to remove impurities from residual adsorption or left-over molecules from previous experiments, before a new experiment is performed. However, a by-product of Ar sputtering is that surface crystalline order is lost due to the removal or displacement of substrate atoms. Order can be regained in the case of Cu by annealing to 900 K in the case of Cu which provides the thermal energy needed for the surface atoms to rearrange themselves into the ideal {311} configuration.

The ion gun used in the UHV system is a Physical Electronics ion sputter gun. The ion gun used in this study is exclusively used for cleaning the single crystal. During the Ar ion sputtering process, Ar (from Messer with a purity of 99.999%) is leaked into the UHV chamber to a pressure of 5×10^{-5} mbar and accelerated onto the surface of the crystal by the ion gun (usually whilst the crystal is at room temperature). The ion gun's emission current

is set to 10-25 mA with a beam voltage of 2.0 kV. The sputtering process is normally run for 25 minutes, making sure that the drain current is constantly monitored using a multi-meter clipped to the crystal's heating wires. The drain current is maintained between 10-15 μA by varying the emission current.

2.4.2 Low Energy Electron Diffraction

Low energy electron diffraction (LEED) is a commonly used method fors determining surface ordering in surface science. The LEED system used for this thesis is a VG Scienta LEED optics attached to a SPECS ErLEED controller. Only the qualitative form of LEED analysis has been used in this thesis, as the quantitative form (LEED IV) is beyond both the necessary work required to study NO adsorption on Cu{311} and the limitations of the control surfaces and sensitivity of the experimental set up.

A LEED image provides information about surface order, which can be used to determine the surface structure and presence of adsorbates. When electron impact a surface, they are diffracted if their de Broglie wavelength matches the atomic spacing of the crystal. If there is no electric or magnetic field, they travel in a straight line, which can be towards the LEED optics screen. As the majority of electrons that come off the surface are inelastically scattered (or are secondary electrons), retarding grids are used to filter them out due to a voltage being applied. The electrons that make it through the grids impact with a phosphorous screen, creating a green image as seen in Figure 2.7. The actual image produced as a result of the electrons colliding with the phosphorous screen is that of the reciprocal lattice of the surface. The spots on the screen of the diffracted pattern correspond to a reciprocal net vector of real space, which can be used to infer the surface order and subsequently the surface structure.

Low energy electrons have a short mean free path length of 5-10 Å which limits their penetration into a crystal to only a few atomic layers. Therefore, in contrast to X-Ray Diffraction (which is a bulk crystal technique), LEED is used to probe surface structure. Realistically the electron beam produced by the LEED optics will not be perfectly collimated, resulting in an upper limit on the order of 100 Å for the surface structure(often

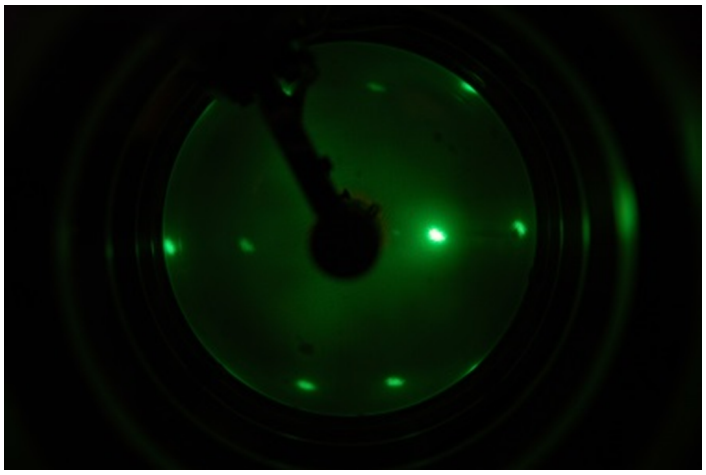

Fig. 2.7 Example photograph of the LEED pattern of the bare Cu{311} surface, taken at 300 K and 50 eV.

referred to as transfer width).

Normally in Surface Science laboratories, Auger Spectroscopy (Section 2.4.3) is used to analyse the cleanliness of surfaces following day-to-day to day cleaning. For this thesis, LEED is used as a proxy for this analysis, following the day-to-day sputtering procedure, by performing a qualitative analysis of surface order. After the cleaning procedure, the single crystal is positioned so that it faces the LEED optics. The single crystal is grounded using the heating wires and a LEED experiment is performed on the surface. Photographs of the LEED image of the surface at 50, 75, 95, 105, 125, and 150 eV are taken using a camera with a 30 second exposure, and kept for reference. This procedure of cleaning and recording the surface order is performed at the start of each experiment.

In addition to being used to verify the cleanliness of the bare Cu{311} surface, LEED is also used to verify the O/Cu{311} phases when they are created before an experiment, as outlined in Chapter 3.

2.4.3 Auger Spectroscopy

Auger Spectroscopy provides information about the elemental composition of a surface (as well as a few atoms under the surface). Figure 2.8 shows the Auger process schematically.

The Auger effect is a process in which an electron in a core level of an atom is ejected

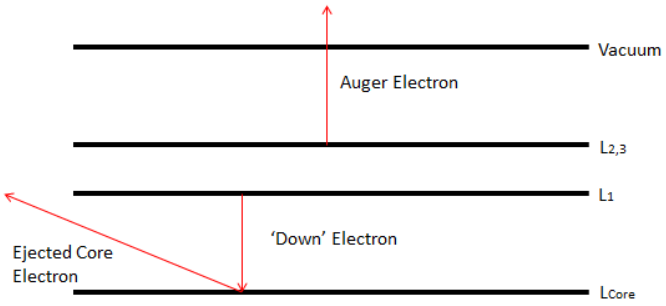

Fig. 2.8 The Auger process. An inner core electron is ejected, which creates an electron hole which is filled by an electron from a higher level. This causes an electron in a higher level to be ejected from the valence level.

from the core (either by incident photon or electron), creating an electron hole. This vacancy is filled by an electron of lower binding energy from the outer shell. The difference in energy between the core vacancy and outer shell electron is then either spent as a photon (via X-ray fluorescence) or the energy is transferred to a third electron that is ejected from the atom. This ejected electron is called the "Auger electron." The energy of the ejected electron follows Equation 2.3, where ϕ is work function and E is energy of the electrons (in the specified state and energy levels).

$$E_{Auger} = E_{Lcore} - E_{L2} - E_{L2,3} - \phi \tag{2.3}$$

The equation shows that the kinetic energy of the Auger electron is independent of the energy of the incident electron and is only affected by the binding energy levels within the atom. This principle allows Auger electrons to be used for elemental identification, as binding energy levels are unique to each element. However, Auger electrons are not the only electrons ejected from an atom after an incident photon or electron has hit it; the vast majority of electrons ejected are inelastically scattered electrons, along with elastically scattered electrons and secondary electrons. In fact, Auger electrons actually only make up a tiny fraction of the electrons that come from the atom. Thus, Auger spectroscopy is performed in derivative mode - the mathematical solution to finding the small Auger electron peaks in a large background of electrons.

The VG LEED optics used in this study can also be used as a retarding field analyzer

(RFA). As electrons are ejected from the sample (including inelastically scattered, secondary, and Auger electrons), they arrive at the LEED optics grids. The RFA works by creating a minimum threshold energy requirement for electrons to pass through. Electrons that pass through the grid collide with the screen, and the resulting current flow into the ground can be measured. This is a high-pass filter system which is able to run an Auger spectroscopy experiment, but have a reduced signal:noise ratio compared to band-pass filter systems on cylindrical mirror or concentric hemispherical analyzers.

In addition to the previously discussed limitations of the high-band pass filter, there is also an additional experimental set-up limitation: LEED optics used in this study is from the manufacturer VG Scienta while the controller is from SPECS. The combination using equipment from two different manufacturers causes the system to have several issues regarding compatibility, which creates problems when performing Auger spectroscopy. Therefore, the Auger spectroscopy used for this thesis was mainly used to determine the relative amounts of impurity on the surface of the single crystal.

An example of an Auger spectra of the clean Cu{311} surface is shown in Figure 2.9 (the spectra was obtained after sputtering the surface with Argon for 120 minutes). There were attempts to maximise the signal:noise ratio along whilst cleaning up the spectra, and the resulting spectra is not too dissimilar to that of previous students who used a similar set-up. In the literature, Cu displays several Auger peaks in the 33 - 110 and 650 - 966 eV regions [36]. The low energy portion of the spectrum exhibits several strong peaks, specifically 31, 66, 96, 132, and 180 eV. The peaks at 31 and 66 eV are likely to be the low kinetic energy peaks for Cu [36]. The other peaks are suspected to be artefacts due to compatibility issues of our set up; they appear in AES spectra regardless of the use of different crystals. The high energy portion of the spectra show several peaks (707, 787, 813, 838, 860, 924, and 940 eV). A few of the peaks are consistent for Cu (mainly 838, 924 and 940 eV peaks [36]). The remaining peaks may be attributed to these peaks that are shifted due to the limitations of our Auger set up. There is noticeably, however, a distinct lack of peaks for carbon (275 eV) and oxygen (510 eV) which suggests a relatively clean surface.

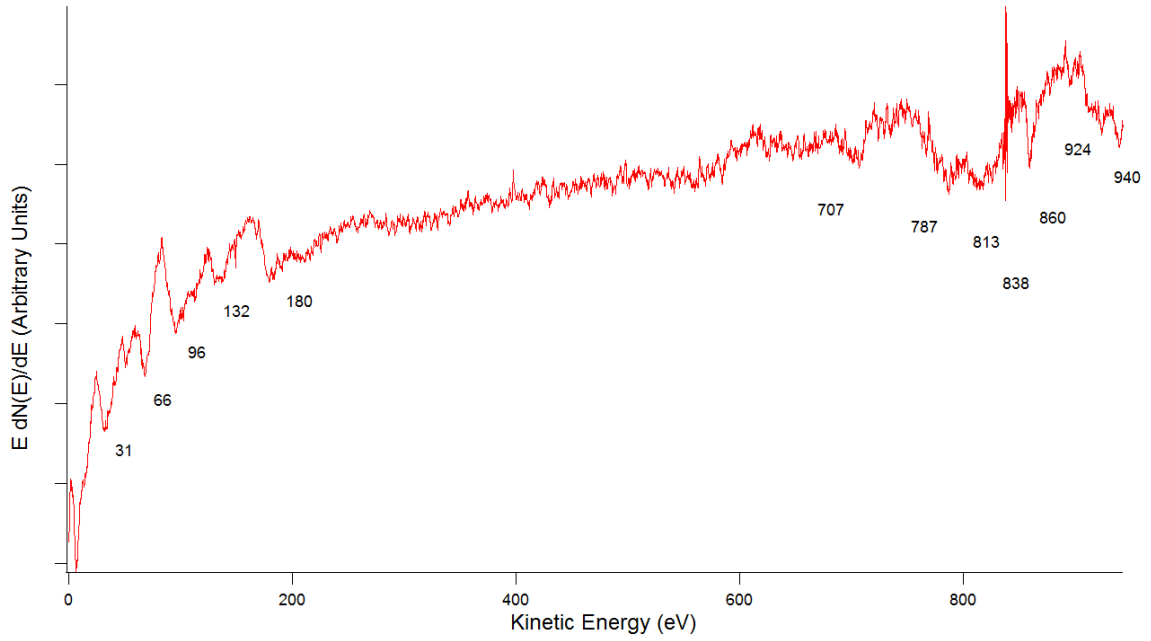

Fig. 2.9 Auger spectrum of the Cu{311} crystal after 120 minutes of cleaning, taken at room temperature.

2.4.4 Mass Spectroscopy

Mass Spectroscopy is a technique that is used to detect the composition of a gas. It can be used both as a qualitative and quantitative tool to investigate the number of molecules present inside the UHV system. The mass spectrometer used in this thesis is a Quadrupole Mass Spectrometer (QMS) - a schematic of the set up is shown in Figure 2.10. The two detectors used in this system are a Faraday Cup and Secondary Electron Multiplier (SEM). In this thesis, the mass spectrometer is used to check for background contaminants, verify the purity of gas molecules, and perform temperature programmed desorption (TPD) experiments.

The mass selection system in a QMS is composed of 4 parallel rods that control the mass of ions that pass into the detector. Gas molecules that have been ionized at the head of the mass spectrometer move towards the QMS rods. A voltage is applied to the rods (controlled by the Hiden Hal 2 Spectrometer) so that only ions of particular mass are able to pass through the entire length of the rod. Ions that are not the right mass will collide with the rods and be pumped out before they reach the detectors. A schematic of this process

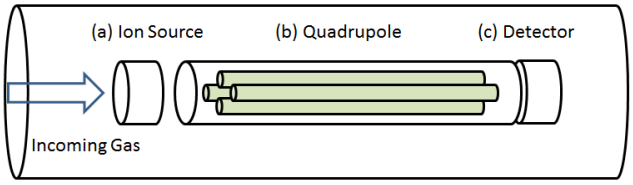

Fig. 2.10 A simplistic schematic of how a Quadrupole Mass Spectrometer functions. (a) shows the ionization source, (b) shows the mass selector (quadrupole), and (c) shows the detector.

is shown in Figure 2.11. Ions that are not rejected by the quadrupole then pass into the detector.

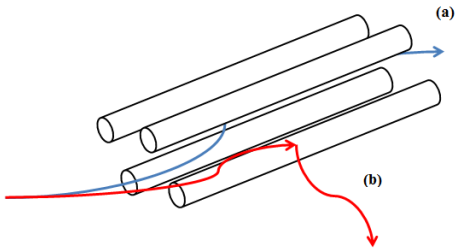

Fig. 2.11 A simplistic schematic (a) example of a molecule traveling through the length of the quadrupole rods and (b) an example of a molecule impacting a rod and being removed.

Once the ion has passed the QMS rods, there are two methods of detection within our mass spectrometer detector. They are called Faraday Cup and Secondary Electron Multiplier (SEM), the prior being used in pressures in the range of 10^{-6} to $^{-9}$ and the latter at 10^{-9} to $^{-11}$ mbar.

Faraday Cups work by using the charge transfer between the charged ion (that came from the QMS) and a metal plate [37]. When an ion collides with the metal plate, the metal becomes slightly charged and the ion returns to a neutral state. The charge from the ion is then discharged and the resulting current can be calibrated to the number of ions impacting the surface. A schematic of this process can be seen in Figure 2.12(a). Faraday cups usually work at higher pressures and are not pressure sensitive in environments below 10^{-8} mbar.

The other detector, the secondary electron multiplier (SEM), is used as a default due to the working pressure of the UHV system in the range of 10^{-11} mbar (Figure 2.12(b)) [38]. SEM works by using the cascading effects of electrons to increase the signal. When an ion

or electron impacts a glass wall which has an electric potential applied, secondary electrons are ejected and the original is reflected off. These electrons then collide with the glass and generate more secondary electrons, creating a cascade [39]. Both the original electron and secondary electrons eventually collide with a metal wire and the number of electrons and ions impacting can be correlated to pressure. The use of a cascade of electrons increases the amount of signal detected, which increases the sensitivity above that achievable by a Faraday Cup.

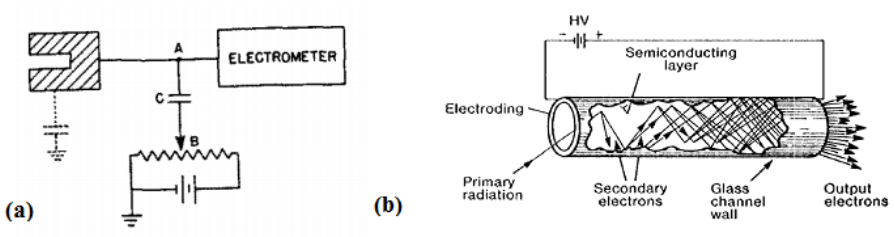

Fig. 2.12 The working concept of (a) Faraday Cup (Brown and Tautfest [37]) and (b) secondary electron multiplier system (Wiza [38]) that is used in this UHV system.

For this thesis, the mass spectrometer has mostly been used to check the amount of contaminants inside the UHV chamber by setting the mass spectrometer to continuously scan between molecular masses in the range of 1 - 70 amu. This is usually done when the system is idling and the pressure is in the order of 10^{-11} mbar. Despite ultra high vacuum conditions, there are residual background gases inside the chamber. The most significant residual gases inside the UHV system used for this thesis are H_2, CO, and CO_2, which have molecular masses of 2, 28, and 44 amu, respectively. By analyzing the composition of the residual gas, information regarding the system can often be inferred. For example, the presence of significant amounts of N_2 and O_2 can indicate a leak in the chamber or the presence of H_2O can indicate that the chamber was inadequately baked. Constant monitoring allows the cleanliness of the inside of the UHV chamber to be checked (to see if there needs to be another round of baking out or if there are any leaks that need to be addressed).

The second main use of the mass spectrometer is for checking the purity of the gas used in experiments. This is always done before Ar sputtering and during the process of dosing chemicals into the chamber to run experiments. This step is undertaken to ensure the quality

of the gas and gas line. Before sputtering, a relatively low amount of Ar (1×10^{-7} mbar) is leaked into the chamber and any significant masses recorded. During NO, O_2, or NH_3 gas dosing, the gas' composition is monitored and recorded as it is leaked into the chamber. If the purity is not within the required limits, the experiment is aborted and either the gas line or gas bottle is changed until a suitable purity is achieved again.

The third use of the mass spectrometer is for temperature programmed desorption (TPD) experiments. TPD experiments allow for information regarding the surface species to be determined; for example, the type of molecule adsorbed and information regarding its binding energy or coverage can be inferred. During a TPD experiment, the Cu{311} crystal is exposed to a pre-determined amount of adsorbate(s) at 100 K; either NO, NH_3, or a mixture of both. The single crystal is then heated at a rate of 0.5 Ks^{-1}. As the single crystal is heated, the partial pressures of significant mass spectrometer fragmentation patterns are monitored using the mass spectrometer. For example, mass 17 and 30 amu (for NH_3 and NO, respectively), were recorded during experiments in Chapter 4, 5, and 6.

One of the significant problems that arose during the course of the PhD was the hard drive failure of the computer that was used to run TPD experiments. This resulted in the loss of customised Hewlett-Packcard Visual Engineering Environment (HP-VEE) software that was used to control the mass spectrometer for TPD experiments. This caused a significant delay of several months due to attempts to recover the hard drive, rewrite the software packages, and out-source the programming. After the failures of these pursuits, TPD experiments were initially scrapped in order to proceed with work on RAIRS. Due to a fortunate discovery several years later, the customised HP-VEE software packages were recovered and TPD experiments were carried out on CO experiments. Unfortunately due to time constraints, TPD experiments were not repeated on NO or NH_3 experiments.

Chapter 3

Cu{311} and Oxides of Cu{311}

3.1 Bare Cu{311}

The single crystal used for this thesis is a Cu{311} single crystal. Figure 3.1(a) shows a ball diagram of the surface, from a top-down view. The surface consists of close packed atoms with {100} and {111} microfacets along the surface in the <01$\bar{1}$> direction as shown in Figure 3.1(a). The unreconstructed surface shows a mirror plane perpendicular to the surface along the <$\bar{2}$33> direction. A LEED pattern of the bare Cu{311} surface is shown in Figure 3.1(b). LEED-IV analysis can show the asymmetry in the surface by examining the difference between the intensities of the spots as a function of voltage. The Cu{311} is structurally very similar to Cu{110} and many comparisons are made throughout this thesis.

3.2 Oxygen Pre-Covered Cu{311} Phases

There is on-going work by members of our group on the oxygen phases of Cu{311} [40–42]. This chapter will give a brief summary of what is known so far, but a more detailed analysis of the phases are in their respective works [40–42].

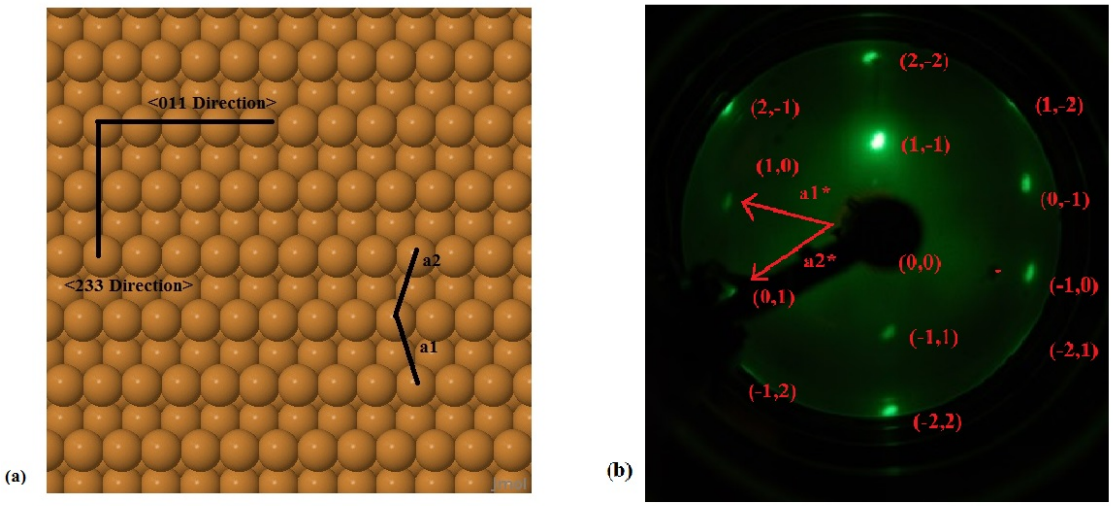

Fig. 3.1 Ball model of the bare unreconstructed Cu{311} surface (a) and the respective LEED pattern (b). The LEED image was produced after sputtering the single crystal with Ar and annealed to 900 K to restore the order. The photograph was taken at 300 K and 50 eV.

3.2.1 O(1×2)/Cu{311}

At a low oxygen exposure onto the bare Cu{311} single, a O(1×2) phase is created. Figure 3.2(a) shows a LEED pattern of this phase taken at 300 K and 50 eV. We would expect the fractional-order sports to indicate a missing row reconstruction, similar to the added row reconstruction on O(2×1)/Cu{110} [43], but this is not all that is seen for the case of O(1×2)/Cu{311}. Upon closer examination of the LEED pattern, there is an additional streaking of spots. These patterns can be attributed to the combination of rectangular and trapezoidal (2×2) unit meshes, as shown in Figure 3.3. Therefore, the resulting LEED pattern of the O(1×2) structure is the combination of the missing row reconstruction of the Cu{311} surface and the rectangular and trapezoidal (2×2) meshes.

STM work [40] done in the group showed that the O(1×2) phase consists of bright linear features running along the <01$\bar{1}$> close packed direction (Figure 3.2(b)). These bright spots have been assigned to Cu-O. Upon closer examination of the STM image, the feature contains a combination of circular and half-moon bright spots. These are inferred to be the unit mesh of the (2×2) oxygen phase, where one of the two structures contain one

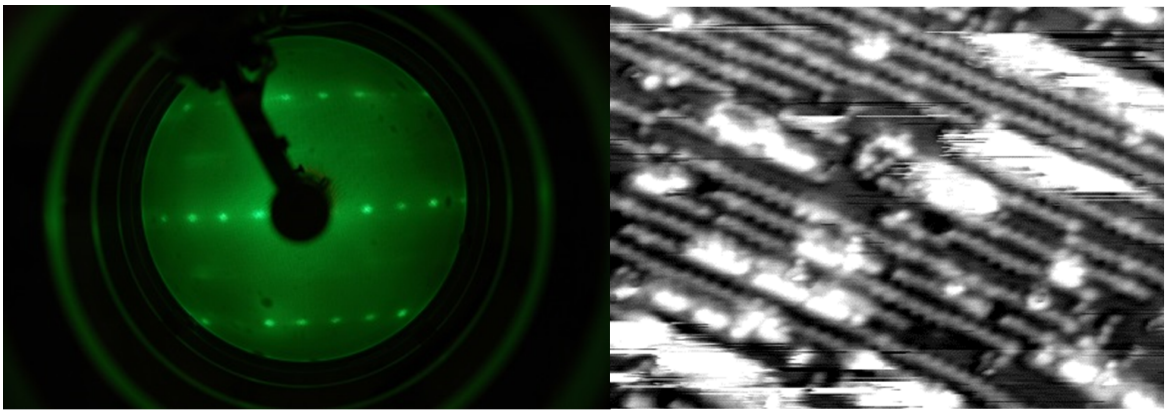

Fig. 3.2 (a) LEED (a) and STM image (Ross [40]) (b) of the "(1×2)" oxygen structure on the Cu{311} single crystal.

oxygen atom and the other contains two. Work undertaken within our group by Hayden [41] using AES suggests that the oxygen coverage of the O(1×2) structure is between 0.45 - 0.52 Monolayers of oxygen.

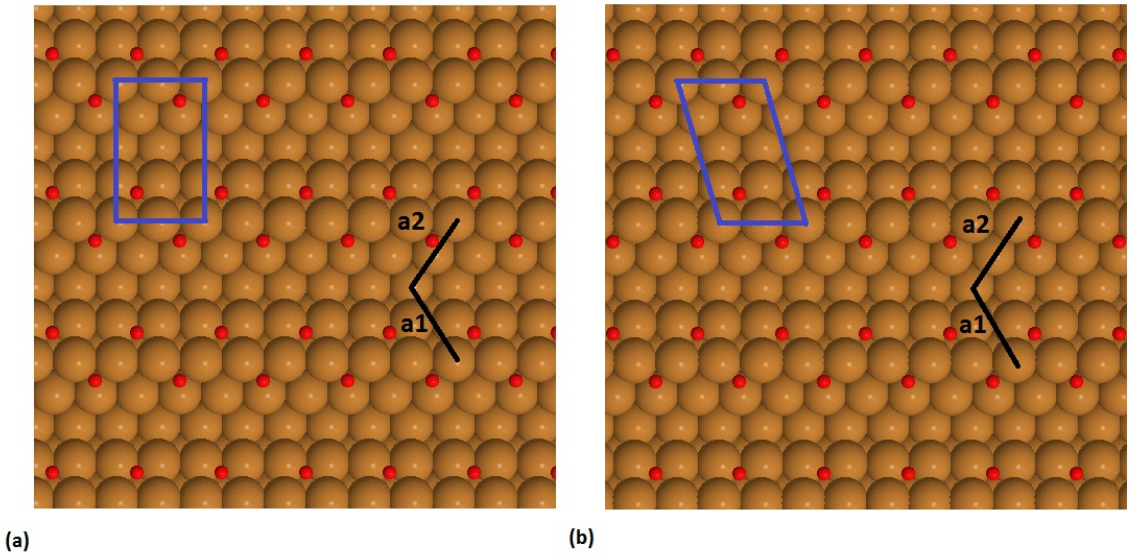

Fig. 3.3 Ball diagram of the (2×2) mesh produced when the O(1×2) LEED pattern is produced on the surface. Note the missing row configuration of the Cu{311} surface. (a) is the rectangular surface and (b) is the trapezoidal (2×2) unit mesh of oxygen adsorbate (Driver [42]).

Therefore, the surface structure of the O(1×2)/Cu{311} phase contains the combination

of a (2×2) oxygen unit mesh (some areas exhibit a 0.25 ML of oxygen coverage with others contain a 0.50 ML oxygen coverage) with a missing row reconstruction of the surface. The procedure used to create the O(1×2)/Cu{311} is to expose the Cu{311} crystal to 3 L of oxygen at 300 K. This is done by leaking 1×10^{-8} mbar of oxygen into the chamber for 6.7 minutes, then flashing the crystal to 750 K for 2 minutes.

3.2.2 O(Runways)/Cu{311}

At medium exposures of oxygen onto the Cu{311} surface, an oxygen phase forms that we have named "runways", shown in Figure 3.4. The runways are structures that extend along the <01$\bar{1}$> direction with a two-fold periodicity and are 20 Å wide along the <$\bar{2}$33> direction, thus looking similar to runways. STM data (Figure 3.4(b)) shows that the runways exhibit mesoscopic ordering. The runways fit between two missing row reconstruction of the Cu{311} surface, almost floating on top of it. The spacing between the runways is usually 20 Å wide, containing defect sites. The most similar structure to the runways is the piano key phase on the O/Cu{110} [44]. The O(Runways)/Cu{311} phase can be described as "more bulk oxide-like"[42]. Work done within our group by Hayden [41] using AES suggest that the oxygen coverage of the O(Runway) structure is between 0.70 - 0.85 Monolayers of oxygen.

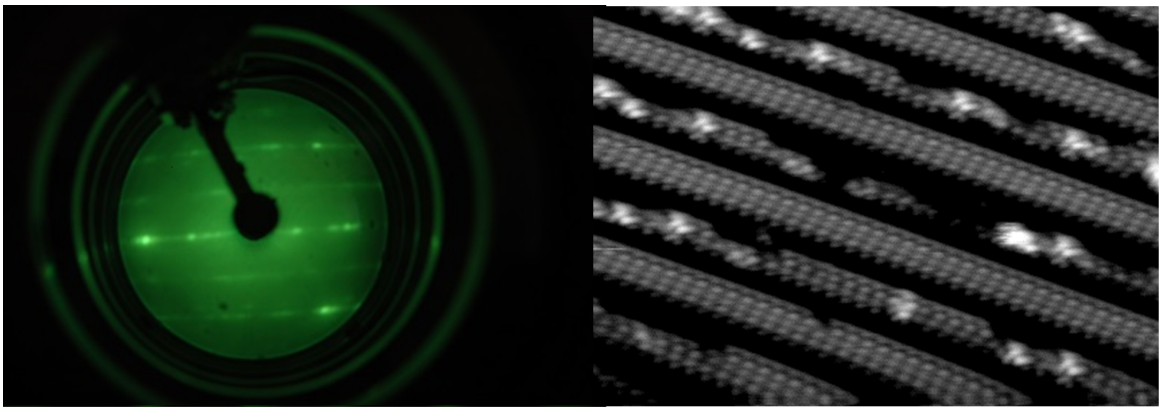

Fig. 3.4 (a) LEED and (b) STM image (Ross [40]) of the "Runways" oxygen structure on the Cu{311} single crystal.

The procedure used to create the O(Runways)/Cu{311} is to expose the Cu{311} crystal to 80 L of oxygen at 300 K. This is done by dosing at 1×10^{-7} mbar for 17.8 minutes, then flashing the crystal to 850 K for 6 seconds.

3.2.3 O(Oxide Clusters)/Cu{311}

At high oxygen coverage, it was found that an oxidic cluster-like structure forms on the surface. STM work done in the group by Ross [40] shows that oxygen forms an oxidic cluster on the surface, with an average diameter of 11 Å $\times$ 13 Å and 2.4 Å high (Figure3.5(b)). The oxide clusters are smaller than the runway structure and exhibit mesoscopic ordering along the <$\bar{2}$33> direction. The structure can be considered as being "oxide-like", due to the high amount of oxygen on the surface. Work done within our group by Hayden [41] using AES suggests that the oxygen coverage of the O(Oxide Cluster) structure is above 0.88 Monolayers of oxygen. The LEED pattern (Figure3.5(a)) is indicative of faceting of the surface, which is in agreement with STM work [40]. The spots generated are a culmination of diffraction of electrons from the clusters on the Cu{311} surface, two facets of the {410} surface, and one from the {210} facet.

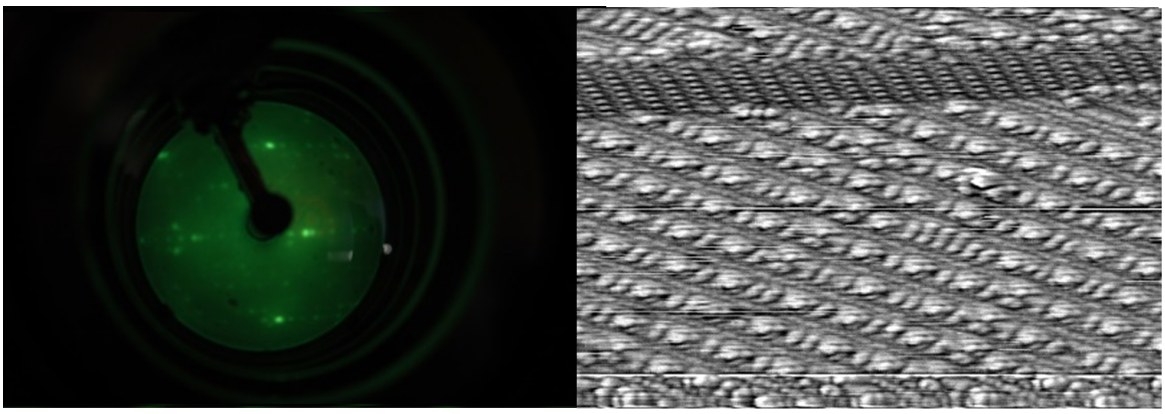

Fig. 3.5 This figure shows the (a) LEED pattern (b) and STM image (Ross [40]) of the Cu{311} crystal after a "Oxide Clusters" oxygen structure procedure is performed on the crystal.

The procedure used to create the O(Oxide Clusters)/Cu{311} is to expose the Cu{311} crystal to 80 L of oxygen, a similar procedure to that used in the creation of runways,

but dosing with the crystal held at 350 K. This is done by leaking oxygen into the chamber at 1×10^{-7} mbar for 17.8 minutes then flashing the crystal to 750 K for 2 minutes. Despite there being the same exposure of oxygen as in the O(Runway) phase, work by Hayden [41] showed that more oxygen adsorbs onto the Cu{311} surface if it is dosed at a higher temperature. Therefore the O(Oxide Clusters) have a higher oxygen coverage than the O(Runways), despite the same oxygen exposure.

3.3 Residual CO Adsorption

One of the major contaminants inside an UHV chamber is carbon monoxide. This is primarily due to degassing from the filaments and outgassing from the metal. Carbon monoxide can impose a restriction on the length of an experiment and can affect the results (as it is a reactive species). Experiments done for this thesis were typically performed for no longer than 30 minutes, whether it be a RAIRS, LEED, or TPD experiment. In addition to this time scale, most experiments were performed at around 100 K. These two conditions are important as CO adsorbs onto the surface of Cu single crystals at temperatures below 200 K with a high sticking coefficient. Therefore it is important to take into account the potential effects of CO on any reaction studied on Cu surfaces. In this chapter, these reactions are examined.

3.3.1 Past CO Adsorption Studies

Before looking at the data from our work, it is worth examining what is already know from existing literature on the subject of CO adsorption onto Cu single crystals. Most studies with CO adsorption on Cu single crystals indicate that CO adsorbs onto the surface at low temperatures. A FT-RAIRS study by Raval *et al* [45] shows large IR peaks assigned to the C-O stretching band as CO is adsorbed onto a Cu{111} surface (Figure 3.6). The figure shows several FT-RAIR spectra associated with the adsorption of CO onto the surface at 95 K at a frequency of 2072 - 2077 cm^{-1}. The spectra show an increase in peak height as CO is dosed onto the surface, starting at 1.22% at 0 L of exposure then increasing to 4.4%

at 0.1 L of exposure, 6.93% at 0.3 L, and 7.5% at 0.45 L of exposure. At face value, the graphs demonstrate that the adsorption of CO onto the Cu{111} is a simple process.

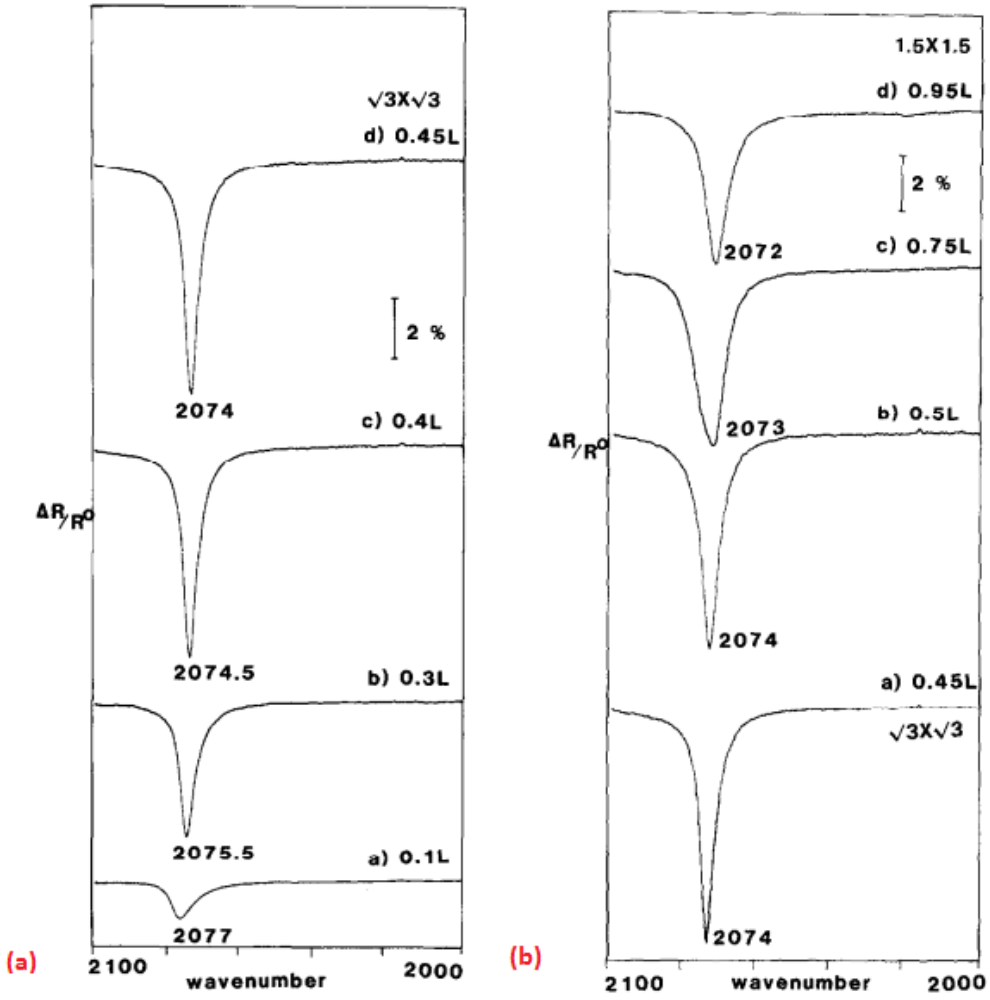

Fig. 3.6 (a) RAIR spectra of CO/Cu{111} at 95 K between 0 - 0.33 ML. (b) RAIR spectra of CO/Cu{111} also at 95 K but with a coverage between 0.33 - 0.44 ML. (Raval *et al* [45])

To understand this process of CO adsorption, it is worth looking at the absolute values of the peak as exposure increases, rather than only at qualitative data. Raval *et al* [45] neatly summarise the behavior of the CO peak by showing a graph that plots peak intensity, full-width half maximum, and $\triangle R/R^0$ against CO exposure (Figure 3.7). The data shows that as the Cu{111} surface is exposed to CO, the $\triangle R/R^0$ value increases until 0.4 L of CO exposure, after which it decreases and plateaus from 0.6 L. The integrated peak intensity

increases up until 0.6 L of CO exposure, after which it decreases.

The behavior of peak $\triangle R/R^0$ and integrated peak intensity is interesting; although the initial increase in the value of the peak can be attributed to CO adsorption onto the surface, we still have to explain the decrease in value after 0.4 L. It is highly unlikely that CO coverage decreases with increased CO exposure, so there must be another reason for the reduction of the CO RAIRS peak size. One simple explanation could be the mutual depolarisation of the CO molecules because of the presence of tightly packed dipoles as CO molecules start to compress into each other. Raval *et al* [45] explain the behavior of CO similarly to Pritchard [46]. They both speculate that the drop in IR peak intensity is due to a tilting of the CO molecule which reduces its vertical component with respect to the surface (making it less RAIRS active due to the selection rule as outlined in Section 3.2). This idea is also supported by the appearance of a frustrated rotational mode of CO in EELS at 293 cm^{-1}. In addition, there is the possibility of adsorption of CO onto different adsorption sites; Raval *et al* [45] have shown evidence for CO on bridge-sites due to a RAIRS peak at 1831 cm^{-1} (although not visible in Figure 3.6, it is shown in their publication [45]).

In addition to RAIRS experiments, Raval *et al* also conducted several LEED experiments and attempted to deduce the surface structure using the combination of both RAIRS and LEED data [45]. Coverage estimates using LEED analysis by the author provides a useful insight into how much CO is on the surface at various CO exposures. At low coverage (0 – 0.33 ML) there is a $(\sqrt{3}\times\sqrt{3})$ R30° LEED pattern, at medium coverage (0.33 – 0.45 ML), a (1.5×1.5)R18° structure forms, and at high coverage (0.45 – 0.52 ML), CO forms a (1.4×1.4) structure. Between the medium and high coverage phases, there are LEED spots for both the (1.5×1.5)R18° and (1.4×1.4) phases until high saturation, where only the (1.4×1.4) structure appears, which suggests that the two phases can exist simultaneously.

When examining the RAIRS and LEED data at the same time, the relationship between RAIRS peak size and coverage can be determined. Raval *et al* [45] note that 0.45 L of CO exposure produced up to 0.33 ML of coverage with 7.9% FT-RAIRS peak intensity, 0.75 L of CO exposure produced 0.44 ML of coverage with 6% FT-RAIRS peak intensity, and

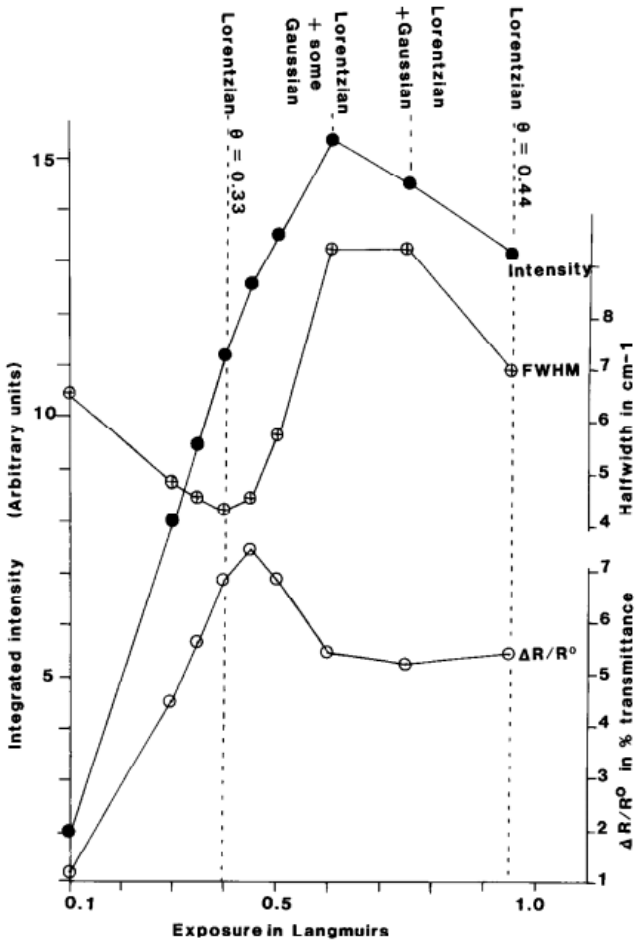

Fig. 3.7 Behavior of the peak assigned to CO by plotting the $\triangle R/R^0$, full-width half maximum, integrated intensity with respect to exposure of CO in Langmuirs. (Raval *et al* [45])

above 2 L of CO exposure produced a maximum of 0.52 ML of CO coverage with 6% FT-RAIRS peak intensity. This shows how at low CO exposure (and subsequently coverage), there is still a large IR peak.

To conclude, work by Raval *et al* indicates that CO initially adsorbs intact upright onto atop sites between 0 – 0.33 ML of CO. Once coverage exceeds 0.33 ML (and is between 0.33 – 0.44 ML), CO molecules may begin to tilt on the surface. This tilting is due to steric repulsion between CO molecules. Once CO coverage exceeds 0.44 ML, bridged species begin to form as shown by the appearance of low frequency CO bands at 1831 cm^{-1} (although not visible in Figure 3.6).

One additional point is the presence of a CO peak even at "0 L" of exposure and the plateauing of the CO peak intensity. The appearance of a RAIRS peak with a 1.22% intensity at "0 L" of CO exposure to the single crystal shows the way in which, background CO persists and inadvertently adsorbs onto the Cu{111} surface in their UHV system, even before their experiment has begun.

Moving on from Cu{111}, of the three main low index surfaces, Cu{110} is most similar to Cu{311} when compared to Cu{100} and Cu{111} in physical and electronic properties, as well as in the arrangement of surface atoms (such as exposure of the second layer of atoms). Horn *et al* [47] performed a coverage estimatation of CO using LEED and surface potential. They show that at medium coverage, CO forms a (2×1) LEED pattern, which corresponds to the adsorption of CO molecules in a simple (2×1) over layer, suggesting a coverage of 0.5 ML. At higher coverage, a c(1.3×2) LEED pattern forms, which would indicate a decrease in distance between each CO molecule along the [100] direction, generating an estimated coverage of 0.7 ML. This is not surprising; there would be compression of the overlayer as more CO molecules adsorb onto the surface, similar to on Cu{111} [45]. This work by Horn *et al* [47] is used by Hollins *et al* [48] to correlate RAIR spectra analysis with CO coverage. Hollins *et al* reported high frequency peaks between 2090 - 2106 cm^{-1}, showing RAIR behavior similar to the Cu{111} surface [45].

Papp and Pritchard [49] in 1975 studied the adsorption of CO onto a Cu{311} single crystal in work that directly relates to our own. Their LEED patterns show extra spots (albeit

streaky) along the [100] direction, which indicate some ordering along the [011] direction, although with limited long range order in real space. They speculated that the CO molecules adsorb into the troughs along the {311} plane with a spacing of 3.81 Å and a coverage of θ = 0.75 ML at the point of maximum surface potential change (Figure 3.8). They proposed that the CO molecules adsorb onto the second layer (trough) with a random mixture of both an atop-like and a bridge-site (due to streaky spots). EELS data indicate two CO species, which could be explained by these two CO configurations. There is no evidence for an extra layer or two-dimensional structures. At the closest packing, the molecule spacing is reported as 3.2 Å, indicating a saturation coverage of 0.9 ML. It is necessary to point out that despite the structure proposed by Papp and Prichard, a similar LEED pattern would also be produced if the CO molecules were on the ridges of the Cu{311} surface, instead of in the troughs.

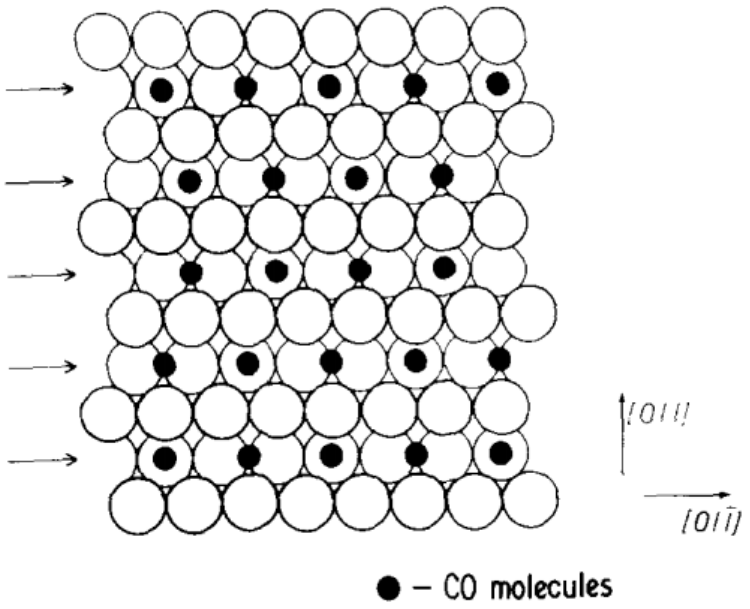

Fig. 3.8 The deduced model for CO adsorption on a Cu{311} surface by Papp and Pritchard based on LEED patterns during CO adsorption onto the surface. This model would have a coverage of θ = 0.75 ML relative to the {311} unit cell. The arrows indicated where compression would occur upon further CO exposure. (Papp and Pritchard [49])

Concerning the work in this thesis, the most relevant point made by these studies is the the maximum coverage attained by CO is at 0.7 ML even with several Langmuirs of CO

exposure (estimating using work on Cu{110} [47]). It is worth mentioning however that the coverage and exposure seems to look like a typical Langmuir isotherm: at low coverages, the growth of coverage parallels exposure; but at higher coverages, more exposure is required to increase the coverage by the same amount.

3.3.2 Experimental

This chapter will look at how CO experiments were performed under similar conditions in order to track the effects of CO in the later NO and NH_3 experiments. In addition, this chapter also provides information about the chemistry of CO adsorption onto the Cu{311} surface.

Before a typical experiment, the single crystal is prepared (either by Ar ion sputtering only or with oxygen pre-covered dosing) and the crystal is aligned with the IR beam from the RAIR spectrometer. The single crystal is then cooled by filling the cold finger inside the manipulator with liquid nitrogen, this will cool the single crystal via conduction. After this preparatory step, the single crystal is annealed to 900 K to desorb contaminants, mainly CO. As the single crystal is then left to cool back down to the experimental temperature (often 100 K), there is inadvertent adsorption of background CO onto the crystal surface. Therefore, these conditions are recreated for the purposes of these CO experiments.

3.3.3 CO/Cu{311} Results

RAIRS Studies of CO/Cu{311}

The first experiment was performed using the RAIR spectrometer to observe contaminants that adsorb onto the Cu{311} surface during the cooling phase. Figure 3.9(a) shows several RAIR spectrum of the surface as the Cu{311} single crystal is cooled from 310 to 100 K, with increasing time from top to bottom spectra as the temperature of the single crystal lowers (after the standard cleaning preparation stage). The figure shows a peak at 2089 cm^{-1} forming when the temperature of the single crystal reaches below 250 K. This peak is assigned to the C-O stretching frequency [47, 48, 50, 51]. Figure 3.9(b) shows an

analysis of the peak area and peak height of the peak at 2089 cm^{-1} by plotting them against temperature.

Figure 3.9(b) shows the increase in both peak area and peak height as the single crystal is cooled towards 100 K during the background CO exposure experiment. Both measurements only begin to rise from 0 after the single crystal has cooled past 250 K, which is expected considering the desorption temperature of CO from Cu single crystals. When the temperature is lower than 250 K, the increase in peak size seems to be relatively linear with respect to cooling and time. This information and buildup of this RAIRS peak during the cooling phase of the single crystal shows the inadvertent adsorption of CO onto the surface despite the ultra-high vacuum conditions. The frequency of the peak is similar to work on other surfaces, with the frequency suggesting that CO is adsorbing onto an atop site.

In addition to the RAIR spectra gathered during the cooling phase of the single crystal, an experiment was performed where the single crystal was left at 100 K while the spectrometer was kept running, shown in Figure 3.10. The intention was to examine what would further adsorb onto the single crystal during a typical experimental run time. Figure 3.10(a) shows RAIR spectra, taken every 12 minutes as the single crystal is held at 100 K for up to 72 minutes. The figure shows a peak at 2089 cm^{-1} which simultaneously grows in size and blue-shifts towards 2118 cm^{-1} as exposure time passes.

Figure 3.10(b) shows both the peak area and height of this peak plotted against exposure time. It is worth noting that Figure 3.10(b) has more data points than that shown in Figure 3.10(a) in an attempt to make Figure 3.10(a) easier to understand (showing one spectra of every 12 minutes instead of every 3 minutes). The figure shows the peak area increasing at a linear rate as exposure time is increased. However, the peak height shows almost no peak growth until 40 minutes of background exposure (which correlates to 1.5 L of exposure), but after which there is a similar growth to the peak area. A key point is the lack of any signs of plateauing, suggesting that it is far from saturation point. This is in contrast to Raval et al's CO studies [45], which shows saturation at very low CO exposures as shown in Figure 3.7. Due to the breaking down of equipment, there were no deliberate CO adsorption experiments so it is difficult to compare the two directly.

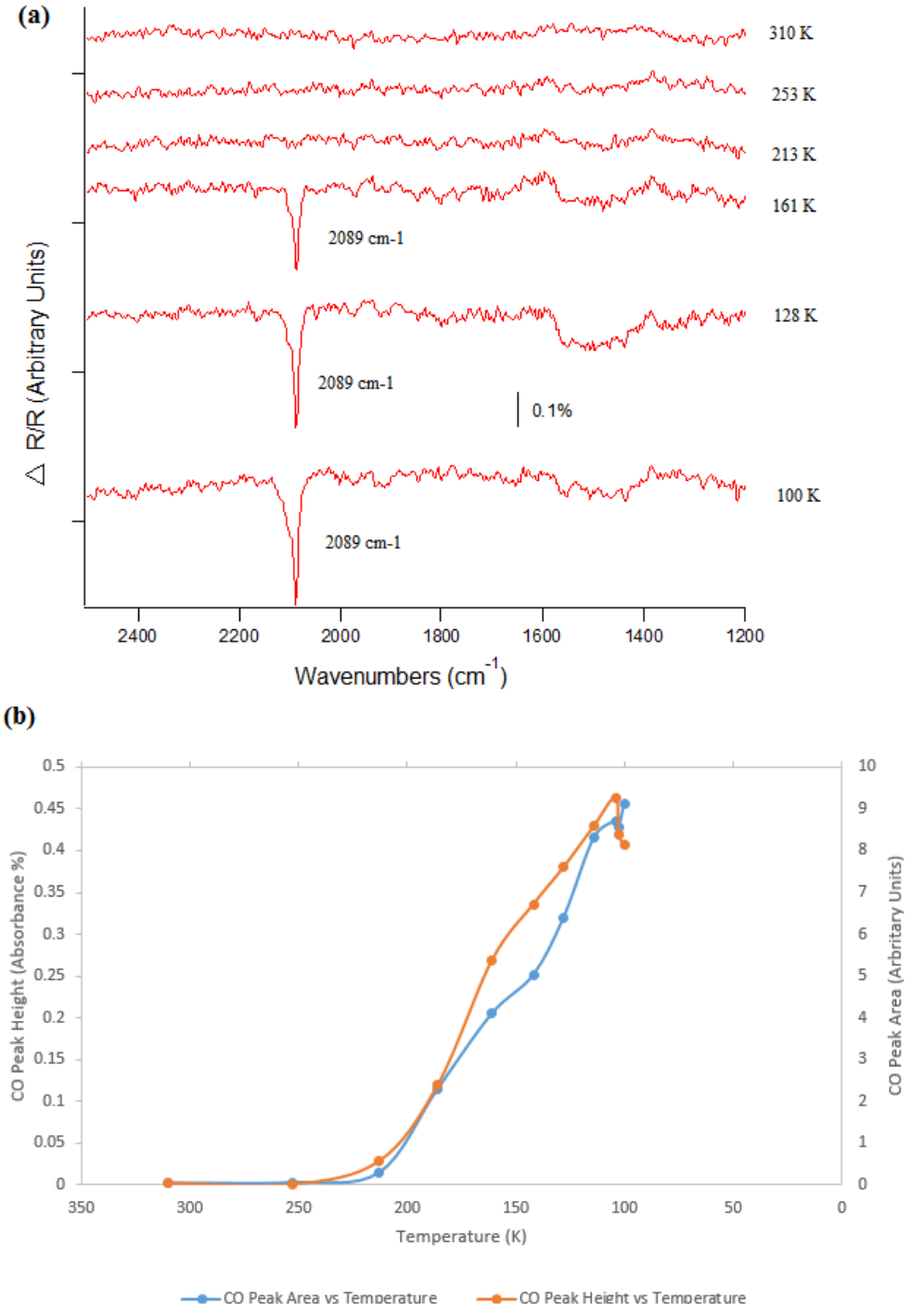

Fig. 3.9 (a) shows the RAIR spectra collected as the Cu{311} single crystal is cooled down to 100 K, with a few spectra omitted to increase clarity of the spectrum. (b) shows a compilation of the peak intensity and peak area of the 2089 cm^{-1} peak plotted against temperature, with one data point every 3 minutes.

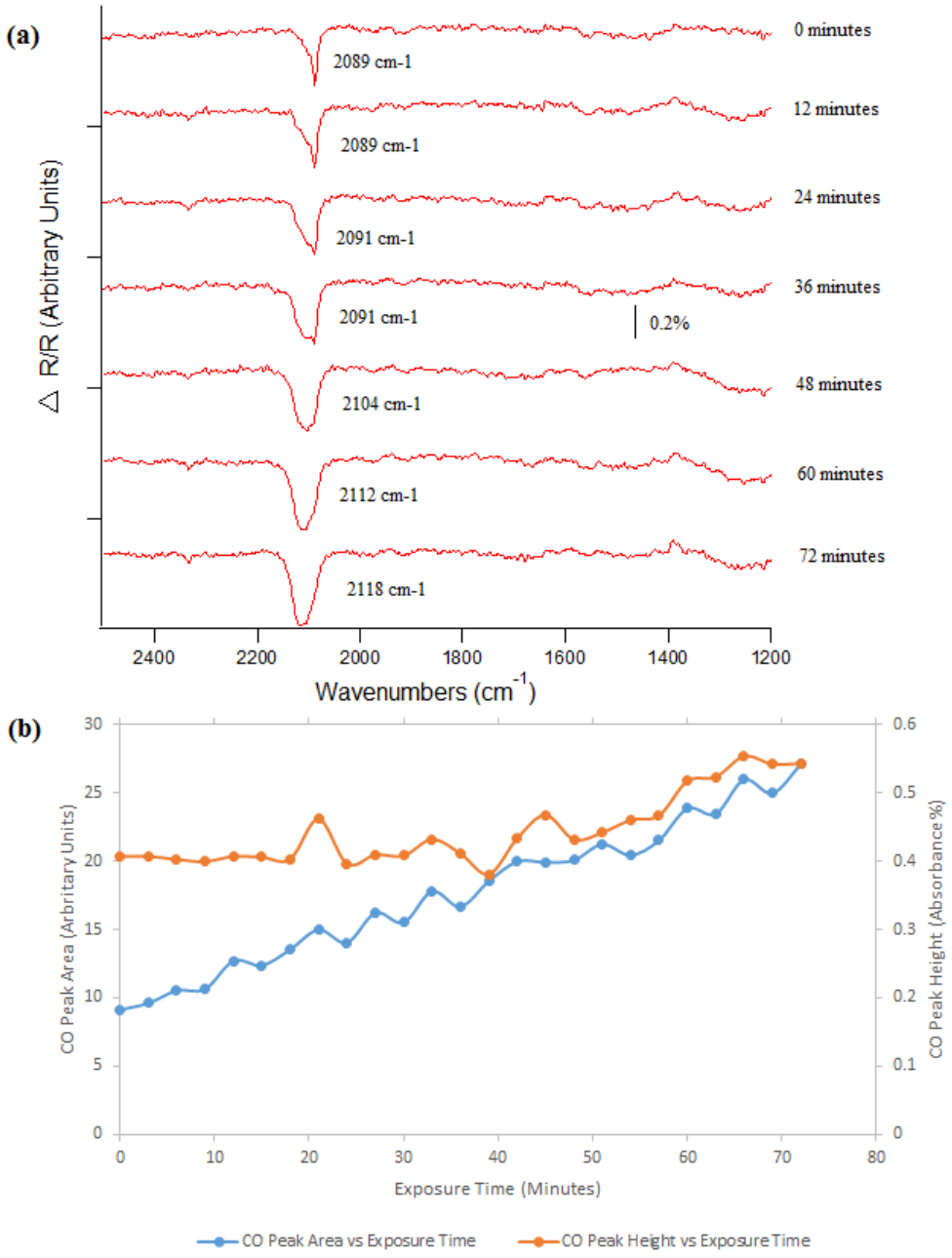

Fig. 3.10 (a) shows the RAIR spectra collected as the Cu{311} single crystal is held at 100 K, collected once every 12 minutes with the resolution at 4 cm^{-1}. (b) shows a compilation of the peak intensity and area of the CO peak plotted against time.

As time and exposure increases, the CO peak shifts in frequency from 2089 to 2118 cm^{-1}, shown in Figure 3.11. It is worth noting that the largest frequency change occurs at roughly the same time as the peak height starts to increase. When CO adsorbs onto the surface, there is dipole-dipole repulsion as coverage increases which causes the shift in frequency. This dipole-dipole repulsion weakens the bond to the surface, causing the molecule to reverse its red shift relative to low coverage, shifting towards the gaseous CO frequency (which is 2143 cm^{-1} [35]).

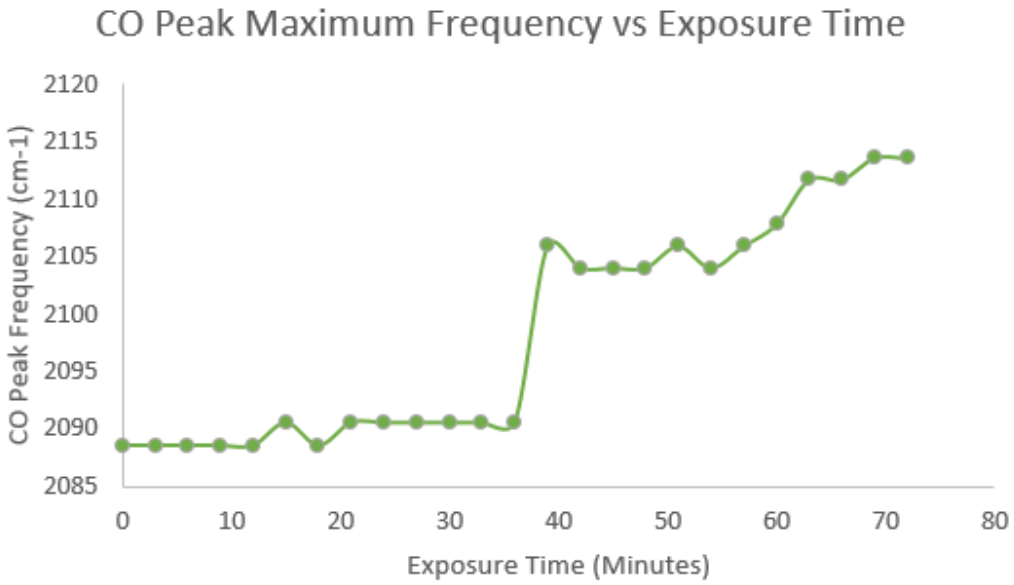

Fig. 3.11 This shows the change in frequency of the CO peak from Figure 3.10. The graph plots the frequency at the peak's maximum against exposure time.

An experiment was performed to compare background CO adsorption onto a bare Cu{311} with one with pre-dosed oxygen, in this case the O(1×2)/Cu{311} surface. Figure 3.12 shows the RAIRS comparison for this experiment. The figure shows a spectrum for the adsorption of 0.2 L of background gases (mainly CO) onto bare Cu{311} and O(1×2)/ Cu{311} surface. It shows a peak at 2089 cm^{-1} and 2129 cm^{-1}, respectively. Both of these peaks are assigned to CO adsorption onto the surface, in keeping with previous experiments and work in the literature. The CO peak on the O(1×2)/Cu{311} surface is shifted probably due to oxygen which withdraws electrons from the surface, reducing the back donation to CO [51, 52]. This destabilises the CO on the surface, causing the CO-Cu bond to weaken

but the C-O bond to strengthen and blue-shift back to towards the gas-phase frequency.

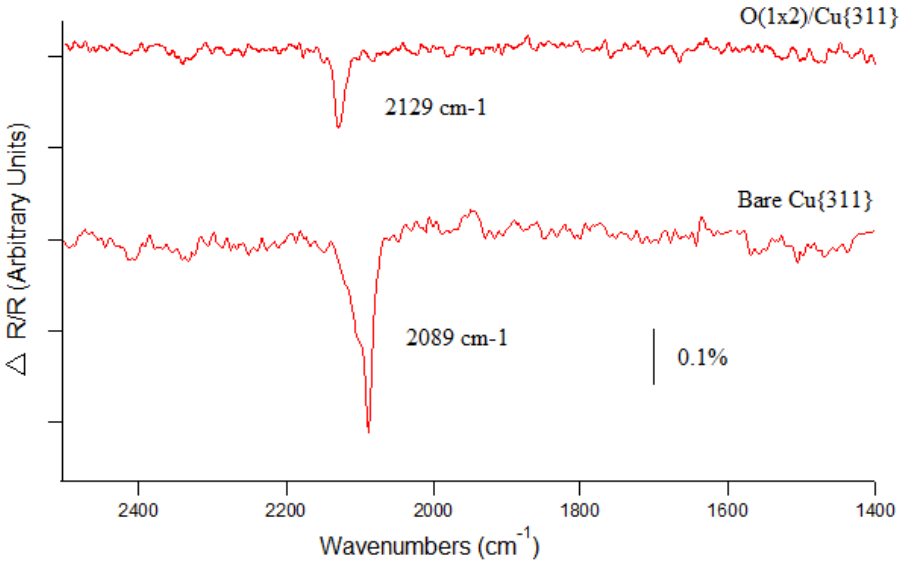

Fig. 3.12 RAIR spectra comparing the adsorption of 0.2 L of residual gas onto the bare Cu{311} and O(1×2)/Cu{311} surface at 100 K.

The combination of both smaller peak height and area along with the blue-shifting of the C-O stretching frequency back towards gaseous CO, suggests that there is reduced CO adsorption when there is oxygen pre-dosed onto the Cu{311} surface.

3.3.4 TPD Studies of CO/Cu{311}

For the TPD experiments, similarly to the RAIRS experiments, the Cu{311} single crystal was cleaned using Ar ion sputtering. The crystal was then cooled to 100 K, flashed to 900 K to remove contaminants, and re-cooled back to 100 K. Once at 100 K, CO was then leaked into the chamber via leak valves to expose the surface to varying amounts of CO exposures (from 0.1 – 20 Langmuirs). In addition to these, a few experiments were also performed where the single crystal was left to adsorb background gases (e.g. no gases were deliberately leaked into the chamber), similar to some of the RAIRS experiments.

Figure 3.13 shows a compilation of several graphs of the desorption of 28 m/z from the Cu{311} surface after various exposures of CO. There is a major desorption peak between

170 - 206 K attributed to the desorption of the CO monolayer. There is also a low temperature desorption peak at roughly 128 K, attributed to the multilayer CO desorption. Although this is not the most useful graph, it allows a side-by-side comparison of the data. An easier analysis can be performed after comparing the peak areas and maximum peak temperatures with respect to coverage in Figure 3.14.

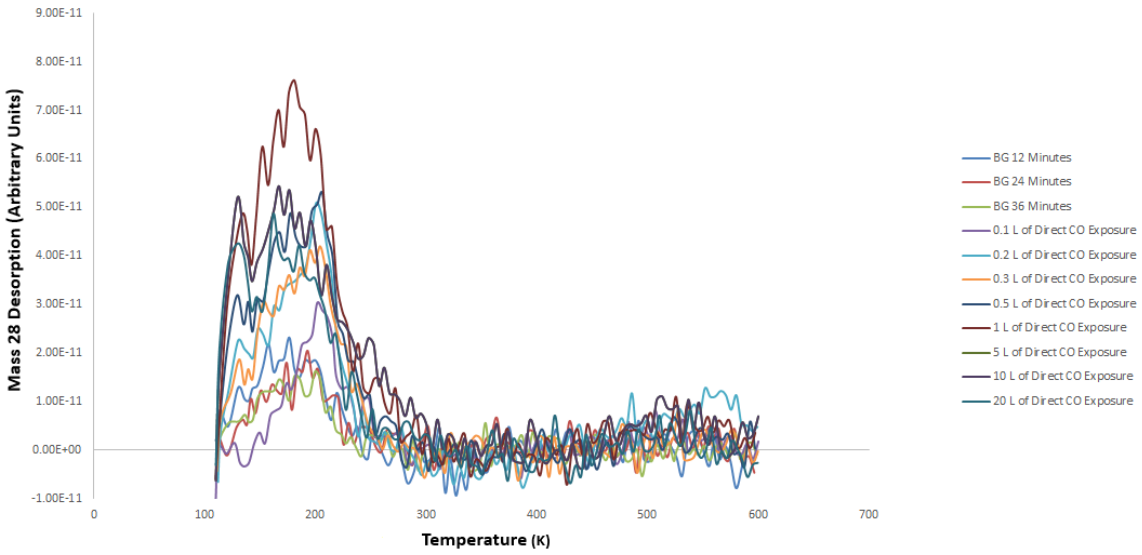

Fig. 3.13 TPD spectra for different CO exposures onto the bare Cu{311} surface. Various CO exposures used for deliberate CO exposure and background CO exposure experiments. In addition to these direct exposure experiments, the graph also shows spectra labelled as "BG12 Minutes", "BG24 Minutes", and "BG36 Minutes". These corresponds to experiments where the single crystal was left at 100 K for 12, 24, and 36 minutes to monitor background adsorption.

Figure 3.14 shows the data from Figure 3.13, with the peak area for the desorption of mass 28 from Cu{311} plotted against CO exposure. The graph shows how the peak area rapidly rises with respect to CO exposure until 5 L of CO exposure, after which it plateaus. The initial rise is to be expected as it corresponds with the amount of CO exposure. The peak area most likely pleateaus due to saturation of the amount of CO on the surface. This is in keeping with previous work which shows that a saturation coverage on various Cu surfaces is reached at similar CO exposures. It is thus shown that it only takes a small amount of CO to reach saturation coverage, but that, after this, the amount of CO on the surface does not increase much with respect to CO exposure, typical of a Langmuir isotherm.

Figure 3.14 also includes the TPD peak areas during background CO exposure, shown by the red data points. These correspond to experiments where the single crystal was left at 100 K for 12, 24, and 36 minutes. The peaks for the background exposure are noticeably smaller than the any of the peaks with deliberate CO exposures, despite a similar amount of CO exposure time and dosage. This discrepancy will be discussed later.

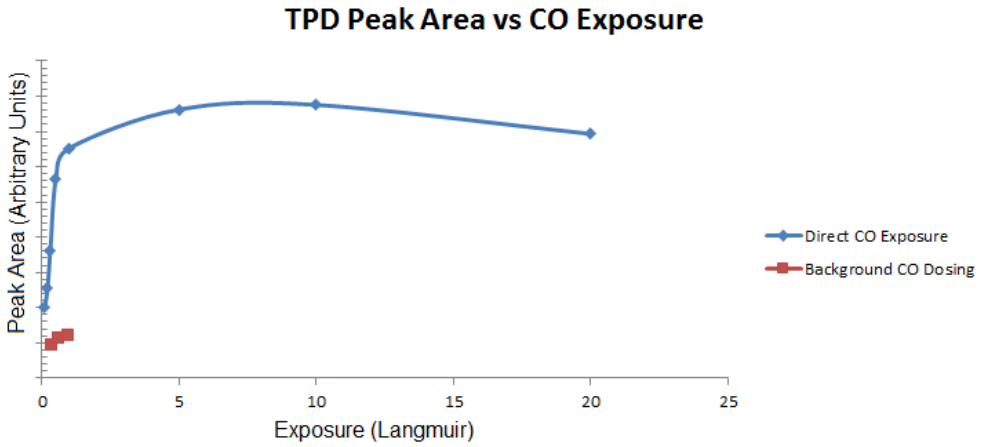

Fig. 3.14 Peak areas of the various TPD spectra from Figure 3.13 plotted against exposure. The blue points are for deliberate CO exposure with the line included to guide the eye. The three red points correspond to background CO exposure.

In addition to the peak area vs exposure analysis, it can also be useful to compare the temperatures of the TPD peak maxima. This is shown in Figure 3.15, where the temperature at which the TPD peak reaches a maximum is plotted against CO exposure (excluding background exposure experiments). The graph shows how the temperature at which the peak reaches its maxima lowers as CO exposure is increased, although the effect is less prominent after 5 L of exposure. At very low exposures of CO (0.1 – 0.3 L), the peak maximum is around 206 K, and drops to 176 K at 0.5 L, but then does not go much below 170 K from 5 L of CO exposure onwards. The drop in peak maximum temperature is most likely due to CO compacting on the surface because of the formation of the monolayer, causing steric repulsion between the CO molecules, which reduces its bond with the Cu surface. The noticeable drop in temperature (20 K) from 0.3 – 0.5 L should indicate that saturation is reached quickly. There is some evidence for a multi-layer forming at 10 and 20 L of

exposure with the extra peak at 128 K.

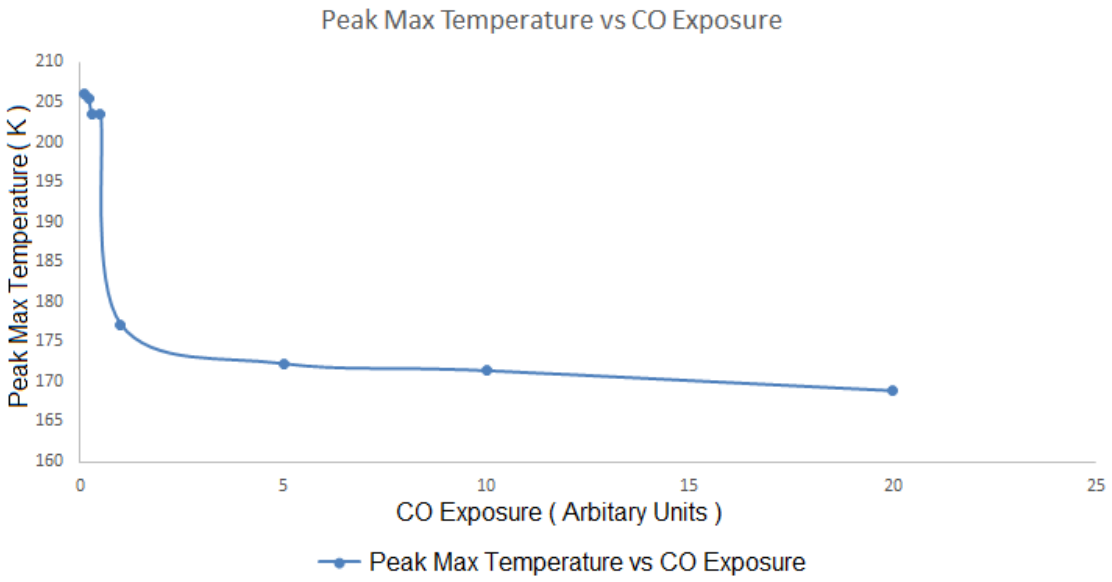

Fig. 3.15 shows a graph that plots the temperature at which there is a peak maxima for various CO exposures to the Cu{311} single crystal plotted against CO exposure.

It is worth mentioning that the peak temperature for (all three) background exposure of CO is 203 K, which is similar to 0.1 – 0.3 L of CO exposure. This suggests that background exposure of up to 36 minutes is far from CO saturation and is similar to 0.1 L of CO exposure.

3.3.5 Discussion

When examining the TPD spectrum, the data suggests that the amount of CO adsorbed during background exposure is far from saturation point and therefore a low amount. Figure 3.14 shows that the TPD peak area of the background CO exposure is roughly 11% of the TPD peak area at saturation. Hollins *et al* [53] estimate that saturation coverage on the Cu{110} surface is 0.77 ML of CO, based on the c(1.3×2) LEED pattern). If purely based only on this data, the CO coverage would be roughly 0.07 ML.

However, the size difference of the unit cell must be taken into account; the Cu{311} unit cell is larger than that of Cu{110}. The unit cell areas of the Cu{311} and Cu{110}

surfaces can be found by examining Jenkins and Pratt's [54] work. It is found that the unit cell of the Cu{311} surface is 1.172 times larger than the Cu{110} surface. Thus, if we assume the same density of CO molecules, there should be more CO molecules inside the Cu{311} unit cell. Using the unit cell area correction from Jenkins and Pratt [54], the saturation coverage of the Cu{311} surface is 0.90 ML (as it is 1.172 times larger). This is in agreement with Papp and Pritchard [49]. As the size of the background CO TPD peak area in our experiments is 11%, this would mean that our background coverage is 0.11 ML, using Cu{110} as an estimate. Similar calculations were done using saturation coverage estimates from Cu{111} (0.52 ML [45]) and Cu{100} (0.7 ML [55]). This produces a coverage estimate of 0.11 ML and 0.12 ML, respectively.

Therefore, based on the TPD data, the estimated CO coverage during 36 minutes of background exposure is estimated to be between 0.11 - 0.12 ML. This estimation suggests that the amount of CO that adsorbs onto the Cu{311} surface during the course of an experiment is moderately low. In addition, the presence of oxygen on the Cu surface reduces the amount of CO on the surface as shown in Figure 3.12 and other works [51, 52].

It is worth noting that, interestingly, the TPD experiments during background exposure of CO show a much lower amount of CO in the TPD spectra when compared to to experiments where CO has been when deliberately leaked into the UHV chamber, despite having a similar Langmuir exposure. Great care has been taken to ensure the purity of CO that is leaked into the chamber. As CO is leaked into the chamber, the mass spectrometer is used to record what gases enter the UHV system, to ensure purity. The gas line is baked out every night and the CO cylinders have been replaced several times. Therefore any leakage from the atmosphere or pumps can be ruled out. A likely reason for the discrepancy between exposure could be due to the inherent limit of the UHV system (Figure 2.1). Within the UHV system, there is most likely a slight pressure gradient (for example, the region nearest to the turbomolecular pump may have slightly lower pressure than the rest of the chamber). During background exposure this gradient is probably very negligible. However, during deliberate CO exposure, the noticeable pressure gradient effect may come from the fact that there is a high pressure at the leak valve and low pressure at the turbomolecular pump, creat-

ing a high pressure differentiation. The proximity of the leak valve to the ion gauge (which is used for pressure detection and therefore dosage reading) may cause the region near both valve to exhibit a slightly larger CO pressure than the region near the single crystal. This discrepancy may explain the difference between deliberate and background CO exposure experiments, despite the same Langmuir exposures.

Figure 3.10 shows the peak height of the CO RAIRS peaks with respect to exposure time. The data shows that the maximum peak height for the CO peak during background exposure does not go above 0.5% of intensity. Although it is difficult to compare RAIRS peaks from other works due to the inherent difference in spectrometer, experimental set-up, data processing, and conditions, it is still a useful tool for comparison. Based on the RAIRS data only, the amount of CO is suggested to be relatively low - but it is far from conclusive. When combined with the TPD data, it does support the assumption that a small amount of CO adsorbs onto the surface during the course of an experiment.

3.3.6 Conclusion

When combining both the TPD and RAIRS data, the adsorption of CO in our work with the current UHV system is in line with the known literature. The work is consistent with standard contamination inside an UHV system. Importantly, the data shows that there is a small amount of CO adsorption onto the Cu{311} surface during standard experimental run time. It is estimated that between 0.11 to 0.12 ML of CO is on the surface during the course of a NO or NH_3 experiment, with even less during an O/Cu{311} experiment.

Chapter 4

NO and Cu{311}

4.1 Literature Review

4.1.1 Catalytic Studies of NO

The vast majority of early work involving NO and Cu is from catalytic studies, which examines the interaction between catalytic mixtures and gases. These studies are different from the gas:metal interface studies within surface science, but are worth examining because they provide a general overview of how NO interacts with Cu based catalysts. In addition to the literature review in this thesis, there have been several reviews published which are not directly addressed here [20, 56–58].

The earliest reported study of NO and catalysts was a paper by Addison *et al* in 1955, showing the formation of N_2O and N_2O_3 from NO in zeolites at 350° C [59]. Isotopic labeling studies found that N_2 forms from the reaction between NO and NH_3 on unsupported CuO. It was found that the nitrogen atoms that mix to create N_2 originate from both NO and NH_3 during the early stages of the reaction [60, 61], but upon reaching steady state, the source of nitrogen comes from NO only. At the same time, N_2O also forms, deriving its nitrogen atoms either from NO only, or from both NH_3 and NO. At steady state, the product mixture was 75% N_2 and 25% N_2O [60, 61]. Mizumoto *et al* [61] speculated about the necessity of the Cu^{2+} ion for the reaction in which NO and NH_3 forms N_2 to take place.

The Cu^{2+} is reduced to Cu^{1+}, which is re-oxidised back to the Cu^{2+} ion by the formation of N_2O. This was later confirmed by other studies [27, 62]. These early studies laid the groundwork for future NO and Cu studies.

The earliest reported study using infrared spectroscopy to investigate NO on CuO (along with various other gases) was by London and Bell in 1973 [63]. They found that the NO molecule is weakly bonded to metallic Cu, with the frequency for $NO_{(a)}$ at 1890 cm^{-1} (similar to NO's gaseous state vibrational peak at 1876 cm^{-1}). The frequency of $N_2O_{(a)}$ is at 2200 cm^{-1}, which is similar to its gas phase frequency of 2240 cm^{-1}.

More recently, most work done with NO and Cu has moved towards Cu-based catalysts inside frameworks such as zeolites [27, 62, 64]. Cu encased inside a ZSM-5 zeolite can produce a conversion rate of up to 97% of NO into N_2 and O_2 at higher temperatures. This zeolite contains Cu^{2+} and is not poisoned by oxygen [27, 62, 65].

Salker and Weiseiler [65] demonstrated how Cu-ZSM-5 is the most active catalyst for NO reduction by NH_3. Their work shows that at temperatures between 673 - 873 K, the formation of N_2 and H_2O from NO and NH_3 is the dominant reaction. Below 673 K, the reaction forming N_2O also takes place, while above 873 K the side reaction between NH_3 and O_2 starts to take place, generating N_2 and NO. They speculated that the side reaction above 873 K occurs because NO does not remain on the catalyst long enough for it to react with NH_3.

Similar to the work of London and Bell on CuO [63], IR spectroscopy was performed on Cu-ZSM-5 catalysts by Hadjiivanoc *et al* [66] and Pietrogiacomi *et al* [67]. Hadjiivanoc *et al* [66] suggest the reaction sequence in Equation 4.1, showing the stepwise oxidation of NO on Cu-ZSM-5 catalysts.

$$NO \rightarrow N_2O_3 \rightarrow N_2O_4 \rightarrow NO_2 \rightarrow NO_3^- \tag{4.1}$$

The authors note that the reaction is poisoned by H_2O, but unaffected by N_2, CO_2, and O_2. Similarly, work done on CuO/ZrO_2 by Pietrogiacomi *et al* [67] and Kantcheva *et al* [68] demonstrated how the reaction in Equation 4.2 dominates, achieving up to 100% conversion

of NO and NH_3 into N_2 and H_2O at 523 K.

$$4NO + 4NH_3 + O_2 \rightarrow 4N_2 + 6H_2O \tag{4.2}$$

When the temperature exceeds a threshold of 523 K, NH_3 oxidation is prevalent (Equation 4.3). Pietrogiacomi *et al* [67] mention that other side reactions occur but do not explicitly state which ones are present.

$$4NH_3 + 5O_2 \rightarrow 4NO + 6H_2O \tag{4.3}$$

Gas phase analysis was performed by Li and Armor [69] with NO on Cu-ZSM-5 using a NO and Ar mixture (0.39% NO) with He at 298.15 K. They found that NO initially decomposes to generate N_2O and N_2 at room temperature, but that the reaction ceases after a few minutes (this is shown in Figure 4.1). The ceasing of the reaction is attributed to the lack of fresh and unoccupied active sites, which have been poisoned by oxygen, in agreement with earlier work [56, 60]. It was suggested by Li and Armor to indicate that the reaction must be self poisoning.

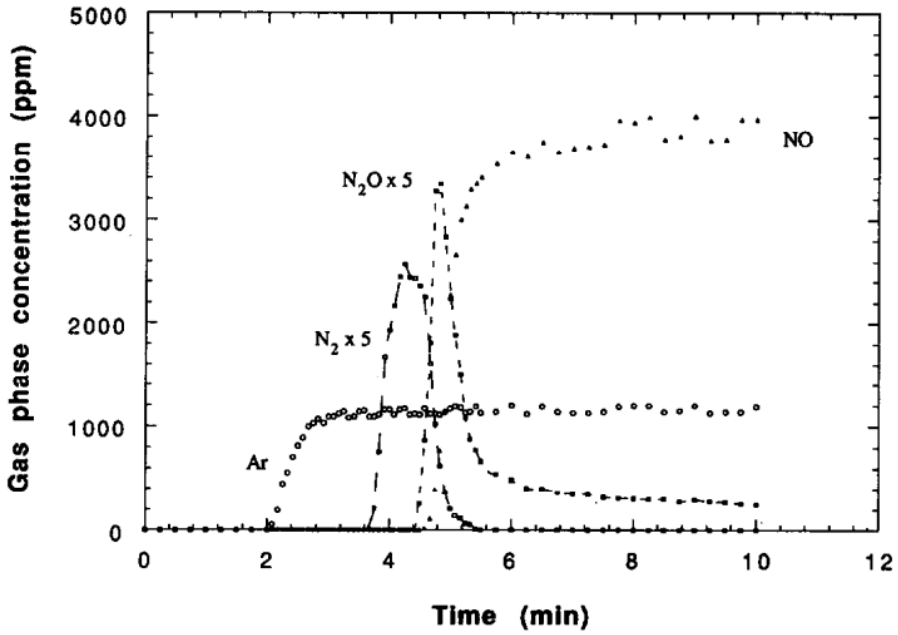

Fig. 4.1 The residual gas analyser (RGA) output of gases following the adsorption (and reaction) of NO onto a Cu-ZSM-5 catalyst at 298 K. (Li and Armor [69])

Temperature programmed desorption (TPD) experiments by Li and Armor performed on the Cu-ZSM-5 catalyst are shown in Figure 4.2. Figure 4.2(a) shows a TPD experiment on an untreated Cu-ZSM-5 catalyst while (b) shows the same experiment on a pre-oxidised, treated Cu-ZSM-5 catalyst. The figure shows that the reaction for NO decomposition occurs on the untreated catalyst, while oxidation of the catalyst inhibits the reaction. Intact NO desorbs from the oxidised catalyst below 673 K, with N_2 desorbing below 473 K.

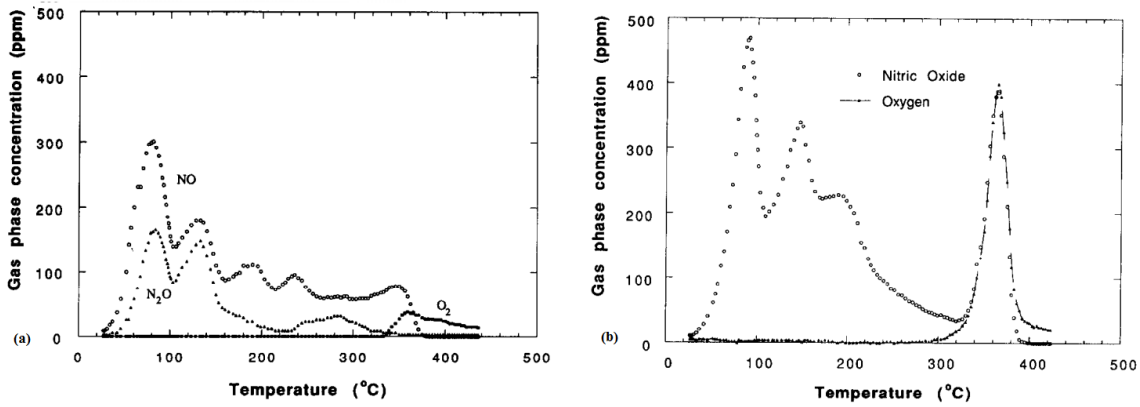

Fig. 4.2 Temperature programmed desorption (TPD) experiment of NO on untreated (a) and pre-oxidised (b) Cu-ZSM-5 catalyst. A heating rate of 8°K/minute was used. (Li and Armor [69])

When compared with other materials, Cu-ZSM-5 has a higher conversion percentage of NO into N_2 than materials such as Cu supported on SiO_2 [70]. Work by Sato *et al* [71] compared the difference in NO decomposition between Cu, Co, Al, Ag, and Zn. The authors reported that NO decomposition on Cu had the lowest temperature for maximum decomposition rate at 573 K compared to 623 K for Co, 673 K for Al, 723-873 K for Ag, and 873 K for Zn. The working temperature for Cu is relevant for selective catalytic reduction as it lies inside the diesel engine exhaust temperature range which is between 523 - 673 K.

Work by Centi *et al* [56] on a Cu-on-alumina catalyst demonstrated how there is a difference in reaction rate between pre-steady state and steady state experiments for the conversation of NO and NH_3. Their work displayed that the reaction is faster pre-steady state than during steady-state. This was suggested to be because of the initial abundance of Cu^{2+} reaction sites on which the reaction can take place. Once the Cu^{2+} reaction sites are used up,

they are replenished slower than the reaction that recovers them (suggesting that it is the rate determining step). This ties into how TPD experiments are more similar to the pre-steady state conditions and therefore have a higher reaction rate.

Interestingly, on the Cu-on-alumina catalyst [56], oxygen increases the rate of reaction between NO and NH_3 (in contrast to on Cu-ZSM-5 where O_2 slows down the reaction [69]). Centi *et al* [56] inferred that this is because there are two pathways for the reaction. The first is the dissociative chemisorption of NO on reduced Cu sites. This reaction is fast and the oxygen atom of NO is said to re-oxidise the reaction site. The second pathway is through a Cu-nitrite-mononitrosyl complex, which decomposes to form N_2 and O_2. This pathway leaves Cu-O, which then reacts with two NO molecules to form N_2 and O_2, reforming the active Cu site. Therefore, oxygen can play an active role in the decomposition of NO, in contrast to inhibiting it on Cu-ZSM-5.

Mizumoto *et al* [61] suggest the following mechanisms for the reaction between NO and NH_3, in which the nitrogen atoms of N_2 originate from both NO and NH_3's nitrogen atoms (Equation 4.4 and 4.7). This is in agreement with isotopic studies [60].

$$\begin{aligned} Cu^{2+}(NH_3)_n + NO \rightarrow Cu^{2+}(NH_3)_n NO \rightarrow \\ Cu^{1+}(NH_3)_m + N_2 + H_2O + (n-m-1)NH_3 + H^+ \end{aligned} \tag{4.4}$$

$$H^+ + NH_3 \rightarrow NH_4^+ \tag{4.5}$$

$$Cu^{1+}(NH_3)_m + 3NO \rightarrow Cu^{2+}(NH_3)_m NO_2^- + N_2O \tag{4.6}$$

$$Cu^{2+}(NH_3)_m NO_2^- + NH_4+ \rightarrow Cu^{2+}(NH_3)_m + N_2 + 2H_2O \tag{4.7}$$

$$Cu^{2+}(NH_3)_m + (n-m)NH_3 \rightarrow Cu^{2+}(NH_3)n \tag{4.8}$$

$$4NO + 2NH_3 \rightarrow 2N_2 + N_2O + 3H_2O \tag{4.9}$$

It can be seen that there is no consensus on the exact mechanism of NO decomposition and reaction with NH_3. There are multiple pathways suggested along with different observed effects of the catalyst support. There has also been work studying other reducing agents, with a review by Iwamoto *et al* [62] in 1994 that extensively compares NO reduction by gases other than NH_3, such as with hydrocarbons.

To conclude this summary of catalytic work with NO and NH_3 on Cu catalysts, it can be suggested that the reaction between the two species readily forms N_2 below certain temperature thresholds (which are material dependent). It is speculated that for Cu in a ZSM-5 zeolite, the active site is a Cu^{2+} ion, which is reduced to Cu^{1+} during the reaction that produces N_2. This is then converted back to Cu^{2+} by a side reaction that produces N_2O. Outside this main reaction pathway, there are also several side reactions such as the oxidation of NH_3 above a temperature threshold. In order to understand the underlying processes that drive the reaction between NO and NH_3, surface science is used to break down the reaction into its components.

4.1.2 Surface Science Studies of NO

In contrast to the catalytic composite and gas mixture approach of catalytic studies, surface science studies employ an alternative method of examining the mechanism of interaction between NO and Cu, namely studying the interface between the gas and the metal in ultra high vacuum. As in the section on catalytic studies, it is worth mentioning that there are several reviews discussing the adsorption of NO onto Cu (and various other metals) [58, 72, 73]. To briefly summarise, NO readily forms N_2O on Cu surfaces, but the mechanism is still being explored. There are two main schools of thought about the formation of N_2O on Cu single crystals, namely the dissociation and dimer formation pathways.

Dissociation Pathway

One of the earliest reported works that used surface science techniques to study NO on Cu was by Matloob and Roberts in 1977 [74]. They studied the adsorption of NO onto Cu films at 295 K, using X-ray photoelectron spectroscopy (XPS), shown in Figure 4.3. The spectra shows that there is both a nitrogen and oxygen species on the Cu film at low temperatures, but that only oxygen species remain on the surface upon heating. The authors commented on the similarities between NO and CO due to the back-donation of electrons from the metal to the NO's anti-bonding orbital, which weakens the N-O bond. In addition to this electronic effect, the authors inferred the existence of two adsorption configurations of the NO molecule - one linearly bonded and the other a bent configuration (with respect to the Metal-N-O bond configuration). They concluded that the linearly bonded form is weakly bonded to the surface, does not react, and simply desorbs from the Cu film at 170 K. In contrast, the bent configuration is the pre-requisite for the dissociation of NO.

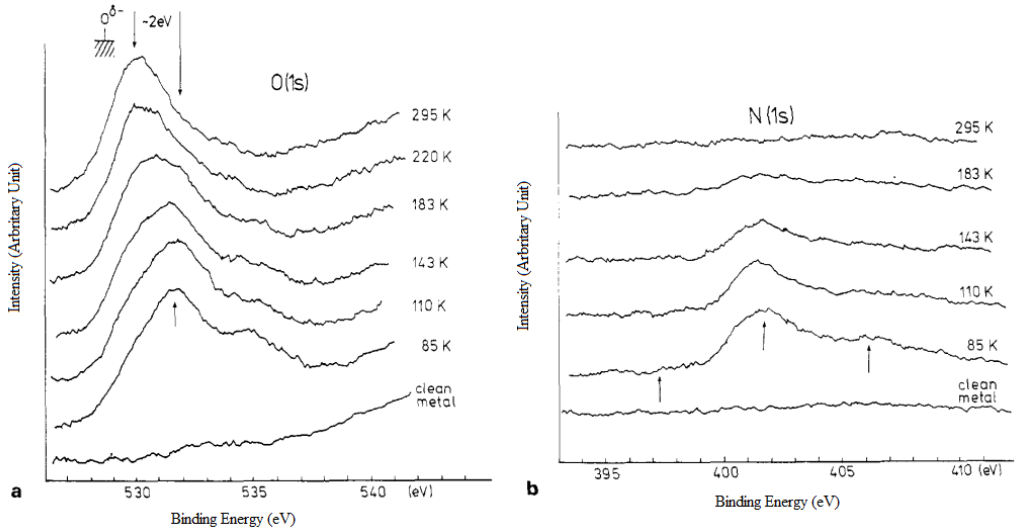

Fig. 4.3 XP spectra of a clean Cu film exposed to NO. The spectra shows the exposure of the bare Cu film exposed to 150 L of NO, which is successively heated to the temperature marked directly on the spectra. (a) is the O(1s) spectral region and (b) is for N(1s) spectra region. (Matloob and Roberts [74])

The first studies of NO on Cu single crystals were reported by Johnson *et al* [75] with their work on Cu{100} and Cu{110}. They speculated that N_2O formation was the result of

the dissociation of NO into $N_{(a)}$ and $O_{(a)}$ as shown in Equation 4.10. Another NO molecule then reacts with $N_{(a)}$, forming N_2O as shown in Equation 4.11. The authors also mention that the reaction rate is faster on the Cu{100} surface than on Cu{110}.

$$NO_{(a)} \rightarrow N_{(a)} + O_{(a)} \tag{4.10}$$

$$NO_{(a)} + N_{(a)} \rightarrow N_2O_{(a)} \tag{4.11}$$

EELS experiments dosing NO onto Cu{110} at 80 K by Wendelken *et al* [76] are shown in Figure 4.4. The authors assigned the peaks at 194 meV (1564 cm^{-1}) and 104 meV (838 cm^{-1}) to the N-O stretching mode of the linearly bonded and bent N-O molecule respectively. Based on this, they speculated that NO initially adsorbs intact in a bent configuration and that this is its pre-dissociation configuration. They demonstrated that NO reacts and dissociates on the surface completely at 113 K (with partial dissociation at 85 K). They mentioned that there is an exposure requirement, with complete dissociation only occurring on the Cu{110} when exposure is above 2.2 L.

LEED experiments show that on Cu{100}, when NO is dosed at 80 K, a $(\sqrt{2}\times\sqrt{2})R45°$ phase forms, identified as derived from an oxygen species [75, 77]. Later work by Dhesi *et al* [78] showed that a weak c(2×2) LEED pattern can form if the dosing pressure is decreased, resulting in a mixture of $N_{(a)}$ and $O_{(a)}$ on the surface.

Dimer Pathway

These early studies provided evidence for the dissociation theory, but the alternative theory of dimer formation has also been considered in the literature. The first paper that reported evidence for $(NO)_2$ dimer formation on Cu surfaces was by Dumas *et al* [79] who used synchrotron infrared reflection absorption spectroscopy to study the process. Previously, Ag{111} was the only surface on which there had been evidence for $(NO)_2$ dimer formation [80, 81].

Figure 4.5(a) shows IR spectra obtained of NO onto a Cu{111} surface as a function

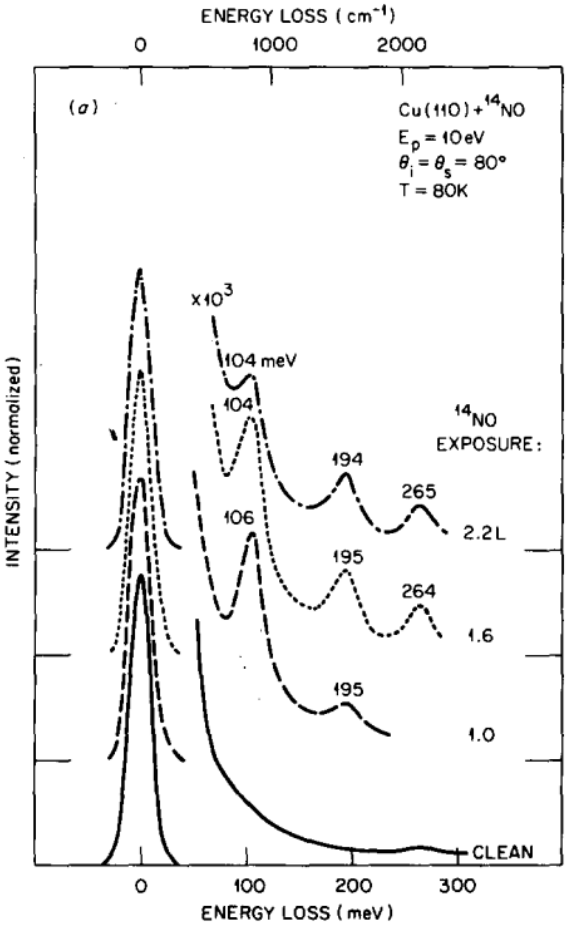

Fig. 4.4 EEL spectra following the adsorption of NO onto Cu{110} at 80 K. The spectra show increasing exposure of NO from bottom to top. (Wendelken *et al* [76])

of exposure (at 88 K). Dumas *et al* [79] assigned the peak at 1525 - 1560 cm^{-1} to NO bonded to a two-fold bridge-site. The peak grows and reaches a maximum at 1.25 L, then vanishes by 2 L, which implies that NO adsorbs and reacts on the surface. The authors identified weak peaks at 1780 and 1850 cm^{-1} as the symmetric and antisymmetric stretches for $(NO)_2$, respectively (Figure 4.5(b)) - though this assignment is questionable, as it is difficult to distinguish the peaks from the noise. The authors inferred from their data that the $(NO)_2$ dimer formation was the intermediate step for N_2O formation, in contrast to the NO dissociation mechanism.

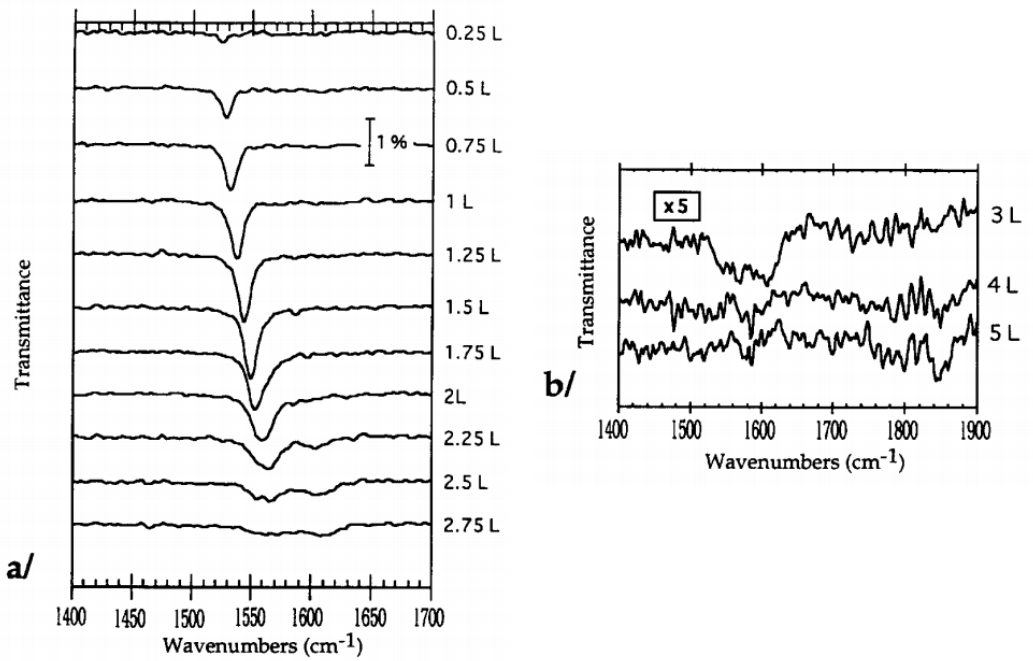

Fig. 4.5 Synchrotron RAIR spectra with increasing exposures of NO onto Cu{111} at 88 K as a function of exposure. (a) shows the adsorption at low coverage, between 0.25 L to 2.75 L. (b) shows 3, 4, and 5 L of exposure. Note that in (b) the intensity is multiplied in an attempt to highlight peaks at 1780 and 1850 cm^{-1}. (Dumas *et al* [79])

The most similar experiments to the work in this thesis were RAIRS studies conducted by Kim *et al* [82] and Brown *et al* [83] with NO on Cu{100} and Cu{110}, respectively. Figure 4.6 shows RAIR spectra following the adsorption of NO on Cu{100} [82]. Kim *et al* attributed the peak at 1657 cm^{-1} to NO on a bridge-site at low exposures of NO [82]. As exposure increases, strong bands at 1773 and 1865 cm^{-1} appear, which were thought to be

due to $(NO)_2$ dimers (antisymmetric and symmetric peaks, respectively). Kim *et al* inferred from the RAIRS data that the peaks give evidence for the $(NO)_2$ dimer mechanism for N_2O formation [82].

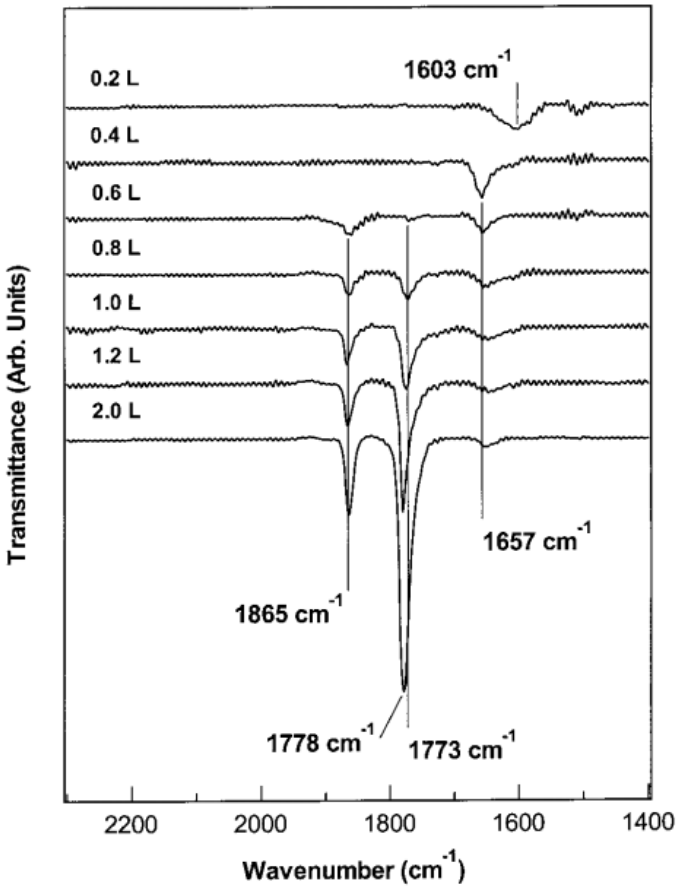

Fig. 4.6 RAIR spectra following the adsorption of NO onto Cu{100} at 25 - 28 K. Exposures marked directly on the spectra. (Kim *et al* [82])

Similar to the work on the Cu{100} surface, Brown *et al* [83] studied NO adsorption on Cu{110} using RAIRS, where similar spectra to those on Cu{100} were observed. The RAIR spectra in Figure 4.7 also displayed similar peaks for NO on the bridge-site, anti-symmetric, and symmetric peaks at 1636, 1780, and 1863 cm^{-1}, respectively. One of the key differences between Cu{100} and Cu{110} is a peak at 2227 cm^{-1}, which Brown *et al* attributed to the N-N stretch of N_2O (based on work with Ag{111} [80, 81]). The authors also mention that $O_{(a)}$ remains on the Cu surface after the exposure of NO.

Both Kim *et al* [82] and Brown *et al* [83] propose that NO forms $(NO)_2$ dimers on the

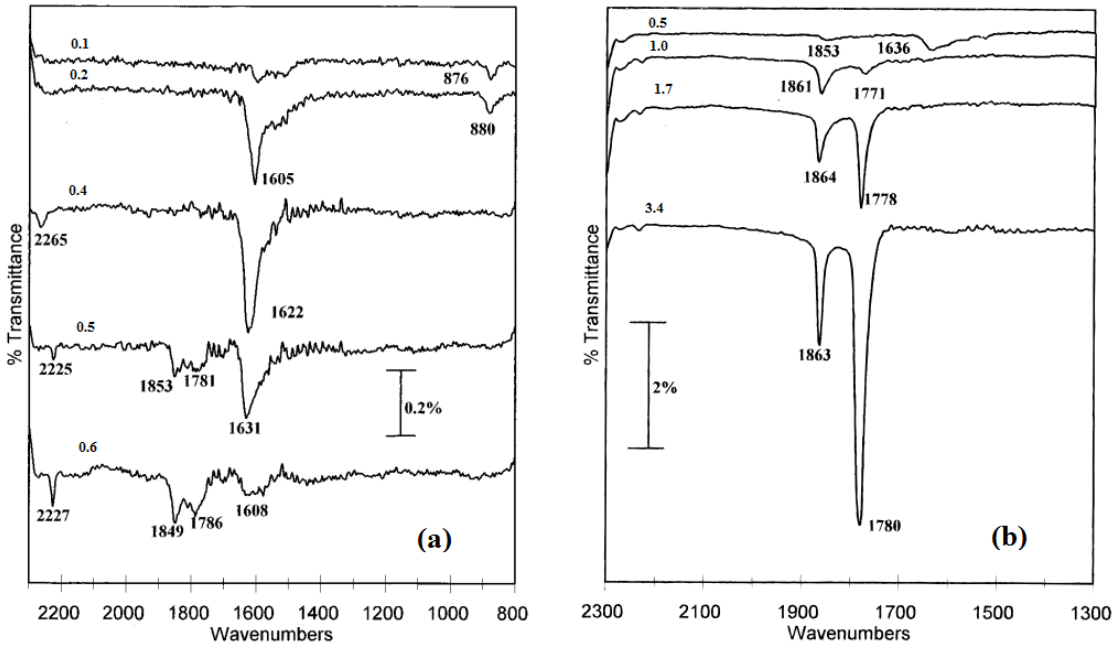

Fig. 4.7 RAIR spectra following the adsorption of NO onto Cu{110} at 40 K. (a) NO exposure between 0.1 - 0.6 L and (b) exposure between 0.5 - 3.4 L. (Brown *et al* [83])

surface, which is the intermediate for N_2O formation. Kim *et al* speculated that the $(NO)_2$ dimer can readily form with almost no activation energy due to the unpaired electrons on each of the NO molecules forming a complete bond (along with an unoccupied anti-bonding orbital). They proposed the mechanism in Equation 4.12 and 4.13.

$$2NO_{(a)} \rightarrow (NO)_{2(a)} \tag{4.12}$$

$$(NO)_{2(a)} \rightarrow N_2O_{(a)} + O_{(a)} \tag{4.13}$$

Figure 4.8 shows the possible orientations of the $(NO)_2$ dimer on a Cu surface as discussed by Kim *et al* [82]. It is most likely that the $(NO)_2$ dimer is oriented in the U-shaped structure (Figure 4.8(b)). This is because it is the only orientation that allows for the appearance of the symmetric peak of the $(NO)_2$ dimer in the RAIR spectra (based on the surface selection rule). The antisymmetric stretching peak can appear if the U-shaped orientation has an additional tilt along the N-N bond axis.

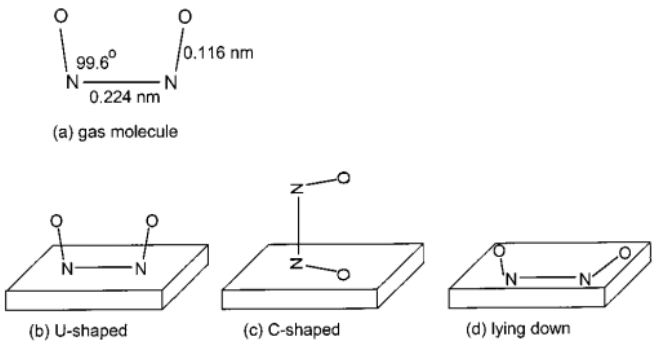

Fig. 4.8 (a) The gas phase structure of the $(NO)_2$ dimer along; (b)-(d) the proposed orientations of the $(NO)_2$ dimer on the Cu surface. (Kim *et al* [82])

There has also been computational work regarding the $(NO)_2$ dimer formation mechanism by various groups. It is suggested that the formation of the dimer is energetically favoured and has a very small activation energy [84–86]. Calculations on Ag{111} by Liu *et al* [86] showed that the barrier for dimer formation is only 0.27 eV. In addition, it was suggested by Liu *et al* that the formation of N_2O via the $(NO)_2$ dimer pathway includes an inversion step of the dimer. Initially, the $(NO)_2$ dimer forms a Cu-N bond (as when NO adsorbs molecularly, it adsorbs with the nitrogen bonded directly to the Cu metal). When the dimer inverts, both oxygen atoms bond to the surface instead of the nitrogen atom. It was calculated that the barrier to inversion is only 0.02 eV, with the resulting Cu-O bonded dimer being more stable by 0.09 eV.

In conclusion, there are two plausible proposed mechanisms for the formation of N_2O, summarised in Table 4.1. There is sufficient evidence for both mechanisms; however, recent work has increasingly focused on the $(NO)_2$ dimer mechanism. This is due to RAIR spectra where the appearance of the symmetric and antisymmetric peaks provide strong evidence for the dimer pathway.

Table 4.1 Proposed Mechanisms of NO Formation

NO Dissociation	$(NO)_2$ Dimer
$NO \rightarrow N + O$	$2NO \rightarrow (NO)_2$
$NO + N \rightarrow N_2O$	$(NO)_2 \rightarrow N_2O + O$

4.2 Experimental

The Cu{311} crystal was cleaned before experiments using Ar ion sputtering and was then annealed to 900 K for 2 minutes to reorder the surface. Surface cleanliness was monitored using Auger Spectroscopy and LEED analysis. NO was then leaked into the chamber at the desired pressure which was constantly monitored using an ion gauge.

As NO was leaked into the chamber, RAIRS was used to monitor surface species as a function of exposure. Varying pressures and dosing times were used to examine any effects of coverage and time of exposure. Various temperature experiments were performed.

After the interaction of NO and bare Cu{311} was examined, oxygen pre-adsorbed Cu{311} was also studied by varying the oxide structure (which was verified using LEED) as described in Section 3.2. Once the desired pre-adsorbed oxygen state was achieved, the same experiments that were run with NO on bare Cu{311} were performed.

Details about the experimental set up and procedures are fully explained in Chapter 2, in their respective sections.

4.3 Results

The RAIRS peak assignments in this chapter were made by comparing the frequencies with work done on similar surfaces such as Cu{110} or from catalytic studies. A compilation of RAIRS mode assignments from similar work is shown in Table 4.2.

Table 4.2 NO RAIRS Peak Assignments

Frequency (cm^{-1})	Assignment	Literature
1601 - 1657	Molecular NO Stretch (Bridge-site)	[72, 79–83, 87]
1773 - 1780	ON-NO Antisymmetric Stretch	[72, 79–83]
1824 - 1865	ON-NO Symmetric Stretch	[72, 79–83]
2080 - 2121	CO stretch	[45, 47–51]
2225 - 2232	Physisorbed N_2O (N-N Bond Stretch)	[80–83]
2260 - 2265	Chemisorbed N_2O (N-N Bond Stretch)	[80, 81, 83]

4.3.1 NO and Bare Cu{311}

Figure 4.9 shows RAIRS spectra following the adsorption of NO onto the Cu{311} single crystals, showing an increase in NO exposure to the bare surface. The spectrum were taken with the single crystal held at 100 K, NO dosing pressure of 6×10^{-10} mbar, and a spectral resolution of 4 cm^{-1}. Each spectra is the average of 400 scans.

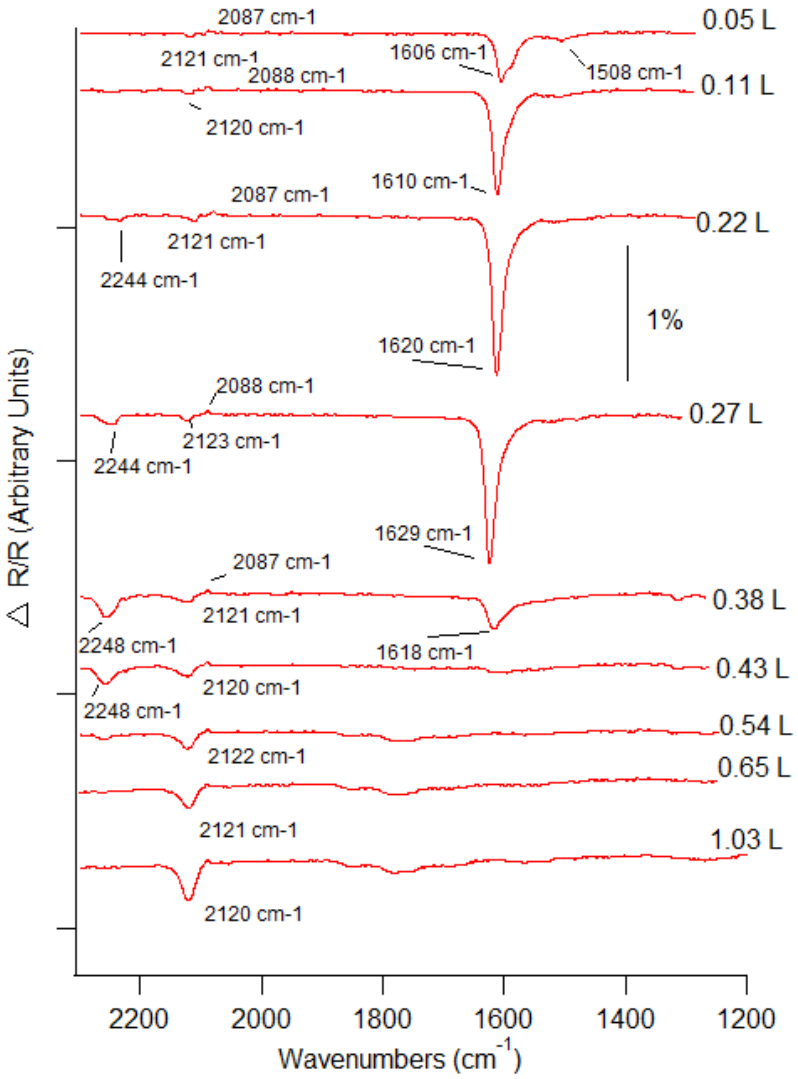

Fig. 4.9 RAIRS spectra following the adsorption of NO onto bare Cu{311} at 100 K with increasing exposure.

During the course of NO adsorption onto the bare Cu{311} surface, multiple peaks form. At 0.05 L of NO exposure, the spectra shows a peak at 1606 cm^{-1} with a peak to peak

intensity of 0.41%. This is assigned to NO on a two fold bridge site [72, 79, 82, 83, 87]. Similarly, the peak also shows a small shoulder at 1508 cm^{-1} with a peak intensity of 0.07%. The 1606 cm^{-1} peak grows with increased NO exposure, reaching a peak at 0.22 L of NO exposure with an intensity of 1.3% and shifts to 1629 cm^{-1}. After 0.22 L of exposure, the 1606 cm^{-1} reduces in intensity and vanishes at 0.43 L of NO exposure (but leaving a broad artifact which remains until higher NO exposures). The peak area of this peak is shown as a function of NO exposure in Figure 4.10. The shoulder of the 1606 cm^{-1} peak at 1508 cm^{-1} disappears at 0.22 L, at the same exposure that the 1606 cm^{-1} peak reaches its maximum.

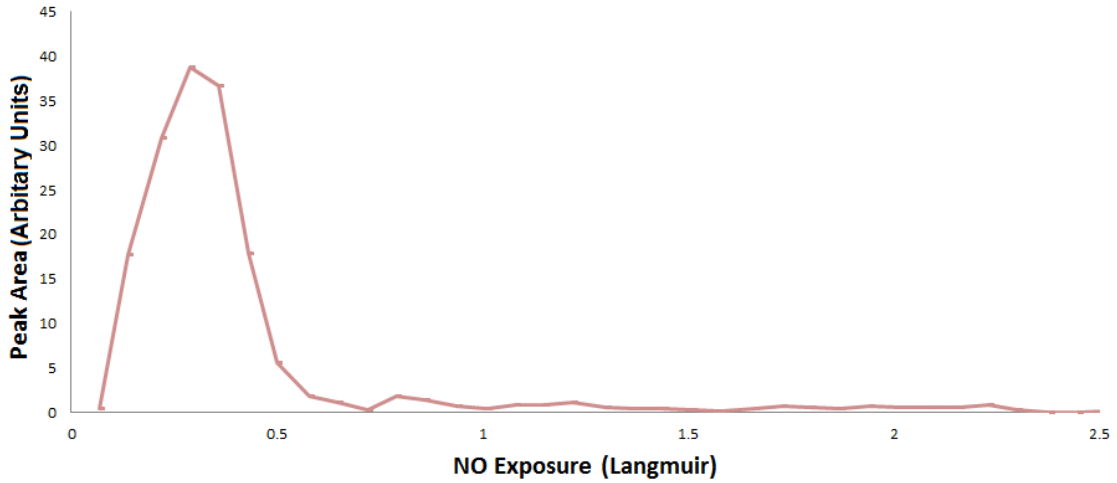

Fig. 4.10 Peak area of the NO bridge-site peak as a function of NO exposure onto the bare Cu{311} surface at 100 K.

At the same time that the 1606 cm^{-1} peak peaks(assigned to the NO monomer on the two fold hollow site), at 0.22 L, a peak at 2244 cm^{-1} appears. This peak is assigned to the N-O stretching mode of N_2O [80, 82, 83]. Similarly, at the same NO exposure there is a tiny peak at 1316 cm^{-1}, which is assigned to the N-N stretching mode of N_2O. These peaks denote the appearance of the N_2O monomer on the surface, caused by the reaction between two NO molecules. After 0.22 L, as NO exposure is increased, the N_2O peaks increase until they reach a maximum at 0.38 L. These two peaks then reduce in size and vanish by 0.65 L of NO exposure.

After the NO monomer peak has vanished (at 0.54 L), there is an appearance of two

broad peaks at 1848 and 1757 cm^{-1}, with the 1757 cm^{-1} having the larger peak intensity of the two. The peak at 1757 has been assigned to the antisymmetric stretching mode of the $(NO)_2$ dimer [72, 79, 82, 83], while the 1848 peak has been assigned to the symmetric stretching mode of the $(NO)_2$ dimer [72, 79, 82, 83]. The size of these two peaks grow from 0.54 L of NO exposure, then stabilises from 0.65 L. The peak area of these two peaks as a function of NO exposure is shown in Figure 4.11. A schematic representation of these modes is shown in Figure 4.12.

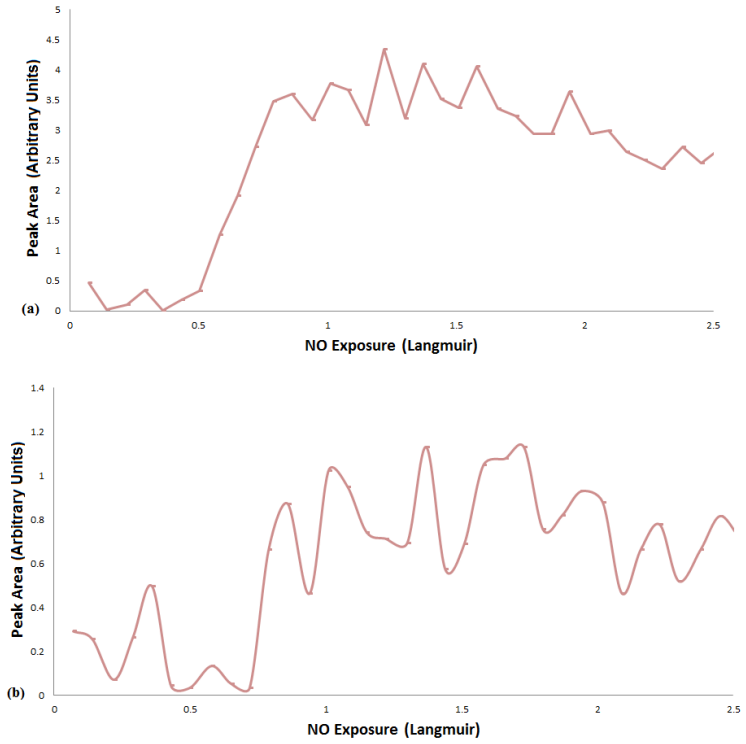

Fig. 4.11 Peak areas for the $(NO)_2$ dimers; (a) symmetric stretching mode and (b) antisymmetrical stretching mode with respect to NO exposure onto bare Cu{311} at 100 K.

At 0.11 L of NO exposure, there is an appearance of a peak and an inverse peak at 2121 cm^{-1} and 2087 cm^{-1}, respectively. As discussed in Section 3.3, the inverse peak at 2087 cm^{-1} is the adsorption of background CO onto the surface and the 2121 cm^{-1} peak is assigned to CO that is absorbed near an oxygen species. Due to the nature of this data processing method, each spectrum is ratioed against a background spectrum taken at 100 K. The inverse peak at 2087 cm^{-1} is assigned to the C-O stretch in CO molecules that adsorbed

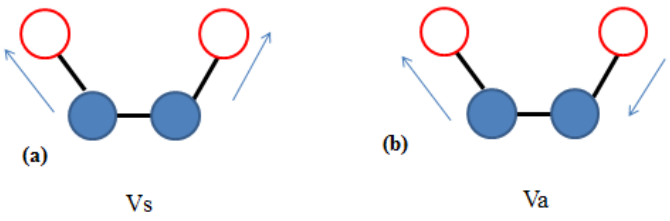

Fig. 4.12 A simple visual representation of the (a) symmetric and (b) antisymmetric vibrational modes of the $(NO)_2$ dimer.

from the residual gases whilst the surface was cooling from 200 to 100 K (as mentioned in Section 3.3). The 2121 cm^{-1} peak is also assigned to CO but it is shifted due to the creation of $O_{(a)}$ on the surface from the NO reaction. These $O_{(a)}$ species then interact with adsorbed CO, causing a shift similar to the adsorption of CO onto oxygen pre-adsorbed Cu{311} resembling that shown in Figure 3.12.

From 0.65 L up until 3 L of NO exposure, the only peaks present are ones assigned to the $(NO)_2$ dimers and CO peaks (with no further peaks appearing after 0.65 L of NO exposure). The 2121 cm^{-1} continues to grow, denoting further CO adsorption onto the Cu{311} surface throughout the course of the experiment. The 1848 and 1757 cm^{-1}, and the inverse peak at 2087 cm^{-1} remains the same size.

Figure 4.13 compiles the spectra of NO on a bridge-site (Figure 4.10), the symmetric and antisymmetric stretching modes of the $(NO)_2$ dimer (Figure 4.11), and the chemisorbed N_2O (Figure 4.15). The spectrum shows how the N_2O peak area rises when the peak for intact NO starts to drop, suggesting that there is a link between the two. This implies that intact NO is used up to form N_2O, but that NO is not replenished at the same time. As the peak for chemisorbed N_2O drops, the peaks for the $(NO)_2$ dimer form. Based on work with NO adsorption onto Ag{111} [80], we know that N_2O forms through the $(NO)_2$ dimer mechanism; it is thus unusual that peaks for N_2O precede peaks for the $(NO)_2$ dimer. This is speculated to be because of the fast speed of the mechanism through which NO forms the $(NO)_2$ dimer and then N_2O. In addition, N_2O desorbs from the surface quickly during this process [41]. Then, as $O_{(a)}$ builds up on the surface, it hinders the formation of N_2O from $(NO)_2$, allowing the dimer to be detected by the RAIRS.

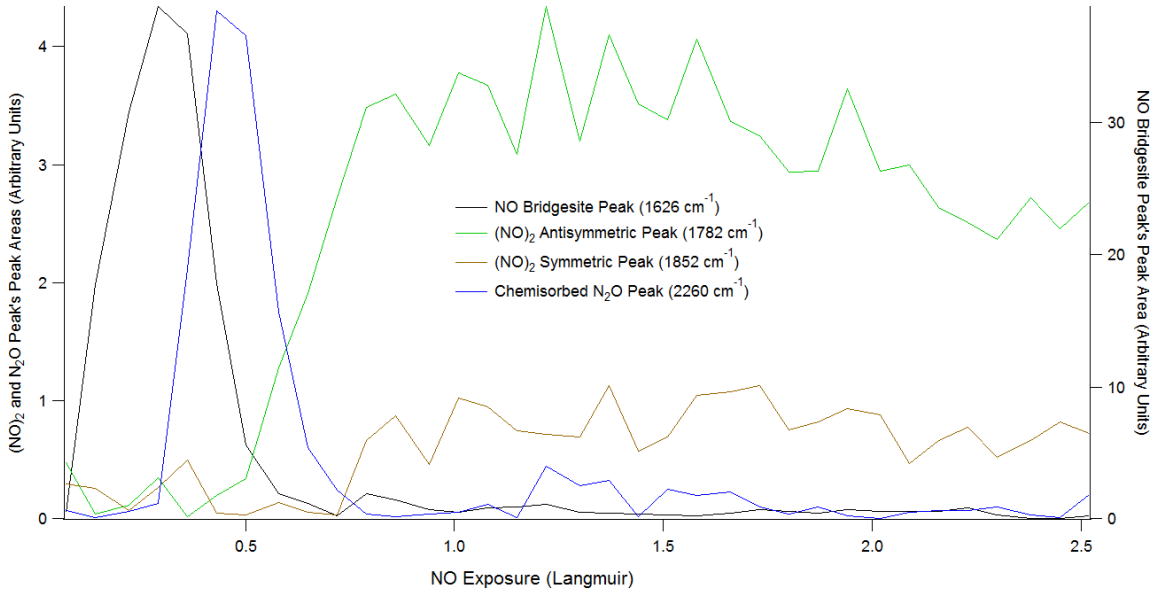

Fig. 4.13 A compilation of the RAIR peak heights of the NO bridge-site, $(NO)_2$, and N_2O as a function of NO exposure with the crystal at 100 K.

High Resolution RAIRS at Low NO Exposure

A series of experiments were performed at an with increased RAIRS resolution (2 cm^{-1} instead of 4 cm^{-1}). However, due to experimental limitations at the time, the base pressure of the UHV machine was an order of magnitude higher, causing there to be a noticeable amount of CO adsorption onto the surface. The overall chemistry of the process does not seem to significantly change, but there are additional insights that can be gained from the higher resolution data.

Figure 4.14 shows how the high resolution RAIR spectrum as a bare Cu{311} surface was exposed to increasing amounts of NO at 100 K (at a NO pressure of 3×10^{-9} mbar). The spectrum shows the lower coverage of NO exposure.

Similarly to in Figure 4.9, several RAIRS peaks appear during the course of NO exposure to the Cu{311} surface. A prominent peak at very low coverage is at 1626 cm^{-1}, which is assigned to NO on a two fold bridge site [72, 79, 82, 83, 87]. The peaks at 1782 and 1853 cm^{-1} begin to appear from 0.26 L, reaching a maximum at 1.0 L, and not changing at NO exposures above 1.5 L. Similarly to in Figure 4.9, these two peaks are assigned to the antisymmetric and symmetric stretching modes of the $(NO)_2$ dimer bond, respec-

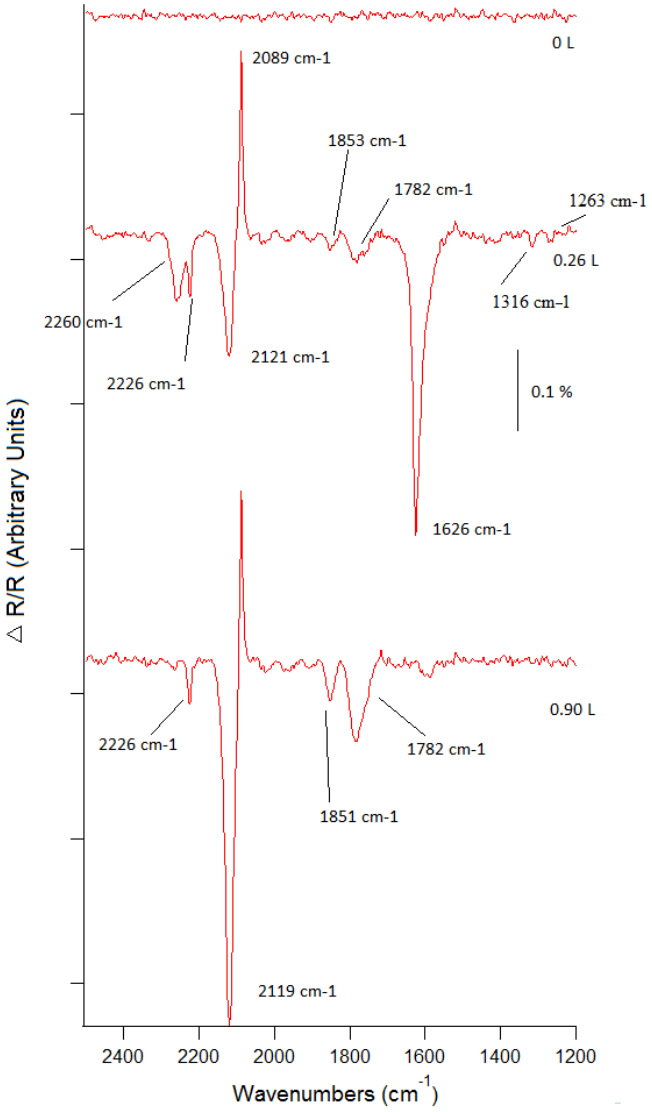

Fig. 4.14 RAIR spectra following the adsorption of NO onto bare Cu{311} at 100 K with increasing exposure.

tively [72, 79, 82, 83].

Due to the higher resolution used by the RAIR spectrometer in these experiments, the 2244 cm^{-1} peak (Figure 4.9) is resolved into two peaks at 2262 and 2226 cm^{-1}, both appearing at 0.2 L of NO exposure. The 2260 cm^{-1} peak quickly grows with respect to increasing exposure, reaching a maximum at 0.4 L and vanishing by 0.7 L. The peak at 2226 cm^{-1} has a much smaller increase, and tails off above 1 L. Both of these peaks are assigned to the N-N stretching frequency of N_2O on the surface based on the N_2O adsorption onto Ag{111} [80] and Cu{110} [82, 83]. The 2226 cm^{-1} peak is most likely physisorbed N_2O as it is similar to the gas phase frequency which is present at 2224 cm^{-1}. The 2260 cm^{-1} peak is assigned to chemisorbed N_2O [83]. Figure 4.15 shows the peak area for physisorbed and chemisorbed N_2O plotted against NO exposure.

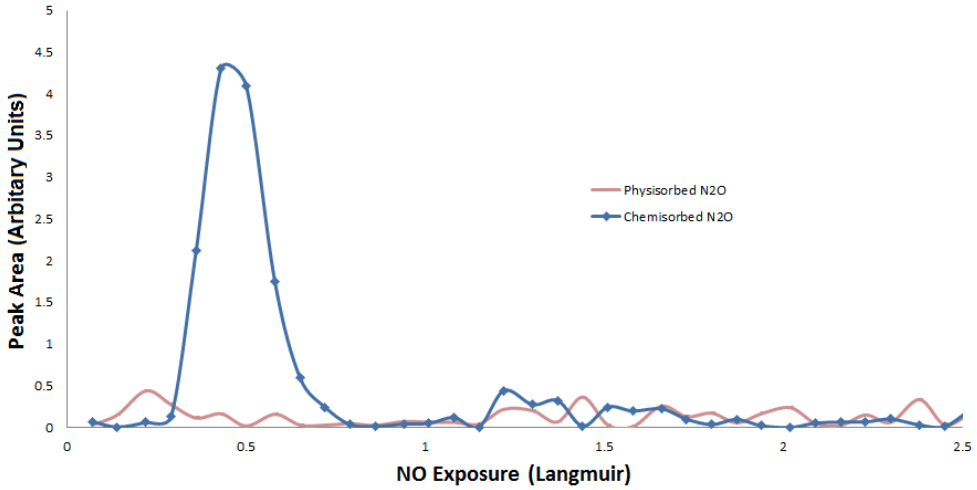

Fig. 4.15 Peak areas for the peaks assigned to physisorbed and chemisorbed N_2O on the bare Cu{311} surface with respect to NO exposure onto bare Cu{311} at 100 K.

Linked to the 2226-2260 cm^{-1} species, during the course of NO exposure, there are peaks at 1316 cm^{-1} and 1263 cm^{-1} (with the latter being barely visible) at 0.26 L of NO exposure. Initially the larger of the two, the 1316 cm^{-1} peak vanishes at 0.90 L of NO exposure. The behaviour of these two peaks is very similar to the N-N modes of N_2O peaks (2260 and 2226 cm^{-1} species), suggesting that they are linked. These two peaks are assigned to the N-O stretching mode of the N_2O species [80, 82, 83], with the 1316 cm^{-1}

peak being assigned to the chemisorbed and the 1263 cm^{-1} peak being assigned to the physisorbed species.

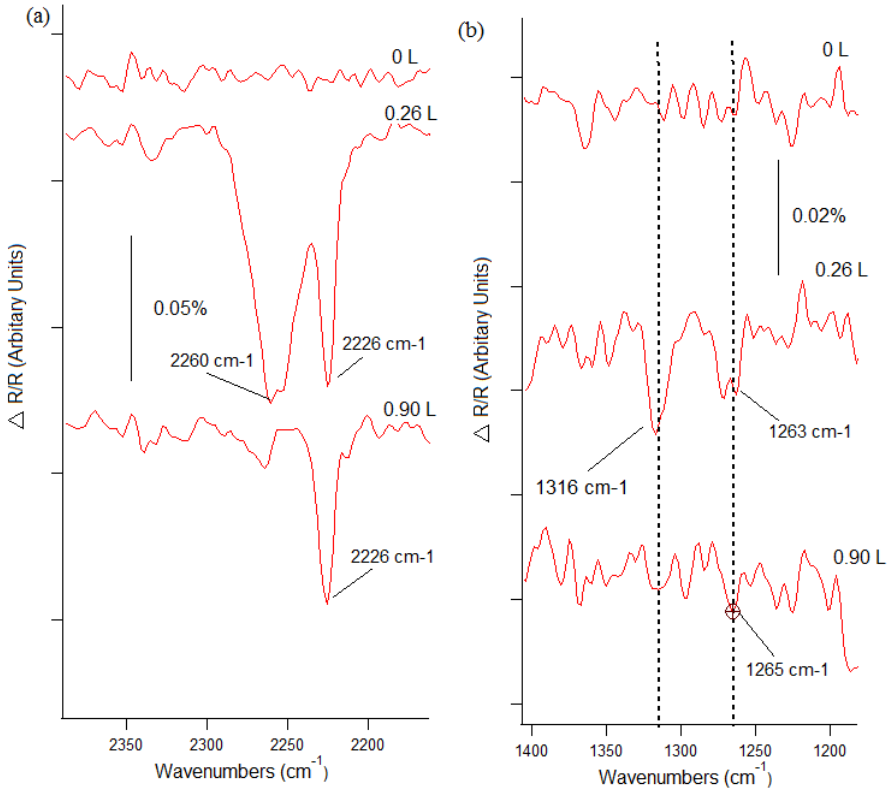

Fig. 4.16 Enlarged image of the high resolution RAIRS data of the peaks assigned to (a) N-N modes of N_2O (2260 cm^{-1} corresponds to chemisorbed and 2226 cm^{-1} to physisorbed species) (b) N-O mode of N_2O (1316 cm^{-1} corresponds to chemisorbed and 1263 cm^{-1} to physisorbed species).

As each spectra is ratioed against a background spectrum taken at 100 K, similar to Figure 4.9, there is an inverse peak at 2089 cm^{-1} that is assigned to the C-O stretch in CO molecules that adsorbed from the residual gases whilst the surface was cooling from 200 to 100 K (as mentioned in Section 3.3 and previously). The 2121 cm^{-1} peak is noticeably larger in Figure 4.14 than in Figure 4.9, but, despite the amount of CO on the surface, the overall chemistry of NO reaction it does not seem to change.

High Resolution RAIRS at High NO Exposure

At NO exposures over 1.0 L, the RAIR spectrum is dominated by a 2123 cm^{-1} peak, shown in Figure 4.17. This peak grows from 0.26 L of exposure. The peak shifts slightly from 2123 cm^{-1} to 2125 cm^{-1} above 40 L of NO exposure. This peak is assigned to residual CO adsorption. For further analysis of the spectra, Figure 4.18 shows NO adsorption onto the bare Cu{311} surface, but with the CO peak omitted in order to highlight the other peaks present. The only other peaks present above 1.5 L are those at roughly 1784 cm^{-1} and 1848 cm^{-1}, which are assigned to the antisymmetric and symmetric stretching modes of the $(NO)_2$ dimer, respectively. These two peaks are present from 0.26 L of NO exposure. The symmetric peak area does not significantly change up to 100 L as shown in Figure 4.19(a), while the antisymmetric peak area (Figure 4.19(b)) reaches a maximum at low exposure but then drops off after roughly 1 L of NO exposure.

4.3.2 NO and Oxygen Pre-Covered Cu{311}

When a low oxygen pre-dosed (O(1×2)/Cu{311}) surface is exposed to NO and monitored by RAIRS, the spectrum is dominated by the 2121 cm^{-1} peak, assigned to CO (Figure 4.20). The only other peaks present are ones at 2220, 1778 and 1851 cm^{-1} assigned to the physisorbed N_2O, antisymmetric mode, and symmetric stretching mode of the $(NO)_2$ dimer, respectively.

When oxygen is pre-dosed to coverages higher than that of the O(1×2) structure (whether the runways or oxide clusters phases) and NO exposed, the only peak present on the RAIR spectra is the CO peak, which has shifted to 2118 cm^{-1} (Figure 4.21 and 4.22). There is a suppression of the CO peak going from the bare Cu{311} surface to the O(1×2)/Cu{311} surface. The area of the CO peak as a function of NO exposure is shown in Figure 4.23. The area of the CO peak increases by a factor of 2.5 going from the O(1×2) phase to the O(runway), but there is minimal change going from the O(runway) phase to the O(Oxide Clusters) phase. There is a peak for physisorbed N_2O with a frequency of 2226 cm^{-1} on the bare Cu{311} surface only.

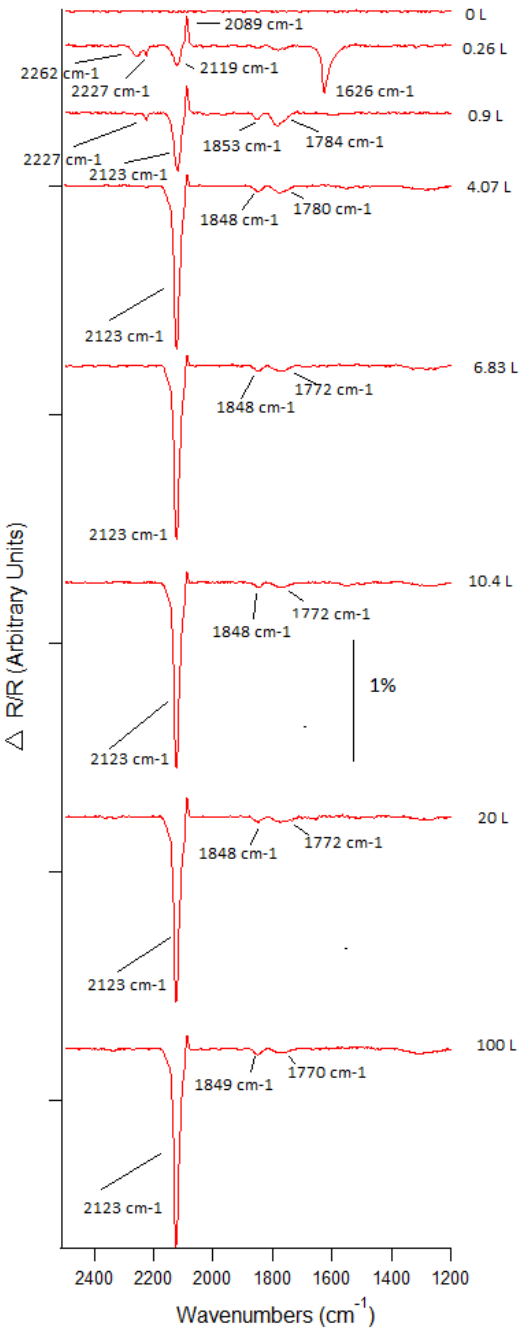

Fig. 4.17 RAIR spectra following the adsorption of NO onto bare Cu{311} at 100 K with increasing exposure.

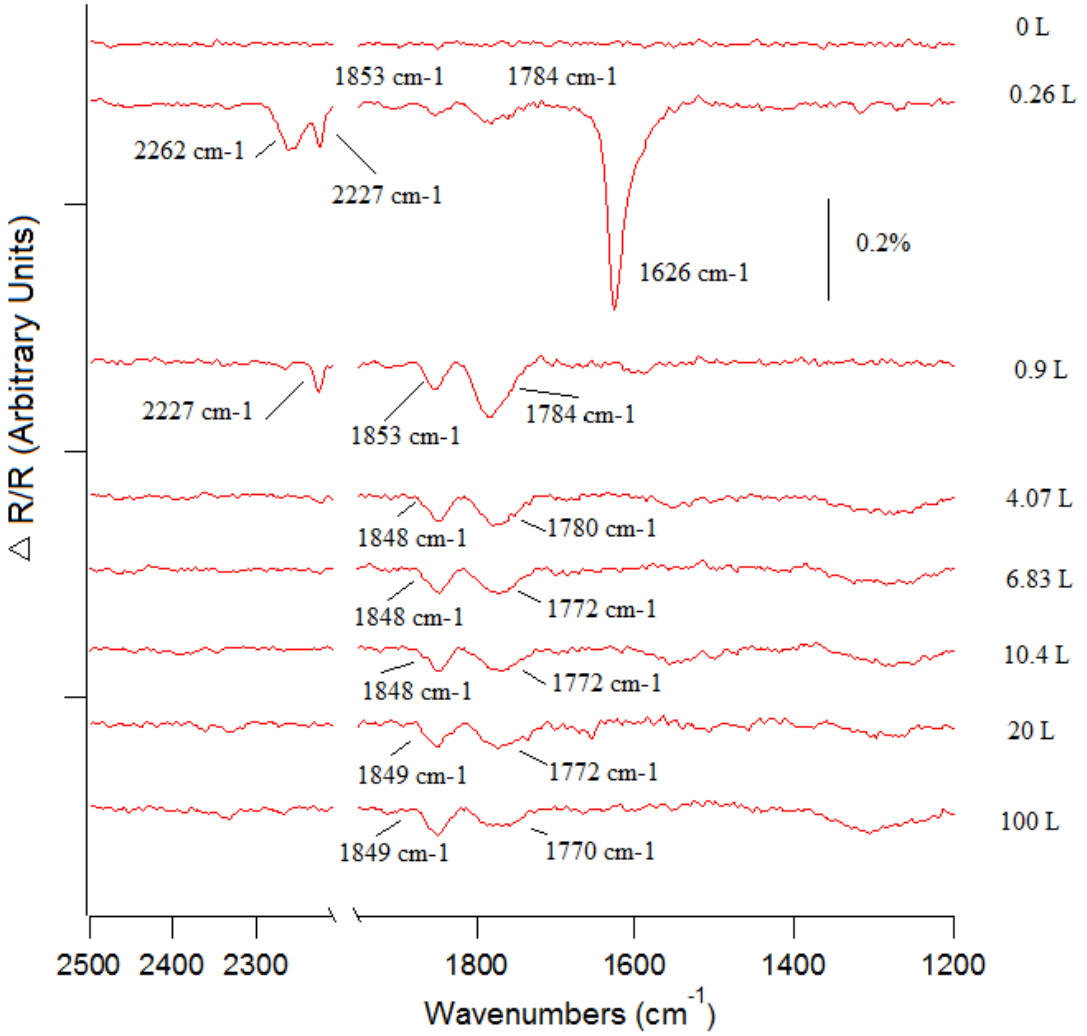

Fig. 4.18 RAIR spectra showing the adsorption of NO onto a bare Cu{311} surface at 100 K, with the prominent CO peak removed to highlight the other peaks present (unaltered spectra is shown in Figure 4.17).

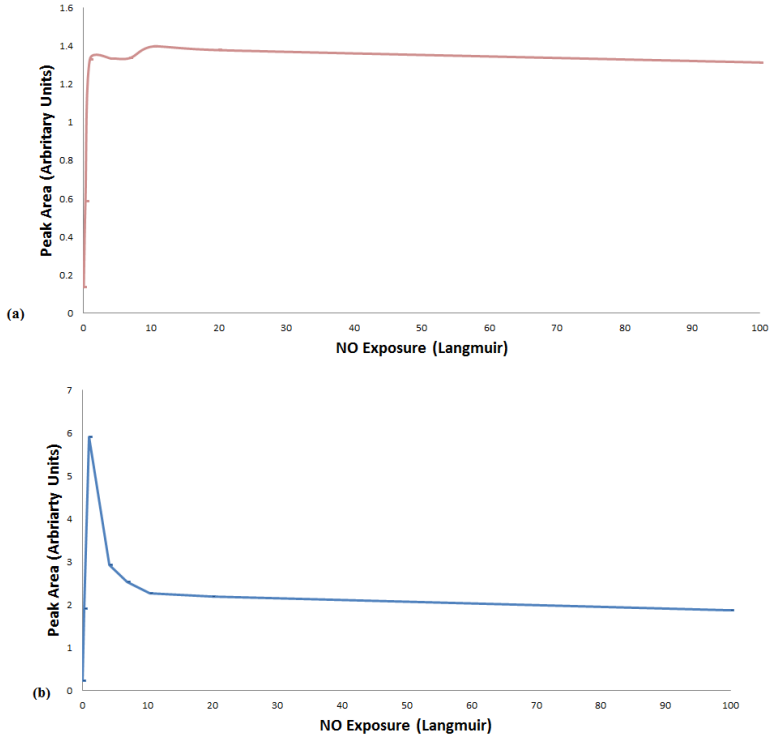

Fig. 4.19 Peak areas for the $(NO)_2$ dimers at high exposures of NO; (a) symmetric stretching mode and (b) antisymmetrical stretching mode with respect to NO exposure onto bare Cu{311} at 100 K.

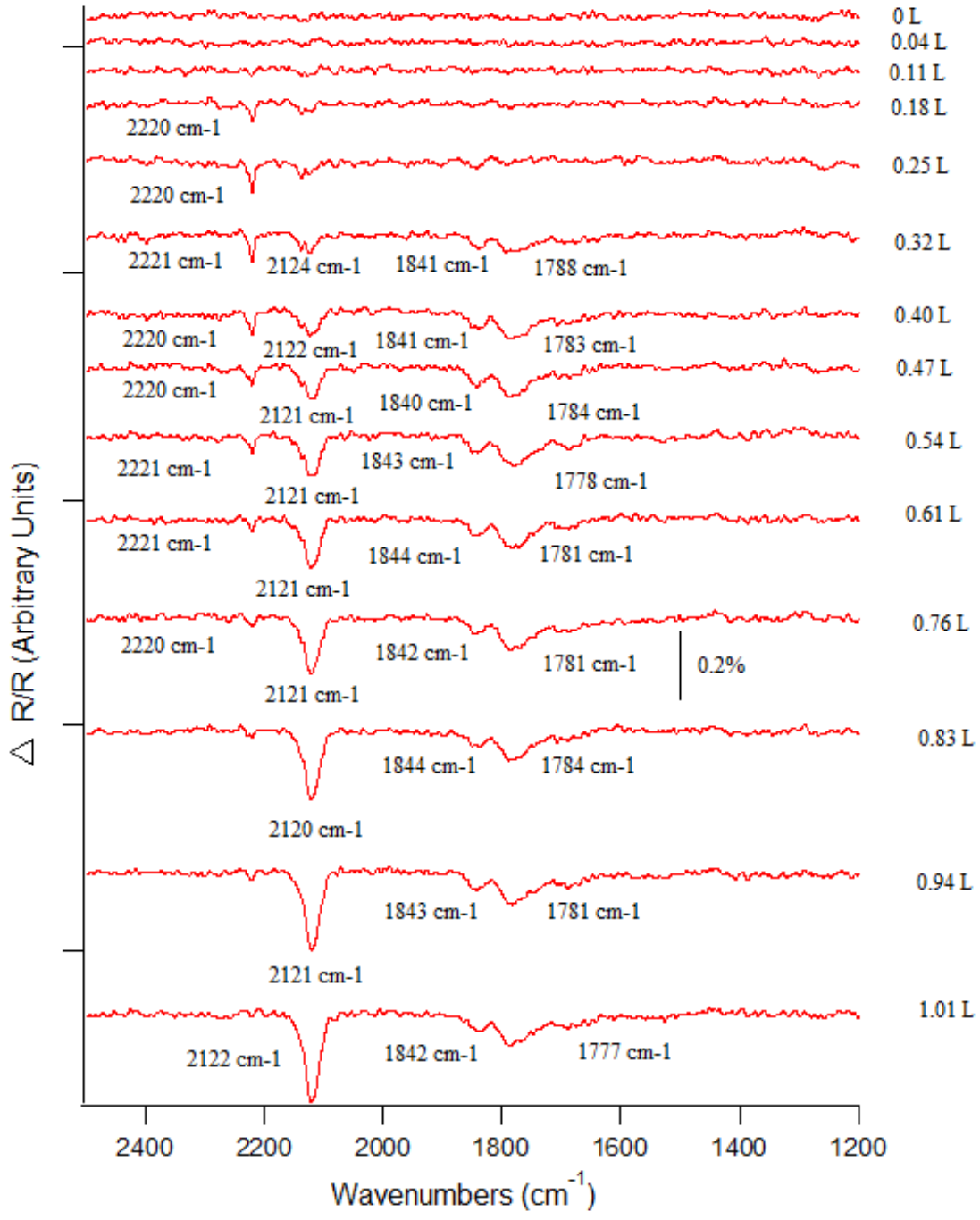

Fig. 4.20 RAIR spectra following the exposure of NO onto the O(1×2) oxygen phase on the Cu{311} surface at 100 K.

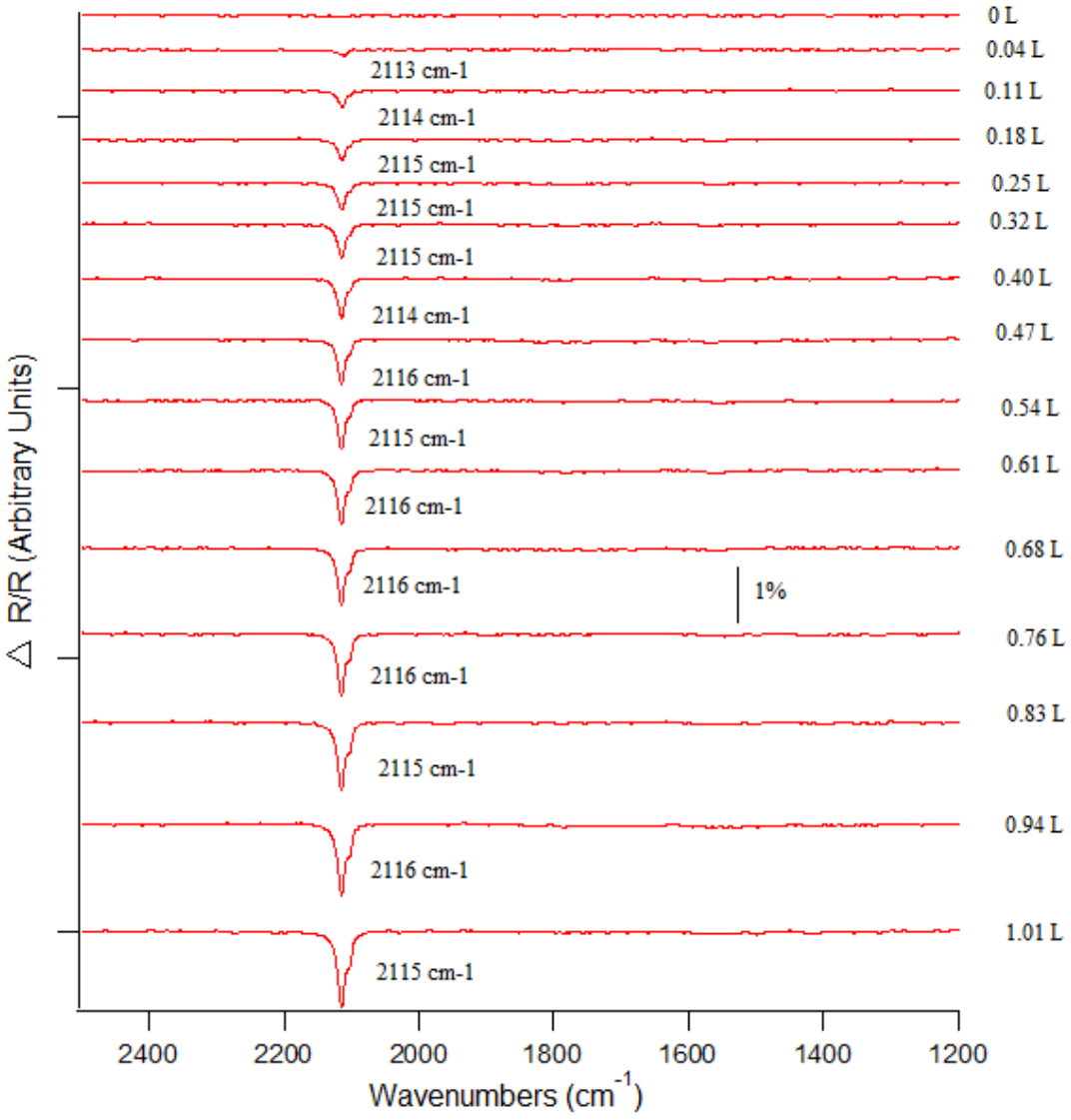

Fig. 4.21 RAIR spectra following the exposure of NO onto the O(Runway) phase of Cu{311} surface at 100 K.

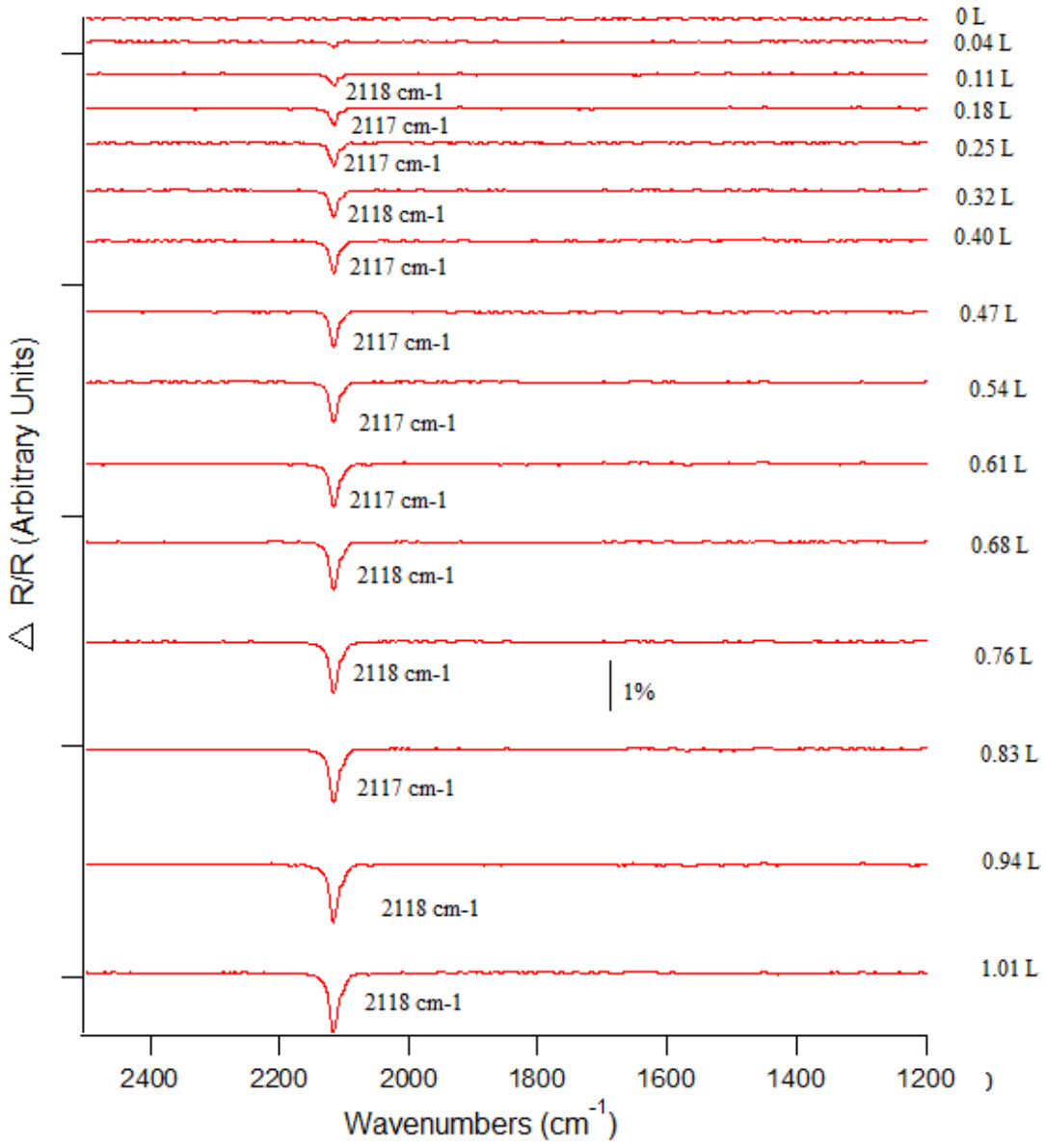

Fig. 4.22 RAIR spectra following the exposure of NO onto the O(Oxide Cluster) phase of Cu{311} surface at 100 K.

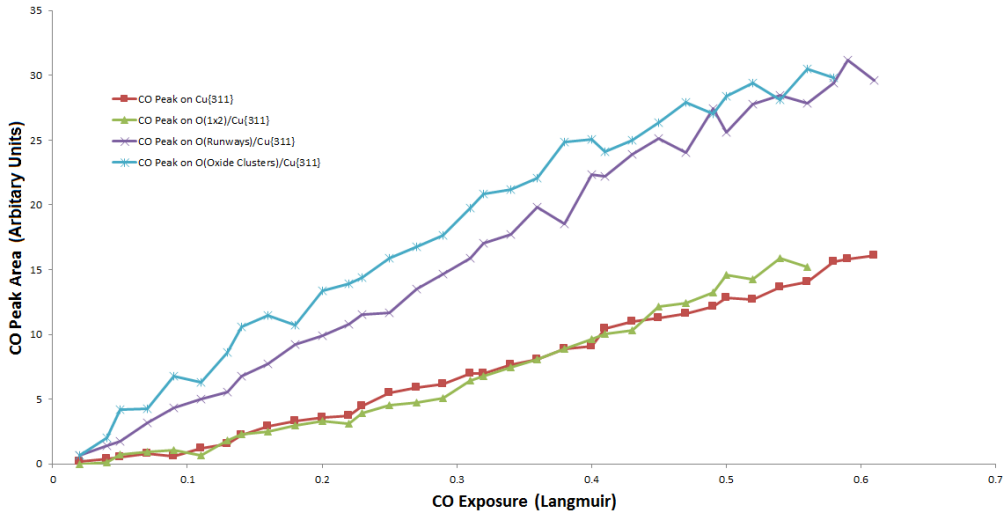

Fig. 4.23 Compilation of multiple experiments showing the CO RAIRS peak area as a function of residual CO exposure for bare and different oxygen pre-covered phases of the Cu{311} crystal. CO, or specifically mass 28 was monitored by the mass spectrometer in parallel with NO during NO exposure.

4.3.3 Temperature Effects

Dosing NO onto the crystal at temperatures above 100 K only show peaks at 1625, 2260, and 2121 cm^{-1}, which have been assigned to the NO on a bridge-site, physisorbed N_2O, and CO species, respectively. An example of the dosing of 1 L of NO onto the bare Cu{311} crystal at 120 K is shown in Figure 4.24.

Figure 4.26 shows the peak area of the NO on the bridge-site after 0.26 L of NO exposure onto the Cu{311} crystal. To examine the effects of temperature, the peaks areas are plotted as a function of both temperature and exposure as seen in Figure 4.26, 4.27, and 4.28.

The NO bridge-site peak has a lower maximum intensity as the temperature of the crystal is increased until it completely vanishes above 150 K (Figure 4.26).

Above 100 K, the peaks for the symmetric and antisymmetric stretching modes of the $(NO)_2$ dimer are not present. However, a peak at 2255-2260 cm^{-1} appears which is attributed to the N-N stretch of the chemisorbed N_2O species. Figure 4.27 shows the change in size of the chemisorbed N_2O peak as a function of both NO exposure and surface temperature. Note that the peak for the corresponding N-N stretch of physisorbed N_2O does not

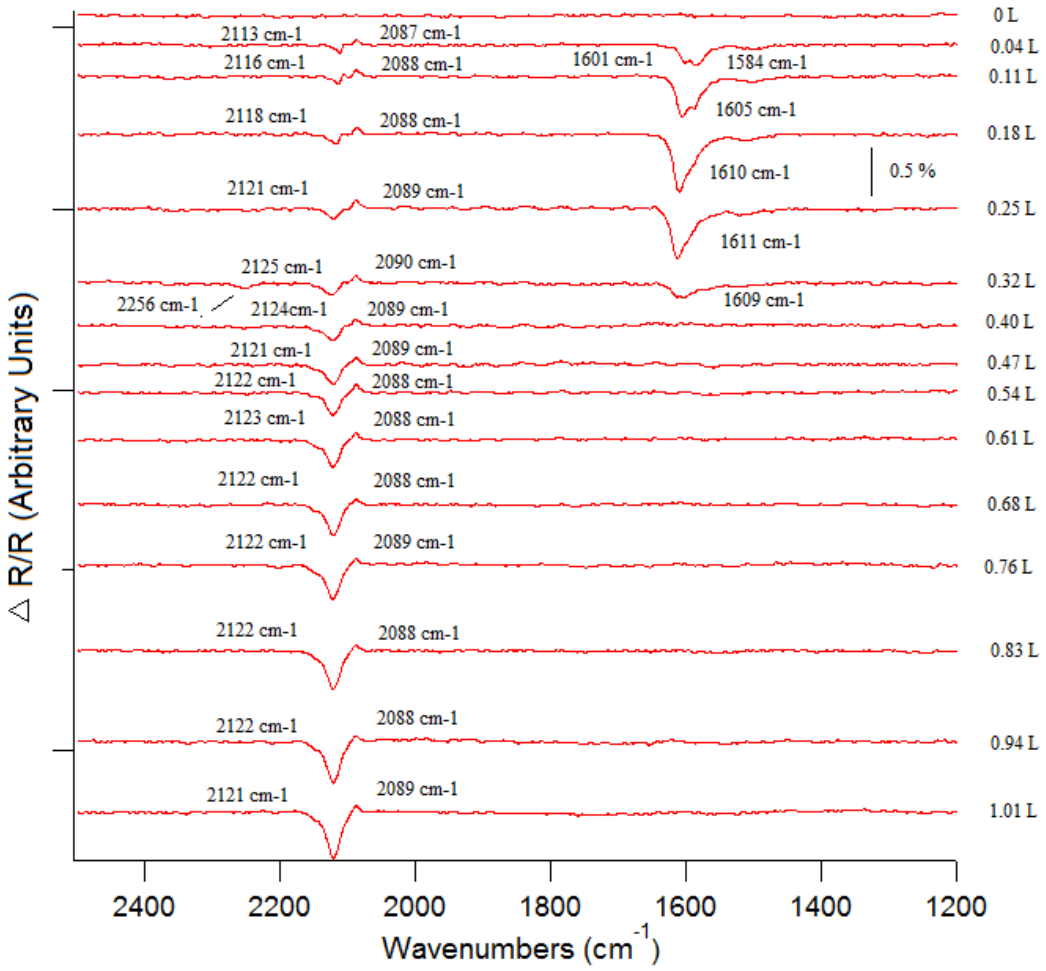

Fig. 4.24 RAIR spectra following the adsorption of NO onto bare Cu{311} at 120 K with increasing exposure.

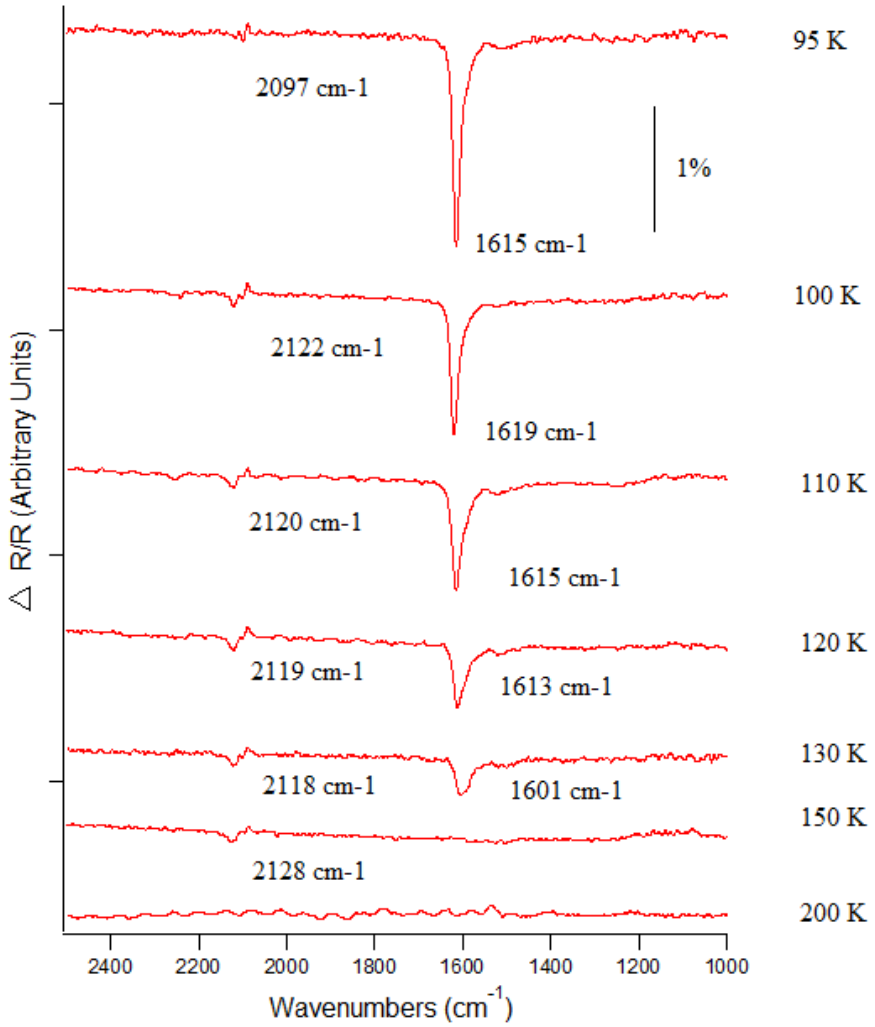

Fig. 4.25 RAIR spectra showing 0.26 L of NO exposure onto different temperatures of the bare Cu{311} surface.

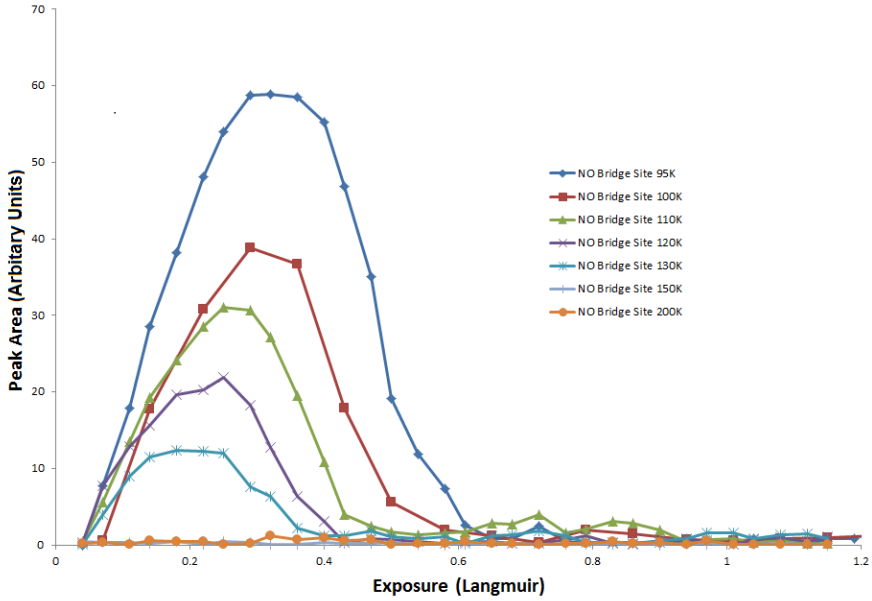

Fig. 4.26 Compilation of the 1618 cm^{-1} RAIRS peak area (assigned to NO bridge site) with increasing NO exposure at various temperatures. All experiments were performed on the bare Cu{311} surface.

appear above 100 K, most likely due to desorption.

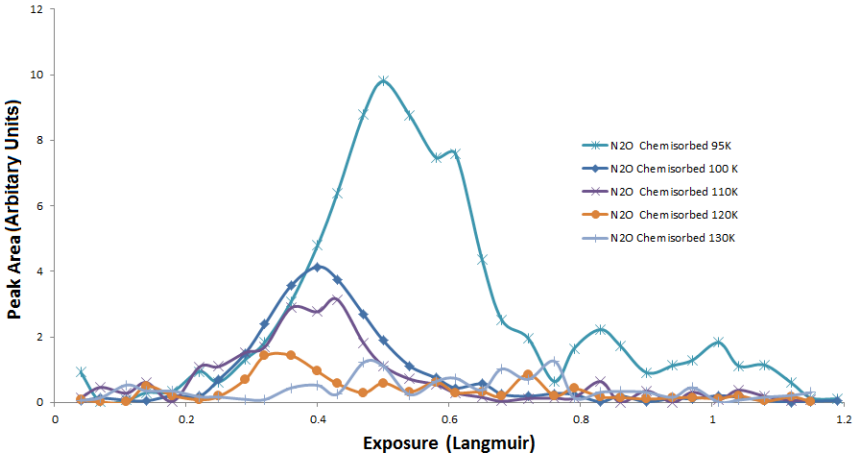

Fig. 4.27 Compilation of the 2251 cm^{-1} RAIRS peak area (assigned to N-N stretch of chemisorbed N_2O) with increasing NO exposure at varying temperatures. All experiments were performed on the bare Cu{311} surface.

The size and rate of increase of the 2121 cm^{-1} peak (which is attributed to CO) does not seem to be directly affected by the temperature below 200 K, above which temperature

it does not appear (Figure 4.28). This is from background CO adsorption, which desorbs from bare Cu{311} at 203 K [88]. This has been discussed in Section 3.3.

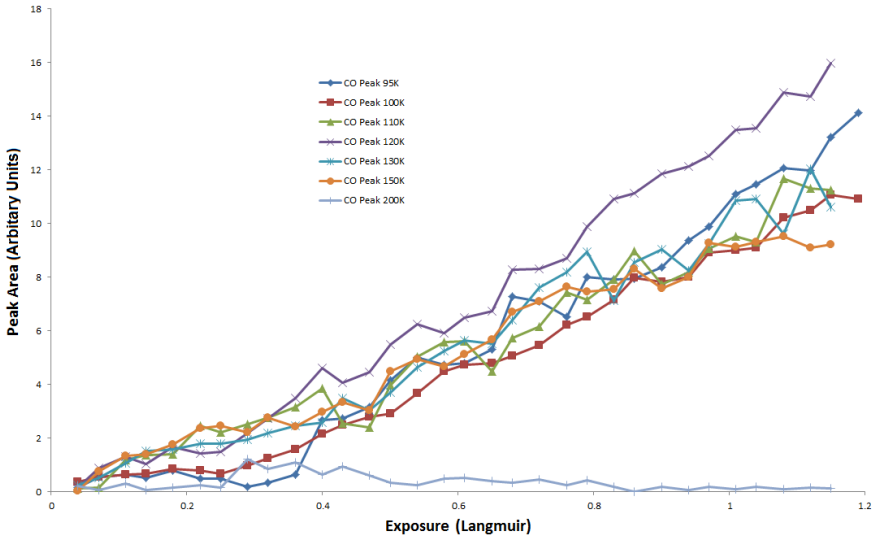

Fig. 4.28 Compilation of the 2120 cm^{-1} RAIRS peak area (assigned to CO) with increasing NO exposure at varying temperatures. All experiments were performed on the bare Cu{311} surface.

4.4 Discussion

4.4.1 RAIRS Analysis

NO Exposure

As NO exposure is increased, the NO bridge-site peak (at 1606 cm^{-1}) area increases until it reaches a maximum at 0.26 L of NO exposure, after which it decreases and vanishes at roughly 0.5 L. At the same NO exposure at which the NO bridge-site peak reaches its maximum, the symmetric and antisymmetric stretching bands for $(NO)_2$ appear. This suggests that NO reacts with itself to form $(NO)_2$ on the bare Cu{311} surface. Based on the behaviour of these peaks, it is therefore thought that when NO is adsorbed onto bare Cu{311}, it readily forms $(NO)_2$ after a coverage threshold (equivalent to an NO exposure of 0.26 L) is passed. This threshold requirement was also proposed by Wendelken *et al* [76].

Our RAIR spectrum is similar to that shown in studies on Cu{100} [82] (Figure 4.6) and Cu{110} [83] (Figure 4.7). Although they used slightly different NO exposures, direct comparisons can still be made. When compared to the Cu{100} surface, the Cu{311} spectra shows a difference in exposures when the peaks reach a maximum but also an additional peak for the physisorbed and chemisorbed N_2O species. These peaks are also seen on the Cu{110} surface spectra (Figure 4.7). The spectrum as NO is exposed to the Cu{110} surface is very similar to our spectrum for Cu{311}, showing the same species although at slightly different NO exposures. It can therefore be concluded that the interaction between NO with bare Cu{311}, Cu{100}, Cu{110} are very similar.

The appearance of the antisymmetric stretching mode is of particular interest as it suggests that the $(NO)_2$ dimer does not simply adsorb onto the surface in the u-shaped configuration. This is because the antisymmetric vibrational mode should be RAIRS inactive; it would only have a dipole moment that is parallel with the surface, making it invisible in the spectra according to the selection rule (explanation of the rule is in Section 2.3). Kim *et al* [82] suggest that the appearance of the antisymmetric band is due to the formation of a multi-layer on the surface. This was inferred from the similar frequency and shape of the peaks to gas phase spectra.

Another possible scenario is that the $(NO)_2$ dimer has a tilt along the horizontal axis of the N-N bond on the surface - a schematic diagram of this is shown in Figure 4.29. This would allow the antisymmetric stretching mode to be RAIRS active, as the tilting would allow it to have non-zero perpendicular dipole moment (with respect to the surface). This could be the result of one of the NO molecules of the $(NO)_2$ dimer sitting bonding to a top-layer surface atom with the other nitrogen bonding to a second-row Cu atom (inside a trough).

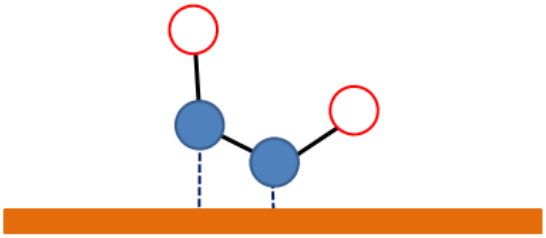

Fig. 4.29 Simple visual representation of the $(NO)_2$ dimer having a tilt along the horizonal axis of the N-N bond.

When considering the two scenarios, the second is more likely. RAIR spectra after dosing a high amount of NO (Figure 4.18) shows that the symmetric and antisymmetric peaks of the $(NO)_2$ dimer stop growing above 3 L. This suggests that the coverage of the dimer reaches a saturation point which would not occur for a multilayer formation of the dimer. It could possibly be argued that the antisymmetric peak is due to a bi-layer, but there is nothing to suggest why the multilayer should not form and therefore that the dimer peaks should keep growing. However, the RAIR peaks show that the symmetric and antisymmetric peaks cease to grow, so it is therefore more likely that the appearance of the antisymmetric band is due to a tilting of the $(NO)_2$ molecule. In addition, the atomic spacing between the Cu atoms on the Cu{311} surface is 0.256 nm, which is just larger than the bond length of gaseous $(NO)_2$ dimer (0.249 nm) - this would allow the two NO molecules to rest on two neighbouring Cu atoms.

It is notable that the antisymmetric $(NO)_2$ peak has a larger peak area than the symmetric peak at low exposures. This difference in size is also seen on the Cu{100} [82] and Cu{110} [83] surfaces. However, with high amounts of NO exposure (10 L), the antisym-

metric peak area halves but the symmetric peak remains the same size (Figure 4.19). This would suggest a reduction in the amount of tilted molecules.

Peaks corresponding to the N-N stretches of physisorbed and chemisorbed N_2O appear at frequencies of 2226 and 2262 cm^{-1}, respectively (Figure 4.16(a)). The N-O stretches of physisorbed and chemisorbed N_2O are also shown in Figure 4.16(b), at frequencies of 1316 and 1263 cm^{-1}, respectively. The chemisorbed species only appears at 0.26 L of NO exposure, while the physisorbed species is present from 0.26 L up to 1.13 L of NO exposure. The disappearance of the peaks is most likely due to desorption of the N_2O molecule as it is displaced, either by NO adsorbing onto the surface, $(NO)_2$ dimers or formation of $O_{(a)}$ on the surface.

It is worth noting that at 0.22-0.38 L, the N_2O peaks are larger than the $(NO)_2$ dimer peaks, which suggests that the reaction to form N_2O from $(NO)_2$ is faster than the formation of $(NO)_2$ from NO although it is not conclusive (as it is not known which species has the higher dynamic dipole moment). As NO exposure is increased, the N_2O peak diminishes, and at the same time the dimer species starts to form (0.38 L). As we know from other Cu surfaces, $O_{(a)}$ is created as a by-product on the surface during NO exposure (due to formation of N_2O) [75, 77, 78]. Therefore, $O_{(a)}$ formation on the surface inhibits both the adsorption of NO and the reaction of the dimer to form N_2O. The lack of any N_2O peaks at higher NO exposure indicates the inhibition of the reaction.

There are two peaks assigned to CO in Figure 4.17: an inverse peak at 2089 cm^{-1} and a much larger peak between 2119 - 2123 cm^{-1}. The inverse peak at 2089 cm^{-1} is most likely due to residual CO adsorbed during the cooling phase of the single crystal preparation (Figure 3.9) and it is inverse due to data processing. The much larger peak is assigned to CO adsorbed near or onto an oxygen species on the Cu{311} surface - the behavior of this peak is show in Figure 4.23. This peak also appears during RAIRS experiments of background CO adsorption onto bare Cu{311} at 100 K (in contrast to deliberate dosing), shown in Figure 3.12. The shift in CO frequency supports the notion that as NO adsorbs and subsequently reacts on the Cu{311} surface, it leaves $O_{(a)}$. The adsorption of CO onto the Cu{311} is explained in more detail in Section 3.3. At high NO exposure, the spectra

only shows a peak for CO, which implies that there is a blocking of the adsorption site for NO and subsequently inhibition of the NO reaction.

NO and Oxygen Phases of Cu{311}

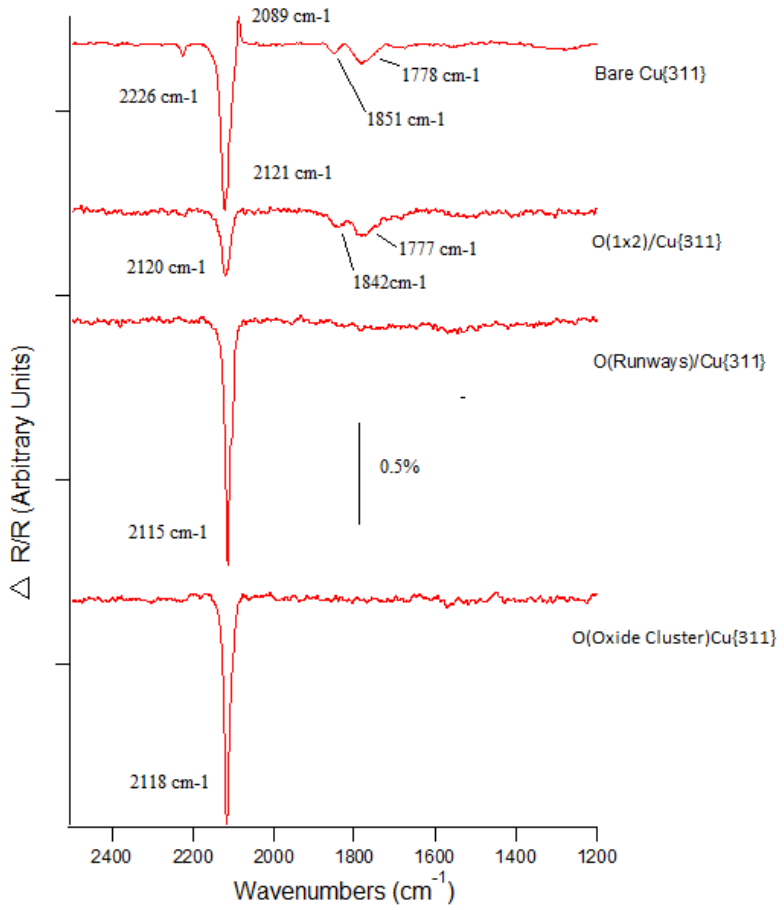

Fig. 4.30 RAIR spectra following the exposure of 1 L of NO onto Cu{311} at 100 K at different oxygen coverage states (oxygen coverage increases going from top to bottom).

Figure 4.30 shows and compares RAIR spectra after 1 L of NO exposure at 100 K onto various oxygen states of the Cu{311} crystal. In general, when NO is dosed onto oxygen pre-covered Cu{311}, the most prominent peak is the CO peak at 2117-2121 cm^{-1}, which can be seen in Figure 4.30. For the O(1×2) phase, there are peaks for physisorbed N_2O, along with the symmetric and antisymmetric stretching peaks of $(NO)_2$ (Figure 4.20). Therefore, it can be seen that the O(1×2) phase allows for the reaction between NO molecules

to form the $(NO)_2$ dimer and N_2O. This is most likely due to the fact that there are still metallic Cu sites available on the O(1×2) phase when compared to the higher oxygen exposures. It is worth mentioning that there are no peaks for the unreacted NO on the surface while there is appearance of peaks for the N_2O species before any $(NO)_2$ dimers form. This suggests that on the O(1×2) phase, NO adsorbs and instantly reacts to form N_2O. Similarly to the bare Cu{311} surface, the N_2O peak diminishes at the same time as the dimer species start to form. This is because of the $O_{(a)}$ formation on the surface which inhibits both the adsorption of NO and the reaction of the dimer to form N_2O.

A direct comparison between the O(1×2) phase and high NO exposure can be made. The behaviour of the $(NO)_2$ dimer and N_2O peaks are very similar. As we know from other Cu surfaces, $O_{(a)}$ is created as a by-product on the surface during NO exposure (due to formation of N_2O). Therefore, the exposure of NO onto a Cu{311} single crystal at high amounts is effectively the exposure of NO onto a O(1×2)/Cu{311} surface due to $O_{(a)}$ build up.

The high oxygen phases (O(Runways) and O(Oxide clusters)) directly inhibits the adsorption of NO or any NO species onto the surface, as the spectra for NO exposure onto them only shows a single peak which corresponds to CO. This is most likely due to the oxide nature of the two oxygen phases. In addition, the two higher oxygen exposure phases have a high oxygen coverage (above 0.70 ML) and have a significantly reduced amount of metallic Cu atoms. This would suggest that adsorption and subsequent reaction of NO requires metallic Cu on the surface, and that oxygen or an oxide inhibits this process. This is similar to the Cu-ZSM-5 catalyst, which is poisoned by oxygen [56, 60, 69].

The variation in CO peak area as a function of NO exposure for various oxidation states of the Cu{311} surface is shown in Figure 4.23. The data shows that there is no direct influence on the adsorption rate of CO onto the surface caused by the O(1×2) structure. Upon adsorption of CO onto the O(Runways)/Cu{311} and O(Oxide Clusters)/Cu{311} phases, there is an increase in the rate of CO adsorption but little difference between the two higher oxygen content phases. It seems that high oxygen pre-coverage phases promotes adsorption of CO onto the surface, while low oxygen pre-coverage (the O(1×2) phase),

inhibits CO adsorption.

There may be some sort of synergetic effect of from the co-adsorption of NO and CO, as the peak areas for CO with NO exposure are slightly larger than from background CO exposure, despite similar conditions (Figure 3.10 and Figure 4.23). This is, however, speculative at best; at higher NO and oxygen pre-dosed experiments there are no peaks associated with NO in the RAIR spectrum. Wee *et al* [89] report that there is minimal interaction between NO and CO on a Cu{100} surface.

Therefore, there is an oxygen coverage effect for the adsorption of CO: below a threshold, oxygen does not influence the adsorption of CO, yet above the threshold, it increases the adsorption. On Cu{110}, Habraken *et al* [90] reported that with low oxygen coverage (the O(1×2) structure), the work function was increased by 370 - 420 meV. Then, as coverage increases (to the c(6×2)O overlayer), the work function decreases by 100 meV. Although this data follows a similar trend, the decrease of 100 meV does not explain why the CO peak after higher oxygen pre-exposures is twice the size of those on the O(1×2) and the bare Cu{311}. It is worth nothing that there may be destabilizing or competitive adsorption between CO and the $(NO)_2$ dimer at low coverage, but this is not possible to infer from the RAIR spectra alone. In contrast, Fu and Somorojai [88] report that a 0.5 monolayer of oxygen coverage on a Cu{311} surface inhibits CO adsorption and do not mention any enhancing effect of oxygen (based on TPD data).

To put the role of oxygen in context of the interaction of NO on the Cu{311} surface, it is seen that oxygen also plays a part in the formation of N_2O from NO. The reaction leaves $O_{(a)}$ as a by-product which itself poisons the reaction. This is evident from RAIR spectra due to the complete lack of peaks apart from that of CO at exposures of NO above 1 L.

Temperature Effects

At higher temperatures, there are only peaks that correspond to NO on a bridge-site, N_2O, and CO. There are two significant changes in the NO bridge-site RAIRS peak (at 1626 cm^{-1}) as dosing temperature is varied. The first is in the size of the peak as temperature increases. Figure 4.31(a) shows the maximum size of the NO bridge-site peak as NO is dosed onto the

bare Cu{311} surface at different temperatures. As the dosing temperature increases, the maximum peak area falls. This can be explained by the fact that higher temperature speeds up the desorption of molecules from the surface after they have bonded or reacted (due to the greater available thermal energy). Therefore, the lower the temperature, the higher the number of adsorbed molecules and therefore the larger the peak size.

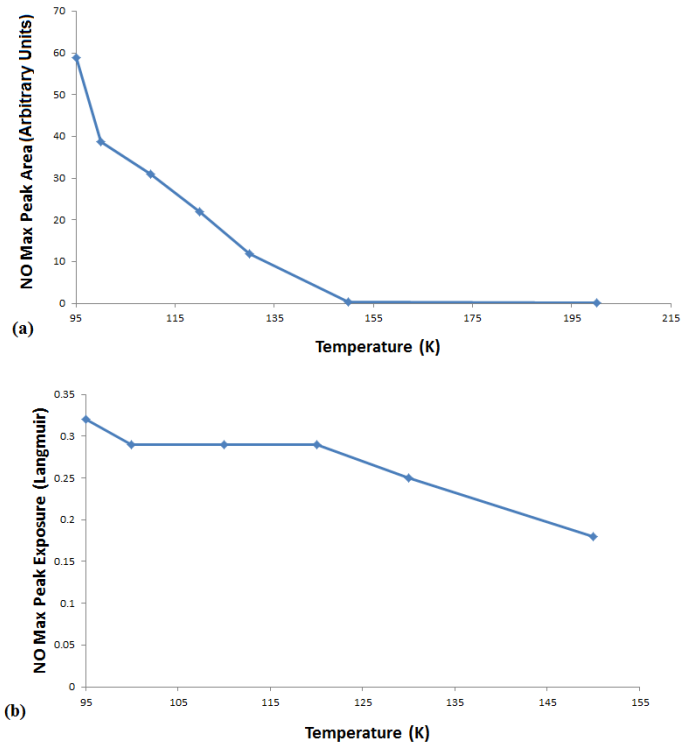

Fig. 4.31 The change in (a) the maximum peak area of the NO bridge-site RAIRS peak (at 1626 cm^{-1}), and (b) the exposure at which this maximum area is reached, at different NO dosing temperatures.

Another change is the exposure at which the NO peak area reaches a maximum shown in Figure 4.31(b). In addition to the effect on size of the maximum peak area, the higher the temperature, the lower the exposure at which this maximum is reached. This is most likely due to the greater available thermal energy at higher temperatures, increasing the rate of diffusion of NO molecules across the surface, which then increases the rate of the reaction to form the $(NO)_2$ dimer.

Figure 4.32(a) shows a similar graph to Figure 4.31(a), but with the peak corresponding

to chemisorbed N_2O instead of that of NO on the bridge-site peak. Again, a larger peak area is seen at a lower temperature. This further suggests that temperature has an affect on the adsorption and desorption of NO and N_2O. In addition, there is a similar shift when the peak reaches a maximum as a function of temperature, similar to the intact NO bridge-site species (Figure 4.32(b)). This implies that temperature similarly affects the mobility of the N_2O molecule, although to a lesser extent (due to less of a temperature change).

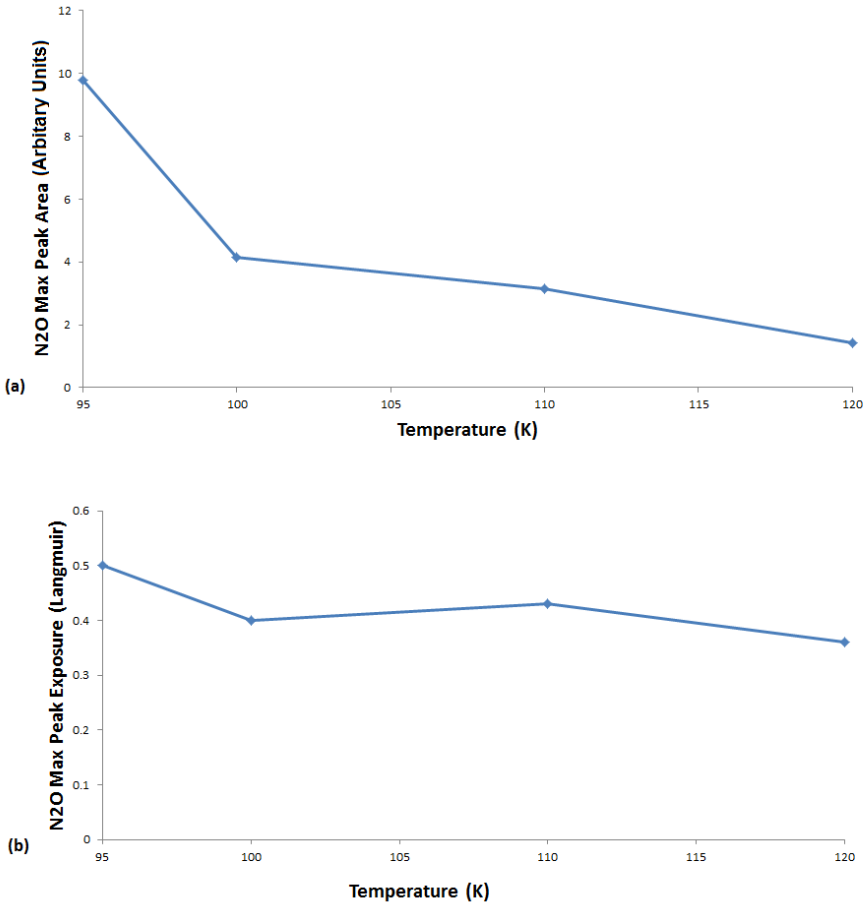

Fig. 4.32 The change in the maximum peak area of the N_2O RAIRS peak at different NO dosing temperatures.

Therefore it seems that temperature plays a role in the desorption and mobility of the NO molecule. At lower temperatures, more NO molecules remain adsorbed on the surface, which act to speed up the reaction. However, the molecules have reduced mobility, which slows down the reaction.

4.4.2 Reaction Mechanism

During the exposure of the bare Cu{311} crystal to NO, the NO RAIRS peak area increases to a maximum at 0.2 - 0.3 L, before decreasing. This increase is due to the adsorption of gaseous NO onto the Cu crystal, creating $NO_{(a)}$. The subsequent decrease suggests that NO reacts faster than it can adsorb (or that adsorption may be inhibited). At a similar exposure to that at which the NO peak starts to decrease (0.3 L), N_2O peaks begin to form. Therefore, it seems that on bare Cu{311}, NO adsorbs as an intact monomer until a threshold coverage (equivalent of 0.2 L of exposure) is reached. At that coverage threshold, there are sufficient nearby adsorbed NO molecules to react to form the $(NO)_2$ dimer, which then forms N_2O. The fact that the NO peak vanishes suggests that the reaction to form N_2O inhibits further NO adsorption on the surface, which is most likely due to $O_{(a)}$ being left behind on the surface after the reaction. The mechanism is shown in the following equations.

$$NO_{(g)} \rightarrow NO_{(a)} \tag{4.14}$$

$$NO_{(a)} + NO_{(a)} \rightarrow (NO)_{2(a)} \tag{4.15}$$

$$NO_{2(a)} \rightarrow N_2O_{(a)} + O_{(a)} \tag{4.16}$$

$$N_2O_{(a)} \rightarrow N_2O_{(g)} \tag{4.17}$$

The role of oxygen in this process is that of an inhibitor: As N_2O forms from the dimer and desorbs, it leaves $O_{(a)}$ on the surface as a by-product, where it acts as an inhibitor in a self poisoning reaction. This oxygen inhibition process is confirmed by pre-adsorbed oxygen experiments. It can be seen from the RAIR spectra (Figure 4.20) that dosing NO onto O(1×2) is similar to dosing NO at higher exposures. At the higher oxygen phases (runways and oxide clusters, Figure 4.30), there is effectively no NO adsorption or reaction taking place on the Cu{311} surface. This means that an oxide-like surface inhibits the

reaction and NO requires metallic Cu to adsorb and react onto.

Temperature primarily affects the desorption of molecules from the surface along with mobility of the NO molecule. There are two conflicting effects of temperatures. At lower temperatures, more NO molecules remain on the surface which speeds up the reaction for N_2O formation. However, these molecules then have reduced mobility, which slows down the reaction.

4.5 Conclusion

The RAIR spectra shown in this Chapter provide evidence for $(NO)_2$ dimer formation on the Cu{311} surface as NO is dosed. Therefore, the mechanism behind N_2O formation on the Cu{311} is via the dimer pathway. The mechanism is similar to that indicated by work done on Cu{110} [82, 83]. The process is inhibited by oxygen on the surface - either from pre-dosing or from the reaction by-product.

The mechanism is different to that on catalysts such Cu-ZSM-5, where after exposure of the catalyst to NO, the reaction only slows down due to the oxygen being produced but does not completely cease like on Cu{311}. As mentioned in the literature, this could be because of the reforming of reaction sites by the side reaction to produce N_2O at higher temperatures [61]. In the context of SCR, the work in this chapter has shown that metallic Cu is extremely active for the reaction to form N_2O from NO, but requires a process to restore the catalytically active site. This process could be mediated by the support or reaction with NH_3. The interaction of Cu{311} and NH_3 is studied in Chapter 5.

Chapter 5

NH_3 and Cu{311}

5.1 Literature Review

5.1.1 Surface Science Studies of NH_3

As described in Chapter 1, the reduction of NO using NH_3 has attracted a great deal of interest, because of concern about the environmental effects of NO and new regulations enforcing the reduction of emissions from cars. The interaction of NH_3 with single crystals has been widely studied in surface science. There are multiple reviews studying the oxidation of NH_3 in the context of selective catalytic reduction [57, 91–94]. A wide range of metallic surfaces have been studied, including Pt, Ir, Fe, Ni, and Cu [95–101]. Various techniques have been used, including ultraviolet photoelectron spectroscopy (UPS), Secondary ion mass spectrometry (SIMS), X-ray photoelectron spectroscopy (XPS), electron energy loss spectroscopy (EELS), temperature programmed desorption (TPD), reflection-absorption infrared spectroscopy (RAIRS), low energy electron diffraction (LEED), and density functional theory (DFT).

For many of the transition metal single crystals, NH_3 adsorbs intact onto the surface at low temperatures under ultra high vacuum conditions. The molecule adsorbs with a near vertical three-fold rotational axis, with the nitrogen atom bonding directly to the metal atom. The hydrogen atoms are situated away from the surface, creating an umbrella-like configu-

ration. The nitrogen-metal bond is a mixture of the donation of the nitrogen's lone electron pair, and an electrostatic component (which involves the nitrogen's permanent dipole and an induced dipole on the surface) [102].

Some of the earliest surface science studies with NH_3 and a metal are with Fe. It has been reported using both UPS [103] and SIMS [104] that on an Fe{110} surface, NH_3 adsorbs intact below room temperature. NH_3 causes the work function of the surface to decrease, with a maximum reduction of 2.4 eV (at saturation coverage), consistent with donation of electrons to the surface. At 350 K, there is dissociation of NH_3 which causes the formation of a stable $NH_{(a)}$ (2×2) structure along with the desorption of H_2 at 400 K [105].

Figure 5.1 shows EEL spectra from work done by Erley and Ibach [98]. The spectra show that at 120 K, NH_3 adsorbs intact onto Fe{110} at 0.05 L of exposure. At 0.05 L, the EEL spectra shows peaks for the NH_3 symmetric deformation mode (1170 cm^{-1}) and Fe-N stretching mode (350 cm^{-1}). As exposure is increased, a peak at 1640 cm^{-1} forms which has been assigned to the antisymmetric deformation mode of NH_3. Erley and Ibach assign the 1450 cm^{-1} peak, which appears at high exposures, to the combination of the peaks at 350 cm^{-1} and 1105 cm^{-1}. However, no peaks for NH_2 (eg. the scissor mode at 1600 cm^{-1}) or NH (inferred to be obscured by the vibrational frequency of NH_3 at 510 cm^{-1}) were reported. The lack of peaks for any dissociated species indicates that NH_3 adsorbs intact onto the Fe{110} surface at 120 K.

Figure 5.2 shows EEL spectra after an Fe{110} surface with 3 L of NH_3 exposure is heated [98]. At 195 K, the EEL spectrum shows the formation of a new vibrational loss peak at 1590 cm^{-1} which is assigned to NH_2. In addition, we see the electron loss peak at 500 cm^{-1}, which was inferred by Erley and Ibach to be the fragmentation of NH_3 into different, unassigned species. This shows that there is dissociation of NH_3 into NH_2 and other species on Fe{110} at higher temperatures. When it is further heated to 315 K, peaks assigned to the dissociated species disappear. This could be due to the recombination and subsequent desorption of the species.

Similarly, on Ni{110}, NH_3 adsorbs intact below 150 K, but decomposes to form NH_2 or NH above 150 K [99]. This can be seen in the XP spectra as Ni{110} is exposed to NH_3

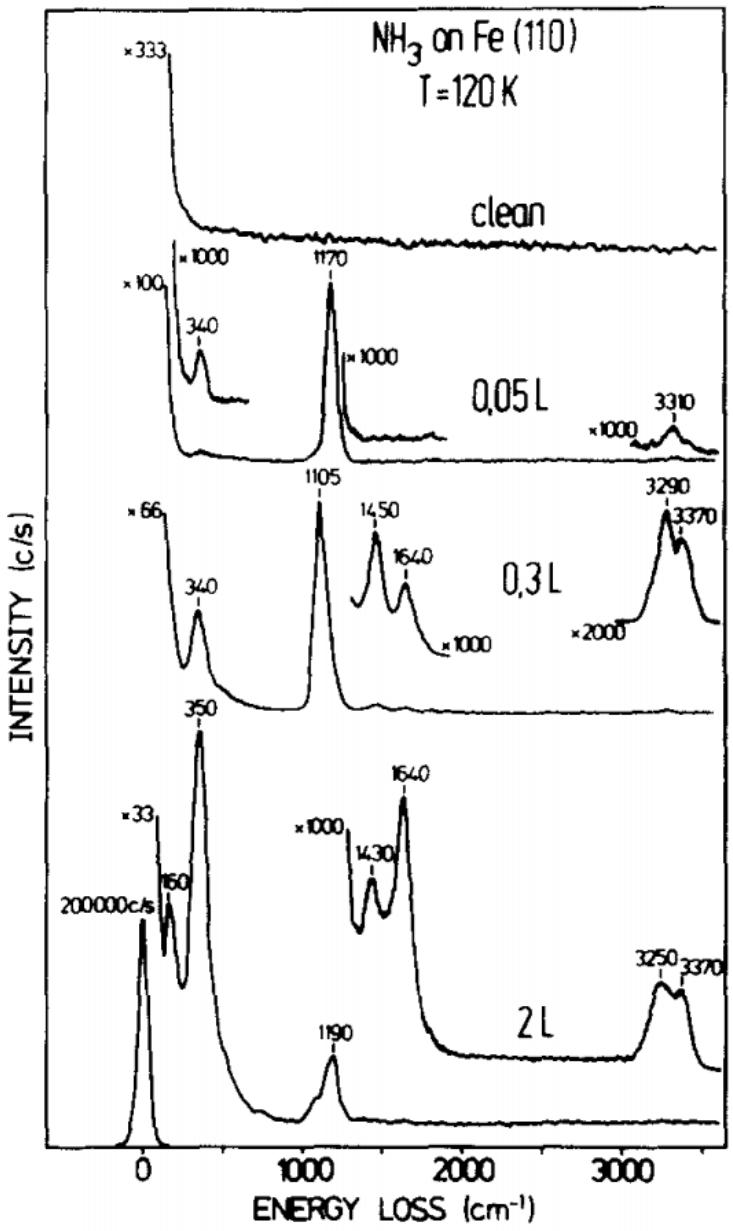

Fig. 5.1 EEL spectra of Fe{110} after three different exposures of NH_3 at 120 K. (Erley and Ibach [98])

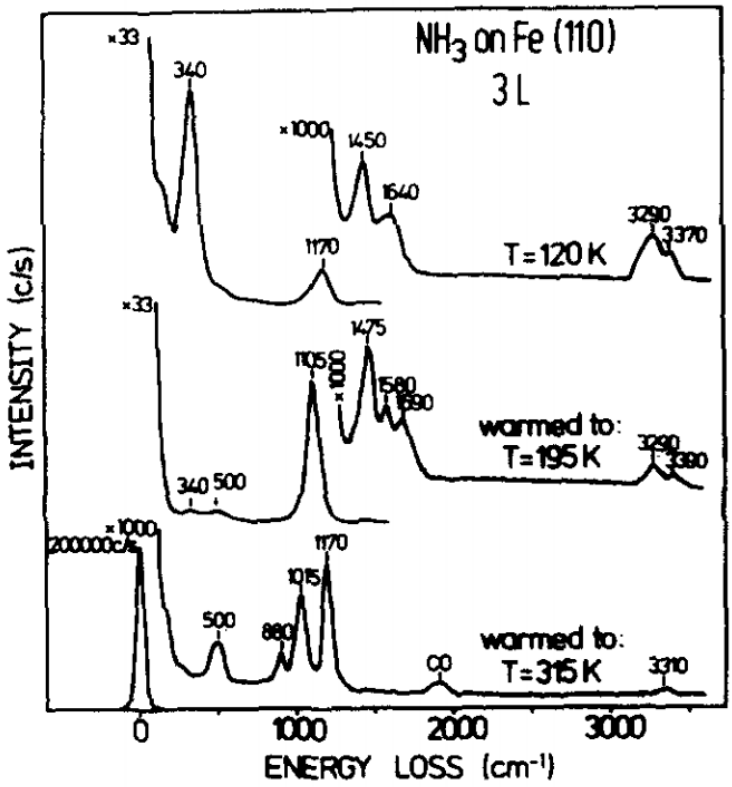

Fig. 5.2 EEL spectra after the exposure of Fe{110} to 3 K of N_3 at 120 K (top most spectra) along with subsequent heating to 195 and 315 K. (Erley and Ibach [98])

(Figure 5.3). The 400.9, 397.4, and 398.0 eV peaks have been assigned to nitrogen atoms in $NH_{3(a)}$, $NH_{2(a)}$, and $NH_{(a)}$, respectively. Initially the XP spectra show the adsorption of a single peak assigned to NH_3 on the Ni{110} surface. As the temperature is increased, there is a reduction in the size of the original $NH_{3(a)}$ peak but the development of peaks assigned to $NH_{2(a)}$ and $NH_{(a)}$. This is similar to that which has been reported on Fe{110}, where NH_3 adsorbs intact at low temperatures but dissociates at higher temperatures.

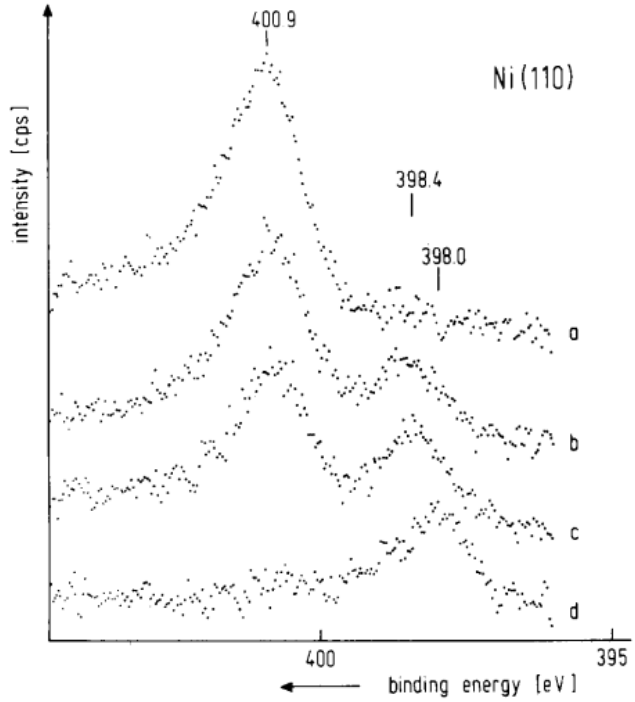

Fig. 5.3 XP spectra as NH_3 is adsorbed onto a Ni{110} single crystal. (a) is the adsorption of 0.75 L of NH_3 at 110 K, (b) is the system heated to 191 K, (c) is the the system heated to 226 K and (d) is the desorption of hydrogen after the system is heated to 426 K. (Grunze *et al* [99])

Calculations done by Chattopadhyay *et al* [100] found that when NH_3 adsorbs onto bare Ni{111}, it adsorbs onto the atop, bridge, and threefold site with similar stability (with adsorption energies of 19, 17, and 18 kcal/mol respectively). The molecule is oriented with the N atom bonded to the Ni atom, with the hydrogen atoms pointing away with respect to the surface, and the H-N-H angle being $108(\pm 2)^\circ$.

Often the behaviour of gas molecules on Cu and Ag surfaces is so a direct comparison

can be made. In addition, a comparison can be made between that way that NH_3 interacts on Ag{110} and on Ag{311}, analogous to the comparisons made in this thesis between Cu{110} and Cu{311}. This is done by examining the EEL spectra when NH_3 is dosed onto both surfaces (Figure 5.4).

Figure 5.4(a) shows EEL spectra as the Ag{110} surface is exposed to NH_3 at 100 K [106]. The spectra show the appearance of peaks at 1050 and 1640 cm^{-1}, which are assigned to the symmetric and antisymmetric deformation modes of NH_3, respectively. The other two peaks at 430 and 3400 cm^{-1} have been assigned to Ag-N and N-H, respectively. The appearance of these peaks and lack of peaks for any fragmented species indicates that NH_3 adsorbs intact onto the Ag{110} surface at 100 K.

The interaction of NH_3 with Ag{311} [107] is very similar to that of Ag{110}, with an almost identical EEL spectrum. Figure 5.4(b) shows the EEL spectra of the Ag{311} surface as it is exposed to NH_3 [107]. The 1100 and 1648 cm^{-1} peaks have again been assigned to the symmetric and antisymmetric deformation mode of NH_3, respectively. The 470 and 3410 cm^{-1} peak are also assigned to the Ag-N and N-H stretching modes, respectively. The peak at 260 cm^{-1} is assigned to the wagging mode of adsorbed NH_3. The EEL spectra shows that NH_3 adsorbs intact onto the Ag{311} surface at 100 K, very similarly to its adsorption onto Ag{110} [106]. It is worth noting how the EEL spectra for NH_3 on Ag{110} and Ag{311} are almost identical, suggesting relatively limited effects of surface orientation on the adsorption of NH_3 between the two surfaces.

TPD experiments on Ag{110} performed by Thornburg and Madix [108] show that the first layer of ammonia desorbs from the surface at 180 K, while the second layer desorbs at 122 K, and the multilayer at 109 K. Ceyer and Yates [107] report a similar behaviour for TPD experiments on Ag{311}. They showed that on the Ag{311} surface, the first layer desorbs at 230 K, the second layer at 160 K, and the multilayer at 120 K. Despite the previously mentioned similarity, TPD experiments indicate that NH_3 binds more strongly to Ag{311} than to Ag{110}.

When oxygen is pre-adsorbed onto metallic surfaces, the interaction between NH_3 and the surface can change. In general, oxygen causes the dissociation and / or dehydrogena-

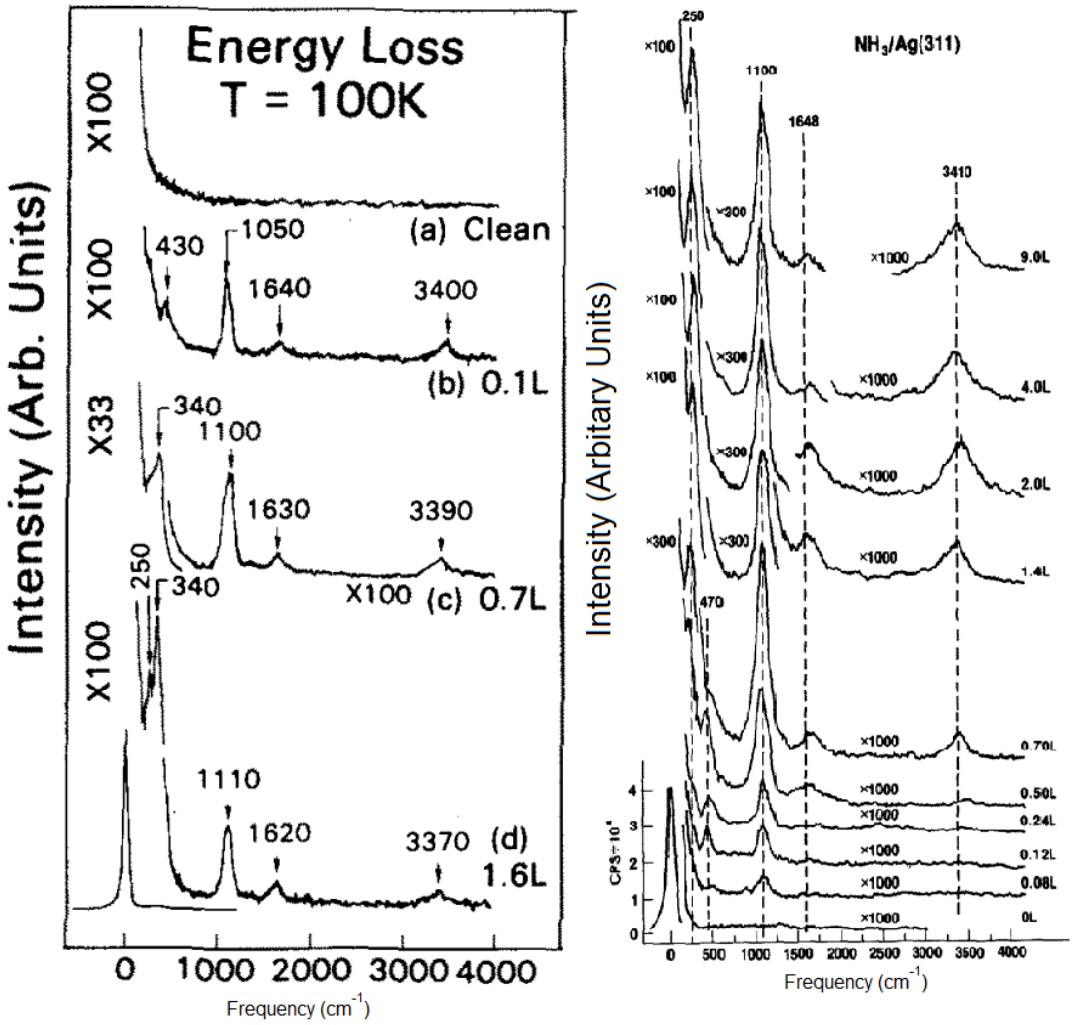

Fig. 5.4 Comparison of the EEL spectra after the adsorption of NH_3 onto (a) Ag{110} (Gland *et al* [106]) and (b) Ag{311} (Ceyer and Yates [107]) single crystal at 100 K.

tion of the NH_3 molecule. On Ag{110}, when ammonia and oxygen are co-adsorbed at 105 K, adsorbed hydroxyl and NH_X species are reported [108]. Ag does not directly de-hydrogenate NH_3, and the hydrogen transfer is direct from the nitrogen to the oxygen atom. When NH_3 is dosed onto the oxygen pre-covered Ag{110} surface and the system is heated to 400 K, NO and N_2 desorb from the surface, indicating a reaction between NH_3 and oxygen. Vibrational spectroscopy shows that NH groups persist on the surface at 310 K and possibly at significantly higher temperatures, indicative of the difficulty of N-H bond cleavage by metallic silver [108].

NH_3 and Cu Single Crystals

The mechanism of NH_3 adsorption onto bare Cu surfaces has been widely studied using EELS, LEED, XPS, DFT, and RAIRS [101, 109–113]. On Cu single crystals, NH_3 is seen to adsorb intact onto the Cu atop site at temperatures below 150 K. NH_3 does not readily dissociate on bare Cu surfaces and simply desorbs when temperature is increased.

Figure 5.5(I) shows EEL spectra following the adsorption of NH_3 onto bare Cu{110} at 170 K [109]. The spectra show electron losses for the symmetric deformation peak at 1150 cm^{-1} and antisymmetric deformation peak at 1600 cm^{-1}. When 0.5 ML of oxygen is pre-adsorbed onto the Cu{110} surface, there is very little change in the adsorption of NH_3, as shown in Figure 5.5(II). The peaks slightly shift in frequency from 1150 to 1195 cm^{-1} and 1600 to 1630 cm^{-1} for the symmetric and antisymmetric deformation modes, respectively. This suggests that at low temperatures and under ultra high vacuum conditions, NH_3 does not dissociate on either Cu{110} or oxygen pre-covered Cu{110}. The relatively smaller size of the NH_3 peaks on the oxygen pre-covered surface may indicate a site-blocking or repulsion effect of oxygen on NH_3 adsorption.

XPS studies by Afsin *et al* [111] reported that an intact NH_3 species adsorbs onto the bare Cu{110} surface and desorbs completely by 200 K, showing no peaks associated with fragmentation. However, the authors also reported peaks for $NH_{2(a)}$, $NH_{(a)}$ and $N_{(a)}$ at 400 K when oxygen is pre-adsorbed, thereby suggesting that the O/Cu{110} surface can dissociate NH_3 at higher temperatures. The authors also note how the de-hydrogenation

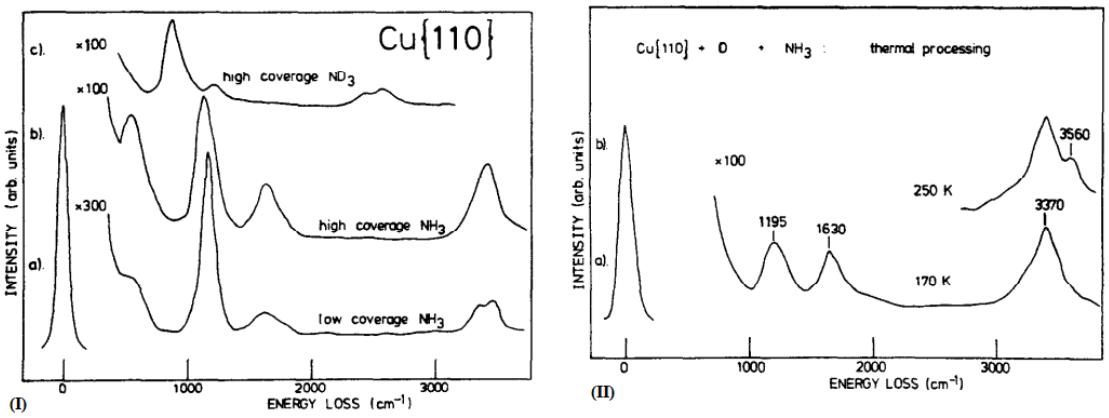

Fig. 5.5 EEL spectra showing the adsorption of NH_3 onto (I) bare and (II) oxygen pre-covered Cu{110} at 170 K. (I)(a) of 0.05 L of NH_3, (b) 1 L of NH_3, and (c) 1 K of ND_3 exposure. (II)(a) half a monolayer of oxygen pre-adsorbed followed by adsorption of 1 L of NH_3 (II)(b) heating of the surface to 250 K in the presence of one third of a monolayer of oxygen. The spectra was recorded with a specular direction at E_p = 5.0 eV, $\alpha = 45^o$. (Lackey et al [109])

process occurs more readily when there is a low amount of oxygen on the surface (0.1 ML), but is slowed when there is very high oxygen coverage (close to 1.0 ML).

STM studies by Guo and Madix [114] suggest that dehydrogenation of NH_3 only occurs if NH_3 is adsorbed onto a clean metallic Cu atom next to a Cu-O species (the Cu-O species is from the boundaries of the -Cu-O- rows or from isolated Cu-O species). Therefore, NH_3 dehydrogenation does not occur when the Cu surface is completely bare or fully oxidised. Thus the role of oxygen on Cu{110} is both as an inhibitor of NH_3 adsorption but also as a promoter of NH_3 dissociation.

FTIR studies under non-UHV conditions dosing with pressures in the order of 10^{-5} mbar have been conducted [101, 113]. When NH_3 is dosed at 10^{-5} mbar onto bare Cu{110}, the spectra only show the appearance of the symmetric deformation mode of NH_3 at 1200 cm^{-1} (Figure 5.6(a)). The oxygen pre-covered Cu{110} surface shows a reduction of the NH_3 peak under similar conditions, suggesting a site blocking effect of oxygen (Figure 5.6(b)), while the co-adsorption of O and NH_3 at room temperature show peaks for NH_2 (1540 cm^{-1}) and NH (1430 cm^{-1})(Figure 5.6(c)). Therefore, it can be inferred that at higher pressures and / or higher temperatures, oxygen pre-covered Cu surfaces cause decomposition (eg.

dehydrogenation) of NH_3.

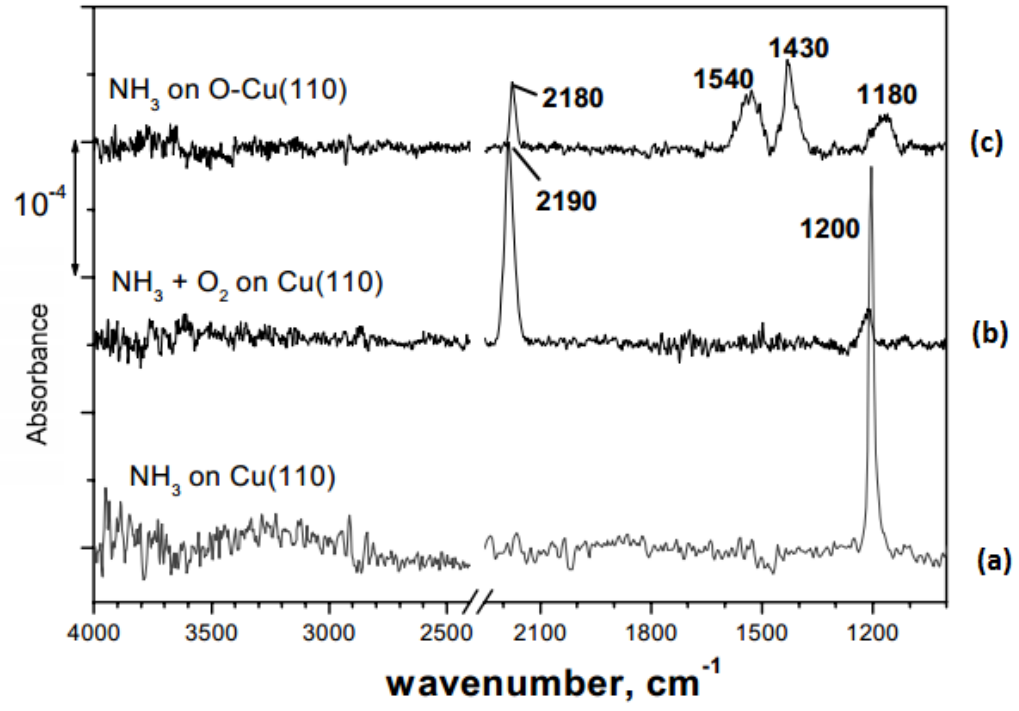

Fig. 5.6 FTIR spectra of the adsorption of NH_3 onto Cu{110} at 300 K after 50 minutes of exposure (with varying pressures). (a) is purely NH_3 with a P_{NH3} of 10^{-5} mbar. (b) is NH_3 and O_2 co-dosing with $P_{NH3} = P_{O2} = 10^{-5}$ mbar. (c) is O - c(6x2)/Cu{110} with NH_3 at P_{NH3} of 10^{-5} mbar. (Louis-Rose *et al* [113])

Therefore, it can be concluded that NH_3 adsorbs intact onto Cu{110} at low temperatures, as inferred from the appearance of EEL peaks for the symmetric and antisymmetric deformation mode of NH_3 at 1150 and 1620 cm^{-1}, respectively. At low temperatures, oxygen does not significantly alter the chemistry between NH_3 and Cu{110} and most likely only inhibits the adsorption of NH_3. However, at temperatures above 300 K, it is speculated that oxygen pre-coverage causes the dehydrogenation of NH_3 to form NH_2 and NH species (with vibrational frequencies at 1540 and 1430 cm^{-1}, respectively).

Figure 5.7 shows the 4 vibrational modes for NH_3 that are referred to extensively in this Chapter to illustrate and interpret the IR data. Table 5.1 shows a compilation of EELS and RAIRS data for the adsorption of NH_3 onto various metal surfaces and their oxides.

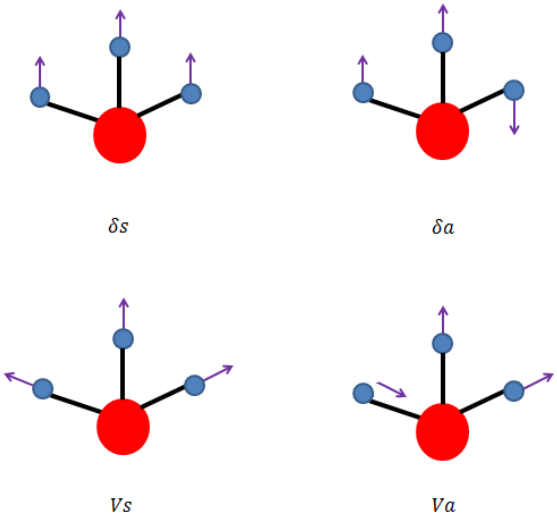

Fig. 5.7 The vibrational modes of NH_3. Clockwise from the top left: symmetric deformation mode, two antisymmetric deformation modes, symmetric stretching mode, and two antisymmetric stretching modes.

Table 5.1 NH_3 RAIRS Peak Assignments

Surface	Reference	δ_s	δ_d	ν_s	ν_d
Ni(110)	[115, 116]	1120	1580	3200	3350
O/Ni(110)	[116]	1160	1632	3328	3328
Ni(111)	[115]	1140	1580	3270	3360
Pt(111)	[96]	1140	1600	3240	3340
Cu(110)	[109]	1150	1600	3360	3430
O/Cu(110)	[109]	1195	1630	3370	3370
Ag(110)	[106]	1050	1640	3320	3400
O/Ag(110)	[108]	1060	1640	3280	3370
Ag(311)	[107]	1100	1648	3410	3410
Gas	[117]	950	1628	3337	3414
Liquid	[118]	1032	1628	3250	3382
Solid	[117, 119]	1060	1646	3223	3378

5.2 Experimental

The experimental set-up used for studying Cu{311} and NH_3 is similar to that used for the work done with NO, as described in Chapter 4.

The Cu{311} crystal was cleaned before experiments using Ar ion sputtering, and was then annealed to 900 K to re-order the surface. NH_3 was then leaked into the chamber at a desired pressure, which was constantly monitored by the ion gauge.

As NH_3 was leaked into the chamber, RAIRS was used to monitor the surface species as a function of exposure. Varying pressures and dosing times were used to examine any effects of coverage and time of exposure. Afterwards, various temperature experiments were performed.

After the interaction of NH_3 and bare Cu{311} was examined, oxygen pre-adsorbed Cu{311} was studied by varying the oxide structure as described in Chapter 3. Similar experiments to those run on bare Cu{311} and NH_3 were performed on various O/Cu{311} surfaces.

More details of the experimental conditions and set-up can be found in Chapter 2.

5.3 Results

5.3.1 NH_3 and Bare Cu{311}

Similarly to in Chapter 4, the RAIRS peaks have been assigned by comparison to work done on similar surfaces. For many of the peaks, the comparison is to work done on Cu{110} by Lackey *et al* (Figure 5.5 [109]), summarised in Table 5.2.

Table 5.2 NH_3 RAIRS peak assignments [104]

Mode	NH_3/Cu{110}	NH_3 Gas	NH_3 Solid
δ_s(HNH)	1130	950	1060
δ_d(HNH)	1600	1628	1646
ν_s(NH)	3400	3337	3223
ν_d(NH)	3400	3414	3378

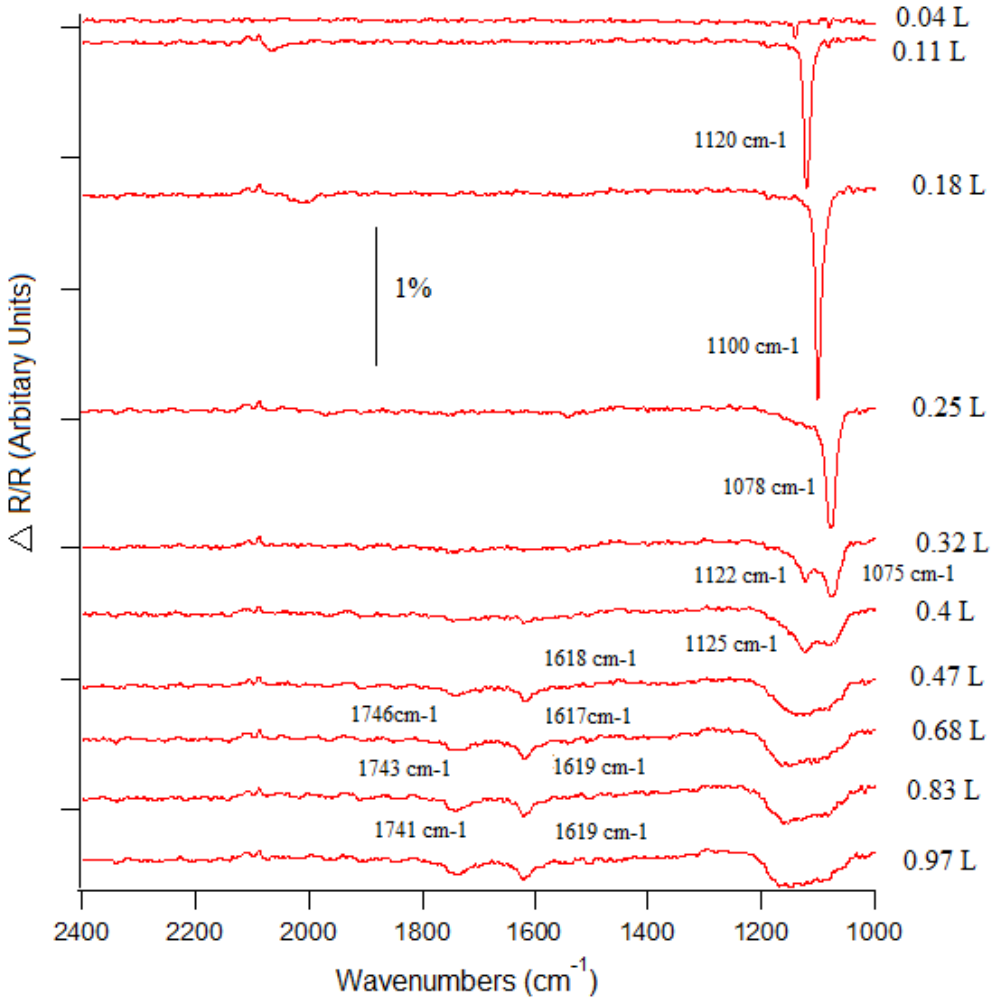

Fig. 5.8 RAIR spectra following the adsorption of up to 1 L of NH_3 onto bare Cu{311} at 100 K.

Figure 5.8 shows RAIR spectra after exposing bare Cu{311} to NH_3 at 100 K. At low exposures (from 0.11 L), there is the formation of a peak at 1120 cm^{-1}, which increases in intensity, until reaching a maximum at 0.27 L of exposure. At the same time, the frequency also shifts towards 1078 cm^{-1}. From 0.32 L, the peak changes into a double peak at 1122 and 1075 cm^{-1}, before turning into a single broad peak above 0.47 L of exposure. The broad peak does not change much with further NH_3 exposure - with the frequency spanning 1157 - 1066 cm^{-1}. All of these peaks have been assigned to the symmetric deformation mode of NH_3 [109]. At NH_3 exposures above 0.47 L, a peak at 1617 cm^{-1} forms. This is assigned to the antisymmetric deformation mode of NH_3 [109, 120, 121]. Another peak also forms at exposures above 0.68 L, at 1746 cm^{-1}; which remains an unknown peak. Figure 5.9 shows the peak areas as a function of NH_3 exposure for all 3 peaks mentioned so far.

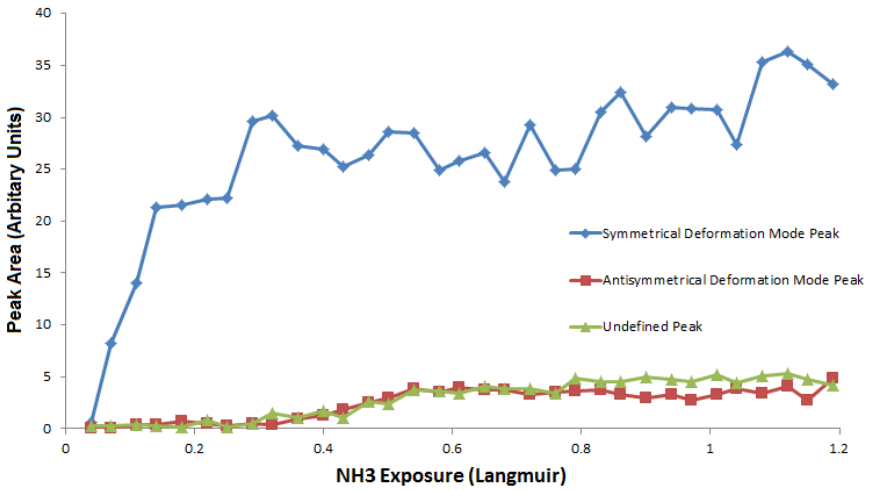

Fig. 5.9 Peak area as a function of NH_3 exposure for the symmetrical, antisymmetric, and undefined peaks when 1 L of NH_3 is exposed to bare Cu{311}.

As NH_3 exposure is increased above 1 L, the spectrum does not significantly change from 1 L onwards (Figure 5.10). There are three major peaks present: the broad peak spanning 1202 - 1017 cm^{-1}, and the two sharper peaks at 1612 and 1749 cm^{-1}. Similarly to in work with NO on the Cu{311} surface, the inverse peak at 2088 cm^{-1} is assigned to residual CO adsorbing onto the surface as explained in Section 3.3. The inverse nature of the peak suggests that NH_3 displaces CO that has adsorbed onto the surface during cooling of the crystal to 100 K. NH_3 also prevents further CO from adsorbing onto the surface.

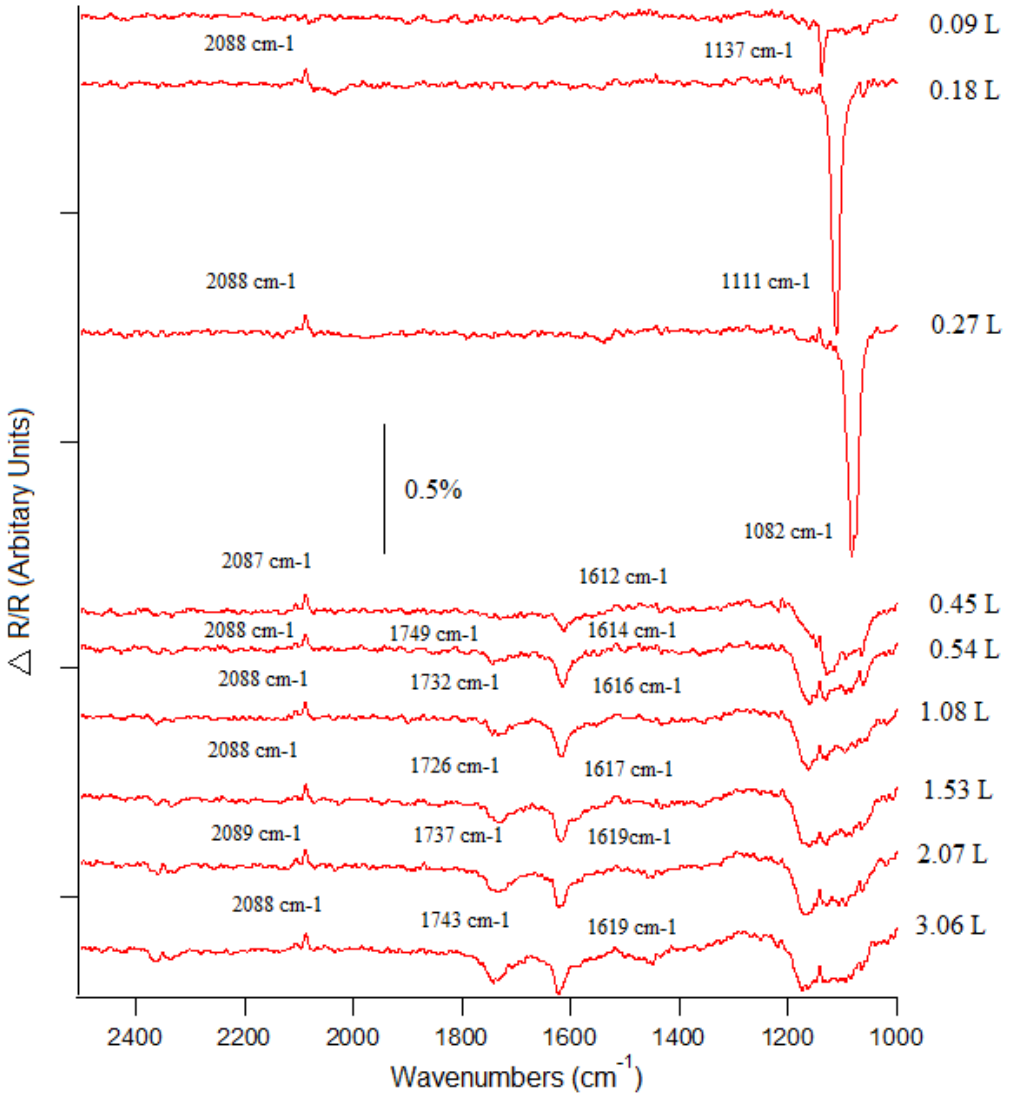

Fig. 5.10 RAIR spectra following the adsorption of up to 3 L of NH_3 onto bare Cu{311} at 100 K.

5.3.2 NH_3 and Oxygen Pre-Covered Cu{311}

As described in Chapter 3, the Cu{311} surface can be pre-covered with oxygen to give different oxide structures on it. A general comparison of the RAIR spectra as 1 L of NH_3 is exposed onto the different oxygen phases is shown in Figures 5.11, 5.12, and 5.13.

Figure 5.11 shows the O(1×2)/Cu{311} surface as it is exposed to 1 L of NH_3, monitored by RAIRS. At 0.07 L exposure, a peak at 1148 cm^{-1} forms. With increasing exposure, the peak shifts towards 1099 cm^{-1} and reaches a maximum at 0.22 L before dropping to 62% of its maximum peak height from 0.4 L onwards. However, in tandem, the area of the peak grows and saturates. Above 0.25 L of exposure, a peak at 1165 cm^{-1} begins to form. The low frequency peak spanning 1099 - 1148 cm^{-1} is assigned to the symmetric deformation mode of NH_3 [109]. The higher frequency peak at 1099 cm^{-1} is also assigned to the symmetric deformation mode of NH_3, but adsorbed onto a different adsorption site.

The other peak present in the spectra is at 1623 cm^{-1}, which appears at 0.32 L exposure. It is assigned to the antisymmetric deformation mode of NH_3 [109], similarly to on bare Cu{311}. It slowly grows until 0.4 L, after which it does not significantly change up to 1 L of NH_3 exposure. A noteworthy observation is the disappearance of the 1740 cm^{-1} peak on the oxygen pre-covered surface; this is explored further in the discussion section.

Figures 5.12 and 5.13 show adsorption of 1 L of NH_3 onto the two higher oxygen coverages, the O(Runways) and O(Oxide Clusters), respectively. The biggest spectrum change when comparing the dosing of NH_3 onto the different oxygen pre-covered phases is when comparing the exposure of NH_3 onto O(1×2)/Cu{311} and O(Runways)/Cu{311} (Figure 5.11 and Figure 5.12). There is, however, very little difference between the adsorption of NH_3 onto the O(Runways) and O(Oxide Clusters). For both of the phases, the spectra show peaks for the symmetric and antisymmetric deformation mode of NH_3 (1111 - 1129 and 1615 - 1620 cm^{-1}, respectively). The spectra also show a peak at 2064 cm^{-1} and inverse peak at 2117 cm^{-1}, both assigned to CO adsorption. The inverse peak is assigned to the displacement of CO that has adsorbed onto the surface as the single crystal is cooled and displaced by NH_3. The much larger peak at 2064 cm^{-1} is assigned to CO adsorption onto the CuO that is near a NH_3 molecule.

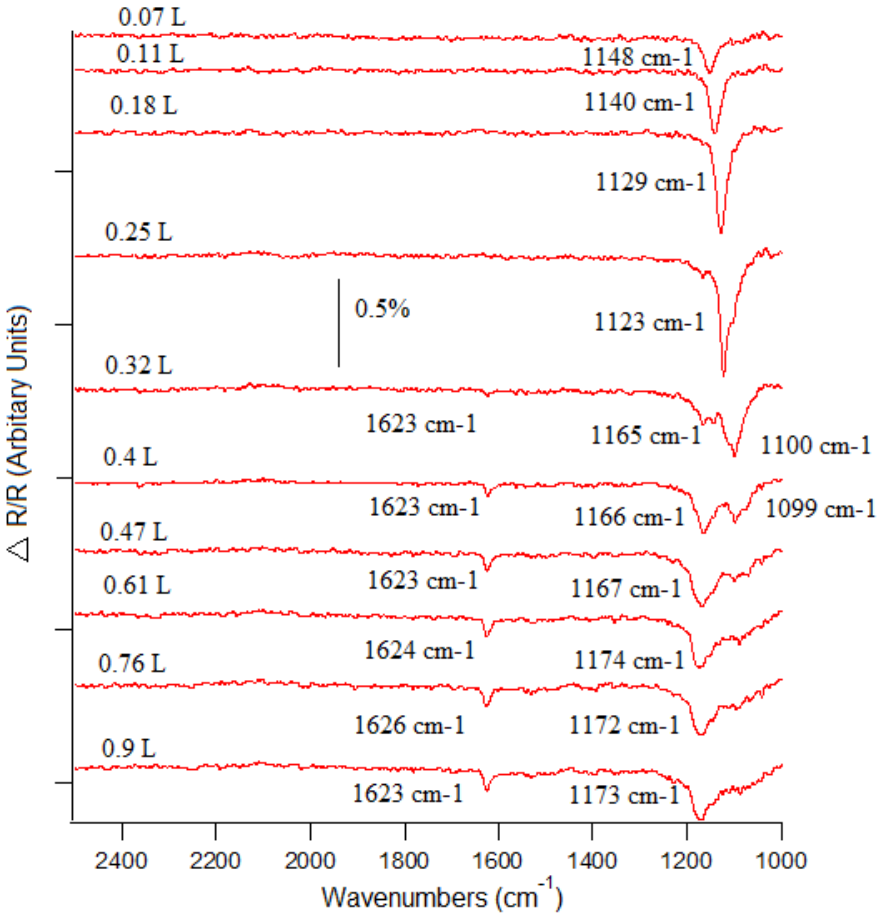

Fig. 5.11 RAIR spectra following the adsorption of up to 1 L of NH_3 onto O(1×2)/Cu{311} at 100 K.

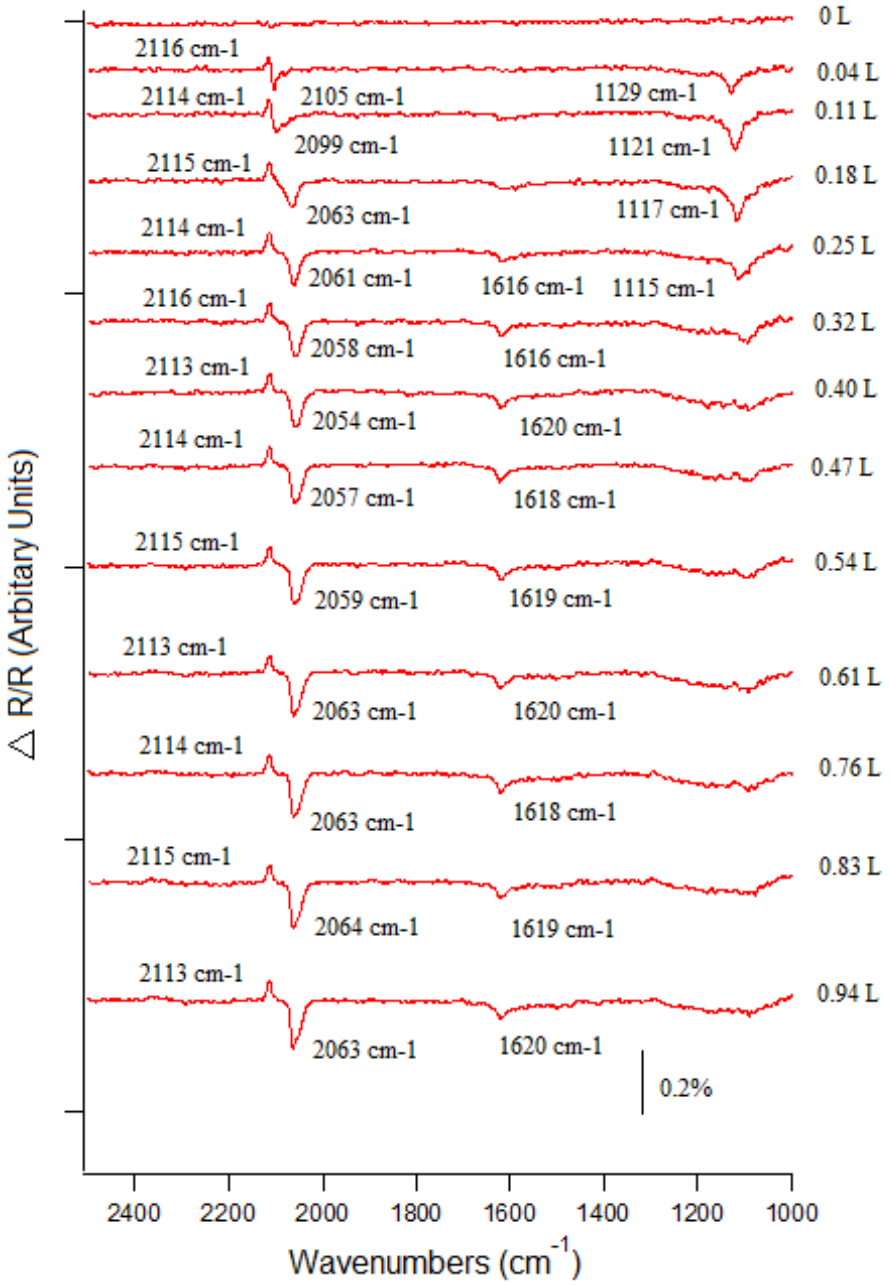

Fig. 5.12 RAIR spectra following the adsorption of up to 1 L of NH_3 onto O(Runways)/Cu{311} surface at 100 K.

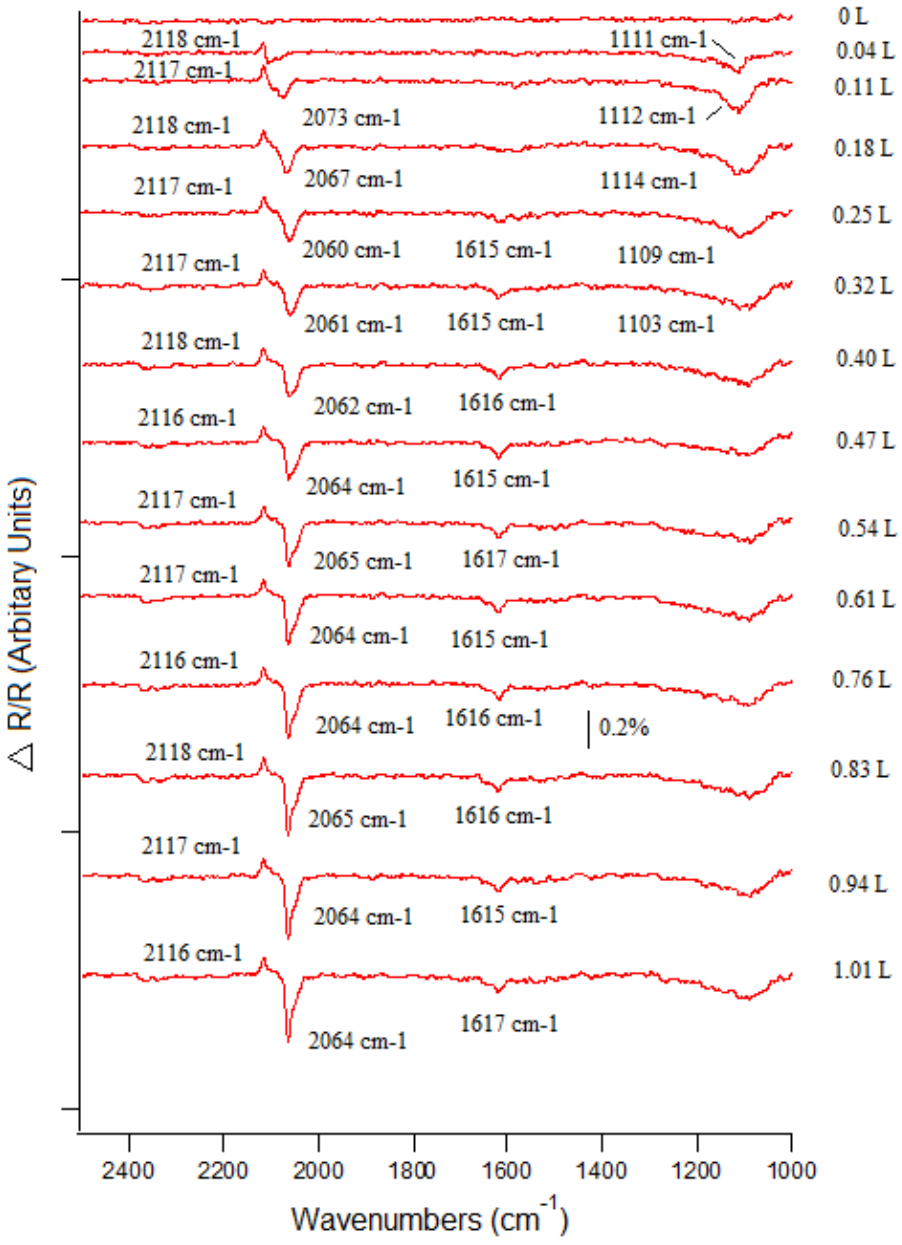

Fig. 5.13 RAIR spectra following the adsorption of up to 1 L of NH_3 onto O(Oxide Clusters)/Cu{311} surface at 100 K.

The most significant change is that the higher the oxygen pre-coverage, the lower the exposure at which the symmetric deformation peak broadens. The peaks that form due to the symmetric and antisymmetric deformation modes of NH_3 (1100-1200 cm^{-1} and 1619 cm^{-1} respectively) are much larger on the bare surface than the oxygen pre-covered ones. This suggests that oxygen acts as an adsorption site blocker.

As the amount of oxygen pre-dosed is increased (going from the O(1×2) towards the O(Oxide Clusters) phases), the peak area of the NH_3 symmetric deformation peak (at 1100 - 1173 cm^{-1}) remains the same despite a difference in oxygen pre-coverage exposure. The peak area of the peak at 1623 cm^{-1} (antisymmetric deformation mode) does not significantly reduce when compared to the bare Cu{311} surface.

.

5.3.3 Temperature Effects

RAIRS experiments were conducted to probe the effects of surface temperature along with oxygen pre-coverage. A comparison between the RAIR spectra as NH_3 is dosed at different temperatures and oxygen coverages is shown in Figures 5.14 - 5.16. When the surface temperature is set to 300 or 400 K and NH_3 is leaked into the chamber, there is a significant change in the RAIR spectre when compared to 100 K.

At 300 K (Figure 5.15) the symmetric deformation mode has a four-fold reduction in size, which suggests NH_3 adsorption is reduced on the surface when compared to NH_3 exposure at 100 K. However, more importantly, at 300 K we note the disappearance of the 1619 cm^{-1} peak and an appearance of a sharp peak at 1530 cm^{-1}. The peak at 1530 cm^{-1} is assigned to the scissor mode of NH_2 [101, 113]. The 1530 cm^{-1} peak is significantly sharper on the oxygen pre-dosed surface than the bare one, although the peak area for the bare Cu{311} surface is twice the size of the oxygen pre-dosed surface. There is also an absence of the antisymmetric deformation mode (usually at 1623 cm^{-1}) for NH_3 along with peaks associated with any CO species.

At 400 K (Figure 5.16), for the bare Cu{311} surface, there is a complete absence of any peaks. However, there is a broad peak spanning 1030 - 1096 cm^{-1} for the O(1×2)/Cu{311}

surface, which indicates presence of a NH_3 species, indicating stabilization of NH_3 at 400 K.

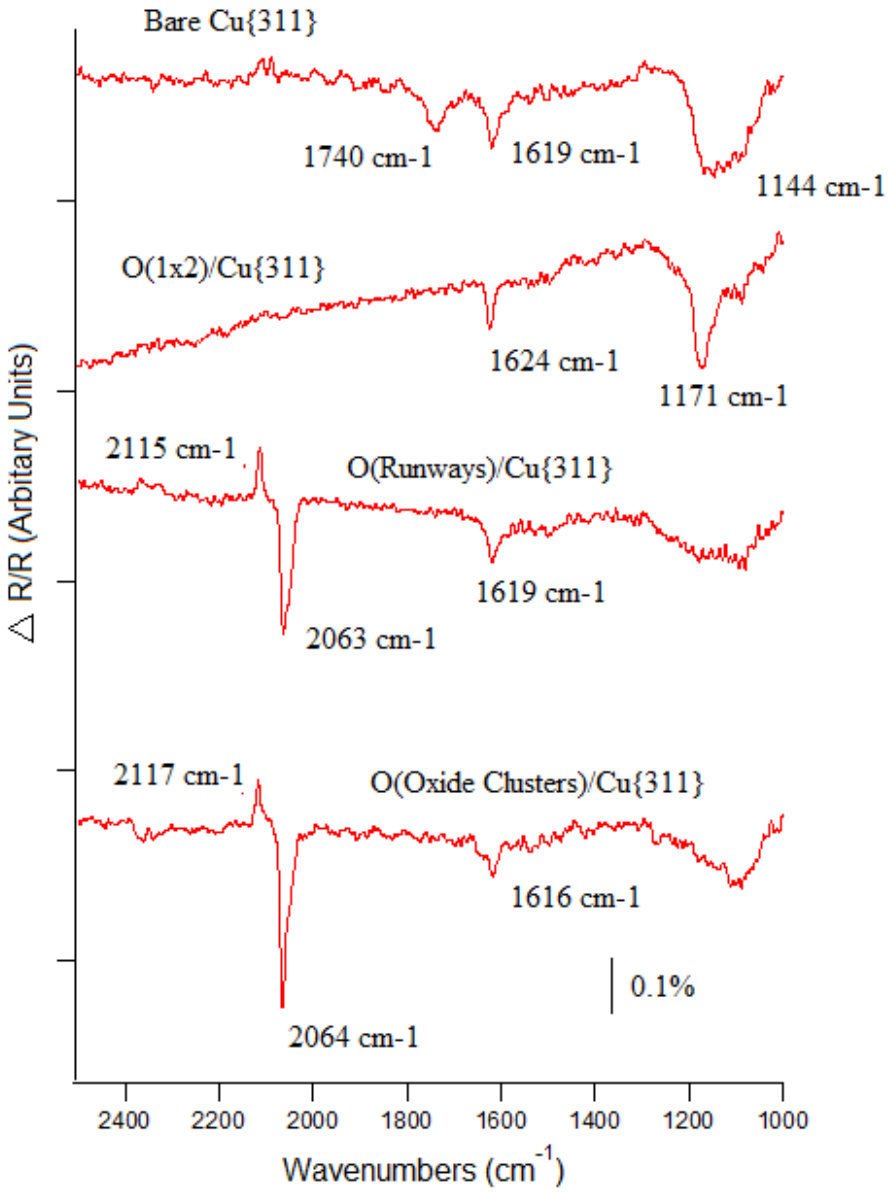

Fig. 5.14 RAIR spectra of dosing 1 L of NH_3 onto different oxygen coverages of the Cu{311} surface at 100 K.

For bare Cu{311}, the major difference between dosing NH_3 at 300 K and 100 K is the lack of any sharp peaks at 300 K, although broad peaks appear at 1148 and 1564 cm^{-1} (assigned to the symmetric deformation mode of NH_3 and NH_2 scissor, respectively).

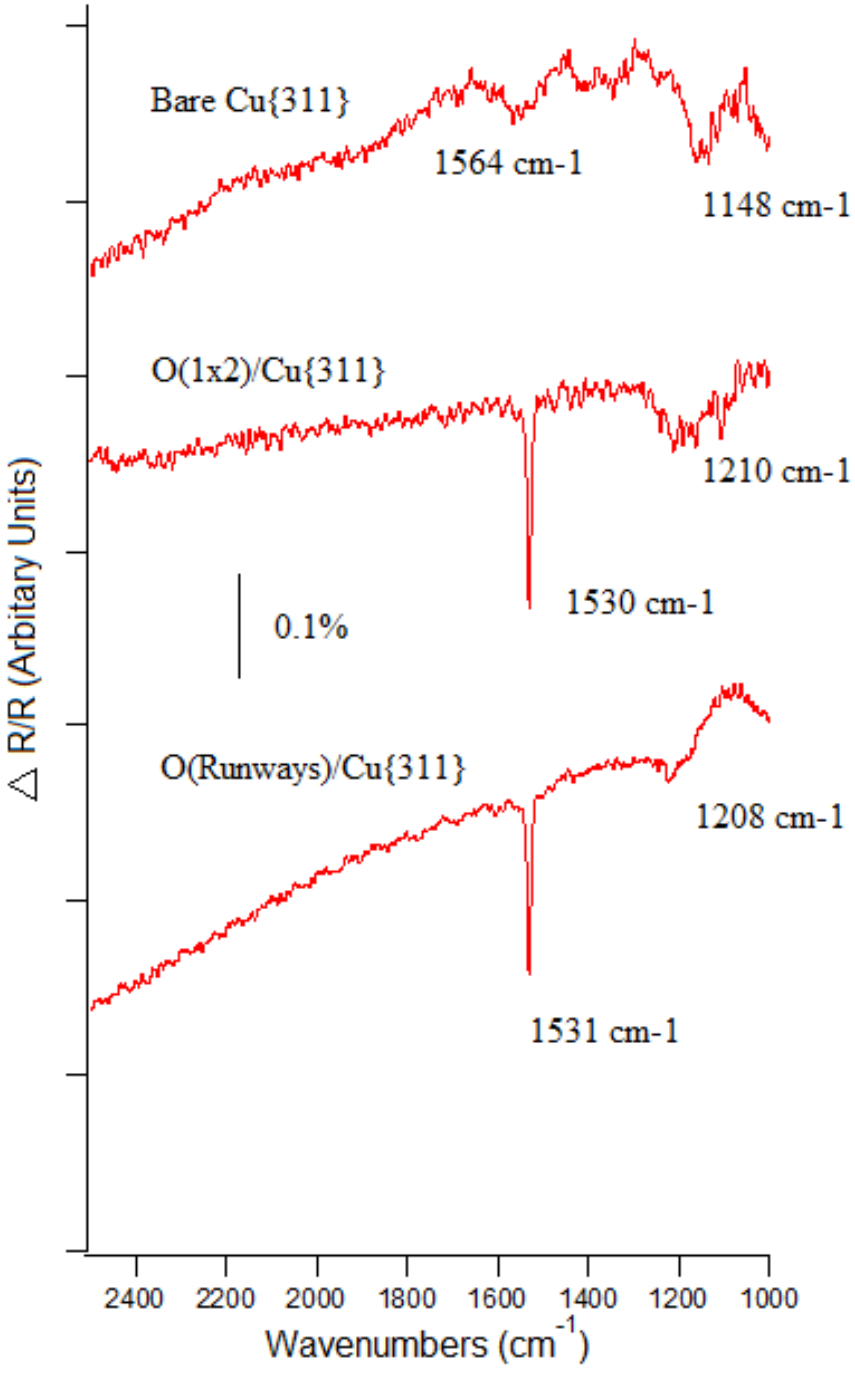

Fig. 5.15 RAIR spectra of dosing 1 L of NH_3 onto different oxygen coverages of the Cu{311} surface at 300 K.

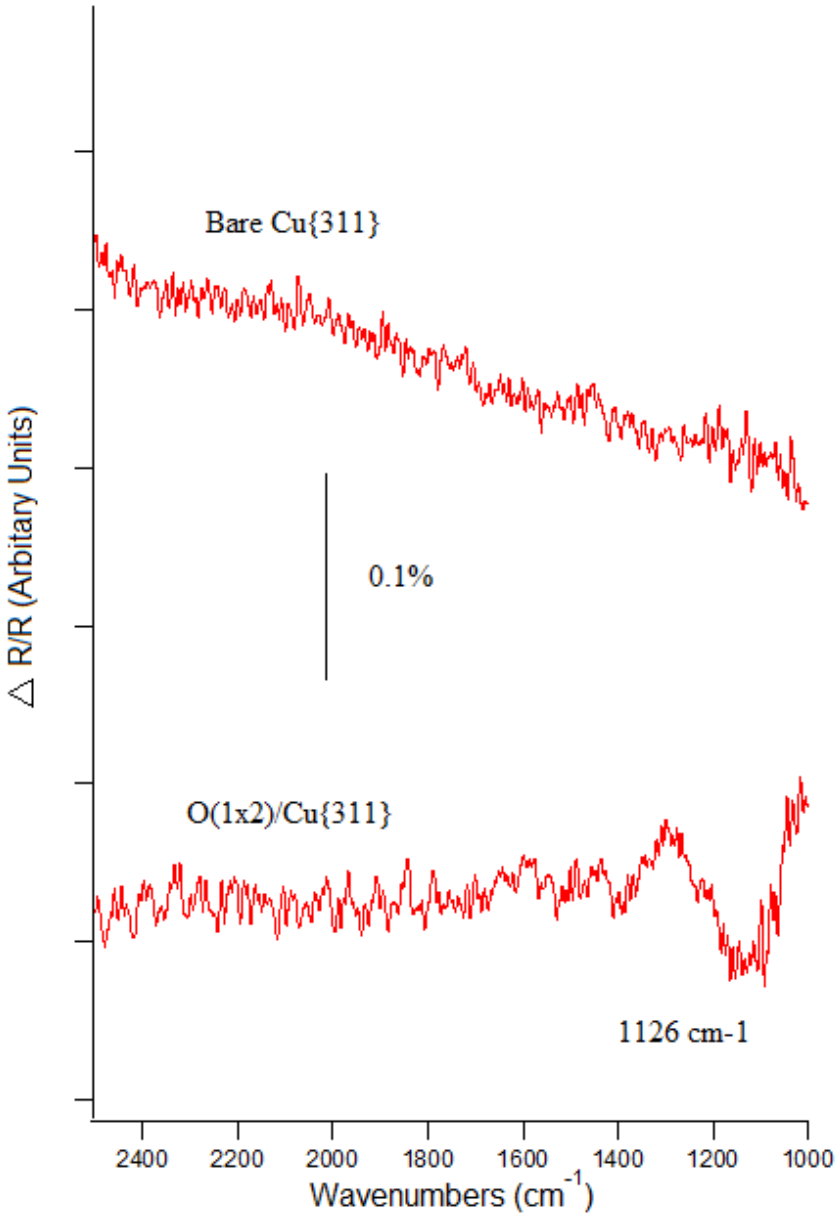

Fig. 5.16 RAIR spectra of dosing 1 L of NH_3 onto the bare Cu{311} and O(1×2)/Cu{311} surface at 400 K.

5.4 Discussion

5.4.1 NH_3 and Bare Cu{311}

The appearance of the symmetric deformation mode peak (1120 cm^{-1}) at low exposures of NH_3 suggests that it adsorbs intact onto the bare Cu{311} surface. However, the gradual shift in frequency, formation of the double peak, and subsequent broadening all suggest that NH_3 adsorption is not simple. There are two possible explanations for the development of the double peak. The first is that NH_3 adsorbs onto two different adsorption sites: the outermost surface layer at low exposures, and the second Cu layer at higher exposures.

The other scenario is the creation of closely packed NH_3 molecules. At low coverage, the NH_3 molecule sits upright on the atop site (consistent with the absence of the antisymmetric deformation mode peak). As more NH_3 molecules adsorb onto the surface, dipole coupling starts to occur. This creates a repulsive electronic interaction between the now closely-packed NH_3 molecules. The repulsion weakens the Cu-NH_3 bond, which shifts the NH_3 symmetric mode back towards the gas phase frequency (which is at 950 cm^{-1}). The broadening above 1 L of NH_3 exposure is attributed to the random and different orientations of the NH_3 molecules on the surface, due to clustering and hydrogen bonding as seen in solid NH_3 [119].

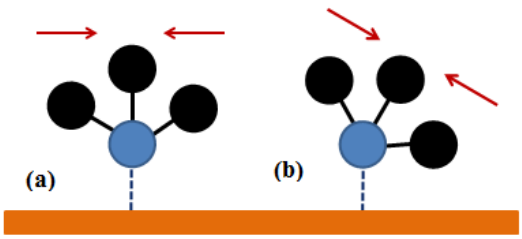

Fig. 5.17 Simple visualization trying to illustrate how the antisymmetric deformation mode gains a vertical movement with respect to the surface. (a) as NH_3 sits up right on the surface and (b) when it is tilted.

At exposures above 0.4 L, there is the appearance of a peak at 1602 cm^{-1}, which is assigned to the NH_3 antisymmetric deformation mode, indicating that there are tilted NH_3 molecules are present on the surface. As the molecule starts to tilt, the dynamic dipole of the

antisymmetric deformation mode, which was previously parallel with respect to the surface, starts to have a non-zero perpendicular component. This makes it become RAIRS active. A simplified diagram can be seen in Figure 5.17 showing how there is now a non-vertical component to the antisymmetric deformation mode. It is worth highlighting that the tilting occurs at roughly the same coverage as the broadening of the peak at 1080 cm^{-1}, suggesting that the two are linked and that there is an exposure requirement. The RAIR spectra were compared to published work done on Cu{110}, where tilting of the NH_3 molecule also happens at coverages above 0.2 ML [121]. Interestingly, however, FTIR studies on Cu{110} at high NH_3 pressure do not show the antisymmetric modes (Figure 5.6 [101, 113]).

It was initially suggested that the creation of densely packed NH_3 species causes them to tilt in order to reduce inter-molecular repulsion [122, 123]. Later DFT modeling by Jones and Jenkins [124] suggested the formation of an intact second layer of NH_3. Jones and Jenkins discussed how a second NH_3 layer is energetically more favoured: hydrogen bonding allows the second layer to be loosely bonded to the surface, while reducing the steric repulsion. The RAIRS data presented in this thesis is consistent with both mechanisms. However, it is speculated that the latter theory is true here; this is because the bi-layer formation allows for the second layer NH_3 to bond weakly to the surface, which would create two NH_3 species on the surface. The formation of the double peak for the symmetric deformation mode indicates the presence of two NH_3 species, thus showing support for the bi-layer theory.

Analogous to the adsorption of NH_3 onto Ag{110} [106] and Ag{311} [107], there is little difference between the spectra for the adsorption of NH_3 onto Cu{110} [109] and Cu{311} under UHV conditions at very low temperatures. This suggests that the surface structure of bare Cu has very little influence on the chemistry of the adsorption of NH_3 onto the surface.

There is, however, one major difference between the adsorption of NH_3 onto Cu{110} and onto Cu{311} in the spectra: the unassigned peak at 1737 cm^{-1}, that appears from 0.54 L of exposure. This is not due to the existence of any of the well-known NH_3-derivative species such as NH_4^+, NH_2, or NH. The only known species with a similar vibrational fre-

quency are carbonyl groups, such as $HCONH_2$, which has a peak for the C=O stretch at 1754 cm^{-1} [125]). However, there are no other peaks associated with formamide in the RAIR spectra, so this is unlikely. It is also unclear where the oxygen and carbon on the bare surface might come from, other than the reaction of NH_3 with adsorbed residual CO.

Another possible explanation could be NH_3 adsorption onto non-atop sites and that the peak at 1737 cm^{-1} corresponds to the antisymmetric mode that is shifted due to NH_3 adsorption onto a different adsorption site. It is worth mentioning that the 1737 cm^{-1} peak does not appear when oxygen is pre-dosed onto the surface (Figure 5.11). This supports the latter theory of NH3 adsorption onto non-atop sites, as oxygen may be blocking the adsorption of NH_3 onto non-atop sites. However, it is unknown why this species is not seen in other surfaces such as Cu{110} [109], Ag{110} [106], and Ag{311} [107].

In contrast to the NO experiments, there is no evidence for CO adsorption as the Cu{311} surface is exposed to NH_3 (Figures 5.10 and 4.17). There is, however, an inverse peak at 2088 - 2089 cm^{-1}, which suggests there is displacement of residual CO from the surface by NH_3. Details of CO adsorption onto the Cu{311} have been discussed in Section 3.3.

To conclude, analysis of the RAIR spectra suggests that as NH_3 is dosed onto bare Cu{311} it adsorbs intact onto an atop site of the surface, with its three fold rotational axis perpendicular to the surface. As the exposure is increased above 0.4 L, the NH_3 molecules on the surface start to tilt (apparent from the appearance of the antisymmetric deformation mode). It is still unclear whether the NH_3 molecules are closely packed or a bi-layer forms, though it is suggested that the latter mechanism is the case.

5.4.2 NH_3 and Oxygen Pre-covered Cu{311}

When an O(1×2)/Cu{311} surface is exposed to NH_3, only two peaks appear in the RAIR spectra, which are for the symmetric and antisymmetric deformation modes (Figure 5.11). The peak areas as a function of NH_3 exposure are shown in Figure 5.18, which shows that for the O(1×2)/Cu{311}, the peak area reaches a similar saturation point at the same NH_3 exposure as the bare Cu{311} surface. However, there are some minor differences as the appearance and frequency of the double peak (1165 and 1100 cm^{-1}) develop at a lower NH_3

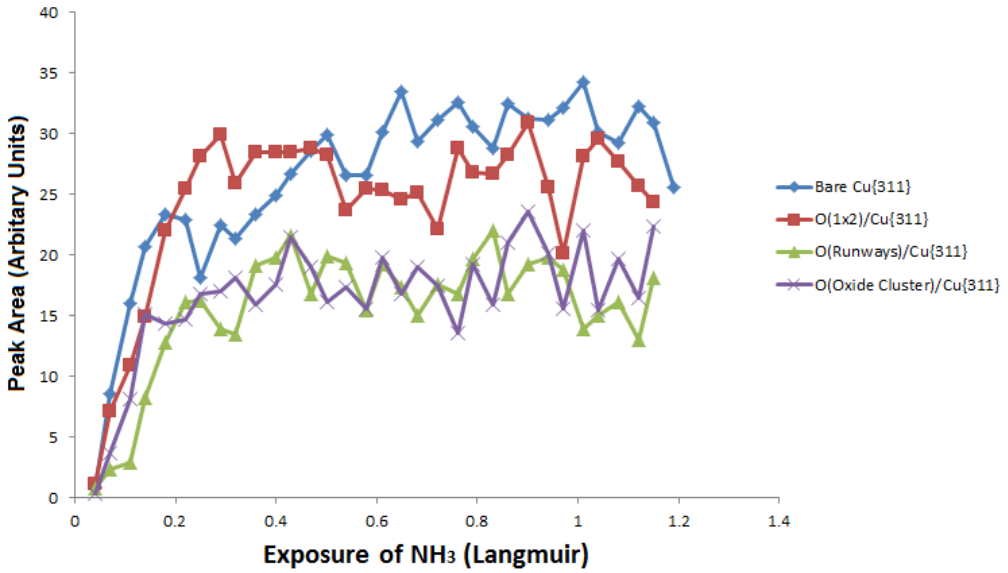

Fig. 5.18 Peak areas for the symmetric deformation peak (1120 cm^{-1}) as a function of NH_3 exposure onto various oxygen pre-covered surfaces of Cu{311} at 100 K.

exposure. The broad peak that forms from 0.5 L of exposure is less broad, but still has a similar frequency when compared to the bare Cu{311}.

The appearance of the double peak suggests that there are two adsorption sites for NH_3, where one is bonded weakly to the surface. The 1100 cm^{-1} peak is more similar to the gas phase vibrational frequency at 950 cm^{-1} than at 1124 cm^{-1}, suggesting that the NH_3 molecule is weakly bonded to the surface, most likely due to the formation of the bi-layer as mentioned in the previous section. At higher coverages (runways and oxide clusters), the lower frequency peak (1100 cm^{-1}) does not appear. This suggests that oxygen blocks NH_3 adsorption sites. The symmetric deformation mode broadens at a lower NH_3 exposure, which suggests that oxygen brings about disorder at a lower exposure, due to the blocking of NH_3 adsorption onto bare Cu atoms.

In addition to the symmetric deformation mode, the peak assigned to the antisymmetric deformation mode at 1624 cm^{-1} is still observed when NH_3 is exposed onto oxygen pre-covered surfaces. The area of this peak as a function of NH_3 exposure onto various oxygen pre-covered phases of the Cu{311} surface can be seen in Figure 5.19. On all the oxygen pre-covered phases, (and the bare surface), the peak saturates, although reaching this point is

reduced to a lower NH_3 exposure when the higher amounts of oxygen are pre-dosed. Whilst on the bare Cu{311}, it takes 0.4 L of NH_3 exposure before it plateaus, when oxygen is pre-covered, it reaches a similar peak area by 0.2 L. This suggests that oxygen promotes the tilting of the NH_3 molecule, either by occupying adsorption sites and causing the NH_3 molecule to tilt (due to reduced available space on the surface) or by stabilizing the second NH_3 bi-layer.

It is worth mentioning how the peak area of the symmetric and antisymmetric peak areas saturates at roughly the same magnitude on the bare and O(1×2)/Cu{311} surface. In contrast, both the O(Runways) and O(Oxide Clusters) have a lower peak area than that of the other oxygen conditions but are the same as each other. As we know from Section 3.2.1, the O(1×2) phase is very similar to the bare Cu{311} phase; although there is a missing row, there is still a large amount of available metallic Cu atoms. As mentioned earlier, there seems to be minimal difference between the two surfaces for the adsorption process of NH_3. This could be because both of these higher oxygen phases exhibit an "oxide-like" surface, which makes them very similar in reactivity to NH_3.

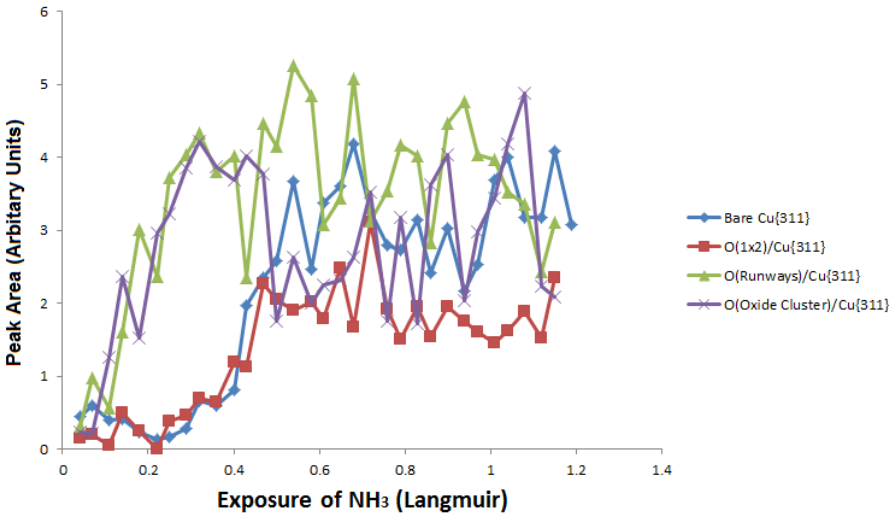

Fig. 5.19 Peak areas for the antisymmetric deformation peak (1620 cm^{-1}) as a function of NH_3 exposure onto various oxygen pre-covered surfaces of Cu{311} at 100 K.

The other major difference as NH_3 is exposed onto the higher oxygen coverages (the runways and oxide clusters) is the appearance of inverse peak and negative peaks at 2116 -

2113 cm^{-1} and 2105 - 2063 cm^{-1}, respectively. Both of these peaks are assigned to CO adsorption onto the surface. The absence of any CO peak at the lower O(1×2) coverage is most likely due to the inhibition effect of oxygen on CO [90]. The appearance of the inverse peak at 2115 cm^{-1} at higher oxygen coverages is due to NH_3 displacing the CO that has adsorbed onto or near CuO as the single crystal is cooled to 100 K (adsorption of CO onto O/Cu{311} as discussed in Section 3.3). The 2064 cm^{-1} peak (only seen on the high oxygen phases) is assigned to CO; as we know from work on NO and oxygen phases, CO readily adsorbs onto the high oxygen pre-covered surfaces (Figure 4.30). The shift in frequency could be due to the adsorption near a NH_3 molecule. NH_3 is known to decrease the work function of the surface by 1.9 eV [126], which can promote CO binding to the surface by increasing back donation of electrons into its pi* orbital. This would explain the shift of the C-O stretch further away from its gaseous phase frequency. Experiments at 300 K (Figure 5.15) do not have these peaks, which is further evidence for them being CO, as CO desorbs from Cu surfaces at 200 K.

To conclude, at 100 K, oxygen mainly acts as an inhibitor for NH_3 adsorption. The difference between the bare and oxygen phases can be viewed together; the bare Cu{311} and O(1×2)/Cu{311} surfaces are very similar to each other. However, they are different from the O(Runways)/ Cu{311} and O(Oxide Clusters)/Cu{311} surface - themselves similar. This is due to the metallic Cu-like surface of the bare and O(1×2)/Cu{311} surfaces and the oxide-like surface of the O(Runways) and O(Oxide Clusters) phases. As mentioned in the previous section, the reason for the disappearance of the 1737 cm^{-1} peak when oxygen is pre-dosed remains, as yet, unknown.

5.4.3 Temperature Effects

As most of the previous work mentioned in this Chapter was done at 100 K, those spectra will not be discussed in detail again, but will be compared to the higher temperature experiments. As the surface dosing temperature is increased from 100 K to 300 K, there is a general reduction in peak area for the symmetric deformation mode peak, suggesting a reduced amount of NH_3 adsorbed on the surface.

The most significant change when NH_3 is dosed on the Cu{311} surfaces at 300 K is the appearance of a peak at 1530 cm^{-1}, which is assigned to the scissor mode of an imide (NH_2) species [109] . This suggests that at 300 K (in contrast to 100 K), Cu{311} is able to dissociate NH_3 into NH_2. It is also worth noting how the 1530 cm^{-1} peak is sharper on the oxygen pre-covered surface sbut has half the peak area of the equivalent peak on the bare surface. This suggests that although oxygen is a site blocker, it promotes the formation of NH_2 on the Cu{311} surface at higher temperatures, but does not at 100 K. Another possible explanation for the much larger NH_2 peak is that $O_{(a)}$ on the surface also stabilizes NH_2 on the surface due to electronic effects. Therefore oxygen has two effects on the interaction of NH_3 with the Cu{311} surface.

This process of NH_3 dissociation is also seen in the XPS studies by Afsin *et al* [111] on oxygen pre-covered Cu{110}, along with low vacuum conditions FTIR O/Cu{110} experiments by Louis-Rose *et al* [113] (Figure 5.6(c)). There is one significant difference: the O/Cu{110} surface also shows peaks for $NH_{(a)}$ species, while we only see a peak for NH_2 (1430 cm^{-1}). This shows that the O/Cu{311} surface, though it promotes dissociation of NH_3 does not promote further cracking of NH_2 into NH.

The disappearance of the antisymmetric deformation peak at 300 K indicates a reduction in the amount of NH_3 on the surface, either due to the desorption of loosely bonded NH_3 molecules (from the second layer or closely packed species) or the reaction to form NH_2. This reduction in the number of NH_3 molecules on the surface would reduce the intermolecular repulsion effect and cause the remaining NH_3 molecules on the surface to return to the upright configuration, making the antisymmetric deformation mode now RAIRS inactive and causing it to disappear from the RAIR spectra. The disappearance of the CO peaks at 2064 and 2115 cm^{-1} at higher temperatures is expected, as CO does not remain on Cu surfaces above 200 K [88].

When NH_3 was dosed at 400 K (Figure 5.16), there are no peaks on the bare Cu{311} surface, but a broad peak at 1126 cm^{-1} on the O(1×2) surface. The 1126 cm^{-1} peak has been assigned to the symmetric deformation mode on the surface, suggesting that there is NH_3 on the surface at high temperatures when oxygen is pre-dosed. This suggests that

oxygen, in addition to being a site blocker, can also stabilize NH_3 on a Cu{311} surface (most likely due to an electronic effect).

It was proposed by Pradier *et al* [101] that on Cu{110} at 300 K, there is de-hydrogenation of NH_3 to form hydroxylamine (O-NH_2), which causes the peaks at 1175 and 1620 cm^{-1} [120, 127]. Although the RAIR spectra in our work show similar peaks, we hesitate to reassign the peaks to the hydroxylamine due the similarity of the frequencies with the two deformation modes of NH_3. In addition, the peaks also appear on the bare Cu{311} surface without the presence of oxygen. Therefore, we still assign the peaks at 1124 and 1624 cm^{-1} to the symmetric and antisymmetric mode, respectively.

To conclude, it is shown that at higher temperatures, such as 300 K, an imide forms when NH_3 is dosed onto an oxygen pre-covered surface. However, at 400 K, NH_3 is seen in the RAIR spectra, suggesting that $O_{(o)}$ has a stabilising effect.

5.5 Conclusion

Similarly to with other onto other well-defined bare metal surfaces, NH_3 adsorbs intact onto the Cu{311} surface. Though initially upright at low exposure, it then tilts after 0.4 L of NH_3 is exposed to the Cu{311} surface. This in-keeping with work on Cu{110} [109], Ag{110} [106], and Ag{311} [107]. Oxygen acts as an inhibitor to NH_3 adsorption at low temperatures, but at high temperatures is seen to promote the dissociation of NH_3 into NH_2.

In the context of SCR, the work in this chapter shows that NH_3 can adsorb onto both bare and oxygen covered Cu surfaces. The presence of oxygen means that NH_3 can remain on a Cu surface at higher temperatures, but it also promotes the formation of NH_2, which is a potentially reactive radical species. NH_2 could be a candidate to react with NO to form N_2 and H_2O.

Chapter 6

NH_3 and NO Co-Adsorption on Cu{311}

6.1 Literature Review

Following on from analyses of the adsorption of NO onto Cu{311} in Chapter 4 and NH_3 onto Cu{311} in Chapter 5, this chapter focuses on the co-adsorption of NO and NH_3 onto Cu{311}. There is limited reported work in the literature on the co-adsorption of NO and NH_3, as the vast majority of studies have concentrated on the individual gases (as explored in the previous two Chapters).

The reported work which is most similar to that presented in this chapter is the study of the co-adsorption of NO and NH_3 onto Cu{111} using EELS and TPD by Sueyoshi *et al* [128]. Figure 6.1 show EEL spectra after the exposure of NO and NH_3 onto the surface along with subsequent annealing. Figure 6.1(i) shows the most similar conditions to the experiments in this chapter as we see the adsorption of 1 L of NO and 2 L of NH_3 onto a Cu{111} surface at 100 K. In contrast to our own RAIRS work with NO on Cu{311}, Sueyoshi *et al* have assigned the reported vibrational frequencies associated with NO differently and have designated their peaks similar to the bent NO configuration mechanism by Wendelken *et al* [76]. As discussed in Section 4.1.1, we are hesitant to make the same assignments (also perhaps based on the fact that we use a different technique). The EEL spectra shows the formation of peaks at 280, 620, 1130, 1180, 1620, 2320, and 3260 cm^{-1}. The authors have assigned the peaks to correspond to $\nu(NH_3)$, $p(NH_3)$, symmetric defor-

mation mode (NH_3), ν(N-O) on a three-fold site, antisymmetric deformation mode (NH_3), combination of ν(N-O) and symmetric deformation mode (NH_3), and ν(N-H), respectively. From our work, we report seeing the NO bridge site peak at 1611 cm^{-1} and therefore hesitate to assign the 1620 cm^{-1} peak purely to the antisymmetric mode of NH_3, as it could be the combination of effects from both molecules.

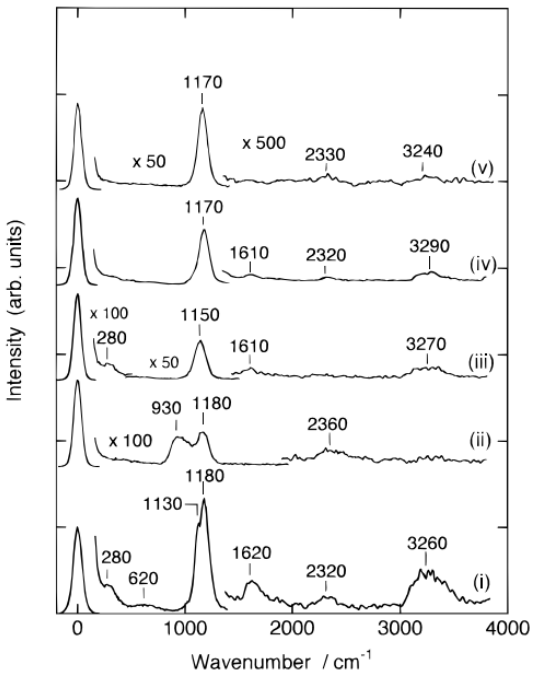

Fig. 6.1 EEL spectra recorded at 100 K for the co-adsorption of NO and NH_3 onto a Cu{111} surface. Spectra (i and ii) were exposed to 1.0 L of NO and 2.0 L of NH_3 and 1.0 L of NO and 2.0 L of ND_3 respectively. Both spectra (i and ii) were taken after the surface was exposed to the adsorbates, annealed to 180 K, and cooled back down to 100 K. The remaining spectra were taken after different exposures of NO and NH_3 were leaked onto the chamber. (iii) 0.4 L of NO and 2.0 L of NH_3 (iv) 2.0 L of NO and 0.8 L of NH_3 (v) 2.0 L of NO and 1.8 L of NH_3. (Sueyoshi *et al* [128])

TPD data (Figure 6.2) shows the desorption of mass 48 and 16 amu, assigned to N_2O and NH_3 respectively [128]. This indicates the presence of both NO and NH_3 on the surface. For the exposure of only NO, N_2O desorbs from the surface between 140 - 150 K (Figure 6.2(a)). For NH_3, desorption occurs at 130 - 150 K (Figure 6.2(b)). When both NO and NH_3 are co-adsorbed there is an increase in desorption temperature. Figure 6.2(c) shows N_2O desorption from the surface at 220 K, 70 K higher than with NO only. Similarly, NH_3 is shown to desorb

at 220 and 270 K, also 70 - 120 K higher than with NH_3 adsorption only.

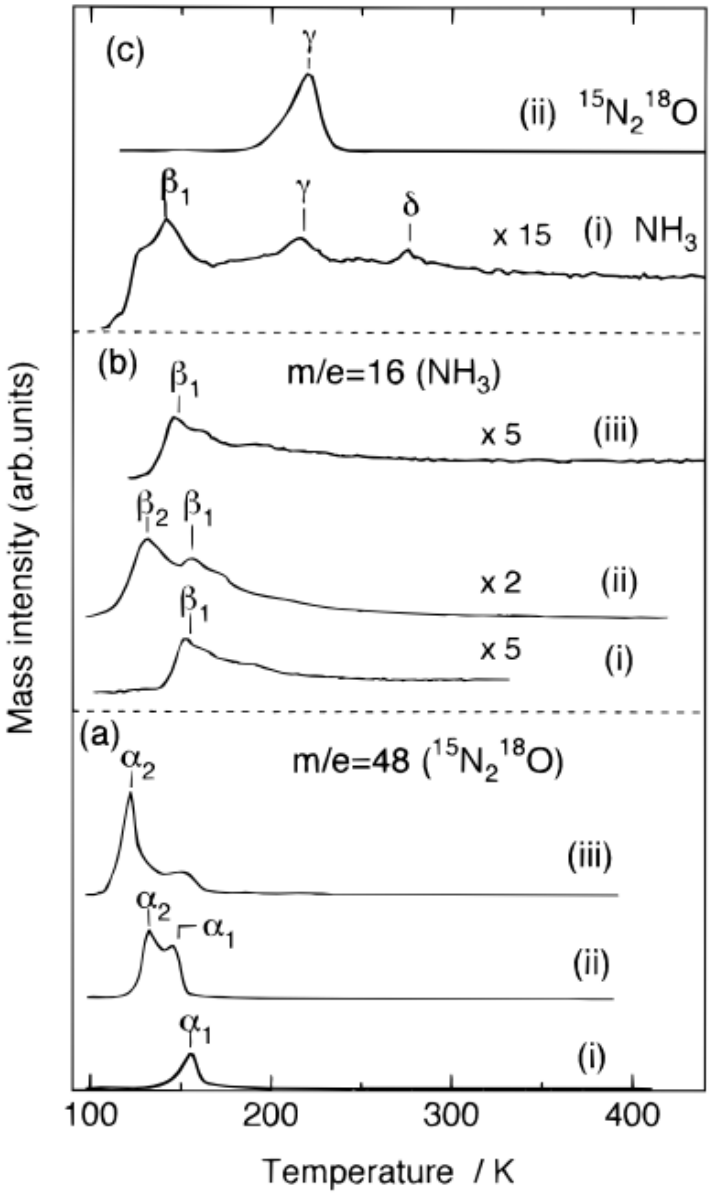

Fig. 6.2 TPD spectra showing the desorption of mass 48 and 16 amu assigned to N_2O and NH_3 from the Cu{111} surface at 100 K after different exposures. (a) is the desorption of mass 48 after (i) 0.4 L (ii) 1.2 L and (iii) 2.0 L exposure of NO. (b) is the desorption of mass 16 amu after (i) 1.0 and (ii) 3.0 L of NH_3 exposure with (iii) being 3.0 L annealed to 120 K and allowed to cool back down to 100 K. (c) is the desorption of mass 48 and 17 amu from the surface after 3.0 L of NH_3 and 2.0 L of NO is exposed to the surface. (Sueyoshi *et al* [128])

Sueyoshi *et al* [128] concluded that the net interaction between NO and NH_3 is attrac-

tive, as the desorption temperature for the NH_3 after co-adsorption is higher than with pure NH_3 or NO on the Cu{111} surface. This is because the work function lowers as NH_3 is adsorbed onto the Cu{111} surface (by up to 1.9 eV [126]). This allows an increase of back donation into the $2\pi^*$ anti-bonding orbital of NO, which enhances the adsorption of NO to the surface. The authors found no direct evidence for any chemical reaction occurring between NO and NH_3, with N_2O being a possible product of the reaction between NO molecules alone.

6.2 Experimental

Work done in this chapter is similar to that presented in Chapter 4 and 5, but differs in its focus on the co-adsorption of both NO and NH_3.

The Cu{311} crystal is cleaned before experiments using Ar ion sputtering and is then annealed to 900 K for 2 minutes to reorder the surface. Surface cleanliness is monitored using Auger Spectroscopy and LEED analysis. NO or NH_3 is leaked into the chamber at a desired pressure, which is constantly monitored by an ion gauge. Afterwards, the gas line is cleaned and flushed with the subsequent gas to be dosed, which is then leaked into the chamber. During this entire dosing process, the surface species is monitored using the RAIRS as a function of exposure (from the first gas leak, to gas line flushing, and to dosing the second gas).

Once the desired exposures of both gases is achieved, a TPD experiment is performed. The crystal is moved towards the mass spectrometer and the heating rate is set to 0.5 K/s. Different masses were recorded, normally mass 17, 30, and 44 amu (for NH_3, NO, and CO_2/N_2O, respectively).

6.3 Results

6.3.1 RAIRS Experiments

The first experiments performed involved exposing the bare Cu{311} surface initially to 5 L of NH_3 and subsequently to 1 L of NO. Figure 6.3 shows RAIRS spectra corresponding to the dosing of 1 L of NO onto 5 L of NH_3. The top five spectra show the dosing of NH_3 while the bottom six show the subsequent dosing of NO onto the NH_3 pre-covered Cu{311} surface. The spectrum that corresponds to the initial dosing of NH_3 onto the Cu{311} is identical to the spectrum of dosing a multilayer of NH_3 as seen in Chapter 5 (Figure 5.10). This is inferred from the appearance of the peaks at 1109 - 1160, 1612 - 1620, and 1740 - 1748 cm^{-1}, which have been assigned to the symmetric, antisymmetric, and unknown peak for NH_3 exposure onto a bare Cu{311} surface [109].

Once NO is leaked into the chamber, the 1612 - 1620 cm^{-1} peak disappears. This peak is assigned to the antisymmetric mode of NH_3 and indicates the reduction in a tilted species of NH_3 on the surface. In addition, the 1740 - 1748 cm^{-1} peak also disappears. Instead, there is a formation of broad peaks at 2011 and 1191 cm^{-1}. The peak at 1191 cm^{-1} is the symmetric deformation mode of NH_3. As NO exposure is increased towards 1 L, both the 2011 - 2021 and 1191 cm^{-1} peaks lower in intensity until 0.5 L of NO exposure. Figure 6.4 shows the change in peak areas as a function of both NH_3 exposure to the Cu{311} surface and subsequent exposure of NO. The inverse peak at 2088 cm^{-1} is assigned to residual CO adsorbing onto the surface as the crystal is cooled, which most likely occurs due to displacement by the adsorption of NH_3 as mentioned in Section 5.3.1. The broad peak at 2011 - 2021 cm^{-1} is similarly assigned to CO with the frequency shifted due to NH_3 co-adsorption changing the work function of the surface (Section 5.4.2.)

The reverse of the first experiment was also performed: NH_3 was dosed onto a NO pre-covered clean Cu{311} surface. Figure 6.5 shows RAIRS spectra following the dosing of 5 L of NH_3 onto 1 L of NO at 100 K. The top seven spectra show dosing of 1 L of NO with the bottom five showing the subsequent dosing of 5 L of NH_3 onto the Cu{311} surface.

The initial dosing of NO onto the Cu{311} is similar to NO adsorption onto the bare

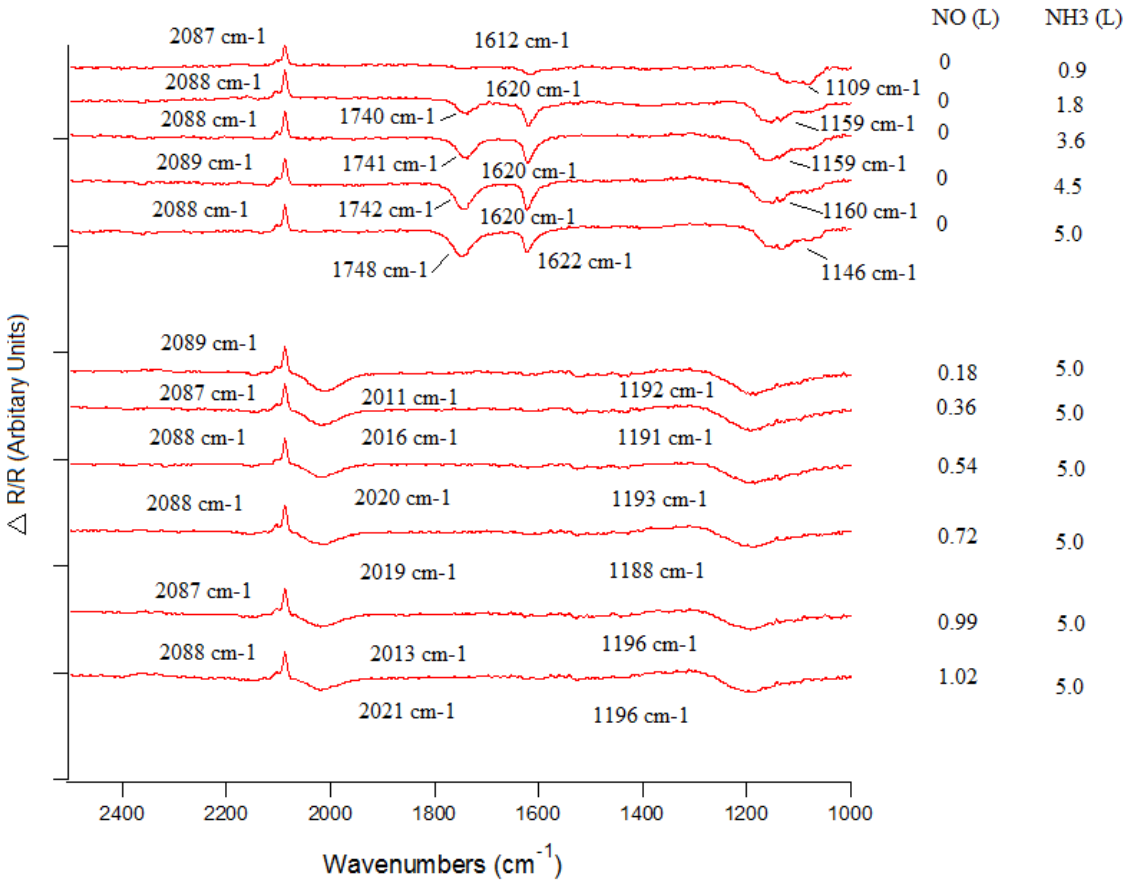

Fig. 6.3 RAIR spectra showing the exposure of the clean Cu{311} surface at 100 K to 5 L of NH_3 followed by a period of gas-line changeover and subsequent exposure of the surface to 1 L of NO. Dosing pressures of NH_3 and NO were at 1×10^{-8} and 1×10^{-9} mbar, respectively.

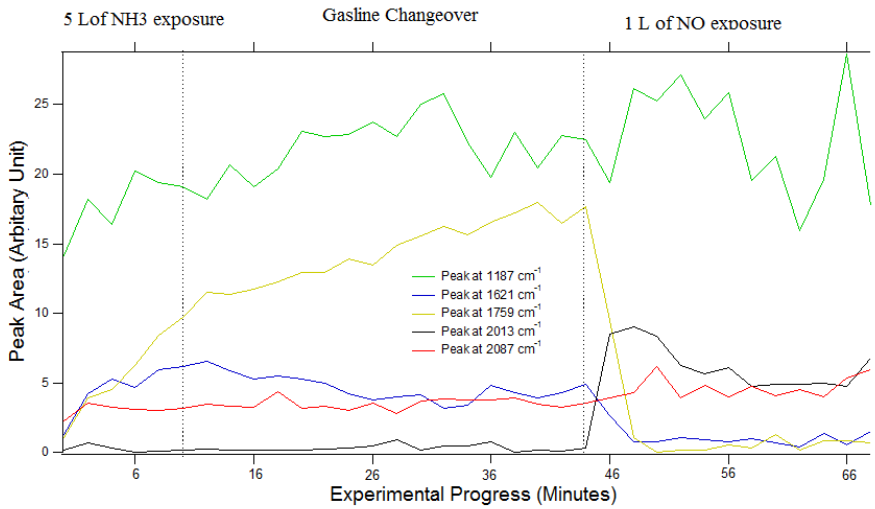

Fig. 6.4 Areas of the peaks from Figure 6.3. The section on the left shows the peaks areas as the Cu{311} surface is exposed to 5 L of NH_3. The middle section shows peak areas as the gas line is changed from NH_3 into NO. The section on the right shows the peak area as the NH_3 covered Cu{311} surface is exposed to 1 L of NO.

Cu{311} surface from Chapter 4 (Figure 4.9). The peaks at 1594 - 1618 and 2250 cm^{-1} are assigned to the NO on a bridge-site and chemisorbed N_2O respectively. As NH_3 is exposed to the NO pre-covered Cu{311} surface, broad peaks appear at 1151 - 1160 and 1610 - 1622 cm^{-1}. The 1151 - 1160 cm^{-1} peak has been assigned to the NH_3 symmetric deformation mode [109]. Although the 1611 - 1622 cm^{-1} peak is similar in frequency to the initial NO bridge-site peak [80–83], it can also be assigned to the antisymmetric deformation mode of NH_3 (but will be discussed in detail later). The two peaks that appear at 2121 and 2089 cm^{-1} are both assigned to CO [51]. Prior to NH_3 exposure, the peak at 2121 cm^{-1} is very prominent but lowers in area once NH_3 is leaked into the chamber and vanishes by 1.8 L of exposure. This is then replaced by the peak at 2069 - 2071 cm^{-1}. The lower frequency peak is assigned to CO, but shifted due to NH_3 changing the work function of the surface [126], causing the C-O bond to strengthen due to increase back of electrons donation from the surface. Figure 6.6 shows the change in peak areas as a function of both NH_3 exposure to the Cu{311} surface and subsequent exposure of NO.

For the last experiment, 5 L of NH_3 was exposed to 0.26 L of NO pre-covered on a bare Cu{311} surface. The 0.26 L of NO exposure was chosen due to it being the highest

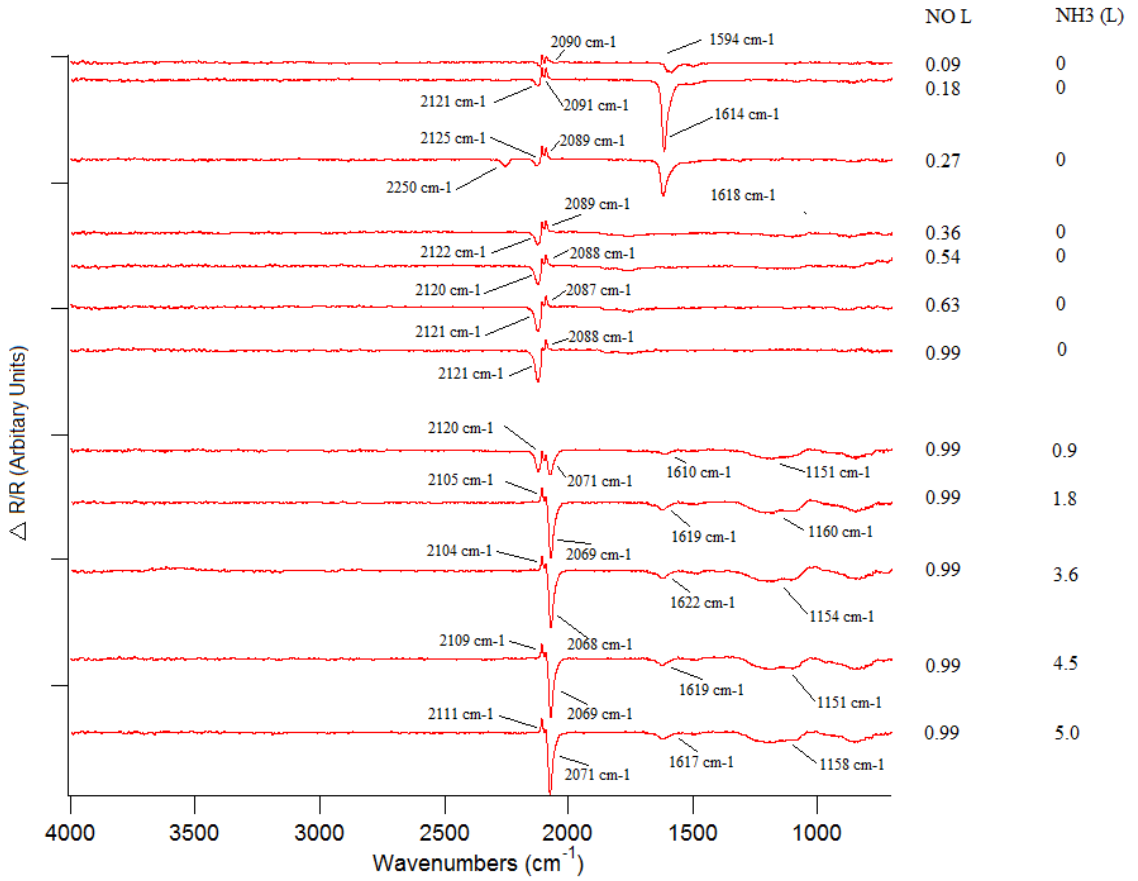

Fig. 6.5 RAIR spectra showing the exposure of the clean Cu{311} surface at 100 K to 1 L of NO followed by a period of gas-line changeover and subsequent exposure of the surface to 5 L of NH_3. Dosing pressure of NO and NH_3 were at 1×10^{-9} and 1×10^{-8} mbar, respectively. This is essentially the reverse order of the experiment performed in Figure 6.3

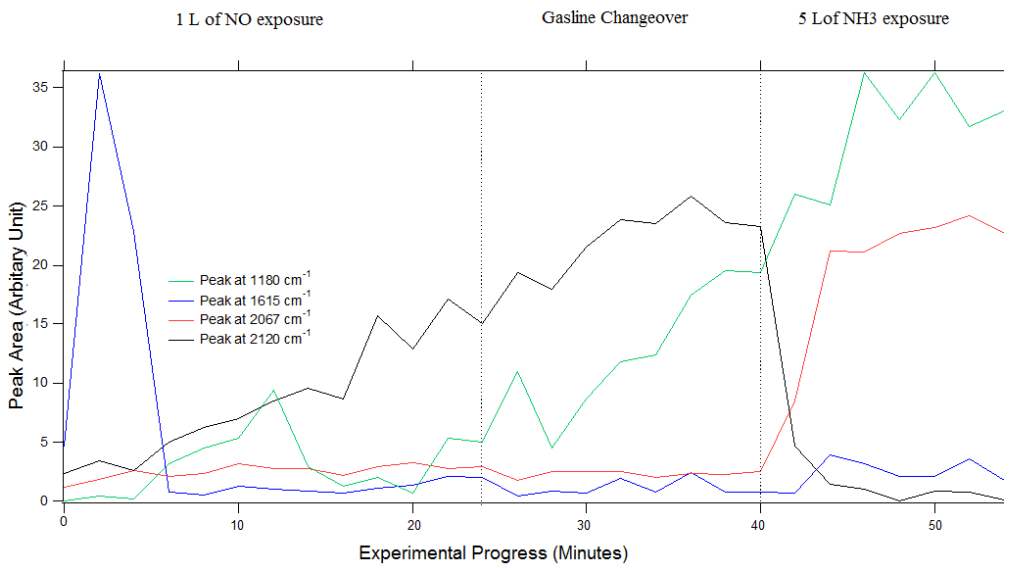

Fig. 6.6 Areas of the peaks from Figure 6.5. The section on the left shows the peaks areas as the Cu{311} surface is exposed to 1 L of NO. The middle section shows peak areas as the gas line is changed from NO into NH_3. The section on the right shows the peak area as the NO covered Cu{311} surface is exposed to 5 L of NH_3.

exposure at which intact NO is still on the surface and does not react completely to form N_2O and $O_{(a)}$. Figure 6.7 shows RAIR spectra following the dosing of 5 L of NH_3 onto 0.26 L of NO on the Cu{311} surface. The top four spectra show the initial dosing 0.26 L of NH_3 with the bottom six spectra showing the subsequent dosing of 5 L of NH_3 onto it.

As NO is exposed onto the clean Cu{311} crystal, NO adsorbs intact, as is evident with the peak NO bridge-site peak at 1583 - 1611 cm^{-1} [80–83]. Once NH_3 is exposed to the surface that was exposed to 0.26 L of NO, the 1611 cm^{-1} peak lowers in area and shifts to 1623 cm^{-1}. This new peak at 1623 cm^{-1} is most likely the combination of two peaks, which are the NO on a bridge-site and antisymmetric deformation mode of NH_3 [109] (both have peaks in the region of 1610 - 1622 cm^{-1}). As with the other two experiments, the inverse peaks at 2119 and 2090 cm^{-1} have both been assigned to residual CO adsorbing onto the surface which has been displaced during the course of the gas dosing [51]. It is worth mentioning that there are no peaks associated with the adsorption of CO onto the surface once NH_3 dosing has begun, most likely due to the inhibition from NH_3. Figure 6.8 shows the change in peak area as a function of coverage for 5 L of NH_3 exposure onto the

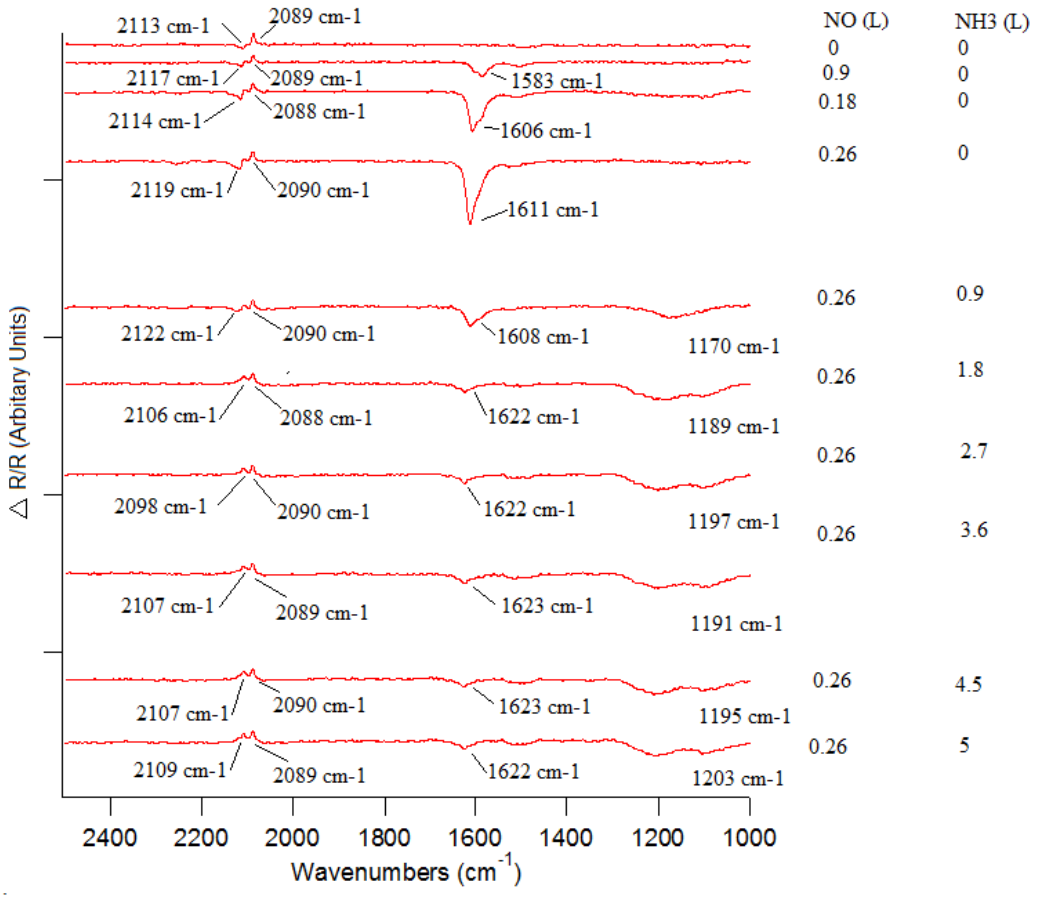

Fig. 6.7 RAIR spectra showing the exposure of the clean Cu{311} surface at 100 K to 0.26 L of NO followed by a period of gas-line changeover and subsequent exposure of the surface to 5 L of NH_3. Dosing pressure of NO and NH_3 were at 1×10^{-9} and 1×10^{-8} mbar, respectively. This is similar to the experiment performed in Figure 6.5, but with a lower exposure of NO.

0.26 L of NO.

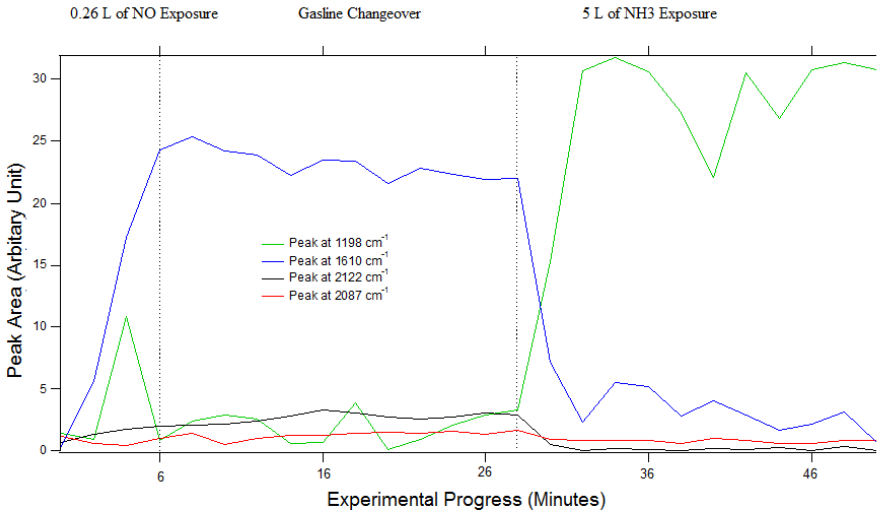

Fig. 6.8 Areas of the peaks from Figure 6.7. The section on the left shows the peaks areas as the Cu{311} surface is exposed to 0.26 L of NO. The middle section shows peak areas as the gas line is changed from NO into NH_3. The section on the right shows the peak area as the NO covered Cu{311} surface is exposed to 5 L of NH_3.

6.3.2 Temperature Programmed Desorption Experiments

Once the RAIRS experiments in Section 6.3.1 were completed, TPD experiments were immediately performed on the resulting coadsorbed species. The masses monitored by the mass spectrometer were mass 17 and 30 amu (assigned to NH_3 and NO) as the temperature is ramped at 0.5 K s^{-1} to 900 K. Figure 6.9 shows the TPD after dosing 1 L of NO onto 5 L of NH_3 on a clean Cu{311} surface. The spectra shows that there is very little NO coming off the surface, while there are poorly resolved desorption peaks for mass 17 amu at 151, 287, and 384 K.

Figure 6.10 shows the TPD after dosing 5 L of NH_3 onto 1 L of NO on a clean Cu{311} surface, essentially the reverse order of Figure 6.9. The TPD data shows very little desorption of NO from the surface but desorption peaks for NH_3 at 151, 270, and 345 K. Fig-

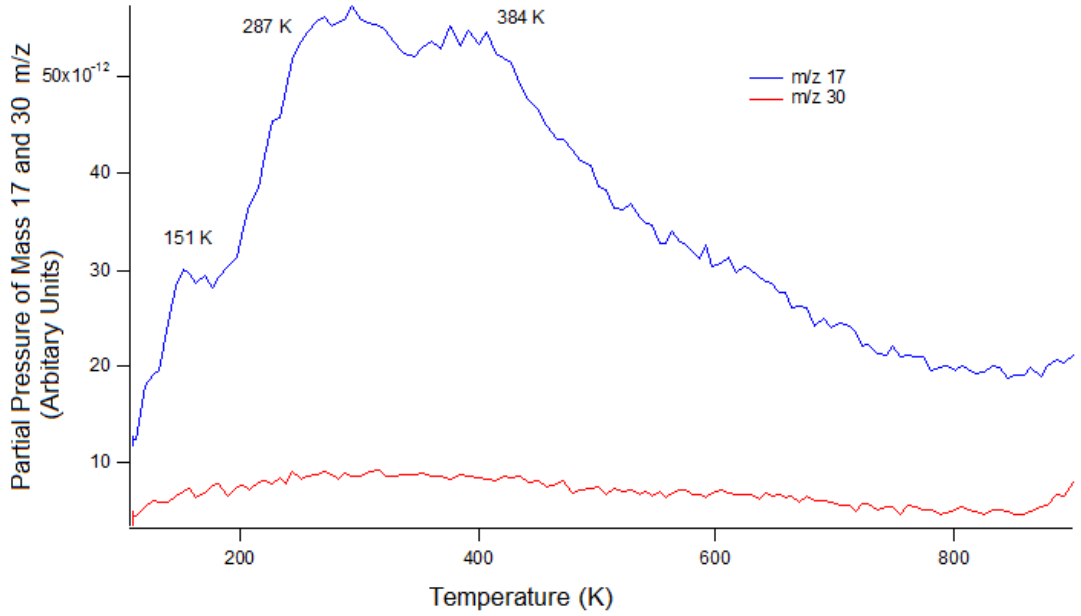

Fig. 6.9 TPD graph after dosing of 1 L of NO onto 5 L of NH_3 on a clean Cu{311} surface.

ure 6.11 shows the TPD experiment after dosing 5 L of NH_3 onto 0.26 L of NO on a clean Cu{311} surface. The mass spectrometer was set to record the partial pressure for mass 17 and 30 amu, which are assigned to NH_3 and NO respectively. The graph shows very little desorption of NO from the surface, but NH_3 desorption from 151, 260, and 341 K.

For comparison, a TPD of 5 L of NH_3 on a clean Cu{311} surface was performed, shown in Figure 6.12. Following both mass 16 and 17, it shows the desorption of NH_3 from the surface at 140, 242, and 350 K.

6.4 Discussion

6.4.1 RAIRS Analysis

When 1 L of NO is dosed onto 5 L of NH_3 pre-covered Cu{311} surface, there is a disappearance of the antisymmetric deformation peak of NH_3. The broad peak assigned to the symmetric deformation mode of NH_3 remains, although with a shift in frequency from 1146

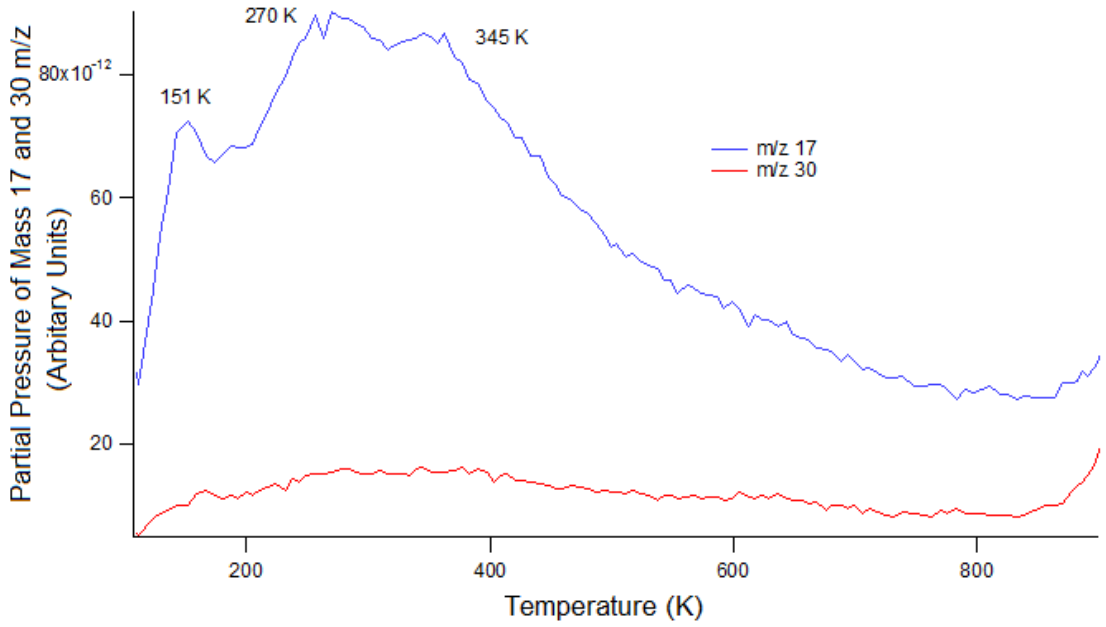

Fig. 6.10 TPD experiment after dosing of 5 L of NH_3 onto 1 L of NO on a clean Cu{311} surface.

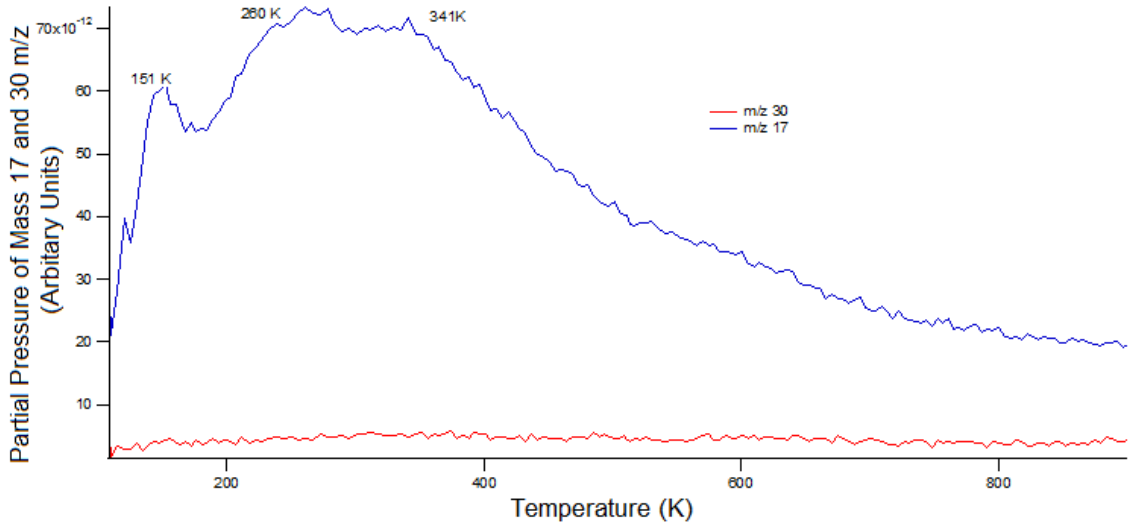

Fig. 6.11 TPD experiment after dosing of 5 L of NH_3 onto 0.26 L of NO on a clean Cu{311} surface.

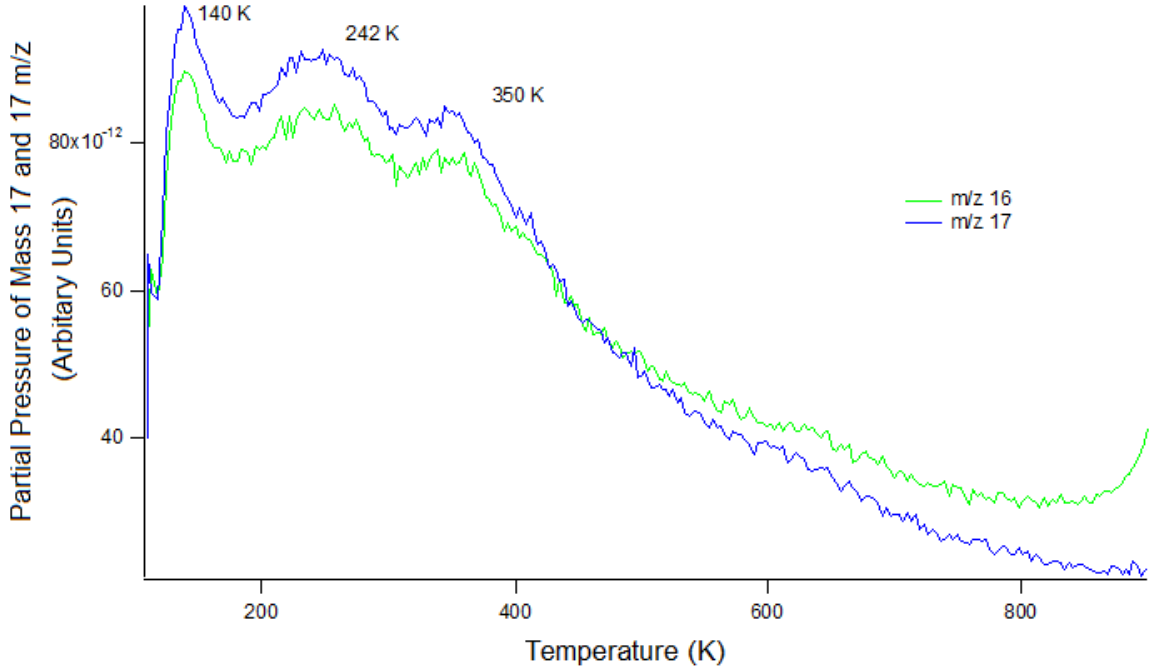

Fig. 6.12 TPD after dosing of 5 L of NH_3 onto a clean Cu{311} surface.

to 1192 cm^{-1}. Despite the noticeable change in frequency, the broad peak at 1191 cm^{-1} is still assigned to NH_3 as later TPD experiments show the desorption of mass 17 amu from the surface (Figure 6.9). The disappearance of the antisymmetric peak for NH_3 at 1612 - 1622 cm^{-1} would suggest that the adsorption of NO leads to the desorption of the tilting (or multilayer) NH_3. This could be due to direct displacement, or the formation of $O_{(a)}$ on the surface, which then reactively removes some of the adsorbed NH_3. It is speculated to be the latter - the shift in the symmetric deformation mode of NH_3 is similar to the effects of oxygen on the surface, which broadens the symmetric deformation peak and shifts it as seen in Section 4.3. However, the broadening and frequency shift is much larger than with oxygen pre-coverage experiments, which could be due to a higher oxygen coverage created by NO reacting on the surface. The complete disappearance of the NH_3 antisymmetric bond also supports the notion that there is a substantially reduced amount of NH_3.

The exposure of 5 L of NH_3 onto 1 L of NO pre-coverage of the Cu{311} surface seems to give more simple results. The spectra shows that as 5 L NH_3 is exposed to the

NO(1 L)/Cu{311} surface, the peaks have frequencies similar to those from the exposure of NH_3 onto the O(1×2) /Cu{311} surface (Figure 5.11(b)). The main difference between the spectra for adsorption of NH_3 onto the NO pre-dosed surface and onto the oxygen pre-dosed Cu{311} surface is that the former has a broader peak for the symmetric deformation mode. As discussed in Section 4.4.1, NO forms N_2O when NO is exposed onto the bare Cu{311} surface (from the $(NO)_2$ dimers) which leaves $O_{(a)}$ on the surface. It is unsurprising that when NH_3 is dosed onto the NO pre-coverage surface - it behaves similarly to when it is dosed onto the oxygen pre-covered Cu{311} surface. Later TPD results indicate a NH_3 multilayer desorbing from the surface, thus the remaining peak at 1610 - 1622 cm^{-1} is likely to be the result of the antisymmetric deformation mode of NH_3.

In a similar experiment to that for 1 L of NO exposure, 5 L of NH_3 was dosed onto a surface that has 0.26 L of NO exposure. This coverage was chosen because it still had intact NO on the surface that had not reacted to form N_2O or $(NO)_2$. Similarly to the previous experiment, the dosing of NH_3 shows the appearance of the peaks associated with the symmetric and antisymmetric deformation mode of NH_3 at 1170 - 1203 and 1608 - 1622 cm^{-1}, respectively. The difference in RAIR spectra (of 0.26 L and 1.0 L of NO pre-coverage) is qualitatively very minor. This suggests that NH_3 simply displaces NO from the surface.

Another of the difference between Figure 6.10 and 6.11 is that the peak area for the CO peak is noticeably higher on the 1.0 L of NO exposure compared to the 0.26 L of NO exposure, which suggests a higher oxygen content in the former. This is due the fact that the higher amount of NO would leave more $O_{(a)}$ on the surface.

6.4.2 Temperature Programmed Desorption Analysis

From the TPD results, only NH_3 is seen to desorb from the surface in significant amounts. This suggests that NH_3 remains intact on the surface, no matter the dosing order. This is in agreement with RAIRS data as the RAIR spectra shows peaks associated with intact NH_3 on the surface (symmetric and antisymmetric deformation mode peaks). Figure 6.13 compares the difference in TPD data from various conditions. Figure 6.13(a) compiles the

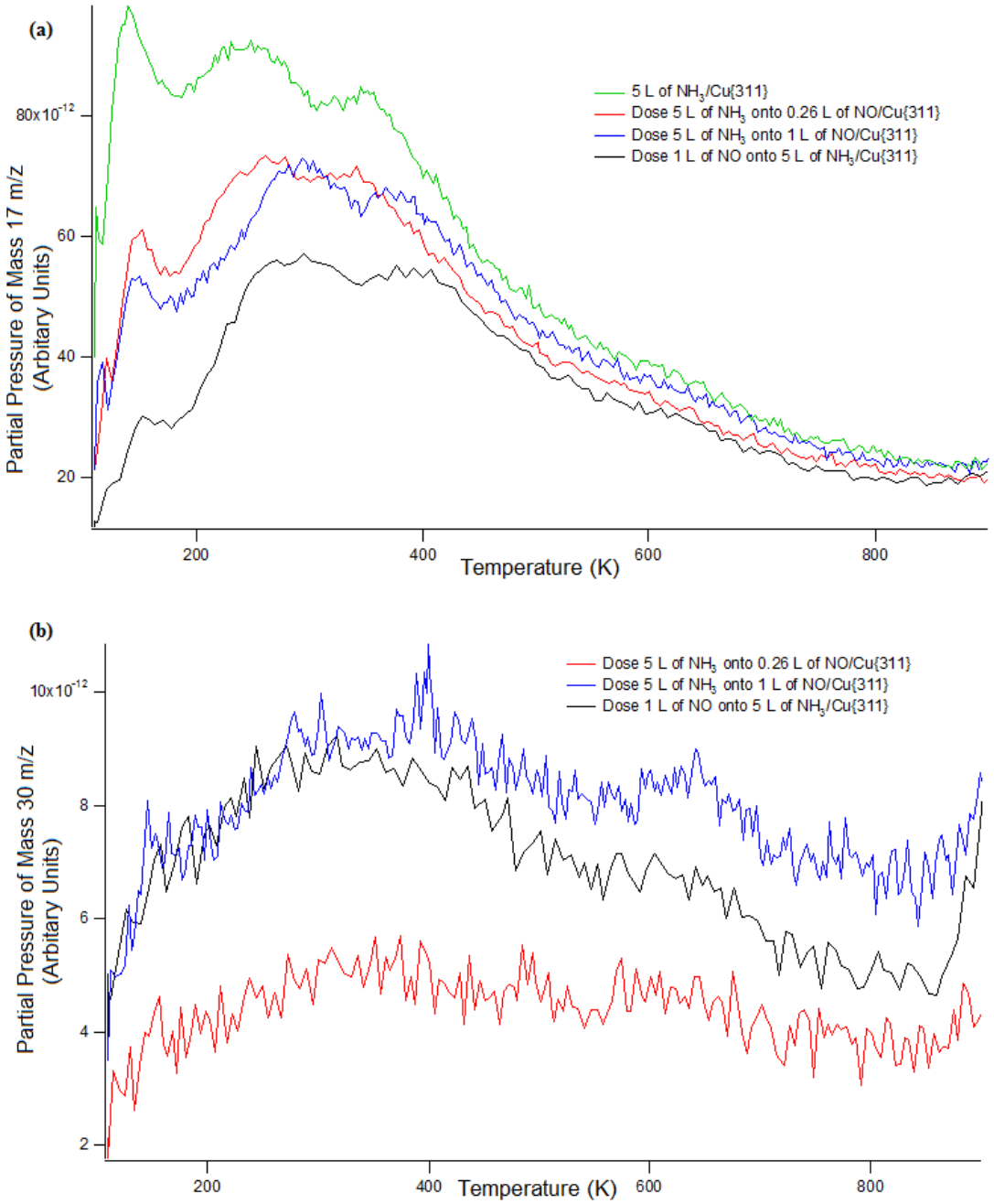

Fig. 6.13 Comparison of the TPD spectra of the various conditions used during the co-adsorption experiments. (a) shows the desorption of mass 17 amu and (b) shows the desorption of mass 30 amu from the surface.

desorption of mass 17 amu from the surface which is assigned to NH_3, Table 6.1 compares the peak sizes and Table 6.2 compares the desorption temperatures of the three experimental conditions. We have assigned Peak 1 to the multilayer, Peak 2 to the bilayer, and Peak 3 to the monolayer of NH_3 respectively. There is a general reduction in the maximum partial pressure of the peaks if NO is exposed to the surface, which suggests a reduction in the total amount of NH_3 adsorbed onto the surface if NO is co-adsoreded onto the surface. Table 6.1 shows the reduction in partial pressure of the mass 17 amu peak maximums of the co-adsorbed experiments, using NH_3 exposure on its own as a reference point.

Table 6.1 Mass 17 desorption peak maximum reduction (using exposure of 5 L of NH_3 onto Cu{311} as the reference).

Condition	Peak 1 (%)	Peak 2 (%)	Peak 3 (%)
5L of NH_3 dosing onto NO(0.26L)/Cu{311}	38	21	14
5L of NH_3 dosing onto NO(1L)/Cu{311}	46	21	18
1L of NO dosing onto NH_3(5L)/Cu{311}	69	38	37

Peak 3, assigned to the monolayer of NH_3 on the surface, is the most strongly bonded species to the Cu{311} surface. It shows the largest change when NO is co-adsorbed, which is not surprising; the shift would be most affected by a change in work function of the surface due to $O_{(a)}$ on the surface. There is a noticeable peak size reduction when NH_3 is dosed onto the NO pre-exposed Cu{311} surface, compared to when it is dosed onto the bare Cu{311} surface. The reduction in peak size is consistent with $O_{(a)}$ blocking adsorption sites. The largest peak area reduction, and the highest desorption temperature (and increase) of the peak assigned to the monolayer occurs when first NH_3 is adsorbed and then NO is adsorbed, in contrast to opposite order. There is little difference between the pre-exposure of 0.26 L or 1 L on the peak size.

Under the same conditions, peak 2 shifts the same way as peak 3. This means that it is affected by the co-adsorption of NO (and therefore $O_{(a)}$) in the same way as the monolayer, and therefore must be a similar species. It is most likely the bilayer of NH_3 as proposed in Chapter 5.

Peak 1 has been assigned to the multilayer of NH_3 on the surface. When 5 L of NH_3 is exposed to the bare Cu{311} surface, this peak is the largest of the 3 peaks and has the

largest reduction when NO is co-adsorbed onto the surface.

Another aspect to discuss is the way which NO, if it is adsorbed onto the surface (either before or after NH_3 exposure), shifts the desorption temperature of the NH_3 desorption peaks upwards by roughly 10 K (Figure 6.2). The largest increase in desorption temperature comes when 1 L of NO is exposed to the surface, especially for Peak 2 and 3.

Table 6.2 Mass 17 amu desorption temperature from various conditions

Condition	Peak 1 (K)	Peak 2 (K)	Peak 3 (K)
5L of NH_3 dosing onto Cu{311}	140	242	350
5L of NH_3 dosing onto NO(0.26L)/Cu{311}	151	260	341
5L of NH_3 dosing onto NO(1L)/Cu{311}	151	270	345
1L of NO dosing onto NH_3(5L)/Cu{311}	151	287	384

As discussed in Chapter 4 and 5, NO leaves $O_{(a)}$ on the surface if NO is dosed onto a Cu{311} surface. It was discussed in Section 5.4.2 that oxygen plays an inhibiting role for NH_3 adsorption due to site blocking, but, because of electronic effects, it also stabilises NH_3 to remain on the surface. This is in agreement with our TPD results as there is a reduction in amount of mass 17 amu coming off the surface but an increase in desorption temperature when NO is co-adsorbed with NH_3. RAIR spectra also show a reduction in the symmetric and antisymmetric deformation mode peaks of NH_3 at 100 K, showing evidence for the inhibiting effect of oxygen on NH_3 adsorption.

When compared to studies on the Cu{111} surface, TPD results only show the desorption of peaks at 140-150 K, which were assigned to the desorption of the chemisorbed NH_3 [126, 128]. Sueyoshi *et al* [128] inferred that the high temperature desorption of mass 16 amu at roughly 250 K is from the NO-NH_3 complex. However, our TPD spectra show that there are also high temperature desorption peaks for NH_3 when only NH_3 is adsorbed onto the bare Cu{311} surface (Figure 6.12). Therefore, the high temperature peak must come from NH_3 only, and not from a NO-NH_3 complex species. Due to limited TPD data, it is not possible to go further in the current analysis of available data.

Figure 6.13(b) compiles the desorption of mass 30 amu from the surface which is assigned to NO desorption from the surface. Compared to mass 17 amu, there is a very small amount of 30 amu desorbing from the surface. This suggests that very little NO remains on

the surface if there is NH_3 pre-adsorbed or exposed after NO. Since no TPD experiments were performed for NO adsorption (without NH_3) onto the Cu{311} surface, it is difficult to infer additional insights from the current available data. There seems to be a very broad peak at 275 K along with one at 600 K although, it is hard to distinguish from the background noise.

There is little difference between the peak size of mass 30 amu desorption when either order of 1 L and 5 L of NH_3 is co-adsorbed. There is a significant reduction when 0.26 L of NO is exposed to the surface (a 55% reduction in maximum peak size). The reduction could be explained by the lower amount of NO exposure, but this does not explain why there is only a 50% reduction despite a 4 fold reduction in dosing amount. This is most likely to be because a significant portion of NO is not on the surface, having reacted to form N_2O, despite the higher dosage of 1 L of exposure. Therefore, the difference between 0.26 and 1.0 L of NO exposure is from unreacted NO on the surface, which is more than just taking exposure into account.

6.4.3 Co-Adsorption and Mechanism

Judging on the RAIR spectra, there is displacement of the NO molecule when NH_3 is exposed to a NO pre-covered Cu{311} surface. This is indicated by the reduction of the NO bridge-site peak as NH_3 is exposed onto it and is confirmed by TPD data indicating that mainly only molecules with mass 17 amu desorb from the surface, which is assigned to NH_3. Therefore the main interaction between NO and NH_3 is the displacement of NO from the surface as NH_3 is dosed onto it.

As there are no other species in the RAIR spectra besides peaks for intact NO and NH_3 when they are co-adsorbed, it seems that NO and NH_3 do not directly interact on the bare Cu{311} surface. However, NO can indirectly influence the adsorption of NH_3 due to the formation of $O_{(a)}$ on the surface after NO has reacted with itself to form the $(NO)_2$ dimer, which eventually forms N_2O, leaving $O_{(a)}$. As mentioned previously, oxygen plays a role as a site blocker for the adsorption of NH_3 onto the surface, but can also stabilize NH_3 to remain on the surface at higher temperatures. Therefore, NO indirectly impacts

the adsorption of NH_3 onto the Cu{311} surface with the creation of $O_{(a)}$. As a result, the amount of NH_3 on the surface is decreased, but that which remains is stabilized.

6.5 Conclusion

To conclude, the co-adsorption of NO and NH_3 seems to be dominated by the displacement of NO from the surface when NH_3 is dosed. However, NO indirectly affects the adsorption of NH_3 by creating $O_{(a)}$ on the surface when it reacts with another NO molecule to form the $(NO)_2$ dimer, eventually forming N_2O. As shown in Chapter 5, $O_{(a)}$ acts both as a site-blocker and electronic stabilizer to affect NH_3 adsorption.

In the context of SCR the process of NO reduction by NH_3 is difficult at low temperatures as NH_3 would simply displace NO on the surface of a Cu catalyst. However, as these experiments were performed at low temperatures, which are distinct from the high temperature conditions of SCR catalysts, they are not purely indicative of how the reaction takes places. Future work should be done on the co-adsorption of NO and NH_3 onto higher surface temperatures.

Chapter 7

Conclusion

7.1 Conclusion

The interaction of NO and NH_3 on a Cu{311} surface has been studied in this thesis, and a brief summary of the results are presented here. It was found that NO forms N_2O and $O_{(a)}$ when dosed onto the Cu{311}, going through the dimer reaction pathway in a process inhibited by oxygen. NH_3 was found to adsorb intact onto the Cu{311} surface at 100 K, but it dissociates at higher temperatures to form NH_2. The co-adsorption of both species onto the Cu{311} surface showed they did not react with each other at low temperatures, and the interaction between NO and NH_3 was dominated by the displacement of NO from the surface by NH_3. In the context of selective catalytic reduction, the work in this thesis has shown that a Cu catalyst needs to be prevented from being fully oxidised (otherwise NO adsorption would cease) but also from being fully metallic (otherwise NH_3 would simply displace NO from the surface rather than dissociating to form NH_2).

NO

RAIRS data shows that when NO is dosed onto the bare Cu{311} surface, it leads to the adsorption of intact NO onto Cu bridge-sites. After a NO exposure of 0.26 L is reached, the formation of $(NO)_2$ dimers on the surface begins to become apparent. With a further increase in NO exposure, the formation of N_2O is seen on the surface. This shows that on

the bare Cu{311} surface, NO adsorption leads to the formation of $(NO)_2$ dimers which subsequently react to form $N_2O_{(a)}$ and $O_{(a)}$ on the surface. As the reaction progresses, $O_{(a)}$ builds up on the surface and eventually inhibits the reaction. Therefore the process of NO adsorption is poisoned by $O_{(a)}$, which is a by-product of the reaction of NO to form N_2O, making it a self-poisoning reaction.

In addition to the inhibition effect of the $O_{(a)}$ when it is produced as a by-product, it also causes the inhibition of the reaction when the Cu{311} surface is pre-covered with oxygen (due to reduction of NO adsorption on the surface). Therefore, the reaction of NO to form the $(NO)_2$ dimer and subsequently N_2O is poisoned by $O_{(a)}$. This result is similar to those from previous work done on Cu{110} [82, 83]. The role of temperature has two effects on the reaction: first, the amount of adsorbed NO on the surface changes (the lower the temperature, the more $NO_{(a)}$ there is), second, a reduction in temperature reduces the mobility of NO on the surface.

In context of SCR, we can see how the bare Cu{311} surface is able to catalyse NO to form N_2O and $O_{(a)}$. Being mindful that N_2O is an extremely harmful greenhouse gas, it is clear that unless the conditions inside the SCR catalyst are carefully controlled, NO may form N_2O instead of environmentally friendly N_2. The poisoning of the reaction due to $O_{(a)}$ also provides useful information, as it highlights the difficulty of using catalysts inside the oxidative conditions of lean burn engine exhausts. This shows that controlling the stoichiometry of the exhaust is essential, since the Cu catalyst would cease to function if fully oxidised.

NH_3

RAIRS data shows that NH_3 adsorbs intact onto the bare Cu{311} surface. Initially, it adsorbs with an upright configuration on the surface. As exposure of NH_3 exceeds 0.32 L, a bilayer of NH_3 starts to form, accompanied by tilting of the NH_3 molecules bonded to the Cu atoms on the surface. This is in line with previous work on Cu{110} [109], Ag{110} [106], and Ag{311} [107]. When the surface temperature is increased to 300 K and NH_3 is dosed, there is some dissociation of NH_3 into NH_2 on the bare Cu{311} surface. At 400 K, the

RAIR spectra shows no adsorbed species on the surface.

When oxygen is pre-dosed onto the Cu{311} surface, at 100 K, it acts as an inhibitor for NH_3 adsorption onto the surface, reducing the amount of NH_3 that is adsorbed. However, when the surface temperature is raised to 300 K and the oxygen pre-covered surface is exposed to NH_3, the RAIR spectra indicates that there is an increase in the amount of NH_3 on the surface when compared to the bare Cu{311} at 300 K. It is inferred that at 300 K, $O_{(a)}$ both promotes the dissociation of NH_3 into NH_2 on the surface but also stabilises it, preventing it from desorbing. Furthermore, at 400 K, when NH_3 is dosed onto a O(1×2)/Cu{311} surface, the RAIRS data shows a peak for intact NH_3 on the surface (no peak is seen on bare Cu{311} in similar conditions). This suggests that oxygen stabilises NH_3 on the surface at higher temperatures.

Therefore, although oxygen inhibits NH_3 adsorption onto the Cu{311} surface, it also stabilises certain NH_3 species on the surface. In the context of SCR, the work in this thesis has shown that NH_3 does not react on a bare or oxygen pre-covered Cu{311} surface at low temperatures, but can form NH_2 at 300 K on bare or oxygen pre-covered Cu{311} surfaces. The work has demonstrated that a low oxygen pre-covered Cu{311} surface is able to promote both the dissociation and the stabilisation of NH_3 to remain on the surface at higher temperatures. This shows how oxygen is a key part of the SCR process and therefore the stoichiometry of the exhaust needs to be controlled so that the Cu surface is neither completely metallic nor oxidised. The formation of NH_2 is useful as it is a potentially reactive radical species - this should be expanded in future work.

NO and NH_3 Co-Adsorption

The culmination of work with NO and NH_3 co-adsorption leads to conclusion that these molecules adsorb onto the surface largely independently from one another at 100 K. The co-adsorption of NO and NH_3 is dominated by the displacement of NO from the surface when NH_3 is dosed, leaving predominately NH_3 on the surface. This is shown in both RAIRS and TPD data, where the prior shows only peaks for intact NH_3 on the surface and the latter primary shows NH_3 desorbing from the surface when both NO and NH_3 are

co-adsorbed. However, as the adsorption of NH_3 is reduced by the presence of $O_{(a)}$, NO indirectly affects the adsorption of NH_3 due to the creation of $O_{(a)}$ on the surface when it reacts with another NO molecule to form the $(NO)_2$ dimer (which eventually forms N_2).

In the context of SCR, at low temperatures NH_3 is seen to displace the NO, which would make it difficult for the reaction to take place on the Cu catalyst. Therefore the mechanism of SCR of NO using NH_3 must be different at higher temperatures at which the bare and oxygen pre-covered Cu surface is able to dissociate NH_3 into a reactive NH_2 species. Further probing of this higher temperature species may yield more information on the mechanism behind NO reduction in selective catalytic reduction.

7.2 Further Work

As most of the work in this thesis was performed at low temperatures, future work should focus on room and high temperature effects on the interaction between of NO and NH_3 on the Cu{311} surface. This should produce different interactions, especially in light of the fact that NH_3 dissociates to NH_2 at 300 K, but not at 100 K. Therefore the exact temperature at which NH_3 dissociates on the Cu{311} surface should also be explored. In addition, the effect of oxygen on the dissociation process of NH_3 as a function of temperature should be explored. This would allow the role of oxygen to be understood; whether it only acts as a promotor for NH_3 dissociation or only stabilises the NH_2 species on the surface, or indeed whether its role is a mixture of both.

Further work should also explore the effects of the various oxygen pre-covered oxides on the co-adsorption of NO and NH_3 on Cu{311}. Although it is very likely that the role of oxygen is simply as an inhibitor on the surface for the co-adsorption of NO and NH_3, it is still worth exploring, especially in the context of SCR. Due to the high oxygen environment of lean burn car exhausts, the effects of the oxides on the co-adsorption is crucial.

A very interesting interaction that should be studied is how $NH_{2(a)}$ reacts with NO and vice versa. NH_2 is a very reactive radical and forms from the dissociation of NH_3 when NH_3 is dosed at 300 K (either on the bare or oxygen pre-covered Cu{311} surface). As discussed

in the NH_3/Cu{311} chapter 5, there is a higher amount of NH_2 when NH_3 is dosed onto an oxygen pre-covered Cu{311} surface at 300 K. Therefore, the interaction between NH_2 and NO should perhaps be studied on the oxygen pre-covered surface at 300 K. This would involve the pre-coverage dosing of oxygen onto the Cu{311} surface. This is then followed by the exposure of the O/Cu{311} surface to NH_3 at 300 K, creating the NH_2 species on the surface, which then further exposed to NO. It is difficult to predict what would occur, but NH_2 is a potentially reactive species and may react with NO to form N_2 or N_2O.

It may also be interesting to probe the nature of the unknown peak observed during NH_3 adsorption onto the bare Cu{311} surface at 1749 cm^{-1}. It may provide useful clues as to both the nature of NH_3 adsorption, and the structure of the Cu{311} surface and its oxides. In addition, the lower frequency peak assigned to CO (at 2069 cm^{-1}) on oxygen pre-covered Cu{311} experiments exposed to NH_3 should also be explored. The shift in frequency indicates a stronger adsorption of CO onto the O/Cu{311} surface. As CO is a major exhaust gas, the effect of NH_3 on CO adsorption is also vital to understand with respect to selective catalytic reduction.

Another area to explore is the interaction of other gases such as N_2O, NO_2 on Cu{311}, in combination with their co-adsorption with NH_3. Studying the RAIRS data of the adsorption of N_2O would most likely yield more insight about how NO forms N_2O and desorbs. NO_2 is another significant gas produced by combustion, so its reduction to NO and then to N_2 would also be valuable.

In conclusion, future work should study NO and NH_3 co-adsorption onto the Cu{311}, surface with a focus on the effects of room and high temperatures on the interaction. Once high temperature effects have been understood, the effects of oxygen should then be studied. In addition to being a new area of study, the higher temperatures and oxygen regimes are more similar to conditions inside the catalytic converter.

References

[1] United States Environmental Protection Agency. Nitrogen Oxides (NO_X), Why and How They are Controlled. 1999.

[2] J.N. Galloway, A.R. Townsend, J.W. Erisman, M. Bekunda, Z. Cai, J.R. Freney, L.A. Martinelli, and S.P. Seitzinger. Transformation of the Nitrogen Cycle: Recent Trends, Questions, and Potential Solutions. *Science*, 320:889–892, 2008.

[3] Intergovernmental Panel on Climate Change. IPCC First Assessment Report. *IPCC Overview*, 1:51–62, 1990.

[4] J.N. Galloway, F.J. Dentener, D.G. Capone, E.W. Boyer, R.W. Howarth, S.P. Seitzinger, G.P. Asner, C.C. Cleveland, P.A. Green, E.A. Holland, D.M. Karl, A.F. Michaels, J.H. Porter, A.R. Townsend, and C.J. Vorosmarty. Nitrogen Cycles: Past, Present, and Future. *Biogeochemistry*, 70:153–226, 2004.

[5] A.R. Townsend, R.W. Howarth, F.A. Bazzaz, M.S. Booth, C.C. Cleveland, S.K. Collinge, A.P. Dobson, P.R. Epstein, E.A. Holland, D.R. Keeney, M.A. Mallin, C.A. Rogers, C.A. Wayne, and A.H. Wolfe. Human Health Effects of a Changing Global Nitrogen Cycle. *The Ecological Society of America*, 1:240–246, 2003.

[6] W.L. Chameides, P.S. Kasibhatla, J. Yienger, and H. Levy. Growth of Continental-Scale Metro-Agro-Plexes, Regional Ozone Pollution, and World Food Production. *Science*, 264:74–77, 1994.

[7] A.R. Ravishankara, J.S. Daniel, and R.W. Portmann. Nitrous Oxide (N_2O): The Dominant Ozone-Depleting Substance Emitted in the 21st Century. *Science*, 326:123–125, 2009.

[8] A. Fritz and V. Pitchon. The current state of research on automotive lean NOx catalysis. *Applied Catalysis B: Environmental*, 13:1–25, 1997.

[9] H.S. Glick, J.J. Klein, and W. Squire. Single-Pulse Shock Tube Studies of the Kinetics of the Reaction $N_2 + O_2 \rightleftarrows$ between 2000-3000° K. *The Journal of Chemical Physics*, 27:850–857, 1957.

[10] Parliament of the United Kingdom. Environmental Protection Act 1990, August 2014.

[11] H.S. Ghandi, G.W. Graham, and R.W. McCabe. Automotive Exhaust Catalysis. *Journal of Catalysis*, 216:432–442, 2003.

[12] J Kaspar, P. Fornasiero, and N. Hickey. Automotive Catalytic Converters: Current Status and Some Perspectives. *Catalysis Today*, 4:419–449, 2003.

[13] R.M. Heck and R.J Farrauto. Automobile Exhaust Catalysts. *Applied Catalysis A: General*, 221:443–457, 2001.

[14] R.J Farrauto and R.M. Heck. Catalytic Converters: State of the Art and Perspetives. *Catalysis Today*, 51:351–360, 1999.

[15] J.H. Baik, S.D. Yim, Y.S. Nam I-S., Mok, B.K. Lee J-H., Cho, and S.H. Oh. Control of NO_X Emissions from Diesel Engine by Selective Catalyric Reduction (SCR) with Urea. *Topics in Catalysis*, 30:37–41, 2004.

[16] M. Koebel, M. Elsener, and T. Marti. NO_X - Reduction in Diesel Exhaust Gas with Urea and Selective Catalytic Reduction. *Combustion Science and Technology*, 121:85–102, 1996.

[17] M. Koebel, M. Elsener, and M. Kleemann. Urea-SCR: a Promising Technique to Reduce NOx Emissions From Automotive Diesel Engines. *Catalysis Today*, 59:335–345, 2000.

[18] M. Radojevic. Reduction of Nitrogen Oxides in Flue Gases. *Environmental Pollution*, 102:685–689, 1998.

[19] M. Iwamoto, H. Yahiro, K. Tanda, MineY. Mizuno, N. and, and S. Kagawa. Removal of Nitrogen Monoxide Through a Novel Catalytic Process. 1. Decomposition on Excessively Copper-Ion-Exchanged ZSM-5 Zeolites. *Journal of Physical Chemistry*, 95:3727—3730, 1991.

[20] M. Shelef. Selective Catalytic Reduction of NOx with N-Free Reducants. *Chemical Reviews*, 95:209–225, 1995.

[21] Z.M. Liu and S.I. Woo. Recent Advances in Catalytic $DeNO_X$ Science and Technology. *Catalysis Reviews*, 48:43–89, 2005.

[22] M. Neeft J.P.A., Makkee and J.A. Moulijn. Diesel Particulate Emission Control. *Fuel Processing Technology*, 47:1–69, 1996.

[23] J.N. Galloway, A.M. Leach, A. Bleeker, and J.W. Erisman. A Chronology of Human Understanding of the Nitrogen Cycle. *Philosophical Transactions of The Royal Society B*, 368, 2013.

[24] M. Appl. *Ammonia*. Ullmann's Encyclopedia of Industrial Chemistry, 1986.

[25] F Haber. The Synthesis of Ammonia from its Elements. *Novel Prize Lecture*, 1920.

[26] TD Kelly and G.R. Matos. Historical Statistics for Mineral and Material Commodities in the United States: U.S. Geological Survey Data. Series 140, 2014.

[27] M. Iwamoto, H. Furukawa, Y. Mine, F. Uemura, S.I. Mikuriya, and S. Kagawa. Coppper(ii) Ion-Exchanged ZSM-5 Zeolites as Highly-Active Catalysts for Direct and Continous Decomposition of Nitrogen Monoxide. *Journal of the Chemical Society - Chemical Communications*, 1(6):1272–1273, 1986.

[28] K. Hermann and F. Rammer. Surface Explorer, November 2014.

[29] J.M. Mundenar, A.P. Baddorf, E.W. Plummer, and L.G. Senddon. Oxygen Chemisorption on Copper (110). *Surface Science*, 188:15–31, 1987.

[30] E.B. Wilson, J.C. Decius, and P.C. Cross. *Molecular Vibrations: The Theory of Infrared and Raman Vibrational Spectra*. McGraw-Hill Book Company, New York, 1955.

[31] H.L Pickering and H.C. Eckstrom. Heterogeneous Reaction Studies by Infrared Adsorption. *Journal of Physical Chemistry*, 63:512–518, 1959.

[32] D.P Woodruff and T.A. Delchar. *Modern Techniques of Surface Science - Second Edition*. Cambridge University Press, Cambridge, 1994.

[33] F.L. Pedrotti, L.M. Pedrotti, and L.S. Pedrotti. *Introduction to Optics (3rd Edition)*. Addison-Wesley, Boston, 2006.

[34] B.E. Hayden. *Vibrational Spectroscopy of Molecules at Surfaces*. Plenum Press, New York, 1987.

[35] N. Sheppard and T. Nguyen. *Advances in Infrared and Raman Spectroscopy*. Hayden & Son, London, 1978.

[36] K.D. Childs, B.A. Carlson, LaVanier L.A., J.F. Moulder, D.F. Paul, W.F. Strickle, and D.G. Watson. *Handbook of Auger Electron Spectroscopy, Third Edition*. Physical Electronics, 1995.

[37] K.L. Brown and G.W. Tautfest. Faraday Cup Monitors for High Energy Electron Beams. *Review of Scientific Instruments*, 27:696–702, 1956.

[38] J.L. Wiza. Microchannel Plate Detectors. *Nuclear Instruments and Methods*, 162:587–601, 1979.

[39] J.S. Allen. An Improved Electron Multiplier Particle Counter. *Review of Scientific Instruments*, 18:739–749, 1947.

[40] M. Ross. *Complex Phenomenology of Model Catalytic Systems: O/Cu{311}, CH_3S-/Au{111}, and S/Au{111} Surfaces Studied by STM*. PhD thesis, University of Cambridge, 2010.

[41] E.W. Hayden. *A Supersonic Molecular Beam Study of Oxygen-Containing Species on Pd{100} and Cu{311}*. PhD thesis, University of Cambridge, 2012.

[42] S.M. Driver. *Private Communication*.

[43] F. Jensen, F. Besenbacher, E. Laesgaard, and Stensgaard I. Surface Reconstruction of Cu(110) Induced by Oxygen Chemisorption. *Physical Review B*, 41:10233–10239, 1990.

[44] H. Schatz A. Zeppenfeld P. Goerge J. Comsa G. Kern, K. Niehus. Long-Range Spatial Self-Organization in the Adsorbate-Induced Restructuring of Surfaces: Cu{110}-(2×1)O. *Physical Review Letters*, 67:855–859, 1991.

[45] R. Raval, S.F. Parker, M.E. Pemble, P. Hollins, J. Pritchard, and M.A. Chesters. FT-rairs, eels and leed studies of the adsorption of carbon monoxide on Cu(111). *Surface Science*, 203:353–377, 1988.

[46] J. Pritchard. On the structure of CO adlayers on Cu(100) and Cu(111). *Surface Science*, 79:231–244, 1979.

[47] K. Horn, M. Hussain, and J. Pritchard. The Adsorption of CO on Cu(110). *Surface Science*, 63:244–253, 1977.

[48] P. Hollins and J. Pritchard. Interactions of CO Molecules Adsorbed On Cu(111). *Surface Science*, 89:486–495, 1979.

[49] H. Papp and J. Pritchard. The adsorption of Xe and CO on a Cu(311) single crystal surface. *Surface Science*, 53:371–385, 1975.

[50] J.F. Wendelken and M.V.K. Ulehla. An ELS Vibrational Study of Carbon Monoxide Adsorbed on the Cu(110) Surface. *Journal of Vacuum Science & Technology*, 16:441–444, 1978.

[51] T. Sueyoshi, T. Sasaki, and Y. Iwasawa. Reactive Oxygen Atoms on Cu(110) Formed at 100 K: Vibrational Spectra and CO Oxidation. *Surface Science*, 343:1–16, 1995.

[52] L.H. Dubois, B.R. Zegarski, and H.S. Luftman. Complex CO-Potassium Interactions on Cu(100): An Electron Energy Loss, Thermal Desorption, and Work Function study. *Journal of Chemical Physics*, 87:1367, 1987.

[53] P. Hollins, Davies K.J., and J. Pritchard. Infrared Spectra of CO Chemisorbed on a Surface Vincinal to Cu(110): The Influence of Defect Sites. *Surface Science*, 138:75–83, 1984.

[54] S.J. Jenkins and Pratt S.J. Beyond the surface atlas: A roadmap and gazetteer for surface symmetry and structure. *Surface Science Reports*, 62:373–426, 2007.

[55] C.J. Hirschmugl, G.P. Williams, F.M. Hoffmann, and Y.J. Chabal. Adsorbate-Substrate Resonant Interactions Observed for CO on Cu(100) in the Far Infrared. *Physical Review Letters*, 65:480–483, 1990.

[56] G. Centi, S. Perathoner, D. Biglino, and E. Giamello. Adsorption and Reactivity of NO on Copper-on-alumina catalysts .2. Adsorbed Species and Competitive Pathways in the Reaction of NO with NH_3 and O_2. *Journal of Catalysis*, 152(1):93–102, 1995.

[57] G. Busca, L. Lietti, G. Ramis, and F. Berti. Chemical and Mechanistic Aspects of the Selective Catalytic Reduction of NOx by Ammonia over Oxide Catalysts: A Review. *Applied Catalysis B - Enviromental*, 18:1–36, 1998.

[58] Y. Hu, K. Griffiths, and R. Norton P. Surface Science Studies of Selective Catalytic Reduction of NO: Progress in the Last Ten Years. *Surface Science*, 603:1740–1750, 2009.

[59] W.E. Addison and R.M. Barrer. Sorption and Reactivity of Nitrious Oxide and Nitric Oxide in Crystalline and Amorphous Siliceous Sorbents. *Journal of the Chemical Society*, 1:757–769, 1955.

[60] K. Otto and M. Shelef. Studies of Surface-Reactions on Nitric-Oxide by Isotope Labeling. 4. Reaction Between Nitric-Oxide and Ammonia Over Copper Surfaces at 150-200 Degrees. *Journal of Physical Chemistry*, 76(1):37–42, 1972.

[61] M. Mizumoto, N. Yamazoe, and T. Seiyama. Catalytic reduction of NO with Ammonia over Cu(ii) Na Y. *Journal of Catalysis*, 55(2):119–128, 1978.

[62] M. Iwamoto and H. Yahiro. Novel Catalyic Decomposition and Reduction of NO. *Catalysis Today*, 22(1):5–18, 1994.

[63] J.W. London and A.T. Bell. Infrared-Spectra of Carbon-Monoxide, Carbon-Dioxide, Nitric-Oxide, Nitrogen-Dioxide, Nitrous-Oxide, and Nitrogen Adsorbed on Copper Oxide. *Journal of Catalysis*, 31(1):32–40, 1973.

[64] W.X. Zhang, H. Yahiro, N. Mizuno, J. Izumi, and M. Iwamoto. Removal of Nitrogen Monoxide on Copper Ion-Exchanged Zeolites by Pressure Swing Adsorption. *Langmuir*, 9(9):2337–2343, 1993.

[65] A.V. Salker and W. Weiweiler. Catalytic Behavior of Metal Based ZSM-5 Catalysts for NOx Reduction with NH_3 in Dry and Humid Conditions. *Applied Catalysis A - General*, 203(2):221–229, 2000.

[66] K. Hadjiivanoc, D. Klissurski, G. Ramis, and G. Busca. Fourier Transform IR study of NOx Adsorption on a CuZSM-5 deNO(x) Catalyst. *Applied Catalysis B - Enviromental*, 7(3-4):251–267, 1996.

[67] D. Pietrogiacomi, D. Sannio, S. Tuti, P. Ciambelli, V. Indovina, and M. Occhiuzzi. The Catalytic Activity of CuO_X/ZrO_2 for the Abatement of NO with Propene or Ammonia in the Prescence of O_2. *Applied Catalysis B - Enviromental*, 21(2):141–150, 1999.

[68] M. Kantcheva. FT-IR Spectroscopic Investigation of the Reactivity of NO_X Species Adsorbed on Cu^{2+}/ZrO_2 and $CuSO_4/ZrO_4$ Catalysts Toward Decane. *Applied Catalysis B - Environmental*, 42(1):89–109, 2003.

[69] Y.J. Li and J.N. Armor. Temperature-Programmed Desorption of Nitric-Oxide over Cu-ZSM-5. *Applied Catalysis*, 76(2):L1–L8, 1991.

[70] M. Shelef, K. Otto, and H. Gandhi. The heterogeneious decomposition of nitric oxide on supported catalysts. *Atmospheric Environment*, 3:107–122, 1969.

[71] S. Sato, Y. Yoshihiro, H. Yahiro, N. Mizuno, and M. Iwamoto. Cu-ZSM-5 Zeolite as Highly-Active Catalysts for Removal of Nitrogen Monoxide from Emission of Diesel Engines. *Applied Catalysis*, 70(1):L1–L5, 1991.

[72] N. Sheppard and C. De la Cruz. A Systematic Review of the Application of Vibrational Spectroscopy to the Determination of the Structures of NO Adsorbed on Single-Crystal Metal Surfaces. *Physical Chemistry Chemical Physics*, 12:2275–2284, 2010.

[73] W.A. Brown and D.A. King. NO Chemisorption and Reactions on Metal Surfaces: A New Perspective. *Journal of Physical Chemistry B*, 104(12):2578–2595, 2000.

[74] M.H. Matloob and M.W. Roberts. Electron Spectroscopic Study of Nitrogen Species Adsorbed on Copper. *Journal of the Chemical Society - Faraday Transactions*, 73:1393–1405, 1977.

[75] D.W. Johnson, M.H. Matloob, and M.W. Roberts. Adsorption of Nitric Oxide on Cu(100) Surfaces - an Electron Spectroscopic Study. *Journal of the Chemical Society-Chemical Communications*, 2:40–41, 1978.

[76] J.F. Wendelken. A Study of Nitric-Oxide Adsorption on Copper-(100) and Copper-(110). *Applied Surface Science*, 11-2(July):172–185, 1982.

[77] A.R. Balkenende, H. Dendaas, M. Huisman, and J.W. Gijeman O.L.J., Geus. The Interaction of NO, O_2, and CO with Cu(100) and Cu(110). *Applied Surface Science*, 47(4):341–353, 1991.

[78] S.S. Dhesi, S. Haq, S.D. Barett, and F.M. Leibsle. LEED and STM Studies of Structures Formed by NO Dissociation on Cu(100) Surfaces. *Surface Science*, 365(3):602–613, 1996.

[79] P. Dumas, M. Suhren, Y.J. Chabal, C.J. Hirschmugl, and G.P. Williams. Adsorption and Reactivity of NO on Cu(111): a Synchroton Infrared Reflection Absorption Spectroscopic Study. *Surface Science*, 371:200–212, 1997.

[80] W.A. Brown, P. Gardner, M.P. Jigato, and D.A. King. Characterization and Orientation of Adsorbed NO Dimers on Ag{111} at Low Temperatures. *Journal of Chemical Physics*, 102:7277–7280, 1995.

[81] W.A. Brown, P. Gardner, and D.A. King. Very-low Temperature Surface-Reaction - N_2O Formation from NO Dimers at 70 K to 90 K on Ag(111). *Journal of Physical Chemistry*, 99:7065–7074, 1995.

[82] C.M. Kim, C.W. Yi, and W.D. Goodman. Adsorption and Reaction of NO on Cu(100): An Infrared Reflection Absorption Spectroscopic Study at 25 K. *Journal of Physical Chemistry B*, 106:7065–7068, 2002.

[83] W.A. Brown, R.K. Sharma, D.A. King, and S. Haq. Adsorption and Reactivity of NO and N_2O on Cu{110}: Combined RAIRS and Molecular Beam Studies. *Journal of Physical Chemistry*, 100(30):12559–12568, 1996.

[84] P.S. Bagus, C.J. Nelin, and P. Avouris. The Interaction of NO with a Metal-Surface - NO/Cu(100). *Journal of Vacuum Science & Technology A- Vacuum Surface and Films*, 5(4):701–702, 1987.

[85] S. Manzhos and K. Yamashita. A Model for the Dissociative Adsorption of N_2O on Cu(100) Using Continuous Potential Energy Surface. *Surface Sciece*, 604(5-6):555–561, 2010.

[86] Z-P. Liu, S.J. Jenkins, and D.A. King. Why is Silver Catalytically Active for NO Reduction? A Unique Pathway via an Inverted $(NO)_2$ Dimer. *Journal of the American Chemical Society*, 126:7336–7340, 2004.

[87] S.K. So, R. Franchy, and W. Ho. Photodesorption of NO from Ag(111) and Cu(111). *Journal of Chemical Physics*, 95:1385–1399, 1991.

[88] S.S. Fu and G.A. Somorojai. Interactions of O_2, CO, CO_2, and D_2 with the Stepped Cu(311) Crystal Face: Comparison to Cu(110). *Surface Science*, 262:68–76, 1992.

[89] A.T.S. Wee, J. Lin, A.C.H. Huan, F.C. Loh, and K.L. Tan. SIMS study of NO, CO adsorption on Cu(100) and Cu(210) surfaces. *Surface Science*, 304:145–158, 1994.

[90] G.A. Habraken F.H.P.M., Bootsma, P. Hofmann, S. Hachicha, and A.M. Bradshaw. The Adsorption and Incorporation of Oxygen on Cu(110) and its Reaction with Carbon Monoxide. *Surface Science*, 88:285–298, 1979.

[91] S. Brandenberger, O. Krocher, A. Tissler, and R. Althoff. The State of the Art in Selective Catalytic Reduction of NOx by Ammonia Using Metal-Exchanged Zeolite Catalysts. *Catalysis Reviews - Science and Engineering*, 50:492–531, 2008.

[92] Z.M. Liu and W. Si. Recent Advances in Catalytic DeNO(X) Science and Technology. *Catalysis REviews - Science and Engineering*, 48:43–89, 2006.

[93] Z.Y. Liu, Q.Y. Liu and C.Y. Li. Adsorption and Activation of NH_3 During Selective Catalytic Reduction of NO by NH_3. *Chinese Journal of Catalysis*, 27:636–646, 2006.

[94] J. Li, H. Chang, L. Ma, and R.T. Hao J. Yang. Low-temperature Selective Catalytic Reduction of NOx with NH_3 Over Metal Oxide and Zeolite Catalysts — A Review. *Catalysis Today*, 175:147–156, 2011.

[95] H. Cheng, B. Reiser D, P.M. Mathias, K. Baumert, and W. Dean Jr S. Investigation of Nitriding Mechanism at Transition Metal Surfaces: NH_3 Adsorption and Decomposition on Fe(100), Ni(100), and Cr(100). *Jornal of Physical Chemistry*, 99:3715–3722, 1995.

[96] B.A. Sexton and G.E. Mitchell. Vibrational Spectra of Ammonia Chemisorbed on Platinum (111). *Surface Science*, 99:523–538, 1980.

[97] C.J. Weststrate, J.W. Bakker, J.R. Rienks E.D.L., Martinez, C.P. Vinod, S. Lizzit, L. Petaccia, A. Baraldi, and B.E. Nieuwenhuysa. Selective NH_3 Oxidation on (110) and (111) Iridium Surfaces. *Journal of Catalysis*, 235:92–102, 2005.

[98] W. Erley and H. Ibach. Vibrational Spectra of Ammonia Adsorbed on Fe(110). *Surface Science Letters*, 119:L357–L362, 1982.

[99] M. Grunze, M. Golze, K. Driscoll R., and P.A. Dowben. Ammonia Adsorption and Decomposition on a Ni(110) Surface. *Jornal of Vacuum Science and Technology*, 18:611–615, 1981.

[100] A. Chattopadhyay, H. Yang, and L. Whitten J. Adsorption of Ammonia on Ni(111). *Journal of Physical Chemistry*, 94:6379–6383, 1990.

[101] A. Pradier C-M, Adamski, C. Methivier, and I. Louis-Rose. Interaction of NH_3 and Oxygen with Cu(110), Investigated by FT-IRAS. *Journal of Molecular Catalysis A: Chemical*, 186:193–201, 2002.

[102] P.S. Bagus and K. Hermann. New Analysis of Lone-Pair Binding-Energy Shifts in Photoemission from Adsorbed Molecules: CO and NH_3 on Cu(100). *Physical Review B*, 33:2987–2991, 1986.

[103] M. Weiss, G. Ertl, and F. Nitschke. Adsorption and Decomposition of Ammonia on Fe(110). *Applied Surface Science*, 00:614–635, 1979.

[104] M. Drechsler, H. Hoinkes, H. Kaaramann, H. Wilsch, G. Ertl, and M. Weiss. Intereaction of NH_3 with Fe(110): Identification of Surface Species by Means of Secondary Ion Mass Spectroscopy (SIMS). *Surface Science*, 3:217–228, 1979.

[105] K. Yoshida and G.A. Somorjai. The Chemisorption of CO, CO_2, C_2H_2, C_2H_2, H_2, and NH_3 on the Clean Fe(110) and (111) Crystal Surfaces. *Surface Science*, 75:46–60, 1978.

[106] J.L. Gland, A. Sexton B., and G.E. Mitchell. Ammonia Adsorption on the Ag(110) Surface. *Surface Science*, 115:623–632, 1982.

[107] S.T. Ceyer and J.T. Yates Jr. Ammonia Adsorption on the Ag(311) Surface. *Surface Science*, 155:584–595, 1985.

[108] D.M. Thornburg and R.J. Madix. Cleavage of N-H bonds by active oxygen on Ag(110). I. Ammonia. *Surface Science*, 220:268–294, 1989.

[109] D. Lackey, M. Surman, and D.A. King. Adsorption of ammonia on Cu{110}. *Vacuum*, 33:867–869, 1983.

[110] B. Afsin, P.R. Davies, A. Pashuski, and M.W. Roberts. The Role of a Dioxygen Precursor in the Selective Formation of Imide NH*a* Species at a Cu(110) Surface. *Surface Science*, 259:L724–L728, 1991.

[111] B. Afsin, P.R. Davies, A. Pashusky, M.W. Roberts, and D. Vincent. Reaction Pathways in the Oxydehydrogenation of Ammonia at Cu(110) Surfaces. *Surface Science*, 284:109–120, 1993.

[112] A.F. Carley, P.R. Davies, M.W. Roberts, and D. Vincent. Oxygen Sites Active in H-Abstraction at a Cu(110)-O Surface: Comparison of a Monte Carlo Simulation with Imide Formation Studied by XPS and VEELS. *Topics in Catalysis*, 1:35–42, 1994.

[113] I. Louis-Rose, C. Methivier, and C.M. Pradier. Oxidation of NH_3 on Polycrystalline Copper and Cu(110): a Combined FT-IRAS and Kinetics Investigation. *Catalysis Today*, 85:267–278, 2003.

[114] R.J. Guo, X-C. Madix. In Situ STM Imaging of Ammonia Oxydehydrogenation on Cu(110): the Reactivity of Preadsorbed and Transient Oxygen Species. *Surface Science*, 387:1–10, 1997.

[115] G.B. Fisher and G.E. Mitchell. A Vibrational Study of Ammonia Chemisorbed on Ni(110) and Ni(111): Whither Goest the Metal-Nitrogen Stretching Mode on Fcc (111) Surfaces? *Studies in Surface Science and Catalysis*, 14:253–259, 1983.

[116] I.C. Bassignana, K. Wagemann, and G. Ertl. Adsorption and Thermal Decomposition of Ammonia on a Ni(110) Surface: Isolation and identification of Adsorbed NH_2 and NH. *Surface Science*, 175:22–44, 1986.

[117] K Nakamoto. *Infrared and Raman Spectra of Inorganic and Coordination Compounds*. Wiley, New York, 1986.

[118] E.B. Burgina, E.N. Yurchenko, and E.A. Paukshtis. Peculiarities of the Vibratioanl Spectra of Molecules Adsorbed on the Surface of Heterogeneous Catalysts: Theoretical Asnalysis. *Journal of Molecular Structure*, 147:193–201, 1986.

[119] O.S. Binbrek and A. Anderson. Raman Spectra of Molecular Crystals. Ammonia and 3-Deutero-Ammonia. *Chemical Physics Letters*, 15:421–427, 1972.

[120] M.A. Larrubia, G. Ramis, and G. Busca. An FT-IR Study of the Adsorption and Oxidation of N-Containing Compounds over Fe_2O_3-TiO_2 SCR Catalysts. *Applied Catalysis B : Environmental*, 30:101–110, 2001.

[121] D. Mocuta, J. Ahner, and J.T. Yates. Adsorption and Electron-Stimulated Dissociation of Ammonia on Cu(110) an ESDIAD Study. *Surface Science*, 383:299–307, 1997.

[122] Davies Booth, NA and, R., Woodruff Toomes, R. and, Hirschmugl D.P. and, Schindler C and, Schaff K.M. and, Fernandez O. and, Theobald V. and, Hofmann A. and, Lindsay Ph. and, Giebel R and, Baumgartel T and, and A.M. P and, Bradshaw and. Structure Determinatio of Ammonia on Cu(110) - a Low-Symmetry Adsorption Site. *Surface Science*, 387:152–159, 1997.

[123] C.J. Hirschmugl, K.M. Schindler, O. Schaff, V. Fernandez, A. Theobald, Ph. Hofmann, A.M. Bradshaw, R. David, N.A. Booth, D.P. Woodruff, and V. Fritzsche. Quantitative Structure Determination of an NH_x Species Adsorbed on Cu(110). *Surface Science*, 352:232–237, 1996.

[124] G. Jones and S.J. Jenkins. Water and Ammonia on Cu{311}: Comparative Structure and Bonding. *Physical Chemistry Chemical Physics*, 15:4785–4798, 2013.

[125] D. McNaughton, C.J. Evans, S. Lane, and C.J. Nielsen. The High-Resolution FTIR Far-Infrared Spectrum of Formamide. *Journal of Molecule Spectroscopy*, 193:104–117, 1999.

[126] T. Hertel, M. Wolf, and G. Ertl. UV Photostimulted Desorption of Ammonia from Cu(111). *Journal of Chemical Physics*, 102:3414–3430, 1995.

[127] G. Ramis, L. Yi, G. Busca, M. Turco, E. Kotur, and R.J. Willey. Adsorption, Activation, and Oxidation of Ammonia over SCR Catalysts. *Journal of Catalysis*, 157:523–535, 1995.

[128] T. Sueyoshi, T. Sasaki, and Y. Iwasawa. Coadsorption of NO and NH_3 on Cu(111): The Formation of the Stabilized (2×2) Coadlayer. *Journal of Physical Chemistry*, 100:13646–13654, 1996.